國 立 交 通 大 學

電 信 工 程 學 系

碩 士 論 文

高階調變符號解碼量度的位元單位分解法則之研究

Bit-wise Decomposition of M-ary Symbol Metric

研 究 生： 張家瑋

指導教授： 陳伯寧 博士

中華民國九十三年六月

高階調變符號解碼量度的位元單位分解法則之研究

Bit-wise Decomposition of M-ary Symbol Metric

研 究 生： 張家瑋　　Student: Chia-Wei Chang

指導教授： 陳伯寧 博士　　Advisor: Dr. Po-Ning Chen

國 立 交 通 大 學

電 信 工 程 學 系

碩 士 論 文

A Thesis

Submitted to Department of Communication Engineering

College of Electrical Engineering and Computer Science

National Chiao Tung University

In Partial Fulfillment of the Requirements

For the Degree of

Master of Science

In

Communication Engineering

June 2004

Hsinchu, Taiwan, Republic of China.

中華民國 九十三 年 六 月

高階調變符號解碼量度的位元單位分解法則之研究

學生： 張家瑋　　指導教授： 陳伯寧 博士

國立交通大學電信工程學系

中文摘要

未來在無線通信的技術,隨著資料量的增加,勢必傳輸速度也要跟著增加。標準 IEEE 802.11a 中,便包含了利用更高階的正交調幅調變符號再加上正交分頻多工的調變技巧來提升傳輸的速度,而在防治錯誤更正上使用(2,1,6)的迴旋碼。為了使迴旋碼達到最好的使用效果,兩層交錯器的設計於是被運用上,第一層先把相鄰已編碼過的位元對應到不相鄰的次載波上然後第二層是把正交調幅調變符號中最重要的位元和最不重要的位元作交錯的變更,而很令人失望的,用此設計雖然簡單但卻限制了威特比演算法只能用硬性決定來做解碼。而本論文就是想找出一個普遍且系統化的近似來設計解碼端能突破硬性決定的限制做到軟性決定更能符合高階正交調幅調變傳輸和位元導向的交錯器。

利用分解原本以正交調幅調變符號符號為基準且使用硬性決定的最大相似方式解迴旋碼變成以位元導向為基準且使用軟性決定,更能契合以位元導向的交錯器和之後的威特比演算法。首先我們由數學推導利用二階逼近看能不能找出跟最大相似方式均方根矩陣達到非常相近的近似,進而達到我們想以位元導向來做軟性決定,接著推導出有系統且規律的公式應用在更高速的正交調幅調變符號中。接下來考慮量化誤差所帶來的影響和個別的高階正交調幅調變符號所需的最少量化位元數。自動增益控制(AGC)對系統所造成的影響,相位誤差所帶來的影響,間空碼技術的影響,也都會在本論文作模擬驗證。最後我們將探討此系統的可行性和未來的應用發展,我們將結合現有的通訊架構利用數位信號處理,類比邏輯電路來探討實作上可能遭遇的問題和相關數學式的推倒與修改,期望能增進系統的效能和速率。

Bit-wise Decomposition of M-ary Symbol Metric

Student: Chia-Wei Chang Advisor: Dr. Po-Ning Chen

Department of Communication Engineering

National Chiao-Tung University

Abstract

In this thesis, we present a systematic approach for bit-wisedecomposition of **M**-ary symbol metric. The decomposed bit metrics can be applied to improve the performance of a system where the information sequence is binary-coded and interleaved before **M**-ary modulated. A straightforward receiver designed for certain system is to de-map or quantize the received **M**-ary symbol into its binary isomorphism to facilitate the subsequent bit-based manipulation, such as hard-decision decoding. In stead, with a bit-wise decomposition of **M**-ary symbol metric, a soft-decision decoder can be readily used to achieve a better system performance. The proposed approach is to decompose the symbol-based maximum-likelihood (ML) metric by equating a number of specific equations that are drawn from squared-error criterion. Systematic solutions for exemplified 16QAM, 64QAM, 256QAM and 1024QAM are then established. Simulation results based on IEEE 802.11a/g system setting show that at the bit-error-rate of 10^{-5}, the proposed bit-wise decomposed metric can provide 3.0 dB, 3.9 dB, 5.1 dB and 6.3 dB improvement over the concatenation of binary–demapper/deinterleaver/hard–decision -decoder for 16QAM, 64QAM, 256QAM and 1024QAM symbols, respectively under the AWGN channel. Further empirical study on system imperfection implies that the proposed bit-wise decomposed metric also improves the system robustness against gain-mismatch and phase-noise. A realization structure for our proposed systematic recursive formula then is established. Different from conventional structure where de-interleaver and decoder are separate circuits, our structure de-interleaves and decodes at the same time; and hence, memory space and processing latency can be reduced.

Acknowledgements

I am deeply grateful to my advisor, Professor Tsern-Huei Lee, for his continuous encouragement, support, and enthusiastic discussion throughout this research. His valuable suggestions help me to the success of this work.

Also this is an opportunity to express my sincere appreciation to all the staff of the Institute of Communication Engineering, National Chiao Tung University, for their encouragement and help. Especially, I would like to thank the members of network technologies laboratory for their stimulating discussion and help.

This thesis is dedicated to my parents for their patience, love, encouragement and long expectation. At last, thank everyone who supports and concerns me so far.

Bit-wise Decomposition of M-ary Symbol Metric

Prepared by Chia-Wei Chang

Advisory by Prof. Po-Ning Chen

In Partial Fulfillment of the Requirements

For the Degree of
Master of Science

Department of Communications Engineering

National Chiao Tung University

Hsinchu, Taiwan 300, R.O.C.

E-mail: sekwan.cm87@nctu.edu.tw

June, 2004

Contents

List of Tables

List of Figures

Chapter 1

Introduction and Background

1.1 Problem Formulation

The state-of-the-art wireless transmission technique of IEEE 802.11a/g [11, 12] incorporated high QAM into OFDM to achieve a high data rate. In order to make a better use of the error correcting capability of the adopted (2,1,6) convolutional code, the standard specified a two-step bit-wise interleaver, where the first step maps adjacent code bits onto non-adjacent sub-carriers, and the second step permutes the code bits alternately onto less and more significant bits of the QAM constellation. Such an interleaver design, although straight and simple in concept, may restrict the potential structures of a receiver in practice.

For a system where the binary information sequence is coded and interleaved before M-ary modulated, a straightforward receiver design is to de-map or quantize the received M-ary symbol into its binary isomorphism to facilitate the subsequent bit-based manipulation (cf. Fig. 1.1). From Figure 1.2, it seems that mapping the two consecutive convolutional code bits directly to a QAM quadrature component and transforming the bit-wise interleaver to a quadrature-component-wise interleaver at the transmitter may improve the receiver performance by taking advantage of the soft-decision Viterbi. However, such an approach cannot be in general used when multiple data rates are implemented through varying QAM

Figure 1.1: An exemplified receiver design.

level and code punctuation, such as 2/3 and 3/4 code rates are resulted from punctuation of a (2, 1, 6) convolutional code together with the selection of 16QAM and 64QAM. In addition, for symbol-based interleaving, one QAM symbol error may render consecutive code bit errors (or burst errors), which the convolutional codes suffers most; hence, the performance may still degrade even if a soft-decision decoding is employed. Question is with a bit-wise interleaving, multi-rate support through varying QAM level and code punctuation, can soft-decision decoder still be employed for a better system performance? The answer is affirmative, if the ML metric corresponding to the received vector due to QAM symbol transmission can be bit-wisely divided. The concern then becomes "How much improvement over the hard-decision decoding can be yielded?" and "Can it be implemented with feasible system complexity?" We will investigate these two issues in the next section.

1.2 Objective of the Research

Take IEEE std. 802.11a as an example (cf. Fig. 1.2), the 4 bits for a 16QAM symbol are interleaved such that the 2 bits for a convolutional code branch in a trellis are constituted by the least significant bit of one QAM quadrature component and the most significant bit of another QAM quadrature component. After de-interleaving (cf. Fig. 1.3, Fig. 1.4), the two code bits, c_1 and c_2, that decide a trellis branch of (2,1,6) convolutional code will respectively come from the least significant bit of 16QAM quadrature component r_1 and the most significant bit of 16QAM quadrature component r_7. The dependence of a single trellis

branch on two time-inconsecutive QAM symbols somehow implicitly and directly suggest that the received M-ary symbol should be hard-mapped before decoding, since other receiver structure such as one with soft-decision decoding may require a branch metric that can be determined by two distant and non-orderly M-ary symbols. Such a soft-decision-based receiver will become more involved, when a receiver structure that also supports multi-rate transmission through code punctuation is further considered.

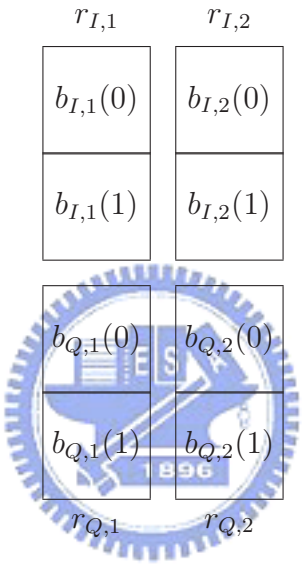

Figure 1.2: The relation between the bits for 16QAM mapping and the bits for a branch in the $(2, 1, 6)$ convolutional code trellis specified in IEEE 802.11a. $(r_{I,1}, r_{Q,1})$ and $(r_{I,2}, r_{Q,2})$ represent the received vectors for two 16QAM symbols, respectively. The 4 bit-pairs that constitute convolutional code branches in a trellis are $[b_{I,1}(0), b_{I,2}(1)]$, $[b_{I,1}(1), b_{I,2}(0)]$, $[b_{Q,1}(0), b_{Q,2}(1)]$ and $[b_{Q,1}(1), b_{Q,2}(0)]$.

In order to design a general receiver for use of M-ary symbol transmission of coded and interleaved information sequence, researchers have proposed several heuristic methods to perform bit-wise decomposition of M-ary symbol metric [4, 5, 6]. With a bit-wise decomposition of M-ary symbol metric, a better system performance can be achieved by adopting a soft-decision decoder, even if code punctuation for dynamic rate transmission is incorporated. Even though some of them perform well in practice, there is still lack of a systematic

method for bit-wise decomposition of M-ary symbol metric. In this thesis, we propose a systematic approach for bit-wise decomposition of M-ary symbol metric. The proposed approach is to approximate the symbol-based maximum-likelihood (ML) metric by equating a number of specific equations that are drawn from squared-error criterion. Notably, when all the listed equations can be simultaneously satisfied, the squared error between symbol-based ML metric and its bit-decomposed approximation reduces to zero, which means that the performance of the symbol-based ML metric can be achieved by taking the proposed bit-wise decomposed metrics. This optimistic result of zero square error however could not be obtained in general due to the bit-wise interleaving. A suboptimal bit-decomposition metric in terms of maximal subset of simultaneously satisfiable equations is then proposed. Exemplified study on QAM modulation interestingly yields a systematic recursive bit metric formula. It is worth mentioning that the recursive bit metric formula can also be applied to some previous work on bit reliability study with different initial condition [5]. Details are given in Section 2.3.2.

Empirical study under the system setting of IEEE 802.11a/g and additive white Gaussian noise (AWGN) channel showed that, at bit error rate (BER) = 10^{-5}, the proposed bit-decomposed metric has 3.0 dB, 3.9 dB, 5.1 dB and 6.3 dB gains over the hard decision system for 16QAM, 64QAM, 256QAM and 1024QAM, respectively. Also, only 0.13 dB performance degradation is resulted by introducing 32-level quantization for 16QAM signals. The quantization impact for 64QAM signals under 64-level uniform quantization can even be reduced to 0.07 dB. No further performance degradation, in addition to that due to quantization, can be observed, when mismatch of AGC gain is limited to be within $\pm 40\%$. The robustness of the proposed bit-decomposed metric against phase noise is also examined. When the phase drift increases up to $\pm 6^o$, the BER due to our bit-decomposed metric will increase from 10^{-5} to around 4×10^{-5} at $E_b/N_0 = 6.7$ dB for 16QAM modulation. This

phase drift tolerance reduces to $\pm 4^o$ at $E_b/N_0 = 9.7$ dB for 64QAM modulation, where E_b/N_0 is chosen so that the no-phase-drift BER is approximately 10^{-5}.

Some previous works on bit reliability study are summarized below. In [6], Zehavi proposed a decoding scheme that consists of a Log-Likelihood-Ratio (LLR) demapping for subsequent use of path metric computation of Viterbi decoder. Later, Pyndiah [4] provided a pragmatic algorithm based on LLR to Turbo codes associated with high QAM modulation, and showed that the block turbo-coded QAM modulation outperforms Trellis-Coded Modulation (TCM) scheme by at least 1dB at BER of 10^{-5}. Tosato and Bisaglia [5] adapted the Pyndiah's algorithm to COFDM system, and proposed a simplified bit reliability decomposition for 16QAM and 64QAM constellations. Their simulations showed that for 64QAM constellation, adopting their bit reliability decomposition results in 8.5dB gain at BER = 10^{-4} over a hard-decision-based receiver under HIPERLAN/2 system model.[1]

1.3 Organization of the Thesis

This thesis is organized in the following fashion. Chapter 2 provides the analysis of the proposed bit-decomposed metric, followed by its comparisons with other soft-demapping schemes. Chapter 3 summarizes the simulation results over the AWGN channel and those over the Rayleigh flat fading channel. Chapter 4 examines the robustness of the proposed bit-decomposed metric against system imperfection. Chapter 5 uses puncture to obtain different coding rate and compares their performances under both AWGN and Rayleigh flat fading channels. Chapter 6 provides a realization structure for our previously proposed systematic recursive formula for bit-wise decomposition of M-ary symbol metric. Concluding remarks appear in Chapter 7. Appendix A is the analysis and general formula of bit-wise metric

[1]Similar to IEEE std 802.11a/g, the scrambled input sequence of HIPERLAN/2 [10] is convolutionally encoded with rate 1/2 and constraint length 7 before bit-wise interleaving and QAM modulation. The technique is often referred to as BICM (Bit-Interleaved Coded Modulation) [16].

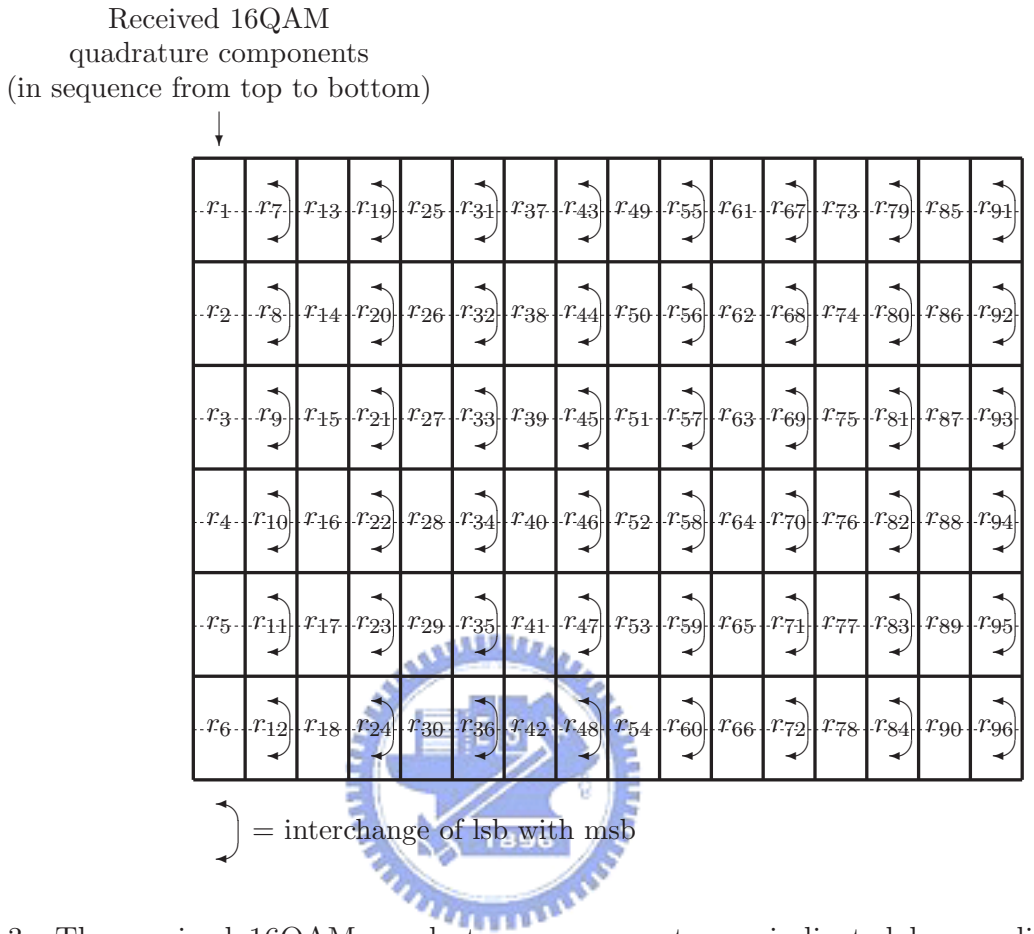

Figure 1.3: The received 16QAM quadrature components are indicated by a solid-lined upright rectangular; each column consists of 6 quadrature components. The de-interleaver should then exchange (the weights of) the least significant bit and the most significant bit of the quadrature components for those columns indicated.

for soft-decision decoding of coded high QAM - 64QAM, 256QAM, 1024QAM. Appendix B gives an intuitive soft-demapping decoding for coded high QAM. Appendix C describes theoretical performances and simulations of QAM modulation over AWGN and Rayleigh flat fading channels that includes symbol error rate and bit error rate, as well as distributions of bit errors given symbol errors.

c_1	c_2	c_3	c_4	c_5	c_6	c_7	c_8	c_9	c_{10}	c_{11}	c_{12}	c_{13}	c_{14}	c_{15}	c_{16}
c_{17}	c_{18}	c_{19}	c_{20}	c_{21}	c_{22}	c_{23}	c_{24}	c_{25}	c_{26}	c_{27}	c_{28}	c_{29}	c_{30}	c_{31}	c_{32}
c_{33}	c_{34}	c_{35}	c_{36}	c_{37}	c_{38}	c_{39}	c_{40}	c_{41}	c_{42}	c_{43}	c_{44}	c_{45}	c_{46}	c_{47}	c_{48}
c_{49}	c_{50}	c_{51}	c_{52}	c_{53}	c_{54}	c_{55}	c_{56}	c_{57}	c_{58}	c_{59}	c_{60}	c_{61}	c_{62}	c_{63}	c_{64}
c_{65}	c_{66}	c_{67}	c_{68}	c_{69}	c_{70}	c_{71}	c_{72}	c_{73}	c_{74}	c_{75}	c_{76}	c_{77}	c_{78}	c_{79}	c_{80}
c_{81}	c_{82}	c_{83}	c_{84}	c_{85}	c_{86}	c_{87}	c_{88}	c_{89}	c_{90}	c_{91}	c_{92}	c_{93}	c_{94}	c_{95}	c_{96}
c_{97}	c_{98}	c_{99}	c_{100}	c_{101}	c_{102}	c_{103}	c_{104}	c_{105}	c_{106}	c_{107}	c_{108}	c_{109}	c_{110}	c_{111}	c_{112}
c_{113}	c_{114}	c_{115}	c_{116}	c_{117}	c_{118}	c_{119}	c_{120}	c_{121}	c_{122}	c_{123}	c_{124}	c_{125}	c_{126}	c_{127}	c_{128}
c_{129}	c_{130}	c_{131}	c_{132}	c_{133}	c_{134}	c_{135}	c_{136}	c_{137}	c_{138}	c_{139}	c_{140}	c_{141}	c_{142}	c_{143}	c_{144}
c_{145}	c_{146}	c_{147}	c_{148}	c_{149}	c_{150}	c_{151}	c_{152}	c_{153}	c_{154}	c_{155}	c_{156}	c_{157}	c_{158}	c_{159}	c_{160}
c_{161}	c_{162}	c_{163}	c_{164}	c_{165}	c_{166}	c_{167}	c_{168}	c_{169}	c_{170}	c_{171}	c_{172}	c_{173}	c_{174}	c_{175}	c_{176}
c_{177}	c_{178}	c_{179}	c_{180}	c_{181}	c_{182}	c_{183}	c_{184}	c_{185}	c_{186}	c_{187}	c_{188}	c_{189}	c_{190}	c_{191}	c_{192}

→ Convolutional code bits (from left to right)

Figure 1.4: After de-interleaving, each 2-bit trellis branch for convolutional decoding is indicated by the flat rectangular in sequences from left to right.

Chapter 2

Systematic Bit-wise Decomposition of M-ary Symbol Metric

2.1 Analysis of Bit-wise Metric for Soft-decision Decoding of Coded High QAM

Denote by $\boldsymbol{r} = (r_1, r_2, \ldots, r_K)$ the real-valued received vector when M-ary symbols $\boldsymbol{s} = (s_1, s_2, \ldots, s_K)$ that are mapped from an interleaved version of encoding output $\boldsymbol{c} = (c_1, c_2, \ldots, c_N) \in \{0,1\}^N$ are transmitted. As an example, $M = 2$, $K = 96$, and $N = 192$ in Fig. 1.3. Assume that the M-ary symbol transmission suffers additive white Gaussian noise (AWGN), $n_1, n_2, n_3, \ldots, n_K$, with single-sided noise power per hertz N_0. The received vector $\boldsymbol{r}$ then satisfies

$$r_i = s_i + n_i$$

for $1 \leq i \leq K$. For AWGN channel, the maximum-likelihood decision upon the receipt of $\boldsymbol{r}$ is given by:

$$
\begin{aligned}
d_{ML}(\boldsymbol{r}) &= \arg\max_{\boldsymbol{s}\in\mathcal{S}} \Pr\{r_1,\ldots,r_K\,|s_1,\ldots,s_K\} \\
&= \arg\max_{\boldsymbol{s}\in\mathcal{S}} \frac{1}{(\pi N_0)^{K/2}} \exp\left\{-\sum_{i=0}^{K}\frac{(r_i-s_i)^2}{N_0}\right\} \\
&= \arg\min_{\boldsymbol{s}\in\mathcal{S}} \sum_{i=1}^{K}(r_i-s_i)^2, \qquad (2.1)
\end{aligned}
$$

where $\mathcal{S}$ represents the set of all possible mappings from the convolutional codeword in $\mathcal{C}$ to its respective symbol word. Due to the non-linear (e.g., interleaving) relation between codeword $\boldsymbol{c}$ and transmitted symbol $\boldsymbol{s}$, Eq. (2.1) cannot be equivalently transformed to the sum of code bit metrics. An approximation is therefore necessary to perform soft-decision decoding. Our goal then becomes to find a sequence of function $\boldsymbol{\lambda} = (\lambda_1, \lambda_2, \ldots, \lambda_N)$ such that the sum of all code symbol metrics, $\sum_{i=1}^{K}(r_i - s_i)^2$, can be well-approximated by $\sum_{i=1}^{N}\lambda_i(c_i, \boldsymbol{r})$ for every mapping pair ($\boldsymbol{c}$, $\boldsymbol{s}$) and the received vector $\boldsymbol{r}$, where functions $\lambda_1, \lambda_2, \ldots, \lambda_N$ can be distinct bit-metric functions.

For clarity, we use the 16QAM modulation in Fig. 1.3 and Fig. 1.4 as an example for the presentation of our subsequent derivation in this section. The general results for 64QAM and 256QAM will be given later.

Let $s(\cdot,\cdot)$ be the 16QAM mapping from code bits to the transmitted symbol. Since code bits c_1, c_2, c_{17} and c_{18} only depend on r_1 and r_7, their contribution to the summation in (2.1) is equal to $[r_1 - s(c_1, c_{17})]^2 + [r_7 - s(c_{18}, c_2)]^2$, where the reverse in order of c_2 and c_{18} is owing to the interleaving procedure. As $r_2, \ldots, r_{96}$ are nothing to do with c_1 and c_{17}, we can simplify our goal to the finding of functions λ_1 and λ_{17} such that $\lambda_1(c_1, r_1) + \lambda_{17}(c_{17}, r_1)$ well-approximates $[r_1 - s(c_1, c_{17})]^2$ for all legal c_1 and c_{17} in the codebook. For the same reasoning, we wish to determine functions λ_{18} and λ_2 such that $\lambda_{18}(c_{18}, r_7) + \lambda_2(c_2, r_7)$ well-approximates $[r_7 - s(c_{18}, c_2)]^2$ for all legal c_2 and c_{18} in the codebook. Since function pairs $(\lambda_1, \lambda_{17})$ and $(\lambda_{18}, \lambda_2)$ are determined according to independent and identical statistical structures, it is

reasonable to presume that they are equal, i.e., $\lambda_1 = \lambda_{18} = f_1$ and $\lambda_{17} = \lambda_2 = f_2$ for some functions f_1 and f_2.[1]

We next address the criterion of "well-approximation" adopted in this thesis.

2.2 Bit-wise Decompositions of 16QAM, 64QAM and 256QAM Symbol Metrics

The criterion we adopt is the minimization of average square error, namely,

$$\min_{f_1,f_2} E\left[\left(f_1(c,r) + f_2(\bar{c},r) - [r - s(c,\bar{c})]^2\right)^2\right] \tag{2.2}$$

To separate the function finding problem from the convolutional code employed, we re-define the cost by assuming uniform prior as:

$$W(f_1,f_2) \triangleq \frac{1}{4}\sum_{c=0}^{1}\sum_{\bar{c}=0}^{1}\int_{-\infty}^{\infty}\left(f_1(r,c) + f_2(r,\bar{c}) - [r - s(c,\bar{c})]^2\right)^2 d\Pr(r|c,\bar{c}), \tag{2.3}$$

where the expectation is taken over the statistics of c, $\bar{c}$ and r. Without loss of generality, we can re-write f_1 and f_2 as[2]:

$$f_1(c,r) = \frac{1}{2}r^2 + a_{1,c,r}r + b_{1,c,r} \quad \text{and} \quad f_2(\bar{c},r) = \frac{1}{2}r^2 + a_{2,\bar{c},r}r + b_{2,\bar{c},r}$$

This transforms (2.2) into:

$$\min_{a_{1,c,r},a_{2,\bar{c},r},b_{1,c,r},b_{2,\bar{c},r}} E\left[\left\{\left(a_{1,c,r} + a_{2,\bar{c},r} + 2s(c,\bar{c})\right)r + \left(b_{1,c,r} + b_{2,\bar{c},r} - s^2(c,\bar{c})\right)\right\}^2\right]. \tag{2.4}$$

It is neither practical nor analytically tractable to consider general coefficient functions, $a_{1,c,r}$, $a_{2,\bar{c},r}$, $b_{1,c,r}$ and $b_{2,\bar{c},r}$, for continuous r. Instead, we consider a piece-wise simplification

[1] As a consequence, the number of distinct functions among $\lambda_1, \lambda_2, \ldots, \lambda_N$ is $\log_2(M)$, which will be denoted by $f_1, f_2, \ldots, f_{\log_2(M)}$ in the sequel. These bit metric functions, $f_1, f_2, \ldots, f_{\log_2(M)}$, will be applied to decompose the symbol metric for every QAM quadrature symbol received.

[2] The optimal $f_1^*(c,r)$ can apparently be re-expressed as $(1/2)r^2 + (f_1^*(c,r)/r - r/2)r + 0$. Therefore, as long as the coefficient $a_{1,c,r}$ and $b_{1,c,r}$ are allowed to be r-dependent, the taken form of $(1/2)r^2 + a_{1,c,r}r + b_{1,c,r}$ covers the optimal solution.

of them by setting $a_{1,c,r}$, $a_{2,\bar{c},r}$, $b_{1,c,r}$ and $b_{2,\bar{c},r}$ equal to constants for r in each interval $\mathcal{I}_\rho = (\lambda_{\rho-1}, \lambda_\rho]$, where $1 \le \rho \le q$, $\lambda_0 = -\infty$ and $\lambda_q = \infty$. For notational convenience, we use $a_{1,c,\rho}$, $a_{2,\bar{c},\rho}$, $b_{1,c,\rho}$ and $b_{2,\bar{c},\rho}$ to denote the constant values specified for each interval. Then the mean squared error between the soft bit metrics and soft symbol metric is given by

$$\begin{aligned}
W(f_1, f_2) &= \frac{1}{4\sqrt{\pi N_0}} \left(\sum_{\rho=1}^{q} \int_{\lambda_{\rho-1}}^{\lambda_\rho} \left[(a_{1,0,\rho} + a_{2,0,\rho} - 6)r + (b_{1,0,\rho} + b_{2,0,\rho} - 9) \right]^2 e^{-(r+3)^2/N_0} dr \right. \\
&\quad + \sum_{\rho=1}^{q} \int_{\lambda_{\rho-1}}^{\lambda_\rho} \left[(a_{1,0,\rho} + a_{2,1,\rho} - 2)r + (b_{1,0,\rho} + b_{2,1,\rho} - 1) \right]^2 e^{-(r+1)^2/N_0} dr \\
&\quad + \sum_{\rho=1}^{q} \int_{\lambda_{\rho-1}}^{\lambda_\rho} \left[(a_{1,1,\rho} + a_{2,1,\rho} + 2)r + (b_{1,1,\rho} + b_{2,1,\rho} - 1) \right]^2 e^{-(r-1)^2/N_0} dr \\
&\quad \left. + \sum_{\rho=1}^{q} \int_{\lambda_{\rho-1}}^{\lambda_\rho} \left[(a_{1,1,\rho} + a_{2,0,\rho} + 6)r + (b_{1,1,\rho} + b_{2,0,\rho} - 9) \right]^2 e^{-(r-3)^2/N_0} dr \right) \\
&= \frac{1}{4\sqrt{\pi N_0}} \sum_{\rho=1}^{q} \left(\int_{\lambda_{\rho-1}}^{\lambda_\rho} \left[(a_{1,0,\rho} + a_{2,0,\rho} - 6)r + (b_{1,0,\rho} + b_{2,0,\rho} - 9) \right]^2 e^{-(r+3)^2/N_0} dr \right. \\
&\quad + \int_{\lambda_{\rho-1}}^{\lambda_\rho} \left[(a_{1,0,\rho} + a_{2,1,\rho} - 2)r + (b_{1,0,\rho} + b_{2,1,\rho} - 1) \right]^2 e^{-(r+1)^2/N_0} dr \\
&\quad + \int_{\lambda_{\rho-1}}^{\lambda_\rho} \left[(a_{1,1,\rho} + a_{2,1,\rho} + 2)r + (b_{1,1,\rho} + b_{2,1,\rho} - 1) \right]^2 e^{-(r-1)^2/N_0} dr \\
&\quad \left. + \int_{\lambda_{\rho-1}}^{\lambda_\rho} \left[(a_{1,1,\rho} + a_{2,0,\rho} + 6)r + (b_{1,1,\rho} + b_{2,0,\rho} - 9) \right]^2 e^{-(r-3)^2/N_0} dr \right), \qquad (2.5)
\end{aligned}$$

where N_0 is the single-sided noise power per hertz.

Intuitively, if more coefficients of r in (2.5) can be made zero, a smaller squared error should be obtained. We then list and number the coefficients of r in (2.5) according to ascending value of $s(c, \bar{c})$ for all possible c and $\bar{c}$, and let them be zero. For example, if $s(c, \bar{c})$ is taken to be the Gray code mapping to 16QAM quadrature component, and c and $\bar{c}$ are

binary, then the coefficient equations listed for each ρ are:

$$s(0,0) = -3 \quad \Rightarrow \quad a_{1,0,\rho} + a_{2,0,\rho} - 6 = 0, \quad b_{1,0,\rho} + b_{2,0,\rho} - 9 = 0 \tag{2.6a}$$

$$s(0,1) = -1 \quad \Rightarrow \quad a_{1,0,\rho} + a_{2,1,\rho} - 2 = 0, \quad b_{1,0,\rho} + b_{2,1,\rho} - 1 = 0 \tag{2.6b}$$

$$s(1,1) = +1 \quad \Rightarrow \quad a_{1,1,\rho} + a_{2,1,\rho} + 2 = 0, \quad b_{1,1,\rho} + b_{2,1,\rho} - 1 = 0 \tag{2.6c}$$

$$s(1,0) = +3 \quad \Rightarrow \quad a_{1,1,\rho} + a_{2,0,\rho} + 6 = 0, \quad b_{1,1,\rho} + b_{2,0,\rho} - 9 = 0 \tag{2.6d}$$

It can be verified that at most three of (2.6a)–(2.6d) can be made valid simultaneously. In addition, in order to minimize the squared error, it is not necessary to equate coefficient equations with non-contiguous equation numbers (because the squared error can be reduced by replacing the non-contiguous numbered equation with one having contiguous equation number), or to equate only part of the three equations that can be made simultaneously valid. This suggests that we should take, for the above example, $q = 2$, for which $\rho = 1$ corresponds to the validity of (2.6a)–(2.6c), and $\rho = 2$ realizes (2.6b)–(2.6d). By experimenting over 64QAM and 256QAM, we found that similar observations can also be made. This motivates us to propose a systematic approach to define a bit-decomposition of M-ary symbol metric as follows.

Step 1. List and number the coefficient equations in ascending value of symbol mapping function value s for all possible code bit combinations.

Step 2. Find all set of coefficient equations that can be simultaneously satisfied, and that are also contiguous in equation number. Remove those sets of coefficient equations that are subset of others. (In this step, the coefficients that validate each set are also determined.)

Step 3. Let q be the number of coefficient equation sets remained in Step 2. Determine the optimal $\boldsymbol{\lambda} = (\lambda_1, \ldots, \lambda_q)$ that minimizes the average squared error in (2.4).

Notably, the solution obtained from the above procedure may be only suboptimal in the minimization of average squared error over all legitimate $f_1(c, r)$ and $f_2(\bar{c}, r)$. However, we will show later that the soft-decision decoding performance by using the bit-decomposed metric above is already close to the optimal but "non-achievable" symbol-based ML performance[3] in (2.1). Specifically, the proposed bit-decomposed metric is only 0.6 dB, $0.8 - 0.9$ dB, or 1.4 dB worse than the symbol-ML performance at $BER = 10^{-5}$.

For completeness, a specific algorithm to exhaust all coefficient equation sets that are not subsets to each other (and hence q is determined) is addressed in the following.

⟨**Algorithm Q**⟩

Initialization: Input L ordered equations with indices 1, 2, ..., L.

Step 1. For each $1 \leq \rho \leq L$, find the largest set A_ρ of equations

- *that can be simultaneously satisfied by some solutions, and*
- *that are contiguous in their equation numbers, and*
- *that contains equation ρ (namely, the equation whose index equals ρ).*

Step 2. Delete all duplicate sets among $A_1, A_2, \ldots, A_L$. (Let q be the number of sets remained.)

Step 3. Output the remaining q (distinct) sets.

Applying Step 1 of Algorithm Q to (2.6a)–(2.6d) results:

[3]As mentioned earlier, with a nonlinear mapping between code word $\boldsymbol{c}$ and symbol word $\boldsymbol{s}$, a receiver can no longer implement (2.1). However, by turning off the interleaver, which in turn linearizes the relation between $\boldsymbol{c}$ and $\boldsymbol{s}$, a M-ary modulated (2,1,6) convolutional codeword can be decoded by forming the trellis of equivalent $(\log_2(M), \log_2(M)/2)$ code trellis in which each branch metric is determined by one received symbol; hence, performance of (2.1) can be simulated. Since a disabled interleaver is not a system option, we therefore term this performance *non-achievable*, and only illustrate it for comparison.

$$\begin{aligned} A_1 &= \{(2.6a), (2.6b), (2.6c)\} \\ A_2 &= \{(2.6a), (2.6b), (2.6c)\} \\ A_3 &= \{(2.6b), (2.6c), (2.6d)\} \\ A_4 &= \{(2.6b), (2.6c), (2.6d)\} \end{aligned}$$

Notably, A_1, A_2, A_3 and A_4 must respectively contain equation (2.6a), (2.6b), (2.6c) and (2.6d) according to the algorithm. Since $A_1 = A_2$ and $A_3 = A_4$, Step 2 yields $q = 2$. The coefficients that validate the equations in sets A_1 and A_3 are respectively:

$$A_1(\rho = 1) \quad : \quad \begin{cases} a_{1,0,1} = 2 - a_{2,1,1} \\ a_{1,1,1} = -2 - a_{2,1,1} \\ a_{2,0,1} = 4 + a_{2,1,1} \\ b_{1,0,1} = b_{1,1,1} = 1 - b_{2,1,1} \\ b_{2,0,1} = 8 + b_{2,1,1} \end{cases}$$

$$A_3(\rho = 2) \quad : \quad \begin{cases} a_{1,0,2} = 2 - a_{2,1,2} \\ a_{1,1,2} = -2 - a_{2,1,2} \\ a_{2,0,2} = -4 + a_{2,1,2} \\ b_{1,0,2} = b_{1,1,2} = 1 - b_{2,1,2} \\ b_{2,0,2} = 8 + b_{2,1,2} \end{cases}$$

Accordingly, with uniform distributed c and $\bar{c}$, the average squared error becomes:

$$\begin{aligned} W(\boldsymbol{\lambda}) &= \frac{1}{4\sqrt{\pi N_0}} \left(\int_{\lambda_0}^{\lambda_1} (8r)^2 e^{-(r-3)^2/N_0} dr + \int_{\lambda_1}^{\lambda_2} (-8r)^2 e^{-(r+3)^2/N_0} dr \right) \\ &= \frac{16}{\sqrt{\pi N_0}} \left(\int_{-\infty}^{\lambda_1} r^2 e^{-(r-3)^2/N_0} dr + \int_{\lambda_1}^{\infty} r^2 e^{-(r+3)^2/N_0} dr \right). \end{aligned} \tag{2.7}$$

By (2.7), we only need to determine λ_1. The derivative of (2.7) with respective to λ_1 is equal to:

$$\frac{\partial W(\boldsymbol{\lambda})}{\partial \lambda_1} = \frac{16}{\sqrt{\pi N_0}} \lambda_1^2 e^{-(\lambda_1^2+9)/N_0} \left(e^{6\lambda_1/N_0} - e^{-6\lambda_1/N_0} \right),$$

the derivative with respective to λ_1 then concludes that the optimal λ_1 that minimizes $W(\boldsymbol{\lambda})$ is zero. Consequently, the average squared error is reduced to:

$$\begin{aligned} W(f_1, f_2) &= \frac{32}{\sqrt{\pi N_0}} \int_{-\infty}^{0} r^2 e^{-(r-3)^2/N_0} dr \\ &= 8(18 + N_0) \operatorname{erfc}\left(\frac{3}{\sqrt{N_0}} \right) - \frac{48\sqrt{N_0}}{\sqrt{\pi}} \exp\left\{ -\frac{9}{N_0} \right\}. \end{aligned} \tag{2.8}$$

We summarize the derivation above as follows:

$$\begin{aligned}
\rho &= \begin{cases} 1, & \text{if } r \in \mathcal{I}_1 \text{ or } r \le 0; \\ 2, & \text{if } r \in \mathcal{I}_2 \text{ or } r > 0 \end{cases} \\
f_1(r,c) &= \frac{1}{2}r^2 + a_{1,c,\rho}r + b_{1,c,\rho} = \frac{1}{2}r^2 + [2(1-2c) - a_{2,1,\rho}]r + (1 - b_{2,1,\rho}) \\
f_2(r,c) &= \frac{1}{2}r^2 + a_{2,c,\rho}r + b_{2,c,\rho} = \frac{1}{2}r^2 + [a_{2,1,\rho} - 4(1-c)\cdot \mathrm{sgn}(r)]r + [b_{2,1,\rho} + 8(1-c)],
\end{aligned}$$

where

$$\mathrm{sgn}(r) = \begin{cases} 1, & \text{if } r > 0; \\ 0, & \text{if } r = 0; \\ -1, & \text{if } r < 0 \end{cases}$$

By the nature of Viterbi algorithm, only those terms that depend on c affect the decoding behavior. Hence, the equivalent soft-demapping functions are:

$$\begin{aligned}
f_1^{\mathrm{eq}}(r,c) &= 2(1-2c)r \\
f_2^{\mathrm{eq}}(r,c) &= -4(1-c)|r| + 8(1-c).
\end{aligned}$$

Since we can remove the constants in $\sum_{i=1}^{N} f_i(c_i, \boldsymbol{r})$ without affecting the decoding result (namely, we can keep only those terms that depend on $\boldsymbol{c}$), and since a universal scaling on all bit-decomposed metric functions also preserves the decoding result, the bit-decomposed metric functions can be equivalently reduced to:

$$\begin{aligned}
f_1^{\mathrm{16QAM}}(c,r) &= c|r| \cdot \mathrm{sgn}(-r) \\
f_2^{\mathrm{16QAM}}(c,r) &= c(|r| - 2).
\end{aligned}$$

As a result, we approximate $[r_1 - s(c_1, c_{17})]^2$ by $f_1^{\mathrm{16QAM}}(r_1, c_1) + f_2^{\mathrm{16QAM}}(r_1, c_{17}) = c_1|r_1| \cdot \mathrm{sgn}(-r) + c_{17}(|r_1| - 2)$ for $c_1, c_{17} \in \{0, 1\}$ for which a decoding algorithm like Viterbi decoding becomes applicable. It is clear that the above f_1^{16QAM} and f_2^{16QAM} can be applied to all c_i and c_j in $s(c_i, c_j)$, respectively.

We can similarly obtain the equivalent bit-decomposed metric functions for 64QAM (where the images of symbol mapping include $-7, -5, -3, -1, 1, 3, 5$ and 7) and 256QAM

(where the images of symbol mapping include $-17, -15, \ldots, 15, 17$) under the IEEE 802.11a system setting[4] as:

$$\begin{cases} f_1^{64\text{QAM}}(c,r) &= c(|r-4|+|r|+|r+4|-8)\cdot\text{sgn}(-r) \\ f_2^{64\text{QAM}}(c,r) &= f_1^{16\text{QAM}}(c,4-|r|) \\ f_3^{64\text{QAM}}(c,r) &= f_2^{16\text{QAM}}(c,|r|-4) \end{cases}$$

and

$$\begin{cases} f_1^{256\text{QAM}}(c,r) &= c(|r-8|+|r-4|+|r|+|r+4|+|r+8|-24)\cdot\text{sgn}(-r) \\ f_2^{256\text{QAM}}(c,r) &= f_1^{64\text{QAM}}(c,8-|r|) \\ f_3^{256\text{QAM}}(c,r) &= f_2^{64\text{QAM}}(c,|r|-8) \\ f_4^{256\text{QAM}}(c,r) &= f_3^{64\text{QAM}}(c,8-|r|) \end{cases}$$

We end this section by noting that the above result suggests a recursive bit-metric decomposition formula. Specifically, for M-ary amplitude modulation (or equivalently, M^2QAM) with amplitude spacing u,[5]

$$\begin{cases} f_1^{(\text{m})}(c,r) &= c\cdot\text{sgn}(-r)\left(\sum_{i=-(m-2)}^{m-2}(|r+2ui|-|2ui|)\right) \\ f_j^{(\text{m})}(c,r) &= f_{j-1}^{(\text{m}-1)}\left(c,(-1)^j\left[2^{m-2}u-|r|\right]\right) \text{ for } 2\le j\le m, \end{cases}$$

where $m=\log_2(M)\ge 2$ and $f_1^{(1)}(c,r)=-cr$. Note that m is respectively 2, 3 and 4 for 16QAM, 64QAM and 256QAM. Consequently, after specifying the first-bit metric f_1, the subsequent bit-metrics are alternately the *left-shift mirror* $f_{j-1}^{(\text{m}-1)}\left(c,2^{m-2}u-|r|\right)$ and *right-shift* $f_{j-1}^{(\text{m}-1)}\left(c,|r|-2^{m-2}u\right)$ of the bit-metrics for one-less m. Such bit-metric assignment somehow even the bit reliability for decoding. The more detailed descriptions are included in Appendix A.

[4]The IEEE 802.11a standard did not specify the interleaver for 256QAM transmission. Here, we simply extend its design philosophy for 16QAM and 64QAM transmission to obtain an extension interleaver for use of 256QAM transmission. To be specific, 96 256QAM quadrature components are tabularized in the same fashion as in Fig. 1.3, where each component is now composed of four bits instead of two bits, and circular shift (from bottom to top) is repeated $(i-1)$ times for those bits belonging to the same quadrature component that locates at ith column.

[5]u is 2 for all QAM considered in this thesis.

2.3 Alternative Structures for Receiver with Soft-decision Decoding

In this section, we briefly describe two existing structures of receiver design for M-ary modulated interleaved code. Performance comparisons of our bit-decomposed metric with these existing schemes will be provided in the next chapter.

2.3.1 Soft-demapping for Bit-interleaved Coded Modulation

An intuitive approach to soft-demap bit-interleaved coded modulation signals is to directly quantize the received vector according to the *inverse* of modulation mapping function [3]. For example, when Gray code mapping is applied to 16QAM modulation, where $s(0,0) = -3$, $s(0,1) = -1$, $s(1,1) = 1$ and $s(1,0) = 3$, the inverse mapping for the first bit position is $b_0^{-1}(-3) = 0$, $b_0^{-1}(-1) = 0$, $b_0^{-1}(1) = 1$ and $b_0^{-1}(3) = 1$, and similarly the inverse mapping for the second bit position can be obtained as $b_1^{-1}(-3) = 0$, $b_1^{-1}(-1) = 1$, $b_1^{-1}(1) = 1$ and $b_1^{-1}(3) = 0$. According to these specified inverse mapping values, we can then form two continuous demapping functions as:

$$b_0^{-1}(r) = \begin{cases} 0, & \text{for } r < -1; \\ (1+r)/2, & \text{for } -1 \le r < 1; \\ 1, & \text{for } r \ge 1 \end{cases} \quad \text{and} \quad b_1^{-1}(r) = \begin{cases} 0, & \text{for } r < -3; \\ (3+r)/2, & \text{for } -3 \le r < -1; \\ 1, & \text{for } -1 \le r < 1; \\ (3-r)/2, & \text{for } 1 \le r < 3; \\ 0, & \text{for } r \ge 3. \end{cases}$$

Fig. 2.1 shows a mapping metric value of 16QAM. Based on the differentiate distribution of the Gray code, we can use weighting to derive better performance. A more detailed discussion refers to Appendix B.

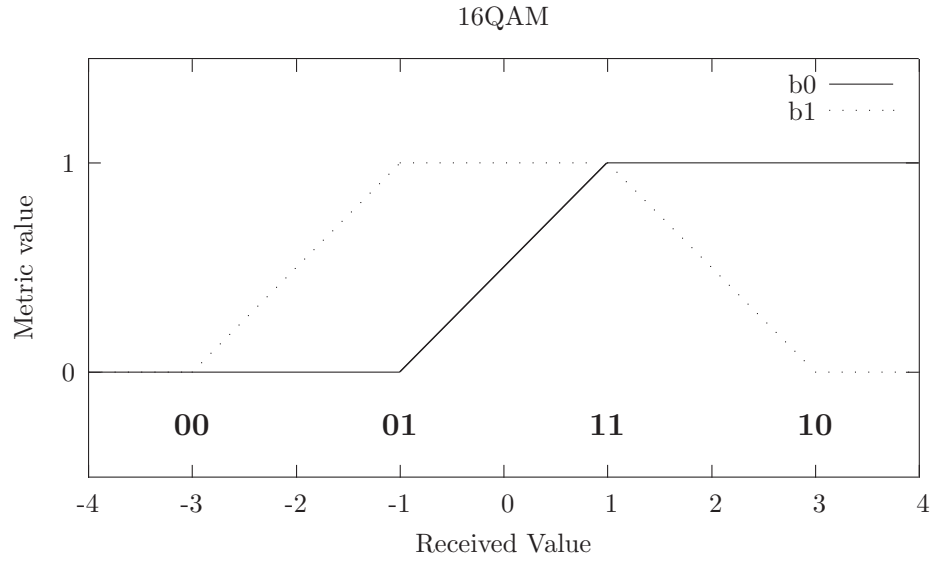

Figure 2.1: The metric values of Soft-demap for 16QAM.

2.3.2 Bit Metrics Recursively Generated from Other First-bit Metric

In 2001, Tosato and Bisaglia [5] proposed and examined a simplified soft-output demapper for binary interleaved COFDM with application to HIPERLAN/2 [10].[6] We interestingly found that their proposed bit metrics $\{g_j^{(m)}(\cdot,\cdot)\}_{1\le j\le m, m\ge 1}$ for 2^{2m}-QAM can be equivalently expressed in terms of our recursive formula as:

$$\begin{aligned} g_1^{(m)}(c,r) &= c(-r) \quad \text{for } m=1,2,3,\ldots \\ g_j^{(\mathrm{m})}(c,r) &= g_{j-1}^{(\mathrm{m}-1)}\big(c,(-1)^j(2^{m-2}u-|r|)\big) \quad \text{for } 2\le j\le m. \end{aligned}$$

The bit metrics $\{g_j^{(m)}(\cdot,\cdot)\}_{1\le j\le m,\ m\ge 1}$ are actually simplified from the bit metrics $\{\bar{g}_j^{(m)}(\cdot,\cdot)\}_{1\le j\le m,\ m\ge 1}$ derived from the bit-based log-likelihood ratio (LLR) decision [5]. Note that the above formula are different from our approach on the initial values. In our approach, instead of being

[6] In fact, their simplified soft-output demapper has appeared in a book published in 1997 [7]. In the book, the soft-output demapper is heuristically obtained through a direct derivation, as opposed to the simplified-from-LLR-decision approach taken by Tosato and Bisaglia.

a constant for all levels of modulations, the initial value $g_1^{(m)}(c,r)$ is related to m, which is determined by the level of modulation. For example, our systematic recursive formula are with initial conditions:

$$\begin{aligned}
\bar{g}_1^{(1)}(c,r) &= c \cdot \frac{1}{2}\left(2|r|\right) \cdot \mathrm{sgn}(-r) \\
\bar{g}_1^{(2)}(c,r) &= c \cdot \frac{1}{2}\left(|r-2| + 2|r| + |r+2| - 4\right) \cdot \mathrm{sgn}(-r) \\
\bar{g}_1^{(3)}(c,r) &= c \cdot \frac{1}{2}\left(|r-6| + |r-4| + |r-2| + 2|r| + |r+2| + |r+4| + |r+6| - 24\right) \cdot \mathrm{sgn}(-r) \\
&\vdots
\end{aligned}$$

This suggests that by varying the first-bit metric, variants of bit-decomposed metrics can be resulted through the recursive formula we established.

As anticipated, with $f_1^{(m)} = g_1^{(m)}$ for $m = 1, 2$, our bit decomposed metric coincides with that proposed in [5] for 16QAM, but is different for 64QAM and 256QAM modulations. In Fig. 2.2, we compare the mapping metric value for 16QAM of our approach named Soft-proposed and the one given in [5] named Soft-TB. After simplifying the metric of Soft-TB, we can derived the same metric as Soft-proposed. Actually the original metric for 64QAM of Soft-TB is more complex than ours as shown in proposed Fig. 2.3.

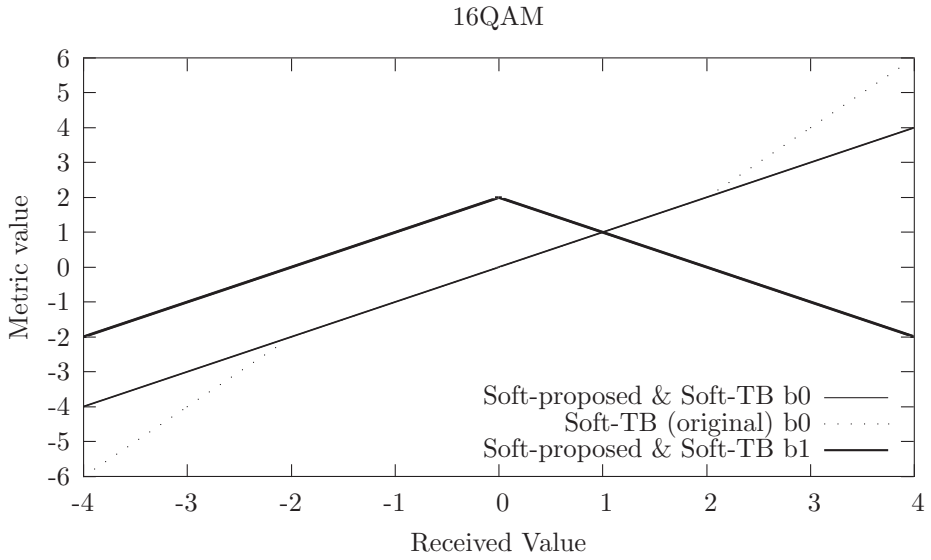

Figure 2.2: The metric values of Soft-TB, simplified Soft-TB, and Soft-proposed for 16QAM.

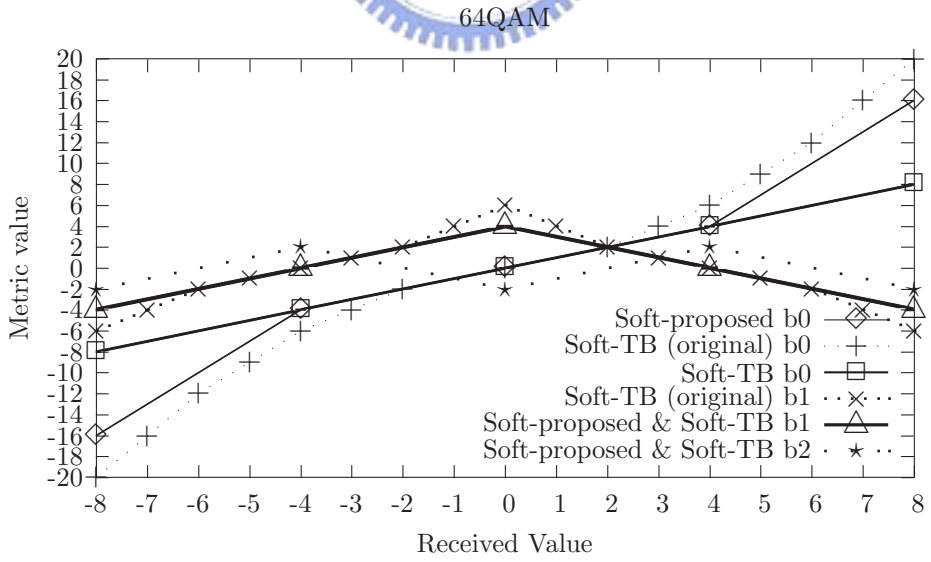

Figure 2.3: The metric values of Soft-TB, simplified Soft-TB, and Soft-proposed for 64QAM.

Chapter 3

Performance Evaluation over the AWGN Channel and the Rayleigh Flat Fading Channel

3.1 Simulation Results for the AWGN Channel

Fig. 3.1 to Fig. 3.3 summarizes the simulated performances under the AWGN channel for *symbol-based ML decision in* (2.1), the *proposed bit-decomposed metrics*, the *soft-demapping in section 2.3.1*, the *simplified bit metrics in chapter 2.3.2* and the straightforward *hard-decision decoding system*. They are respectively abbreviated as Symbol-ML, Soft-proposed, Soft-demap, Soft-TB and Hard in all subsequent figures. From these figures, we observed that at BER = 10^{-5} and under BPSK, QPSK modulation, Soft-demap has 2.0 dB gain over Hard; Soft-proposed (equivalently, Soft-TB) has 2.3 dB gain over Hard, but is 0.12 dB inferior to the ideal Symbol-ML. At the same rate under 16QAM modulation, Soft-demap has 2.3 dB gain over Hard; Soft-proposed (equivalently, Soft-TB) has 3.0 dB gain over Hard, but is 0.7 dB inferior to the ideal Symbol-ML. At the same BER, the superiority of Soft-proposed and Soft-TB over Hard is extended to 3.9 dB for 64QAM, where Soft-demap only provides 2.9 dB gain over Hard. Note that although Soft-proposed and Soft-TB use different bit metrics under 64QAM modulation, they have comparable performance. More advantage

can be obtained under 256QAM, where the gain of Soft-proposed and Soft-TB over Hard is enlarged to 5.1 dB, yet the gain of Soft-demap over Hard remains around 3.0 dB. Similarly, under 1024QAM, the gain of Soft-proposed and Soft-TB over hard is more than 6.3 db, yet the gain of Soft-demap over hard still around 3.4 db. This indicates that the intuitive Soft-demap can only provide limited improvement over Hard. Even though Soft-TB has similar performance to the proposed bit-decomposed metrics on the AWGN channels, the superiority of the latter over the former on the fading channels will be demonstrated in the next section.

3.2 Simulation Results for Rayleigh Flat Fading Channel

In section 2.2, we obtained a recursive bit-decomposed metric formula through the approximation of symbol-based Euclidean metric under the AWGN channel. In this section, we want to adapt our recursive bit-decomposed metric formula for Rayleigh flat fading channel as shown in Fig. 3.4 . Assume that the M-ary symbol transmission suffers Rayleigh flat fading with $\alpha_1, \alpha_2, \alpha_3, \ldots, \alpha_K$, and with single-sided noise power per hertz N_0. The received vector $\boldsymbol{r}$ then becomes:

$$r_i = \alpha_i * s_i + n_i$$

for $1 \leq i \leq K$. For flat fading Rayleigh channel, the maximum-likelihood decision upon the

receipt of $\boldsymbol{r}$ is given by:

$$\begin{aligned} d_{ML}(\boldsymbol{r}) &= \arg\max_{\boldsymbol{s}\in\mathcal{S}} \Pr\left\{r_1,\ldots,r_K \,|\alpha_1 * s_1,\ldots,\alpha_K * s_K\right\} \\ &= \arg\max_{\boldsymbol{s}\in\mathcal{S}} \frac{1}{(\pi N_0)^{K/2}} \exp\left\{-\sum_{i=1}^{K}\frac{(r_i-\alpha_i * s_i)^2}{N_0}\right\} \\ &= \arg\min_{\boldsymbol{s}\in\mathcal{S}} \sum_{i=1}^{K}(r_i-\alpha_i * s_i)^2, \end{aligned} \tag{3.1}$$

where $\mathcal{S}$ represents the set of all possible mappings from the convolutional codeword in $\mathcal{C}$ to its respective symbol word. The criterion we adopt is the minimization of average square error, namely,

$$\min_{f_1,f_2} E\left[\left(f_1(c,r)+f_2(\bar{c},r)-[r-\alpha * s(c,\bar{c})]^2\right)^2\right]. \tag{3.2}$$

Without loss of generality, we can re-write f_1 and f_2 as:

$$f_1(c,r)=\frac{1}{2}r^2+\alpha_i * a_{1,c,r}r+\alpha_i^2 * b_{1,c,r} \quad \text{and} \quad f_2(\bar{c},r)=\frac{1}{2}r^2+\alpha_i * a_{2,\bar{c},r}r+\alpha_i^2 * b_{2,\bar{c},r}$$

What we need to adapt is the coefficient α. Specifically, for M-ary amplitude modulation (or equivalently, M^2QAM) with amplitude spacing u, the former recursive bit-metric decomposition formulas then become,

$$\begin{cases} f_1^{(\mathrm{m})}(c,r) &= c\cdot\mathrm{sgn}(-r)\left(\sum_{i=-(m-2)}^{m-2}(|\alpha * r+\alpha^2 * 2ui|-|\alpha^2 * 2ui|)\right) \\ f_j^{(\mathrm{m})}(c,r) &= f_{j-1}^{(\mathrm{m}-1)}\left(c,(-1)^j\left[2^{m-2}u-|r|\right]\right) \text{ for } 2\le j\le m, \end{cases}$$

where $m=\log_2(M)\ge 2$ and $f_1^{(1)}(c,r)=-\alpha * cr$. Note that m is respectively 2, 3 and 4 for 16QAM, 64QAM and 256QAM.

As mentioned before, our recursive formula can also be applied to the bit reliability proposed by Tosato and Bisaglia with different initial function [5]. We subsequently compare the performances of our Soft-proposed metric, Soft-TB, Soft-demap and Hard. As anticipated, Soft-proposed and Soft-TB perform better than Soft-demap, which in turn is superior to Hard.

The superiority of our proposed bit-decomposed metric over Soft-TB becomes a little more apparent under fading environment. For example in 1024QAM at BER=10^{-5}, Soft-proposed gains 0.5 dB over Soft-TB (cf. Fig. 3.7). Also, we can observe from Fig. 3.5 to Fig. 3.7 that in a fading environment, the performance superiority of Soft-proposed and Soft-TB over Hard respectively extends to 7.7 dB, 8.1 dB, 8.5 dB and 9.1 dB under 16QAM, 64QAM, 256QAM and 1024QAM modulations at BER=10^{-5}.

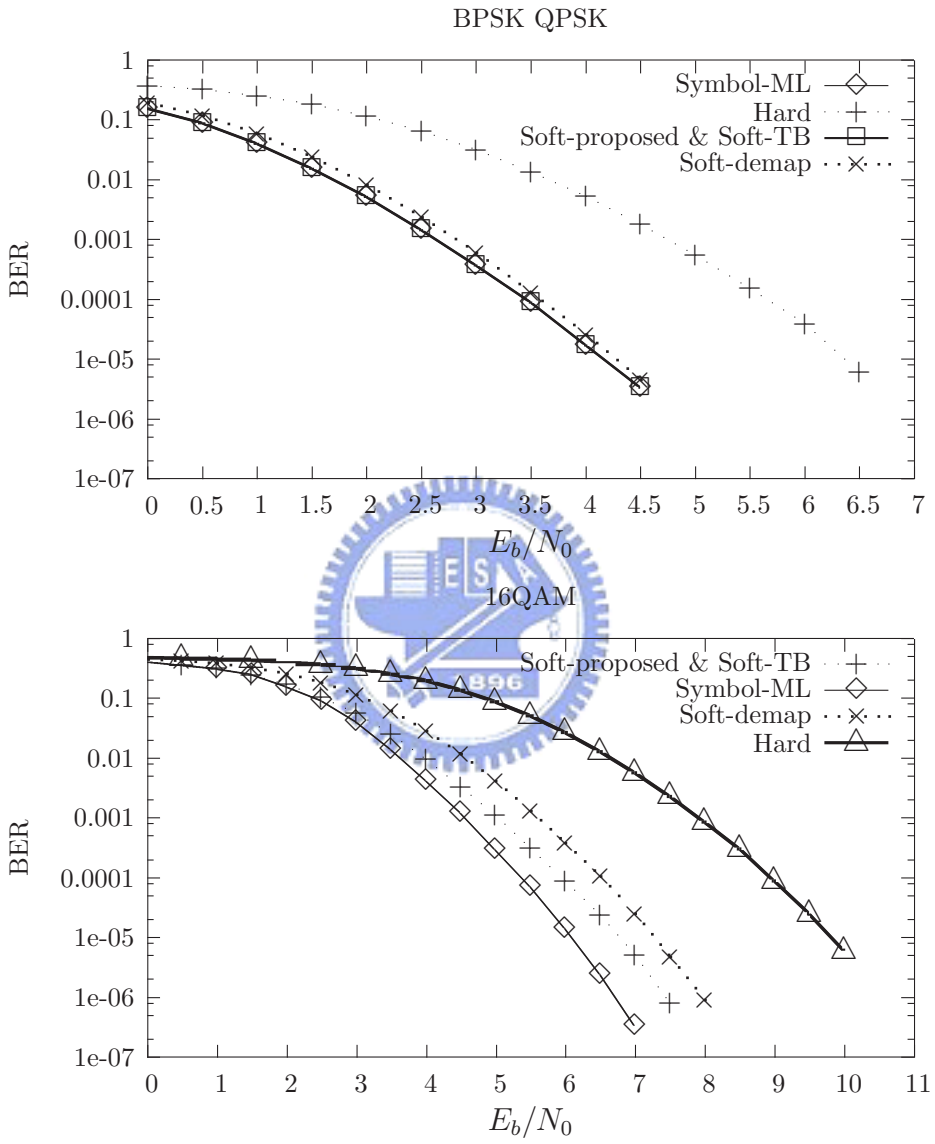

Figure 3.1: System performances under the AWGN channel for BPSK, QPSK, and 16QAM modulations.

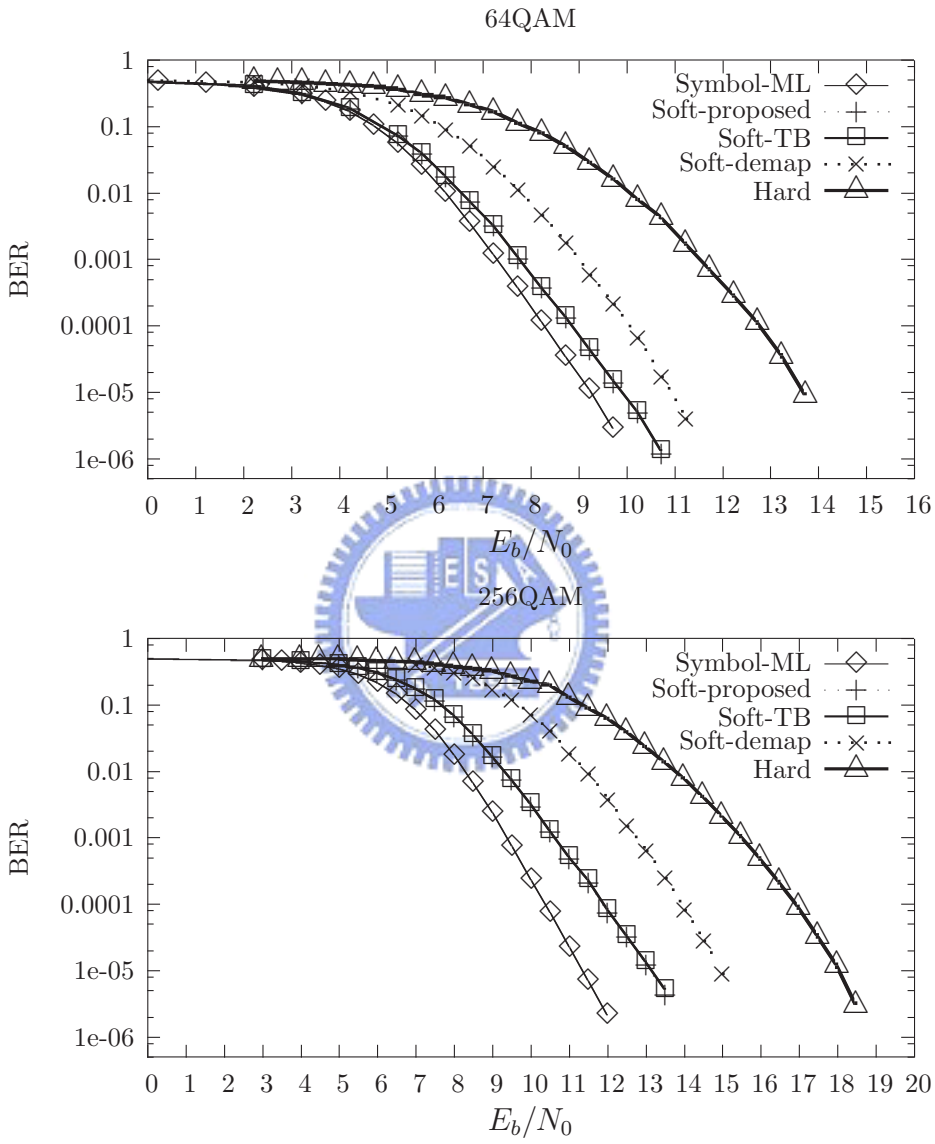

Figure 3.2: System performances under the AWGN channel for 64QAM and 256QAM modulations.

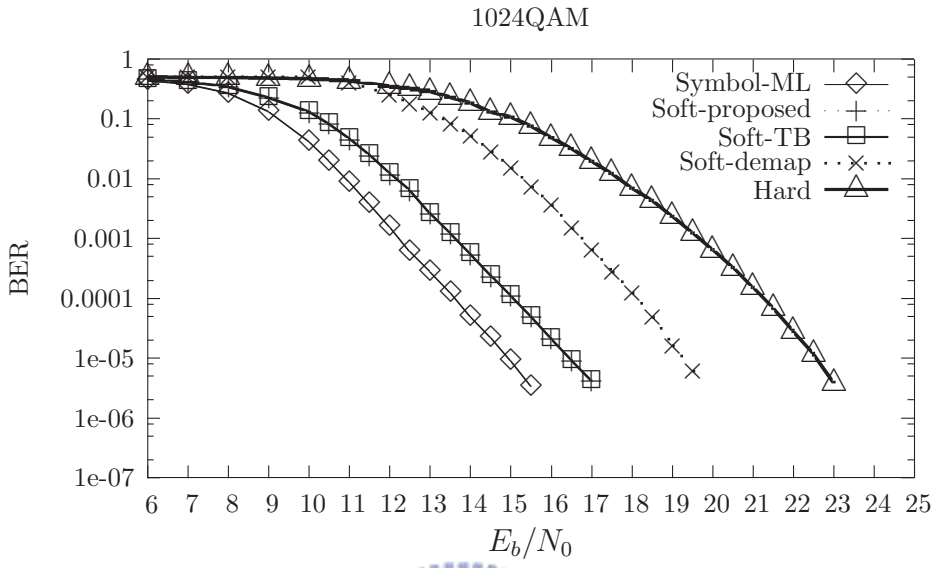

Figure 3.3: System performances under the AWGN channel for 1024QAM modulation.

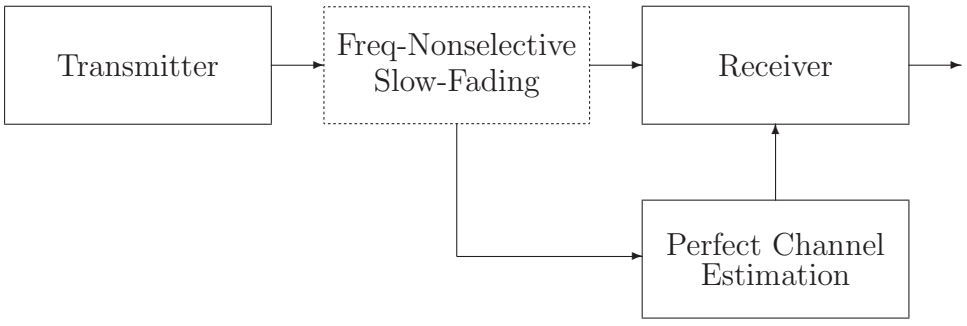

Figure 3.4: Block diagram of a frequency-nonselective slowly fading channel with perfect channel knowledge, which can be described as $r = \alpha \cdot s + n$, where s and r are respectively channel input and output symbols, α is Raileigh distributed channel attenuation that can be perfectly estimated, and n denotes the additive white Gaussian noise.

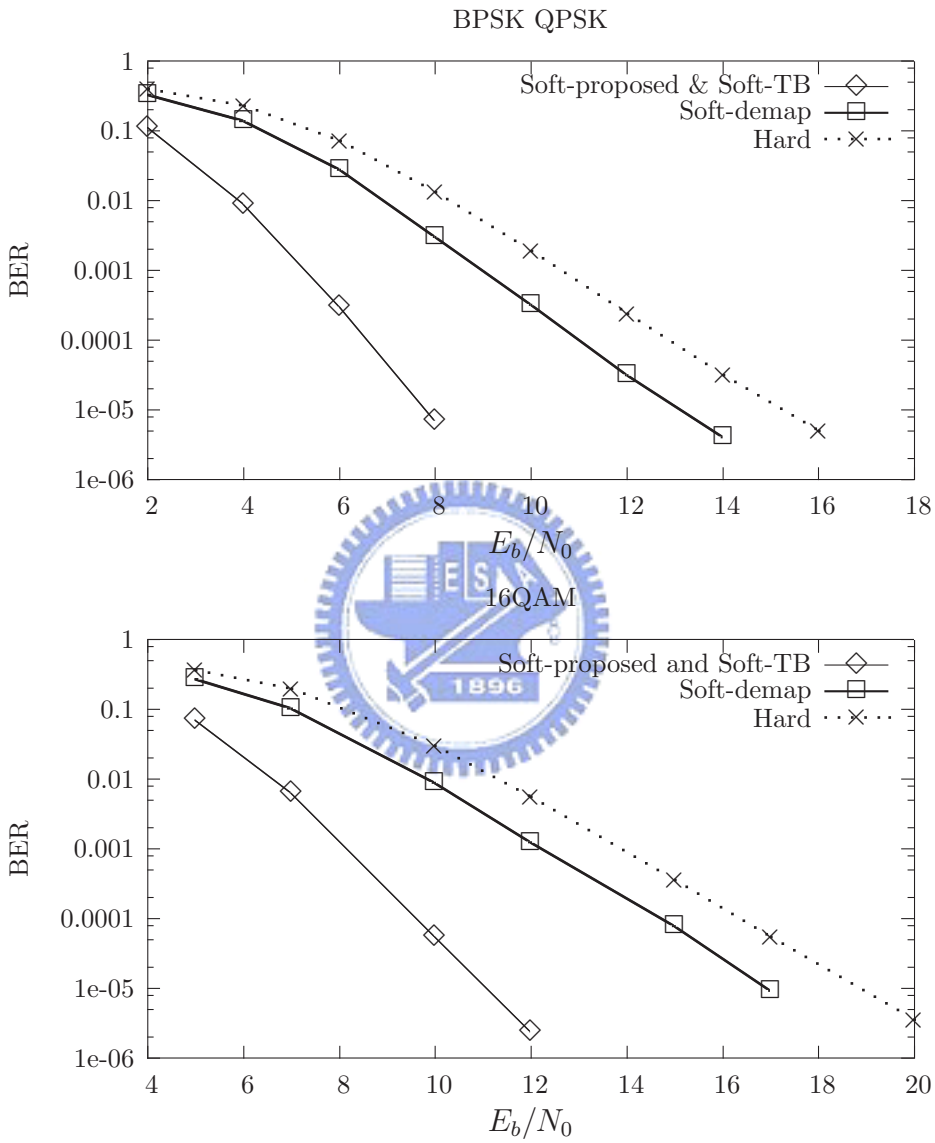

Figure 3.5: System performances under the Rayleigh flat fading channel for BPSK, QPSK, and 16QAM modulations.

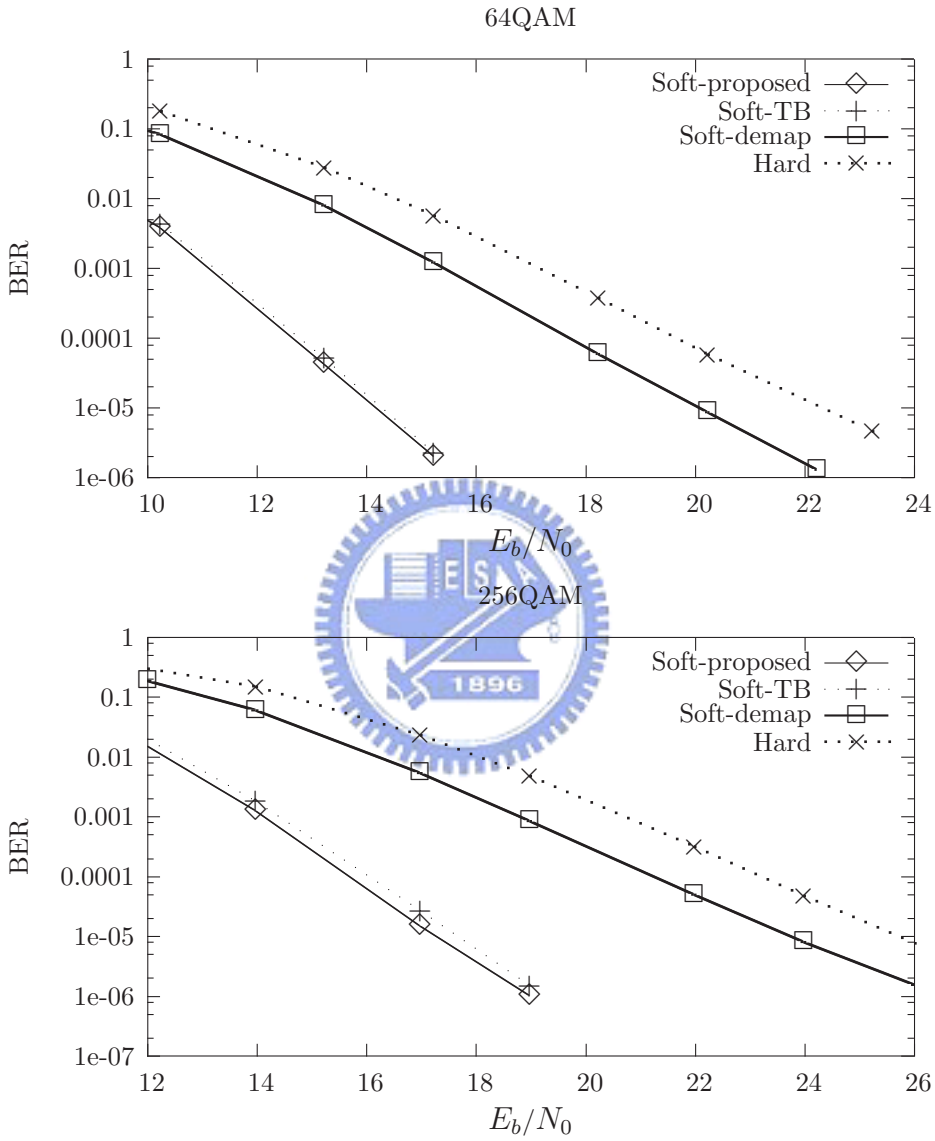

Figure 3.6: System performances under the Rayleigh flat fading channel for 64QAM and 256QAM modulations.

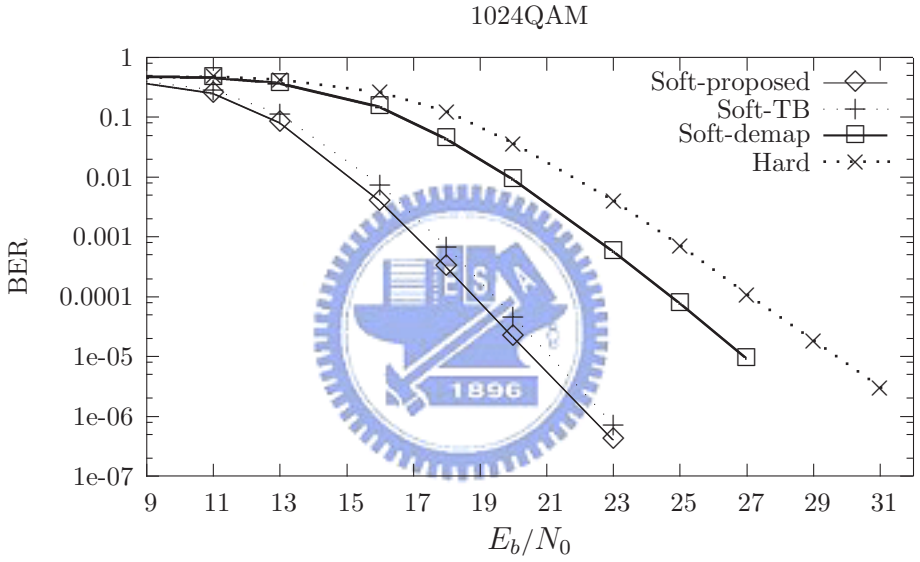

Figure 3.7: System performances under the Rayleigh flat fading channel for 1024QAM modulation.

Chapter 4

Robustness Against Imperfect System Parameters

4.1 Effect of Quantization

Figures 4.1, 4.3, 4.5, 4.7 illustrate the performance impact of uniform quantization under the AWGN channel. Similar to [1, 2], the received scalar is first multiplied by the appropriate normalization factor in order to make the average QAM symbol power equal to unity, and then is quantized with the step size equal to $2 \times u$ divided by the number of quantization levels, where $u = 2$ is the amplitude spacing for QAM signals. Another intuitional quantization is employed on Soft-demap since Soft-demap has imposed a quantization on the metric it uses (cf. Appendix B).

For example, for 8-level (3 bit) quantization in 16QAM as shown in Fig. B.2, it only quantizes 3 interval values. We observed from these figures that, under 16QAM modulation, adopting 32-level quantizer to Soft-proposed and Soft-TB only yields 0.13 dB performance loss at BER $= 10^{-5}$. The performance loss due to 16-level quantization is around 0.11 dB at BER $= 10^{-5}$ for Soft-demap. Under 64QAM modulation and BER $= 10^{-5}$, the performance loss can be reduced to 0.07 dB for Soft-proposed/Soft-TB by taking 64-level quantization. The performance loss due to 16-level quantization is around 0.13 dB at BER $= 10^{-5}$ for

Soft-demap.

Under 256QAM modulation and the same BER, the performance loss of 64-level quantization is restricted within 0.20 dB for Soft-proposed and Soft-TB. The performance loss due to 16-level quantization is around 0.15 dB for Soft-demap. At the same BER under 1024QAM modulation, the performance loss of 128-level quantization is around 0.20 dB for Soft-proposed and Soft-TB. The performance loss due to 16-level quantization is about 0.17 dB for Soft-demap. These figures conclude that for 16QAM, 64QAM, 256QAM and 1024QAM modulations, it is sufficient to take 5-bit, 6-bit, 6-bit and 7-bit quantizations for the proposed bit-decomposed metrics to perform close to the system without performing quantization. Same conclusion can be made on Tosato/Bisaglia's bit metrics and for Soft-demap approach in Section 2.3.1.

Figs. 4.2, 4.4, 4.6, 4.8 illustrate the performance impact of quantization under the Rayleigh flat fading channel. We adjust quantization of Soft-proposed and Soft-TB to fit the new assumed channel. By assuming known fading-coefficient α, we divide the received value with the known-fading factor and then apply the adopted uniform quantizer of Lloyd-Max algorithm to the metric. When BER = 10^{-5} under 16QAM modulation, adopting 32-level quantizer to Soft-proposed and Soft-TB only yields 0.11 dB performance loss. The performance loss due to 16-level quantization is around 0.08 dB for Soft-demap. Under 64QAM modulation and BER = 10^{-5}, the performance loss is still 0.11 dB for Soft-proposed/Soft-TB by taking 64-level quantization. The performance loss due to 16-level quantization is around 0.1 dB at BER = 10^{-5} for Soft-demap. Under 256QAM modulation and the same BER, the performance loss of 64-level quantization is restricted within 0.27 dB and 0.35 dB respectively for Soft-proposed and Soft-TB. The performance loss due to 16-level quantization is around 0.12 dB for Soft-demap. At the same BER under 1024QAM modulation, the performance loss of 128-level quantization is around 0.16 dB and 0.34 dB respectively

for Soft-proposed and Soft-TB. The performance loss due to 16-level quantization is about 0.14 dB for Soft-demap. We then proceed to examine the robustness of these quantized bit metrics in terms of the above quantization levels against gain mismatch and phase noise in later sections.

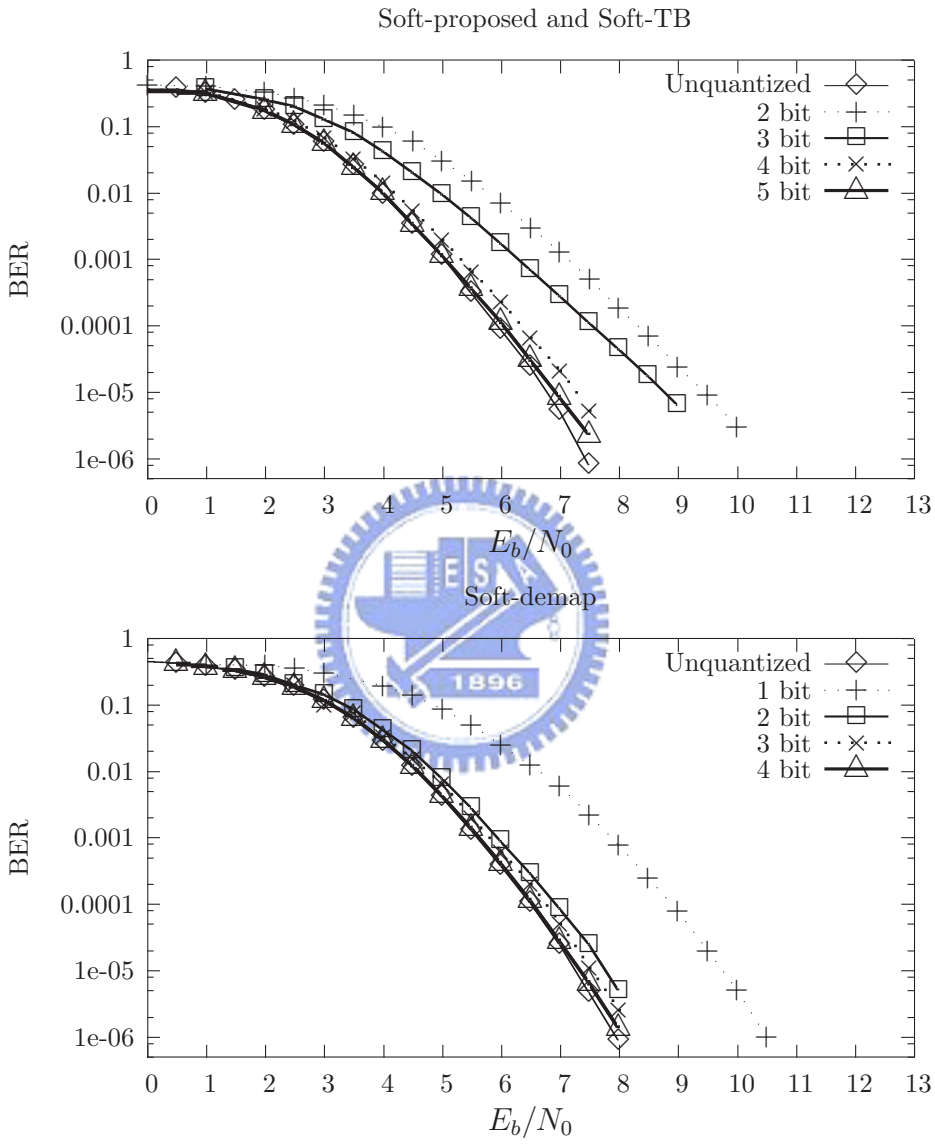

Figure 4.1: Performance impact of quantization for 16QAM modulation under the AWGN channel .

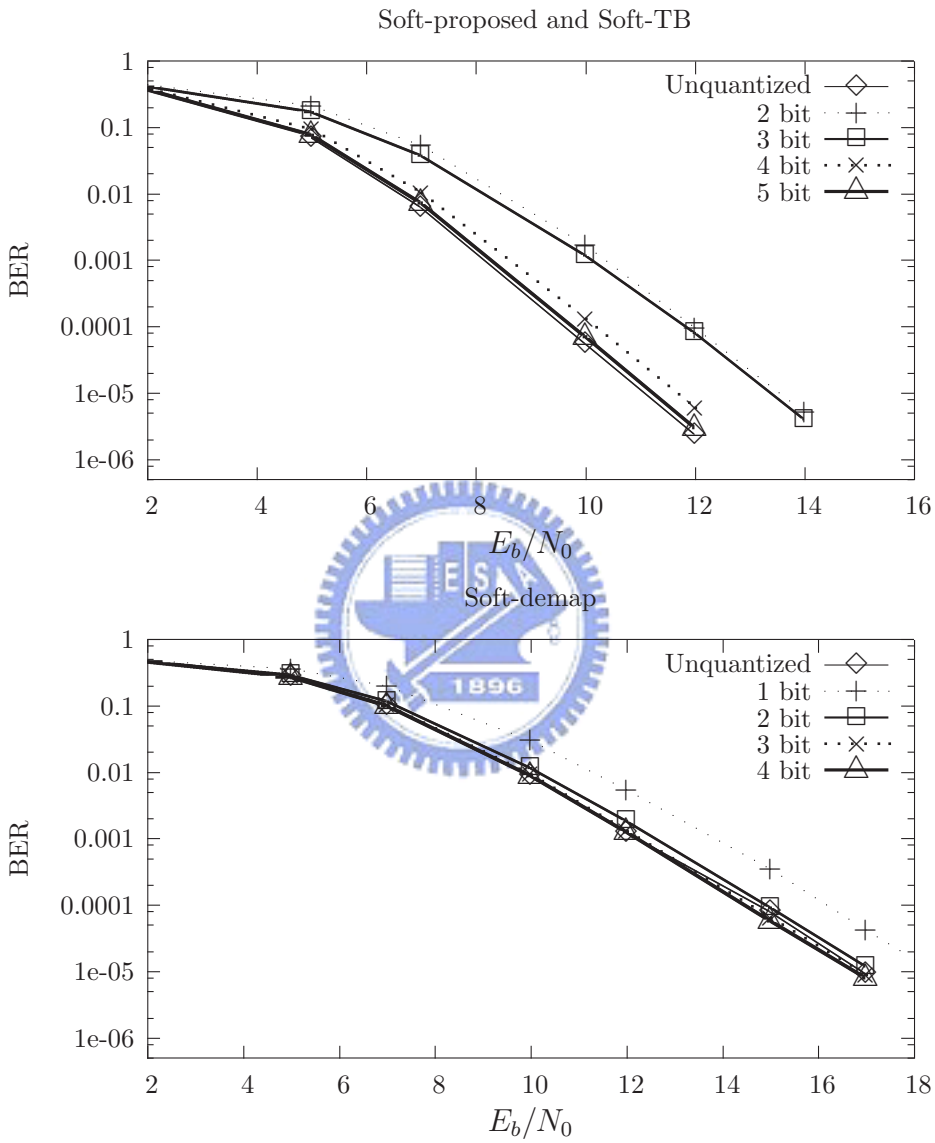

Figure 4.2: Performance impact of quantization for 16QAM modulation under the Rayleigh flat fading channel.

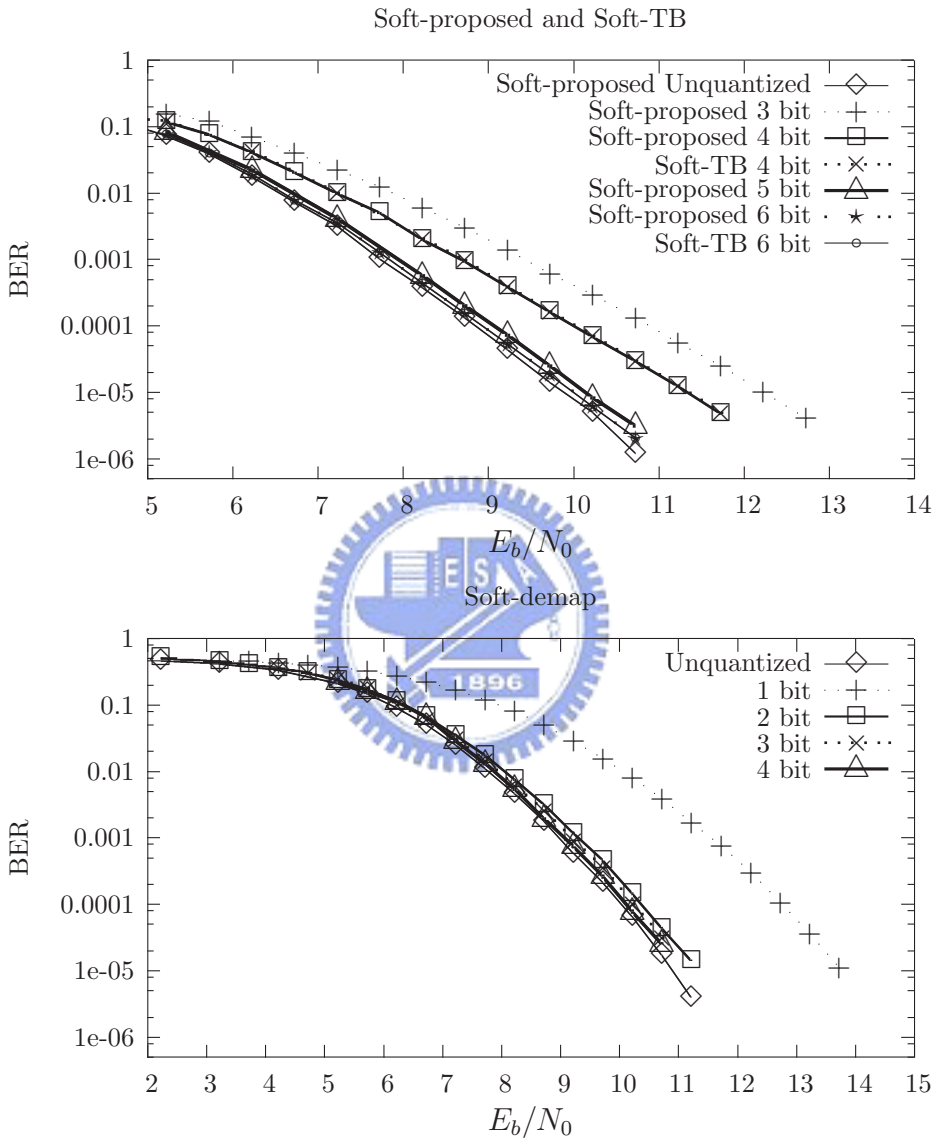

Figure 4.3: Performance impact of quantization for 64QAM modulation under the AWGN channel .

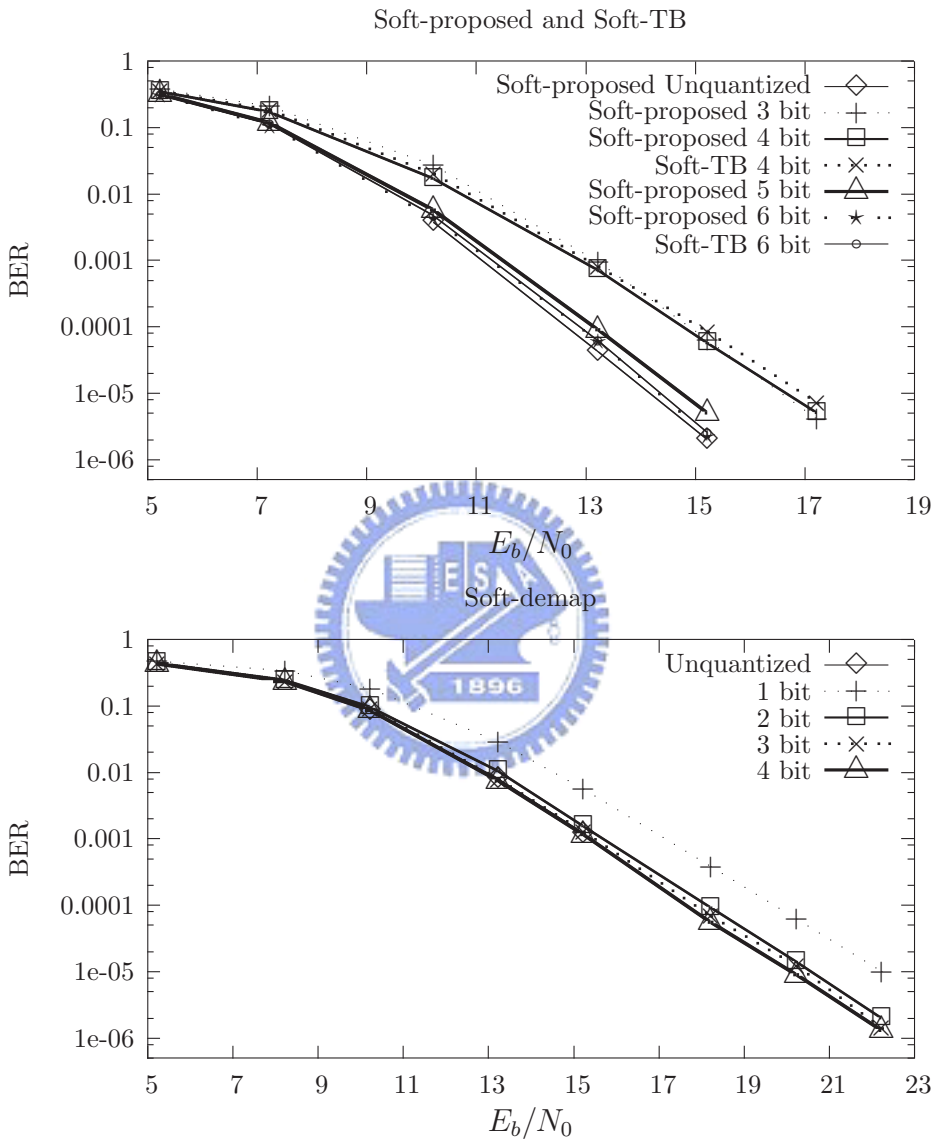

Figure 4.4: Performance impact of quantization for 64QAM modulation under the Rayleigh flat fading channel.

4.2 Effect of Imperfect Automatic Gain Control

Coded systems that quantize the matched filter output to more than two levels for use of subsequent digital manipulation require an analog-to-digital converter, whose level thresholds should depend on a correct measurement of the noise variance. Usually, the level-setting is effectively controlled by the automatic gain control (AGC) circuitry in a modem. In this section, we are interested in the sensitivity of decoder performance to an inaccurate (or drifting) quantized AGC signal.

Our performance comparisons between Soft-proposed, Soft-TB, Soft-demap and Hard are employed at BER=10^{-5}. Due to different BER performances, different E_b/N_0's are accordingly used for each bit-decomposition approach. Specifically, under 16QAM modulation, we use 6.8 dB, 7.5 dB, 9.7 dB for Soft-proposed, Soft-demap and Hard, respectively, to obtain the required BER under the AWGN channel. The taken values of E_b/N_0 under 64QAM modulation are listed in Fig. 4.11 to Fig. 4.13. The step size without AGC drift is taken as $2 \times u$ divided by the number of quantization levels [1, 2] which are employed except Soft-demap because it has its own step-size already. A drift to the above value is then caused by an inaccurate AGC circuitry.

From Fig. 4.9 to Fig. 4.13, we found that the performances of Soft-proposed ,Soft-TB, and Soft-demap are quite insensitive to wide range of variation in AGC gain based on the same step-size. The resultant BER remains between 1.0×10^{-5} and 1.4×10^{-5} over a step-size range of 0.075∼0.175 for 32-level[1] quantized 16QAM signals under the AWGN channel. This allows an AGC gain margin[2] of

$$\frac{|0.075-(0.075+0.175)/2|}{(0.075+0.175)/2}=\frac{|0.175-(0.075+0.175)/2|}{(0.075+0.175)/2}=40\%.$$

[1]As mentioned before, the step size is $2 \times u$ divided by 32 equal to 0.125

[2]When AGC-drift goes up to 60%, the BER increases from 1.0×10^{-5} to 3.1×10^{-5}.

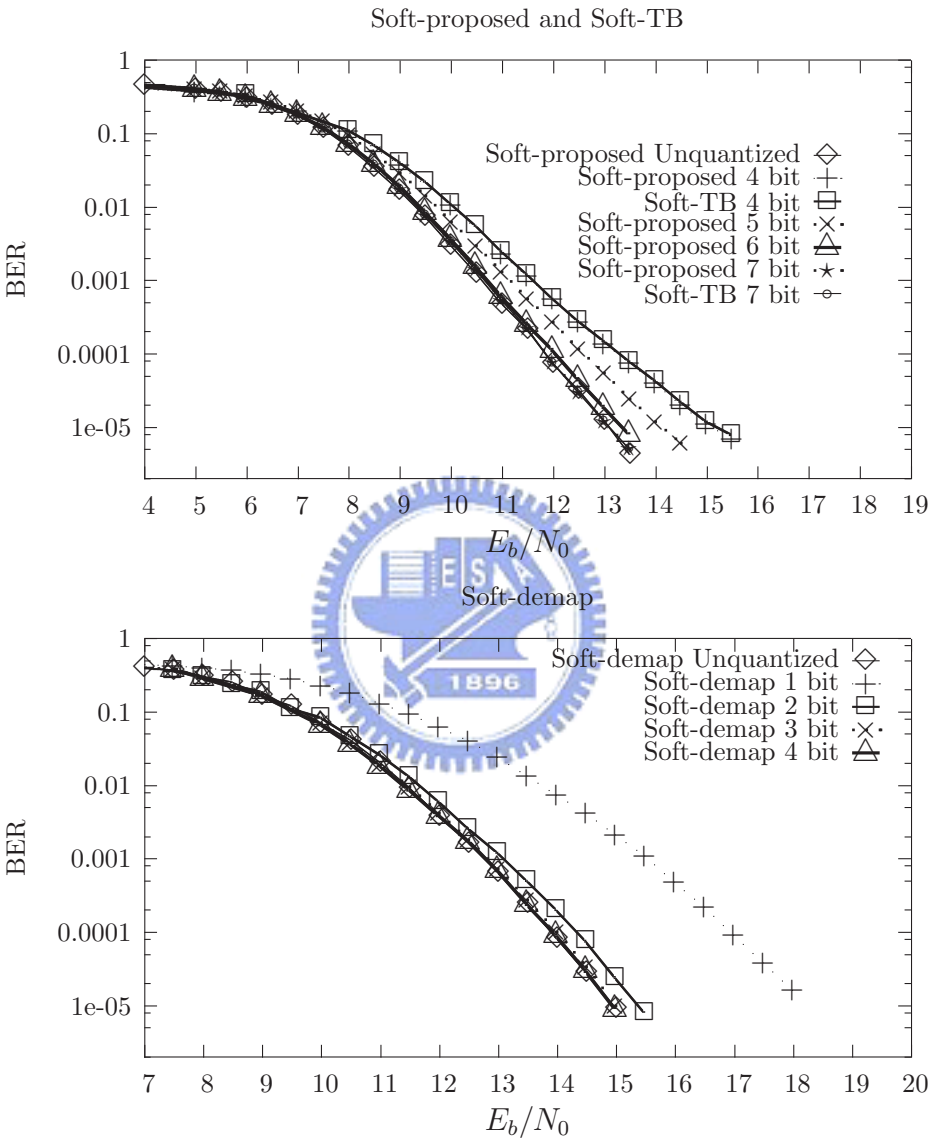

Figure 4.5: Performance impact of quantization for 256QAM modulation under the AWGN channel.

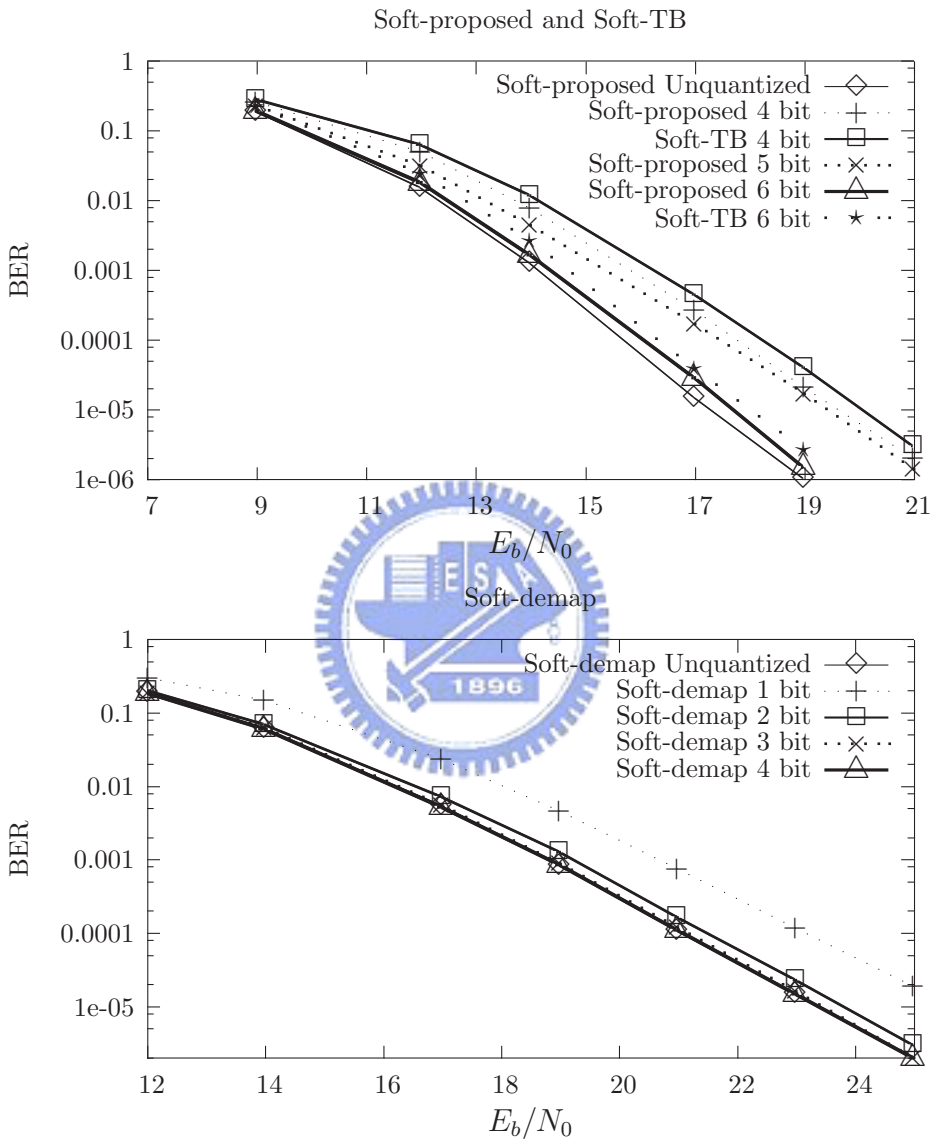

Figure 4.6: Performance impact of quantization for 256QAM modulation under the Rayleigh flat fading channel.

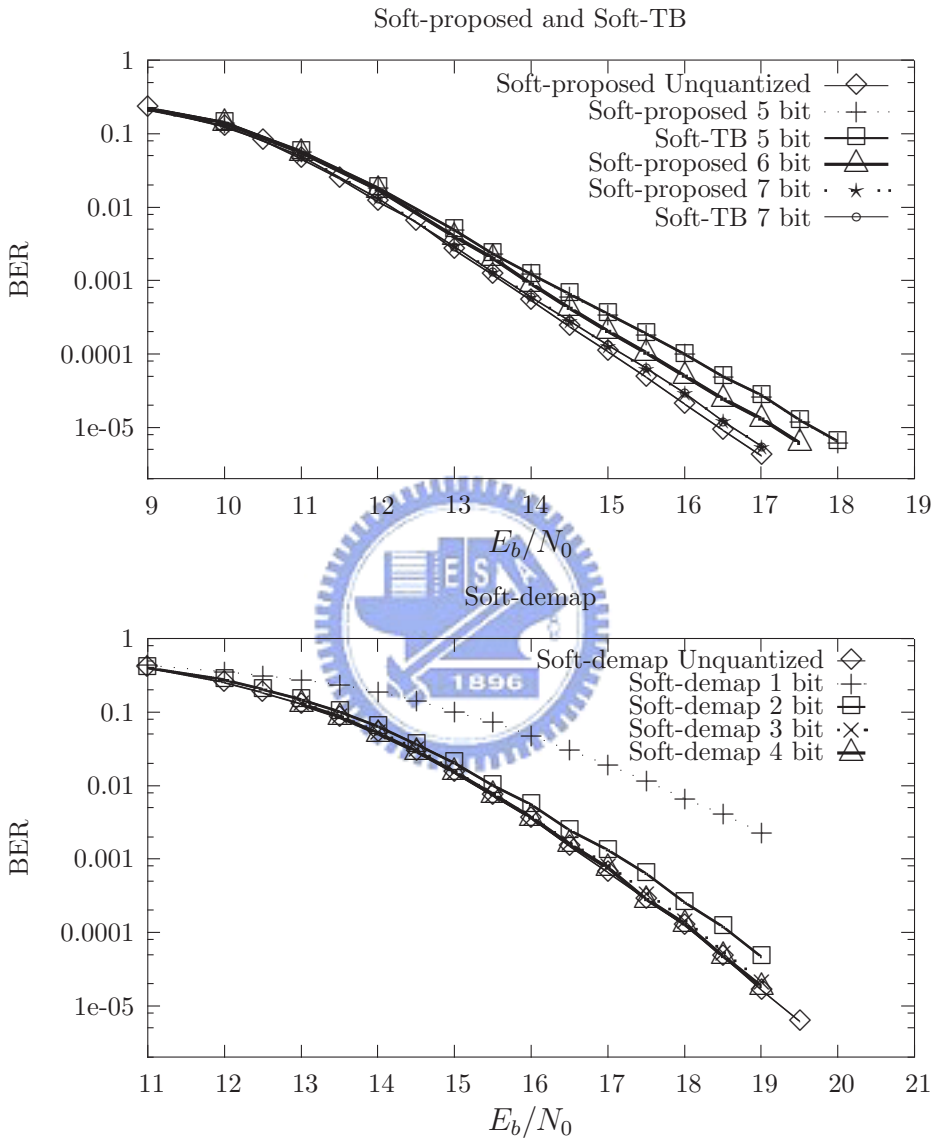

Figure 4.7: Performance impact of quantization for 1024QAM modulation under the AWGN channel .

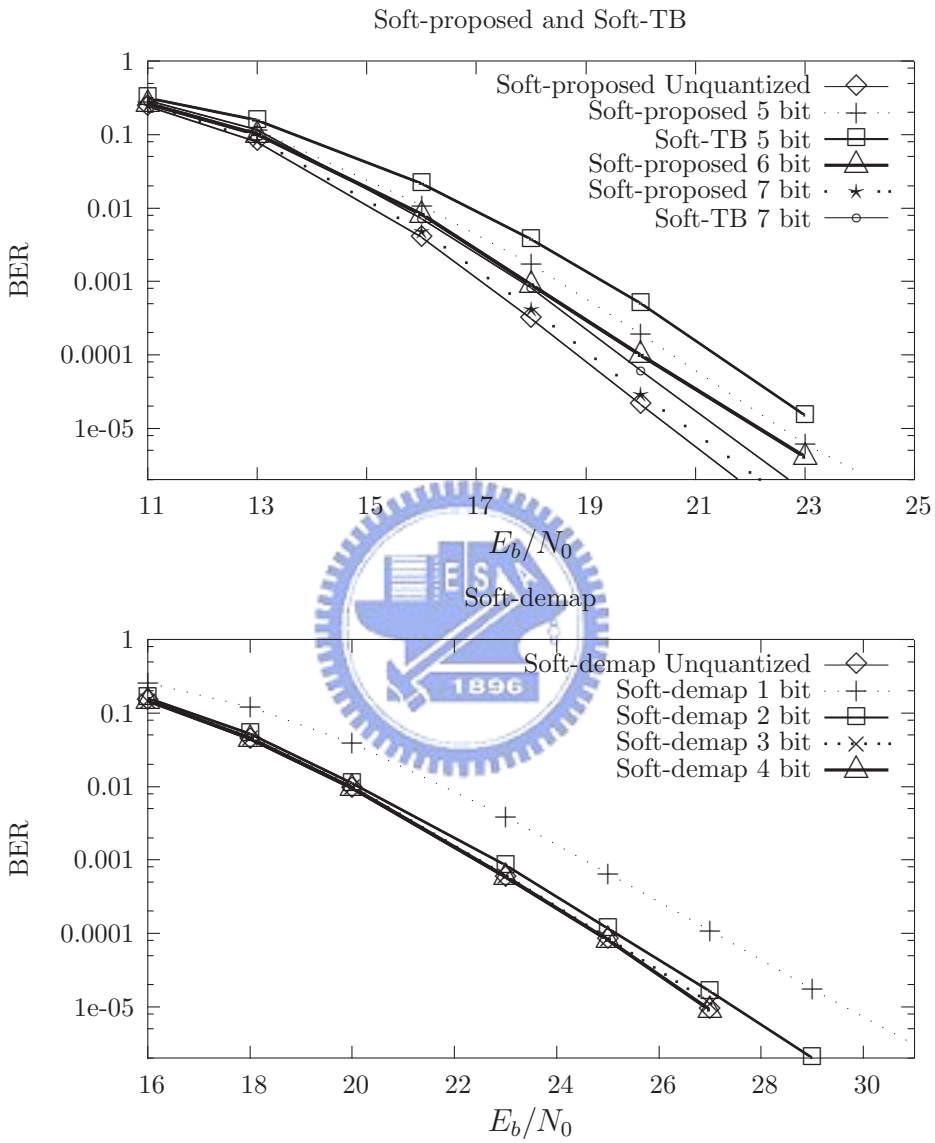

Figure 4.8: Performance impact of quantization for 1024QAM modulation under the Rayleigh flat fading channel.

For 16-level quantized Soft-demap[3] under the AWGN channel, if we allow BER to increase up to 1.8×10^{-5}, the AGC gain margin will be

$$\frac{|0.2 - 0.125|}{0.125} = \frac{|0.05 - 0.125|}{0.125} = 60\%.$$

But for Hard, even if we allow BER to increase up to 1.0×10^{-4}, the AGC gain margin is only

$$\frac{|0.1375 - 0.125|}{0.125} = \frac{|0.1125 - 0.125|}{0.125} = 10\%.$$

A similar calculation for 64-level quantized 64QAM signals under the AWGN channel of Soft-proposed and Soft-TB yields a gain margin[4] of $|0.0375 - 0.0625|$ / $0.0625 = |0.0875 - 0.0625|$ / $0.0625 = 40\%$ for BER ranging from 1.7×10^{-5} to 2.0×10^{-5}. Similarly, if we allow BER ranging from 8×10^{-6} to 1.2×10^{-5} for 16-level quantized Soft-demap yield 60% AGC gain margin and the BER allowance from 1×10^{-5} increasing up to 1×10^{-4} for Hard only leads to 11% AGC gain margin. At the same time we can find that all of these bit-decomposed methods can get better tolerance of AGC drift under the Rayleigh flat fading channel than the AWGN channel. Fig. 4.14 to Fig. 4.16 shows the impact of AGC performances of Soft-proposed, Soft-TB, Soft-demap and Hard for 256QAM modulation under the AWGN and the Rayleigh flat fading channels. For 128-level quantized 256QAM signals under the AWGN channel of Soft-proposed and Soft-TB yields a gain margin of $|0.04375 - 0.03125|$ / $0.03125 = |0.03125 - 0.01875|$ / $0.03125 = 40\%$ for BER ranging from 1.2×10^{-5} to 1.4×10^{-5}. Similarly, if we allow BER ranging from 7×10^{-6} to 1.1×10^{-5} for 16-level quantized Soft-demap yield 50% AGC gain margin and the BER allowance from 1×10^{-5} increasing up to 1×10^{-4} for Hard only leads to 3% AGC gain margin.

[3]See Appendix B, the step size is 2 divided by 16 equal to 0.125

[4]The BERs for step-size 0.0375, 0.0625 and 0.0875 are respectively 2.0×10^{-5}, 1.8×10^{-5} and 1.7×10^{-5}.

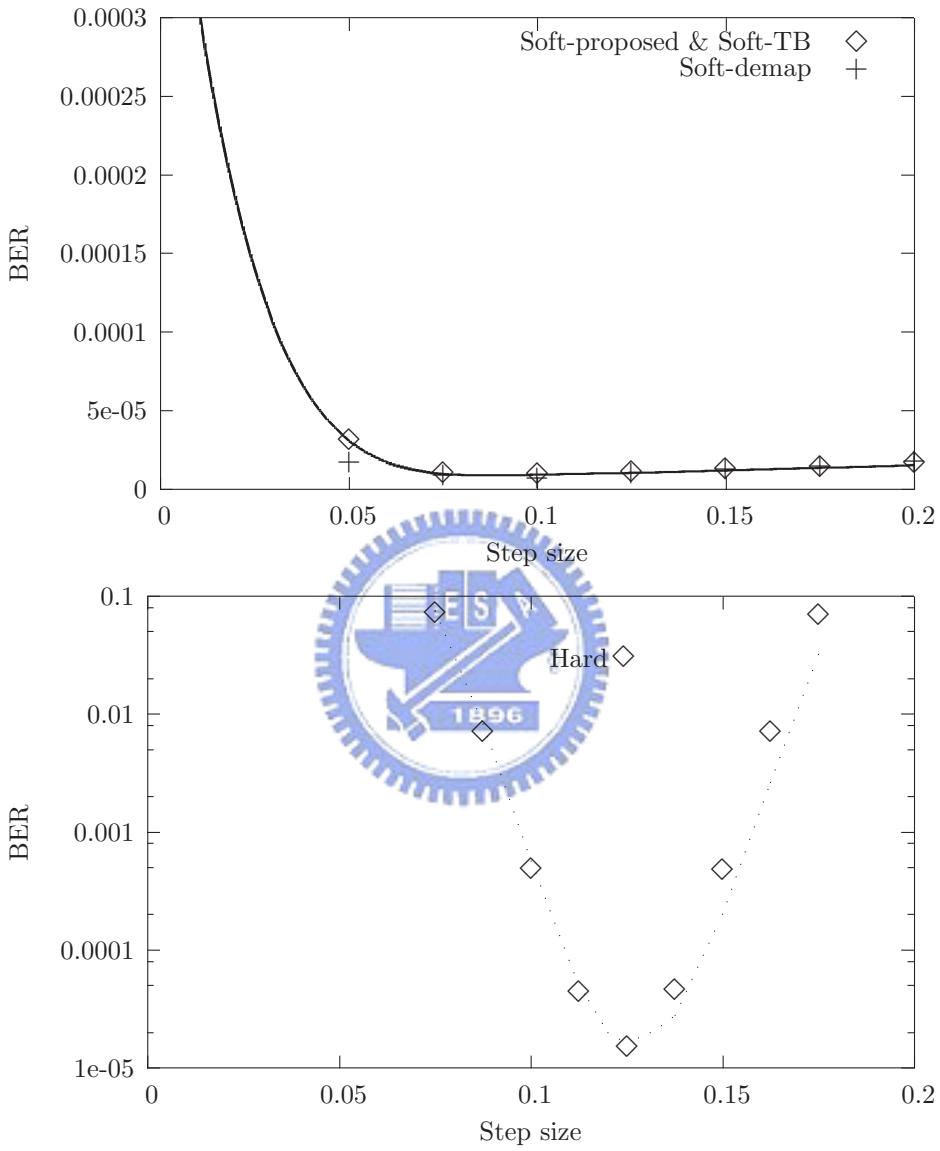

Figure 4.9: Sensitivity to gain-mismatch for 16QAM under the AWGN channel. The taken values of E_b/N_0 for Soft-proposed & Soft-TB, Soft-demap and Hard are respectively 6.8 dB, 7.5 dB and 9.7 dB. The non-drift step-size is 0.125

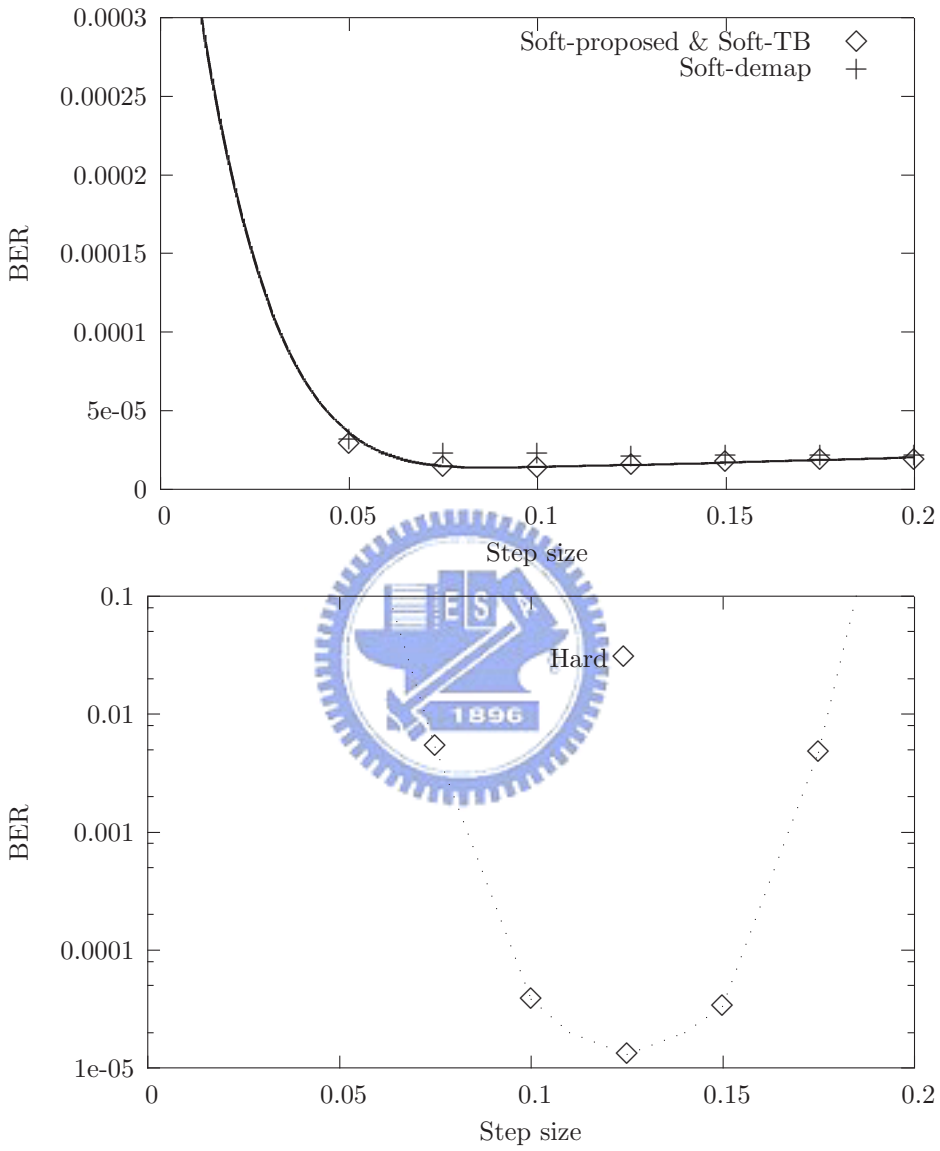

Figure 4.10: Sensitivity to gain-mismatch for 16QAM under the Rayleigh flat fading. The taken values of E_b/N_0 for Soft-proposed & Soft-TB, Soft-demap and Hard are respectively 11.0 dB, 16.0 dB and 18.5 dB. The non-drift step-size is 0.125

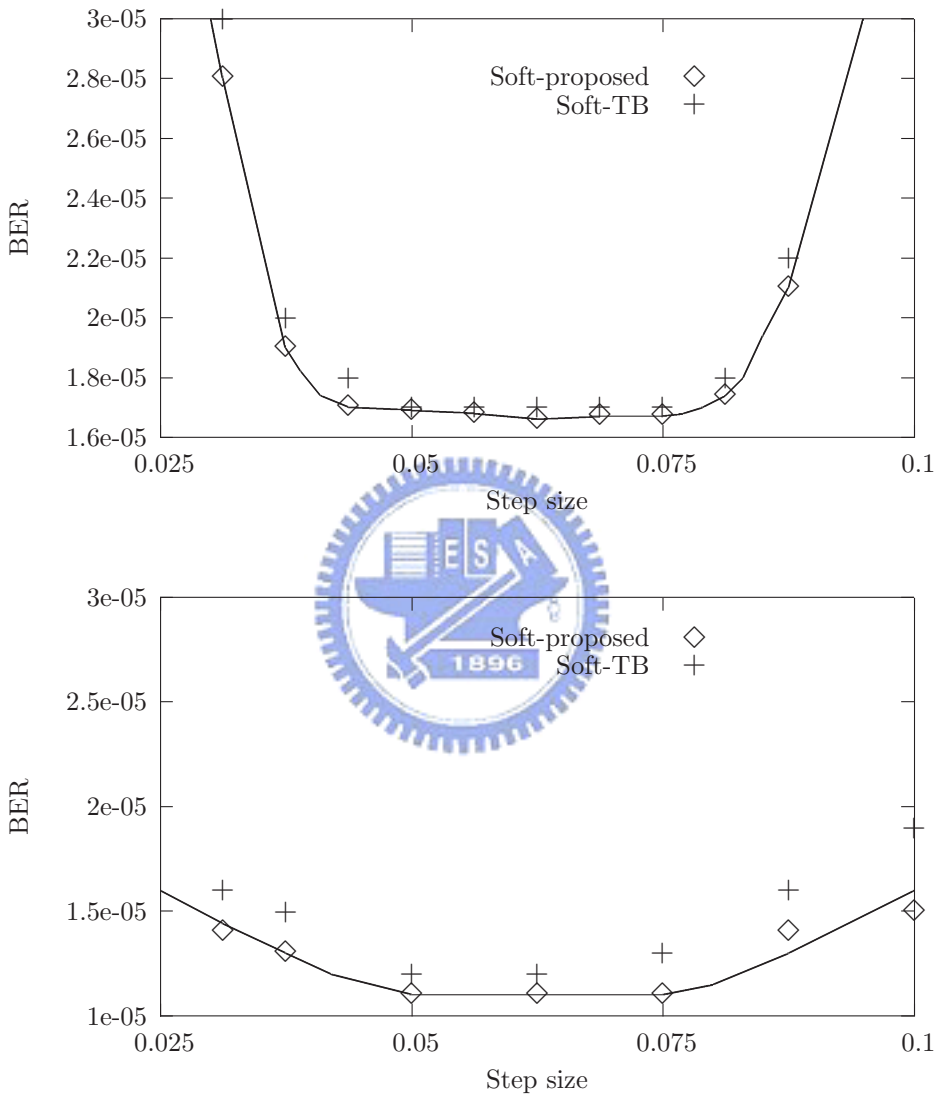

Figure 4.11: Sensitivity to gain-mismatch for 64QAM. The taken values of E_b/N_0 for Soft-proposed & Soft-TB are respectively 9.8 dB and 14.2 dB under the AWGN and the Rayleigh flat fading channels. The non-drift step-size is 0.0625

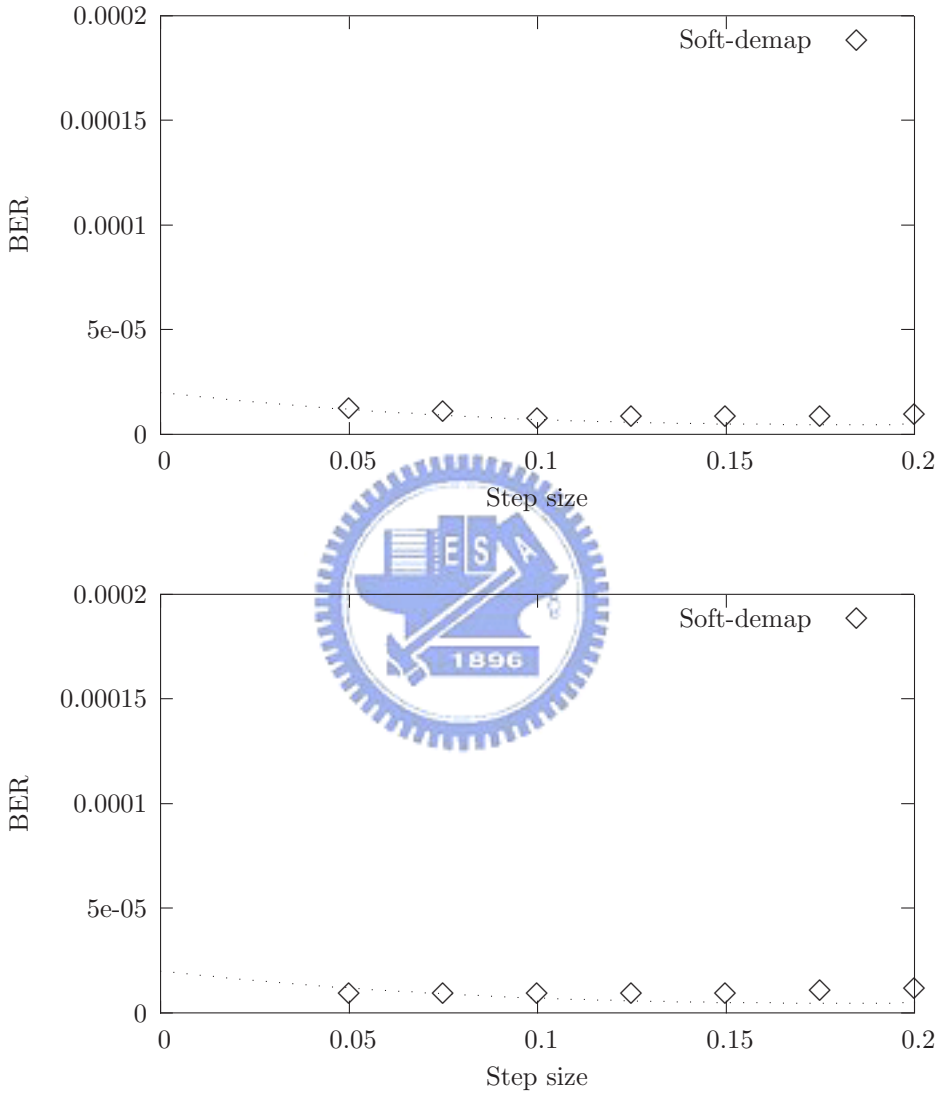

Figure 4.12: Sensitivity to gain-mismatch for 64QAM. The taken values of E_b/N_0 for Soft-demap are respectively 11.1 dB and 20.2 dB under the AWGN and the Rayleigh flat fading channels. The non-drift step-size is 0.125

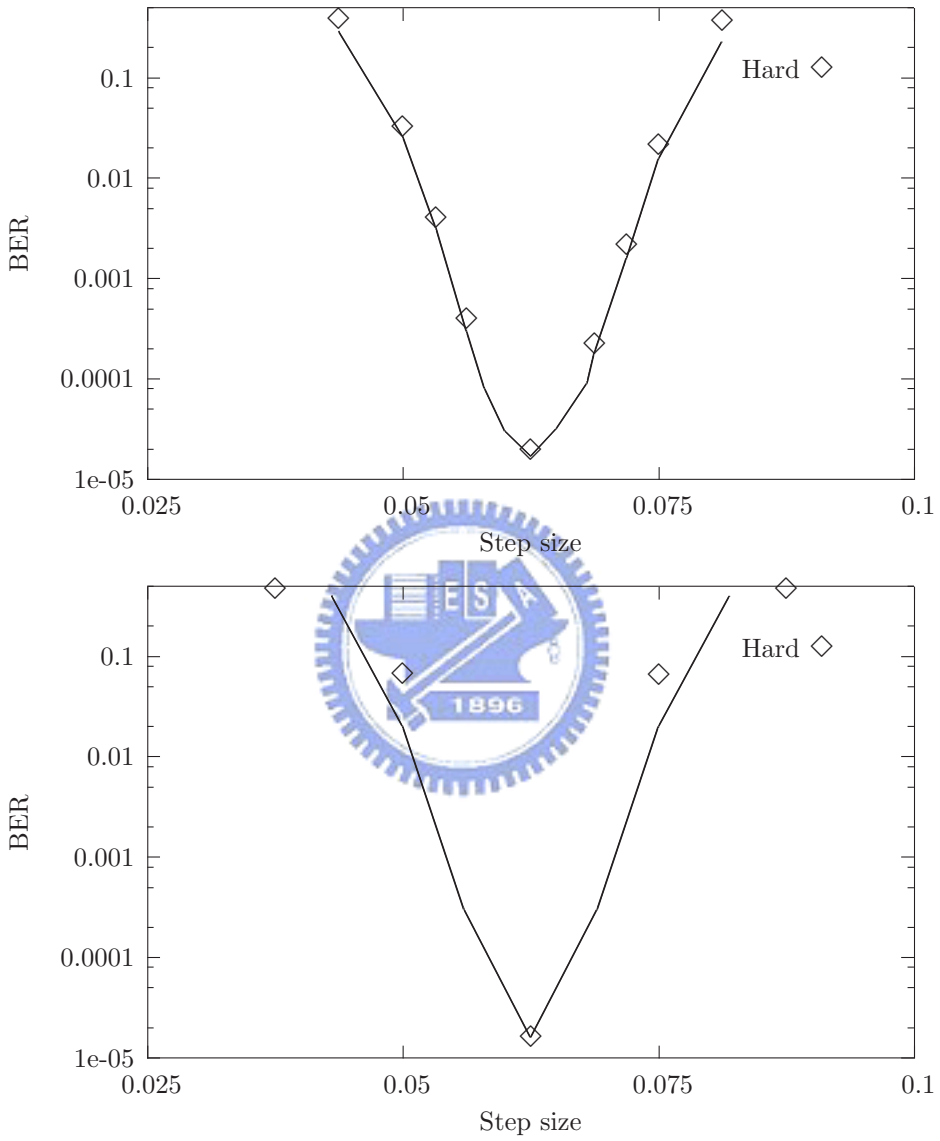

Figure 4.13: Sensitivity to gain-mismatch for 64QAM. The taken values of E_b/N_0 for hard are respectively 13.5 dB and 21.7 dB under the AWGN and the Rayleigh flat fading channels. The non-drift step-size is 0.0625

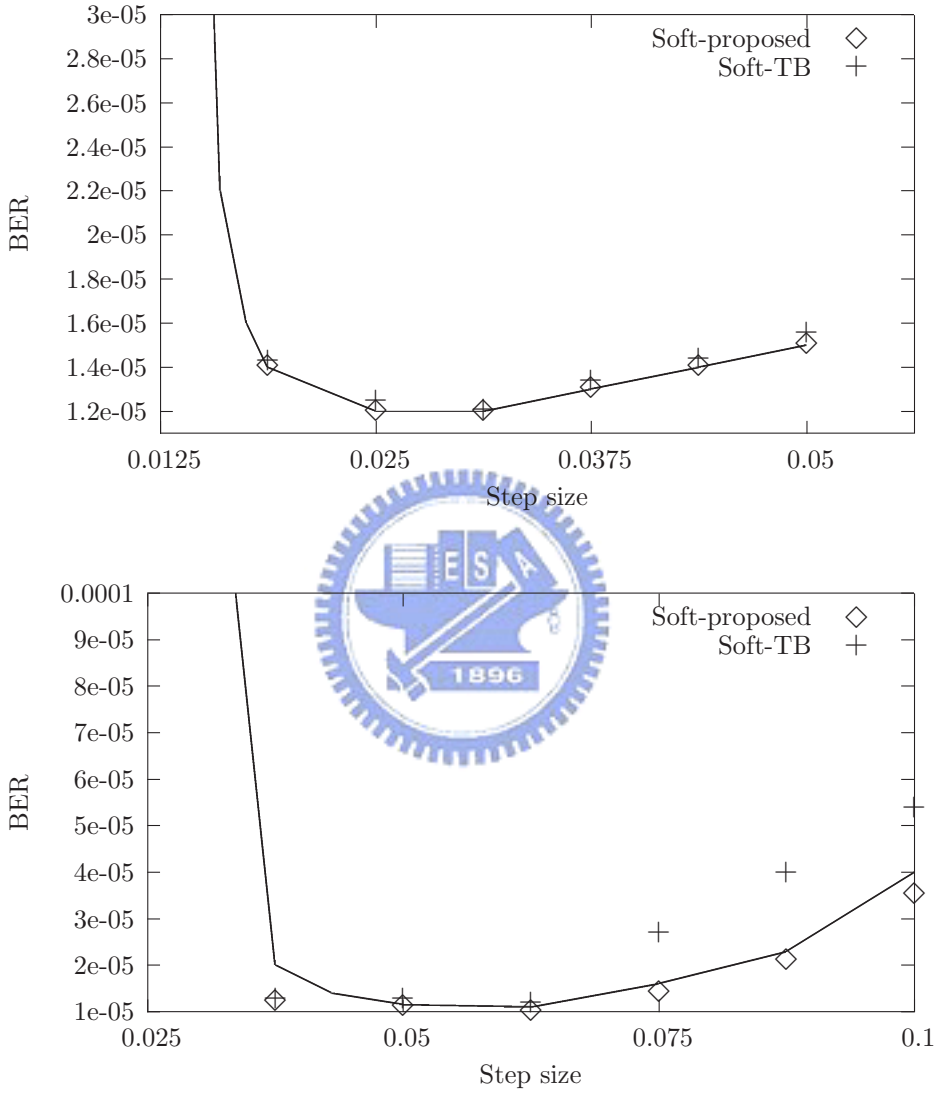

Figure 4.14: Sensitivity to gain-mismatch for 256QAM. The taken values of E_b/N_0 for Soft-proposed & Soft-TB are respectively 13.0 dB and 17.5 dB under the AWGN and the Rayleigh flat fading channels. The non-drift step-size is 0.03125 and 0.0625 respectively for each channel.

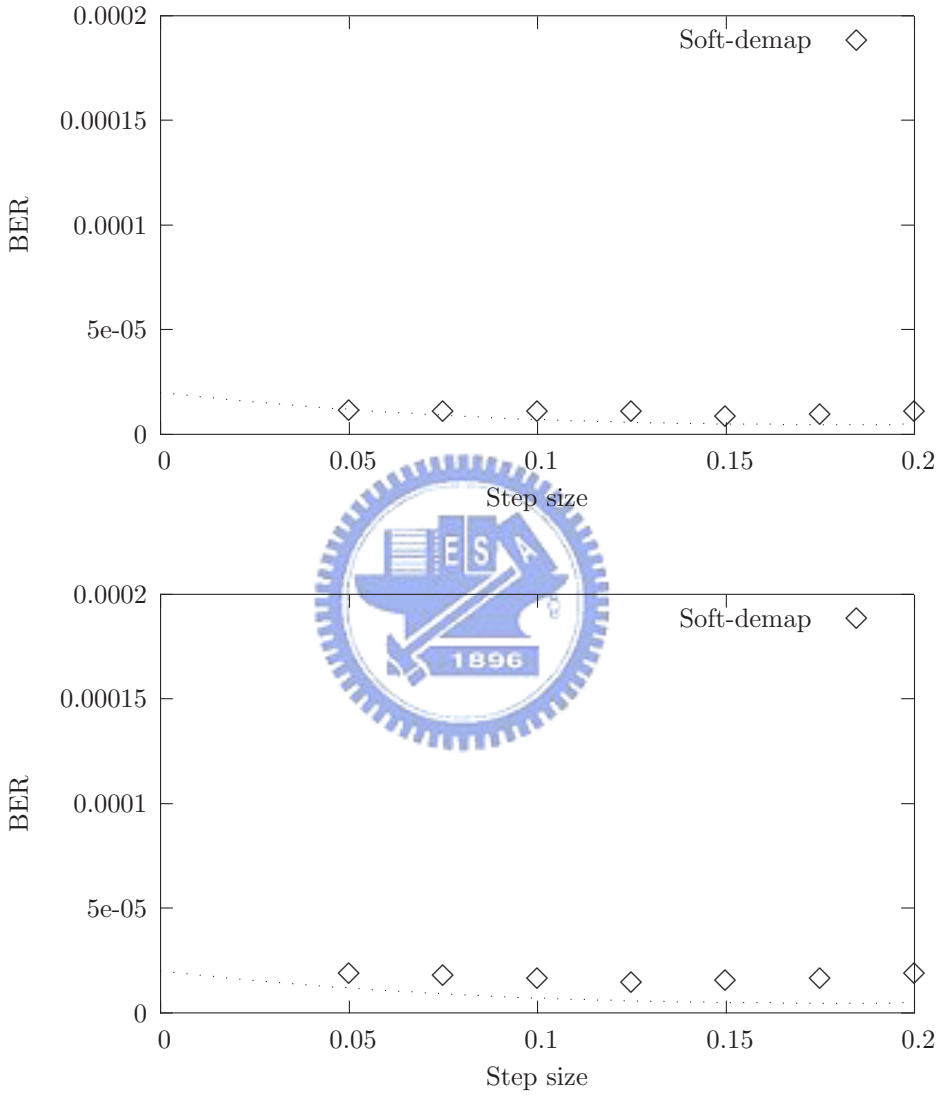

Figure 4.15: Sensitivity to gain-mismatch for 256QAM. The taken values of E_b/N_0 for Soft-demap are respectively 15.0 dB and 23.0 dB under the AWGN and the Rayleigh flat fading channels. The non-drift step-size is 0.125

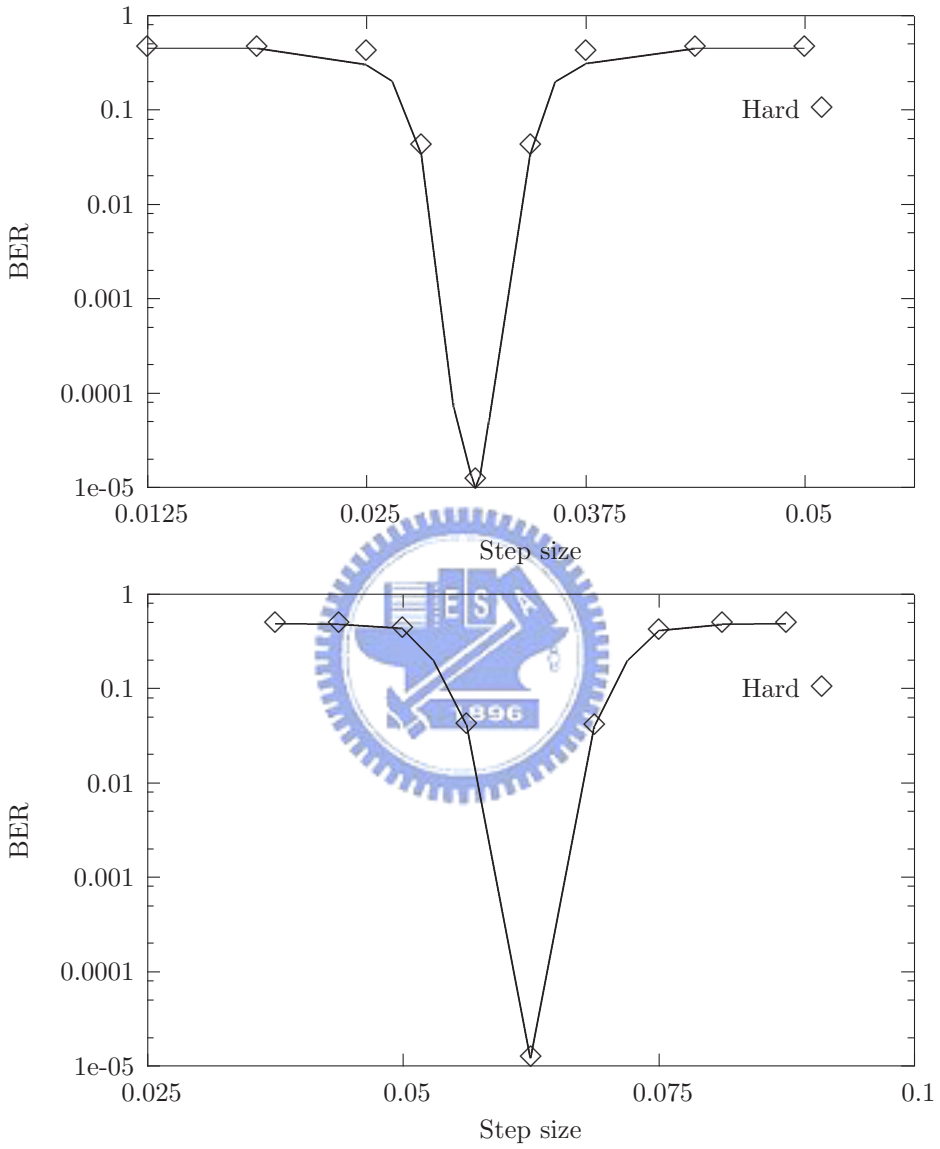

Figure 4.16: Sensitivity to gain-mismatch for 256QAM. The taken values of E_b/N_0 for hard are respectively 18.0 dB and 25.5 dB under the AWGN and the Rayleigh flat fading channels. The non-drift step-size is 0.03125 and 0.0625 respectively for each channel.

4.3 Effect of Phase Noise

In all previous simulations, perfect synchronization without phase noise is implicitly assumed. However, the real systems often suffer certain degree of uncompensated oscillator instabilities and Doppler shifts even a carrier phase tracking circuitry is implemented at the receiver.

A common way to compute the average symbol error rate under phase noise is as follows:

$$f_{\text{phase-noise}} = \int_{-\pi}^{\pi} f\left(\gamma \cos^2(\phi)\right) dP\ (\phi),$$

where function $f(\gamma)$ characterizes the symbol error rate with respect to the symbol signal-to-noise ratio γ, and $P\ (\cdot)$ denotes the distribution of the phase imperfection ϕ. This result is obtained under the assumption that the received symbol energy is degraded by a factor of $\cos^2(\phi)$ for a phase error ϕ. For the second-order phase-locked loop, the distribution of phase imperfection can be set to [9, 2]

$$\frac{dP\ (\phi)}{d\phi} = \frac{1}{2\pi I_0(\alpha)} \exp\{\alpha \cdot \cos(\phi)\},$$

where $I_0(\cdot)$ is the modified Bessel function of the first kind of order zero, and α is a system constant which is often much larger than unity. The above approach however cannot be applied to determine the bit error rate for any system in which the relationship between the symbol error and the bit error cannot be explicitly formulated. By introducing an interleaver before modulation, no general expression between the symbol error and the bit error can be obtained.

Accordingly, we obtain the bit error rate as a function of phase error ϕ by computer simulations. Note that both quantization imperfection and gain mismatch are eliminated in the simulations of Fig. 4.17 to Fig. 4.20. Under perfect gain control and no quantization, the signal-to-noise ratios per information bit (E_b/N_0) under the AWGN channel that can achieve the required BER of 10^{-5} then become 6.7 dB, 7.5 dB and 9.7 dB respectively for

Soft-proposed/Soft-TB, Soft-demap and Hard under 16QAM modulation, 9.7 dB, 10.7 dB and 13.5 dB respectively for Soft-proposed/Soft-TB, Soft-demap and Hard under 64QAM modulation, 13.2 dB, 15.0 dB and 18.0 dB respectively for Soft-proposed/Soft-TB, Soft-demap and Hard under 256QAM modulation, and 16.4 dB, 19.2 dB and 22.5 dB respectively for Soft-proposed/Soft-TB, Soft-demap and Hard under 1024QAM modulation. Similarly Under perfect gain control and no quantization, the signal-to-noise ratios per information bit (E_b/N_0) under the Rayleigh flat fading channel that can achieve the required BER of 10^{-5} then become 11.0 dB, 16.5 dB and 18.5 dB respectively for Soft-proposed/Soft-TB, Soft-demap and Hard under 16QAM modulation, 14.2 dB, 20.2 dB and 21.7 dB respectively for Soft-proposed/Soft-TB, Soft-demap and Hard under 64QAM modulation, 17.5 dB, 23.0 dB and 25.5 dB respectively for Soft-proposed/Soft-TB, Soft-demap and Hard under 256QAM modulation, and 21.0 dB, 26.8 dB and 29.0 dB respectively for Soft-proposed/Soft-TB, Soft-demap and Hard under 1024QAM modulation.

From Fig. 4.17, we observed that, for 16QAM signals under the AWGN channel, if BER is allowed to increase (from 1.0×10^{-5}) up to 4.0×10^{-5}, then Soft-proposed can tolerate up to $\pm 6^o$ phase drift, while Soft-demap and Hard only allow $\pm 5^o$ and $\pm 4^o$ phase drifts, respectively. Under the same BER degradation range, for the Rayleigh flat fading channel, the tolerant phase drifts for Soft-proposed/Soft-TB, Soft-demap and Hard are increase to $\pm 7^o$, $\pm 8^o$ and $\pm 8^o$, respectively. From Fig. 4.18, under the same BER degradation range and 64QAM modulation, the tolerant phase drifts for Soft-proposed/Soft-TB, Soft-demap and Hard are reduced to $\pm 4^o$, $\pm 3^o$ and $\pm 2^o$ under the AWGN channel, and $\pm 5^o$, $\pm 6^o$ and $\pm 4^o$ under the Rayleigh flat fading channel. These results conclude that Soft-proposed and Soft-TB are less sensitive to phase drift than Soft-demap and Hard under the AWGN channel. However, under the Rayleigh flat fading channel, although all of them can get better tolerableness than under the AWGN channel, Soft-demap is the least sensitive to phase drift

instead of Soft-proposed/Soft-TB. From Fig. 4.19 and Fig. 4.20, we also can observe that, along with the high-QAM modulation, the tolerance of phase drift declines.

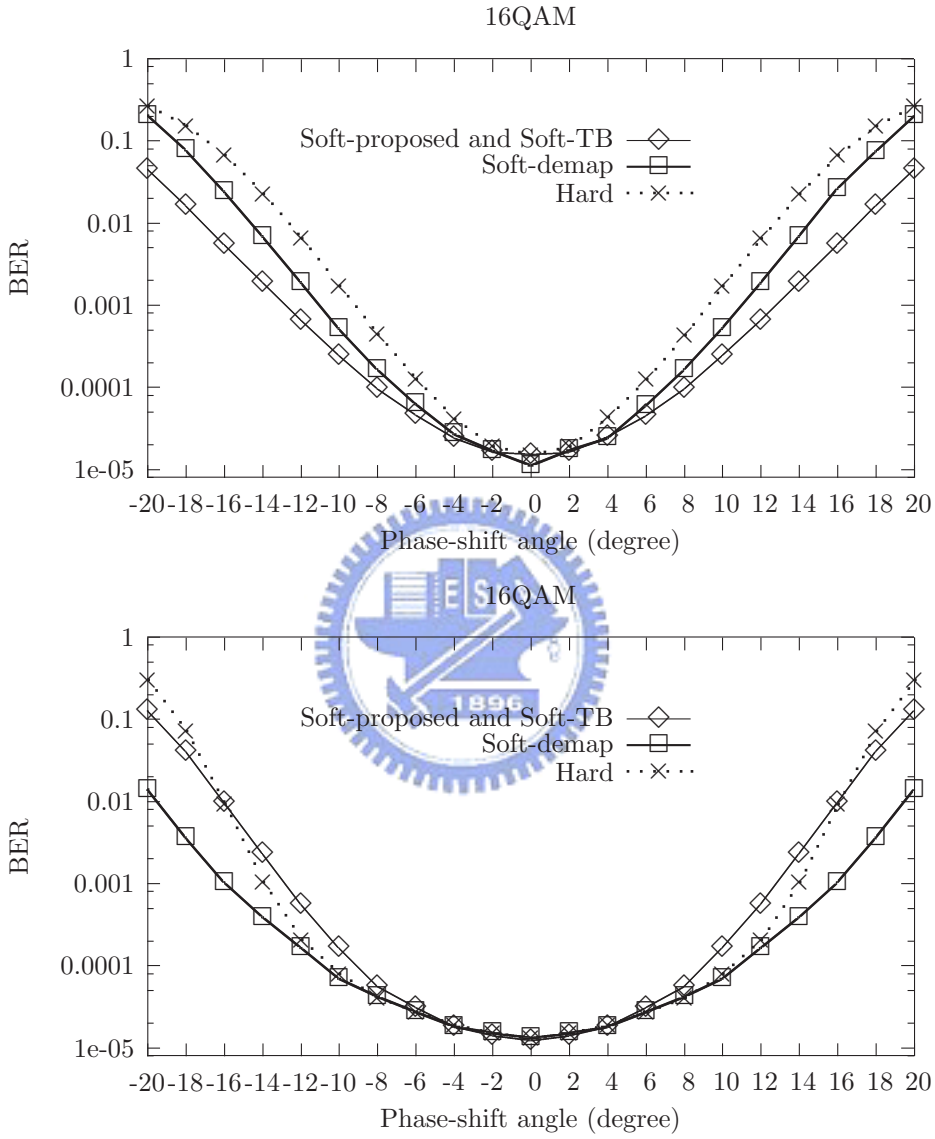

Figure 4.17: Performance impact of the phase noise. The values of E_b/N_0 taken for Soft-proposed/Soft-TB, Soft-demap and Hard are respectively 6.7 dB, 7.5 dB and 9.7 dB under the AWGN channel, 11.0 dB, 16.5 dB and 18.5 dB under the Rayleigh flat fading channel.

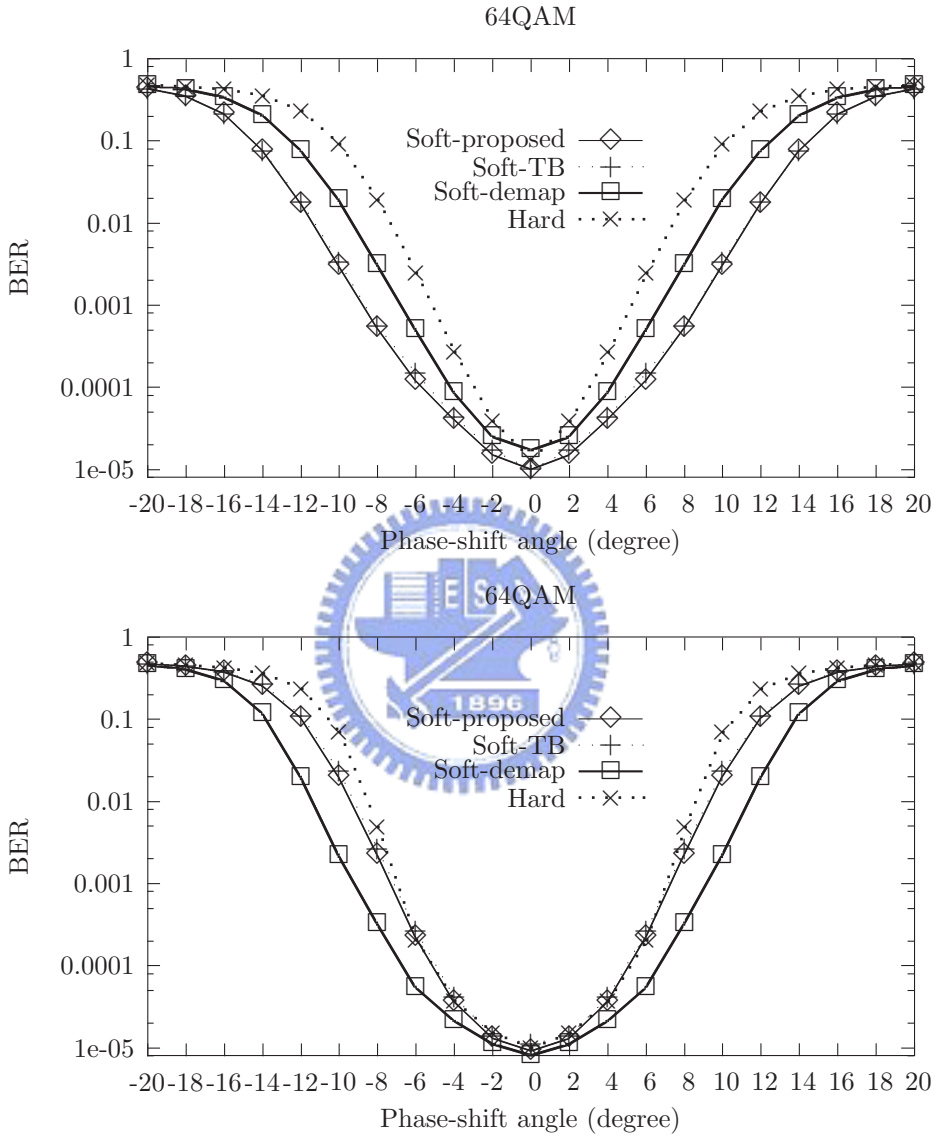

Figure 4.18: Performance impact of the phase noise. The values of E_b/N_0 taken for Soft-proposed/Soft-TB, Soft-demap and Hard are respectively 9.7 dB, 10.7 dB and 13.5 dB under the AWGN channel, 14.2 dB, 20.2 dB and 21.7 dB under the Rayleigh flat fading channel.

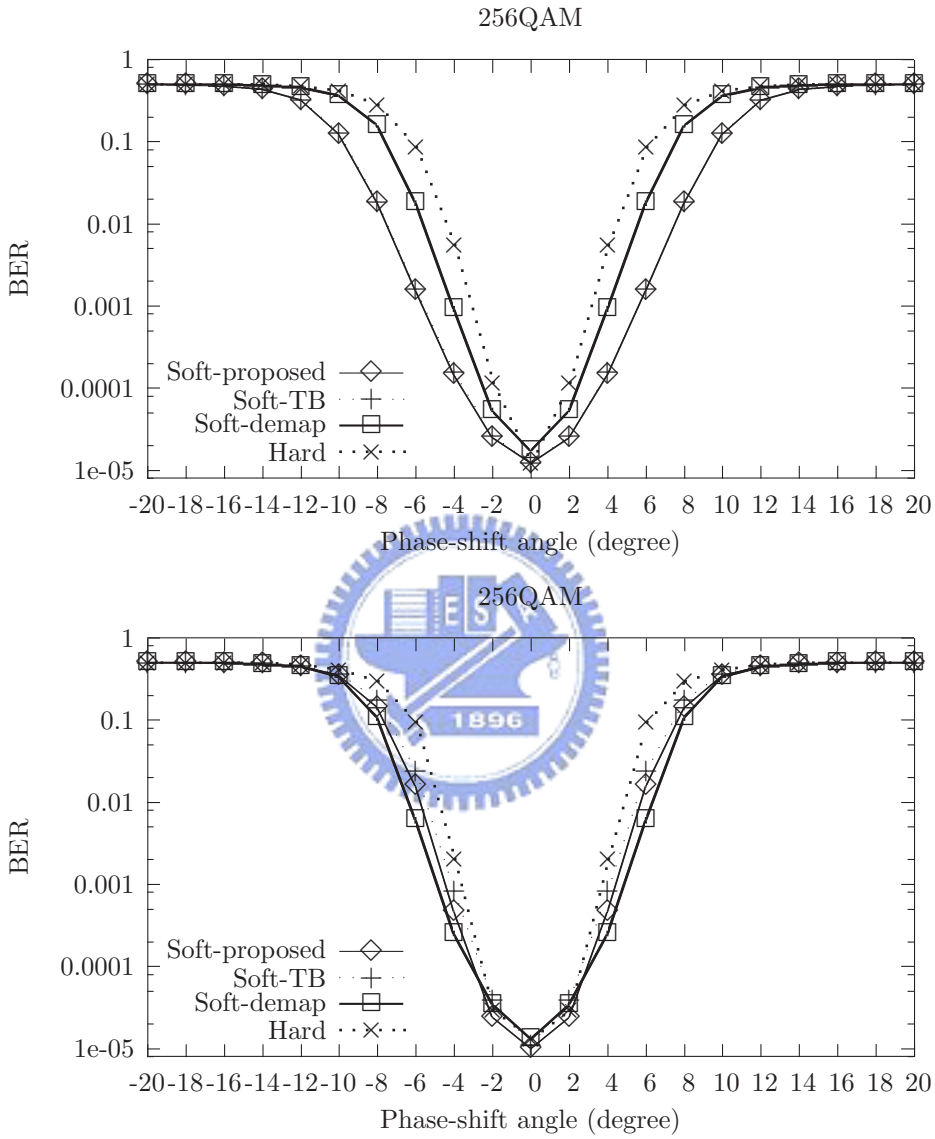

Figure 4.19: Performance impact of the phase noise. The values of E_b/N_0 taken for Soft-proposed/Soft-TB, Soft-demap and Hard are respectively 13.2 dB, 15.0 dB and 18.0 dB under the AWGN channel, 17.5 dB, 23.0 dB and 25.5 dB under the Rayleigh flat fading channel.

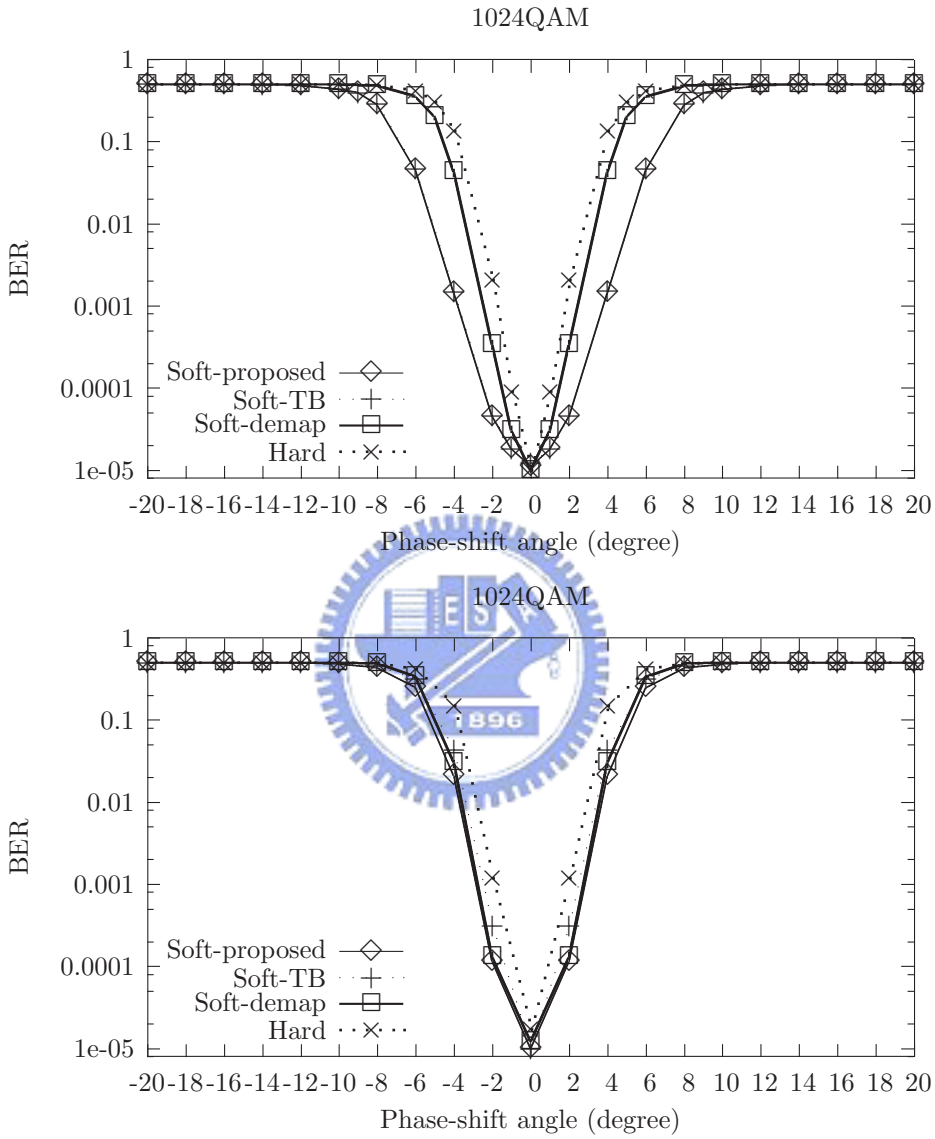

Figure 4.20: Performance impact of the phase noise. The values of E_b/N_0 taken for Soft-proposed/Soft-TB, Soft-demap and Hard are respectively 16.4 dB, 19.2 dB and 22.5 dB under the AWGN channel, 21.0 dB, 26.8 dB and 29.0 dB under the Rayleigh flat fading channel.

Chapter 5

Performance Evaluation Over the Punctured Codes

5.1 Description of the Puncture Procedure

The DATA field of IEEE 802.11a/g [11, 12], composed of SERVICE, PSDU, tail, and pad parts, shall be coded with a convolutional encoder of desired coding rate R = 1/2, 2/3, or 3/4. The convolutional encoder is implemented according to the industry-standard generator polynomials, $g_0 = 133_8$ and $g_1 = 171_8$, of rate R = 1/2, as shown in Fig. 5.1. The bit denoted as "A" is output from the encoder before the bit denoted as B. Codes with higher rates are derived from this mother code by employing puncturing. Puncturing is a procedure to omit some of the encoded bits in the transmitter (thus reducing the number of transmitted bits and increasing the coding rate) and inserting a dummy "zero" metric into the convolutional decoder on the receiver in the positions of the received vector corresponding to that of the omitted bits. The recommended puncturing patterns are illustrated in Fig. 5.2 and decoding by the Viterbi algorithm is recommended.

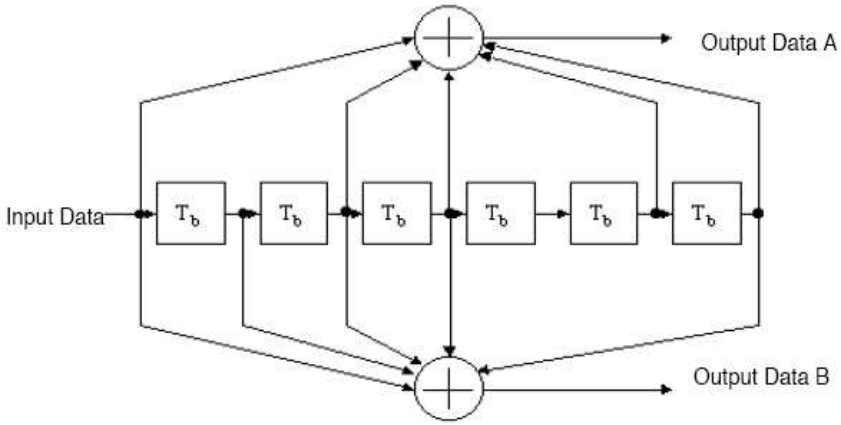

Figure 5.1: The convolutional encoder (k = 7).

5.2 Performance of Punctured Codes

Fig. 5.3 and Fig. 5.4 summarize the simulated performance of codes with different coding rates under the AWGN channel for *symbol-based ML decision in* (2.1), the *proposed bit-decomposed metrics*, the *soft-demapping in Chapter 2.3.1*, the *simplified bit metrics in Chapter 2.3.2*, and the straightforward *hard-decision decoding system*. As stated in the previous chapter, they are respectively abbreviated as Symbol-ML, Soft-proposed, Soft-demap, Soft-TB and Hard in all subsequent figures. Under 16QAM modulation and at BER = 10^{-5}, for coding rates 1/2, 2/3, and 3/4, Soft-proposed (equivalently, Soft-TB) has 3.0 dB, 2.7 dB, and 2.6 dB gain over Hard respectively. Under 64QAM modulation and at BER = 10^{-5}, for coding rates 1/2, 2/3, and 3/4, Soft-proposed (equivalently, Soft-TB) has 3.9 dB, 3.0 dB, and 2.8 dB gain over Hard respectively. Under 256QAM modulation and at BER = 10^{-5}, for coding rates 1/2, 2/3, and 3/4, Soft-proposed (equivalently, Soft-TB) has 5.1 dB, 3.7 dB, and 3.3 dB gain over Hard respectively. One can see that, with the higher puncture coding rate, the coding gain reduces. Furthermore, the three soft-decision decoding algorithms considered have similar performance when higher puncture coding rates are employed.

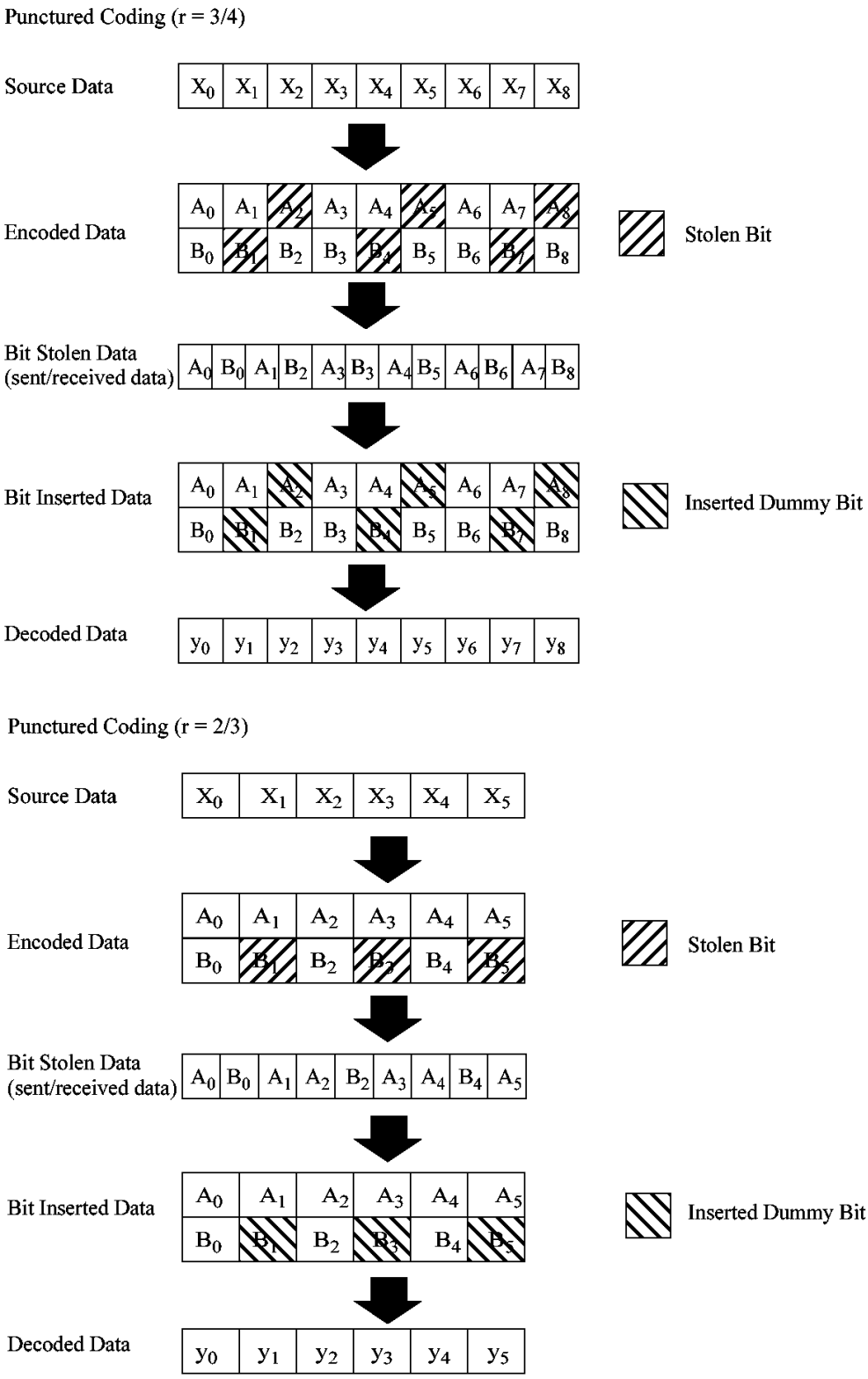

Figure 5.2: An example of the bit-stealing and bit-insertion procedure (r = 3/4, 2/3).

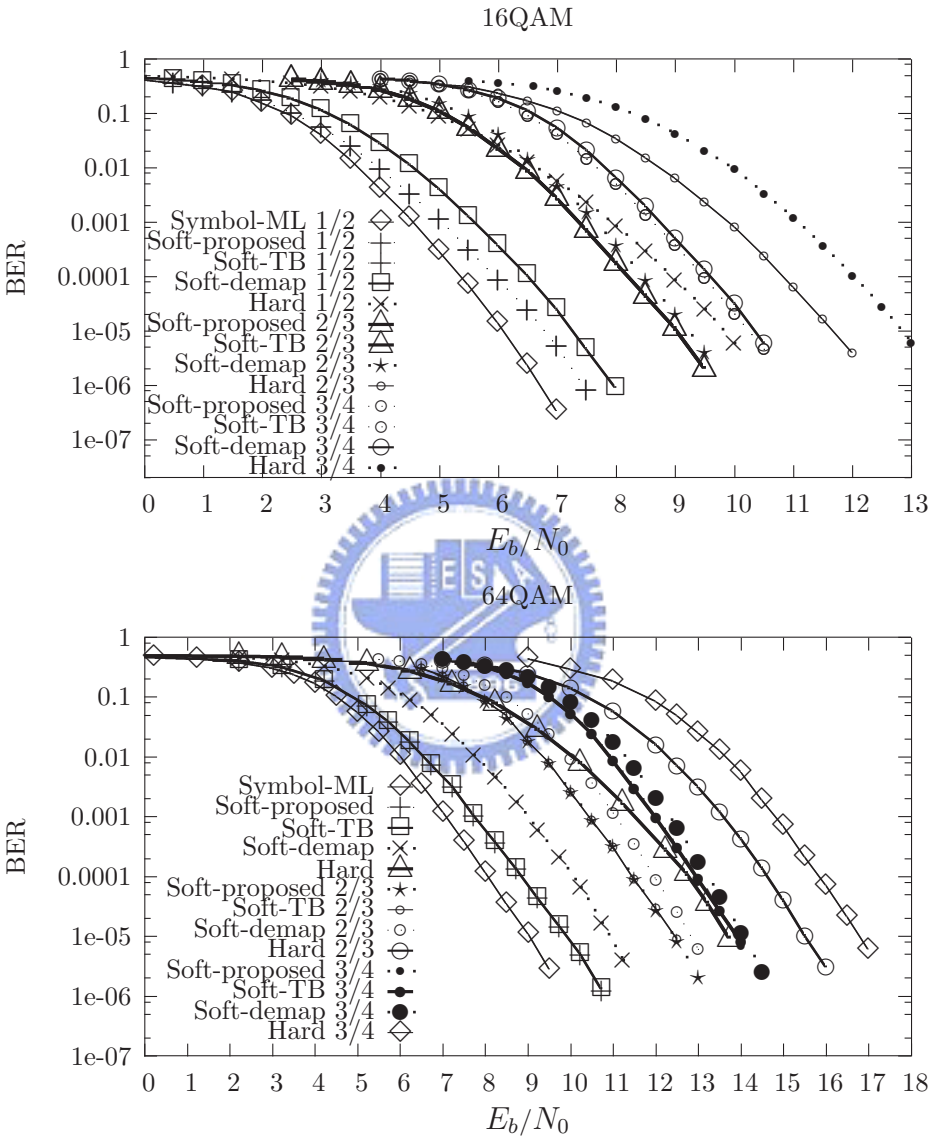

Figure 5.3: System performance of punctured codes with different coding rates under the AWGN channel for 16QAM and 64QAM modulations.

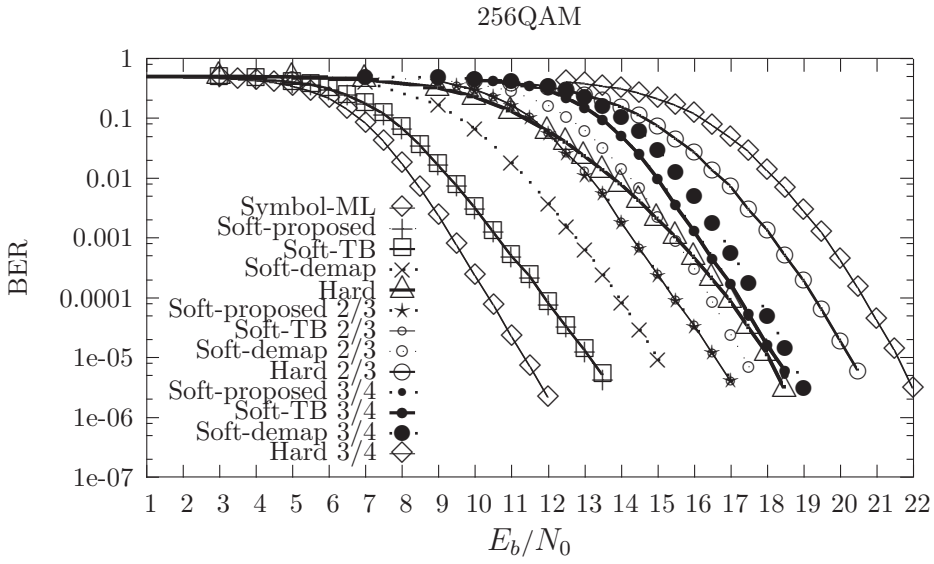

Figure 5.4: System performance of punctured codes with different coding rates under the AWGN channel for 256QAM modulation.

There are several rate-dependent parameters recommended in the standard of IEEE 802.11a/g [11, 12] (see Table 5.1). However, there are still some alternatives. For example, the punctured code with coding rate 1/2 under 64QAM modulation has the same information bit rate as the punctured code with coding rate 3/4 under 16QAM modulation that is recommended in the standard. Furthermore, the punctured code with coding rate 1/2 under 256QAM modulation has the same information bit rate as the punctured code with coding rate 2/3 under 64QAM modulation that is recommended in the standard. In the following we will investigate the BER performance of all codes recommended in the standard under 16QAM and 64QAM modulations and the above two alternatives.

Fig. 5.5 illustrates the BER performance of punctured codes for Hard and Soft-demap under the AWGN channel for 16QAM, 64QAM, and 256QAM modulations. Under 16QAM modulation and at BER = 10^{-5}, the punctured code with coding rate 3/4 has 0.9 dB and 0.56 dB gain over the code with coding rate 1/2 under 64QAM modulation for Hard and Soft-

Table 5.1: Rate-dependent parameters in the std. of IEEE 802.11a/g

$Date-rate$ $(Mbits/s)$	$Modulation$	$Coding$ rate (R)	$Coded-bits$ per $subcarrier$ (N_{BPSC})	$Coded-bits$ $per-OFDM$ $symbol$ (N_{CBPS})	$Data-bits$ $per-OFDM$ $symbol$ (N_{DBPS})
6	BPSK	1/2	1	48	24
9	BPSK	3/4	1	48	36
12	QPSK	1/2	2	96	48
18	QPSK	3/4	2	96	72
24	16QAM	1/2	4	192	96
36	16QAM	3/4	4	192	144
48	64QAM	2/3	6	288	192
54	64QAM	3/4	6	288	216

demap, respectively. At the same bit error rate, under 64QAM modulations the punctured code with coding rate 2/3 has 2.6 dB and 2.1 dB gain over that with coding rate 1/2 under 256QAM modulation for Hard and Soft-demap, respectively. Hence, the code with rate 1/2 under 64QAM modulation can be replaced by the code with coding rate 3/4 under 16QAM modulation. Similarly, the code with coding rate 1/2 under 256QAM can be replaced by the code with code rate 2/3 under 64QAM modulation. These results reveal that the codes recommended in the standard indeed superior to the above two alternatives for Hard and Soft-demap.

Fig. 5.6 presents the BER performance of punctured codes for Soft-proposed and Soft-TB under the AWGN channel for 16QAM, 64QAM, and 256QAM modulations. At BER $= 10^{-5}$, under 64QAM modulation the code with coding rate 1/2 has 0.33 dB gain over that with coding rate 3/4 under 16QAM modulation for Soft-proposed and Soft-TB. This indicates that, when employing Soft-proposed or Soft-TB, the code with coding rate 1/2 under 64QAM modulation is preferred to the code with rate 3/4 under 16QAM modulation recommended in the standard. At the same bit error rate, the code with code rate 2/3

under 64QAM modulation recommended in the standard still has 0.67 dB gain over that with coding rate 1/2 under 256QAM modulation for Soft-proposed and Soft-TB.

Fig. 5.7 summarizes the BER performance of punctured codes with different coding rates under the Rayleigh flat fading channel for Symbol-ML, Soft-proposed, Soft-demap, Soft-TB and Hard. Under 16QAM modulation and at BER = 10^{-5}, for coding rates 1/2, 2/3, and 3/4, Soft-proposed (equivalently, Soft-TB) has 7.7 dB, 10.4 dB, and 13.0 dB gain over Hard respectively. Under 64QAM modulation and at BER = 10^{-5}, for coding rates 1/2, 2/3, and 3/4, Soft-proposed (equivalently, Soft-TB) has 8.1 dB, 10.7 dB, and 13.3 dB gain over Hard, respectively. In contrast to the cases under the AWGN channel, with the higher puncture coding rate the coding gain increases under the Rayleigh flat fading channel. Furthermore, unlike the cases under the AWGN channel, the three soft-decision decoding algorithms considered have quite different performance when higher puncture coding rates are employed under the Rayleigh flat fading channel.

Fig. 5.8 and Fig. 5.9 illustrate the BER performance of punctured codes for Hard, Soft-demap, Soft-proposed, and Soft-TB under the Rayleigh flat fading channel for 16QAM and 64QAM modulations. Under 64QAM modulation and at BER = 10^{-5}, the punctured code with coding rate 1/2 has 9.3 dB, 8.3 dB, and 5.1 dB gain over the code with coding rate 3/4 under 16QAM modulation for Hard, Soft-demap, Soft-proposed, and Soft-TB, respectively. This indicates that, when under the Rayleigh flat fading channel, employing not only Soft-proposed or Soft-TB but also Soft-demap and Hard, the code with coding rate 1/2 under 64QAM modulation is preferred to the code with rate 3/4 under 16 QAM modulation.

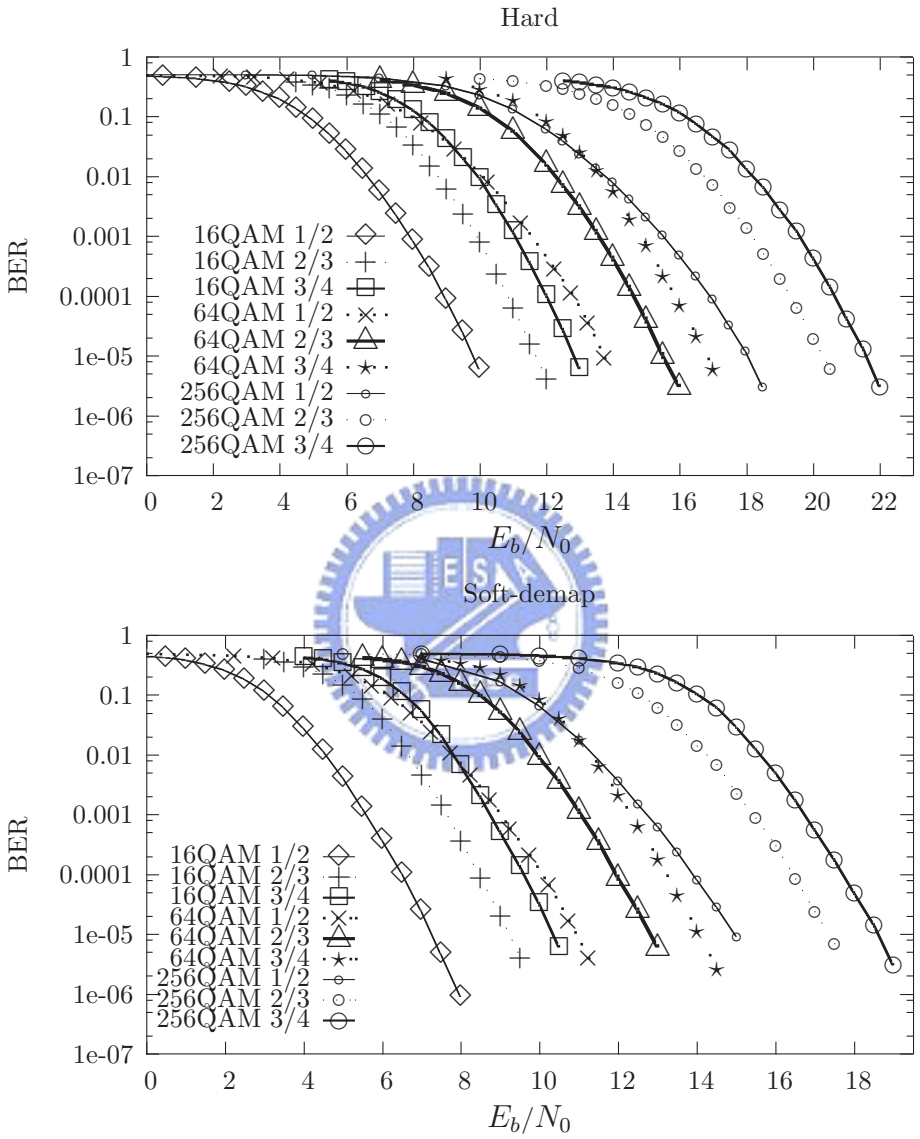

Figure 5.5: System performance of punctured codes with different coding rates under the AWGN channel for Hard and Soft-demap.

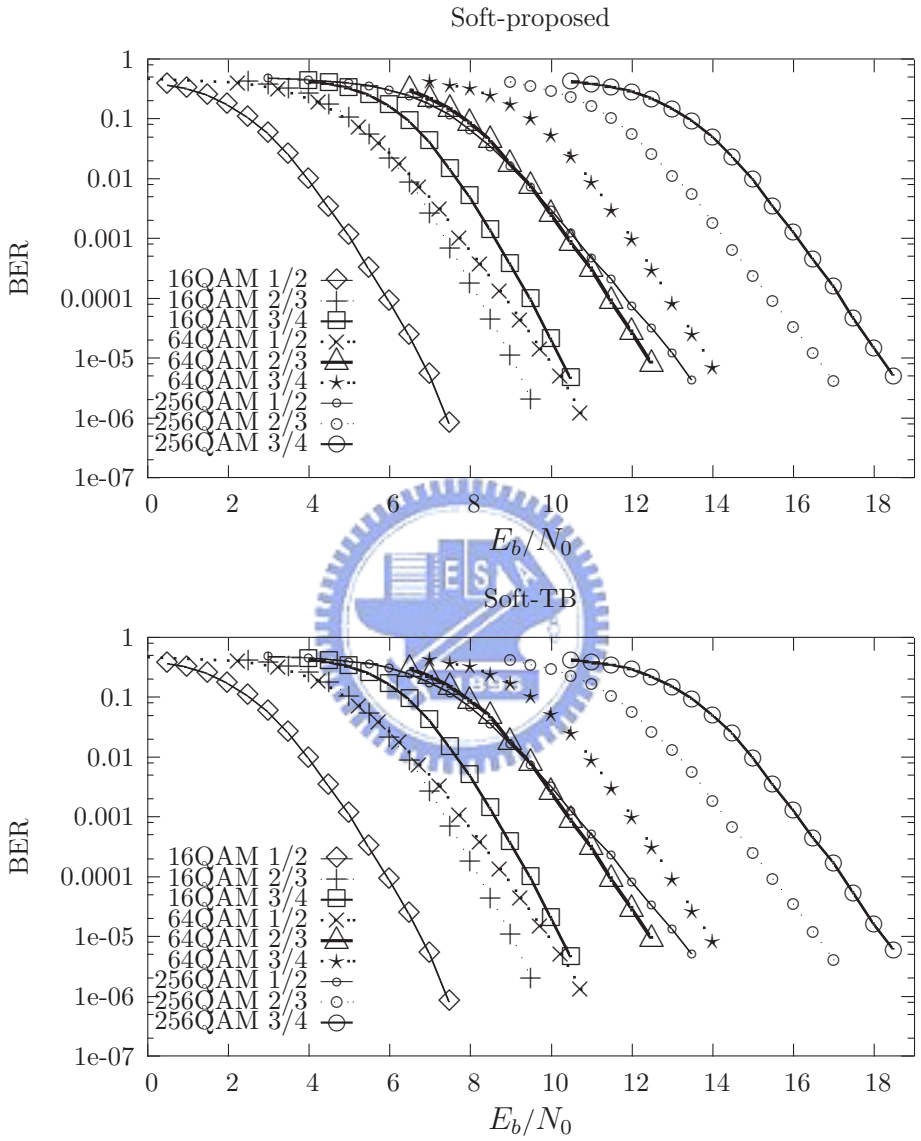

Figure 5.6: System performance of punctured codes with different coding rates under the AWGN channel for Soft-proposed and Soft-TB.

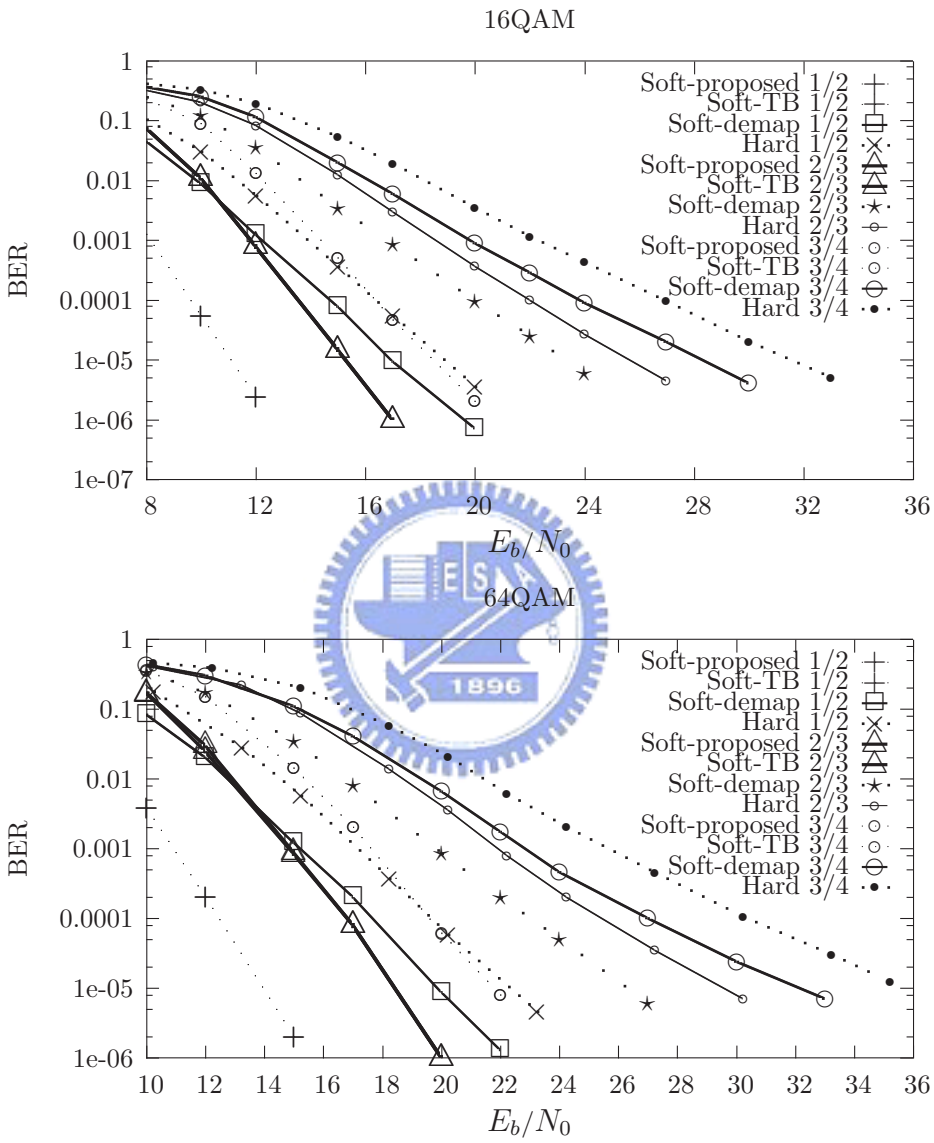

Figure 5.7: System performance of punctured codes with different coding rates under the Rayleigh flat fading channel for 16QAM and 64QAM modulations.

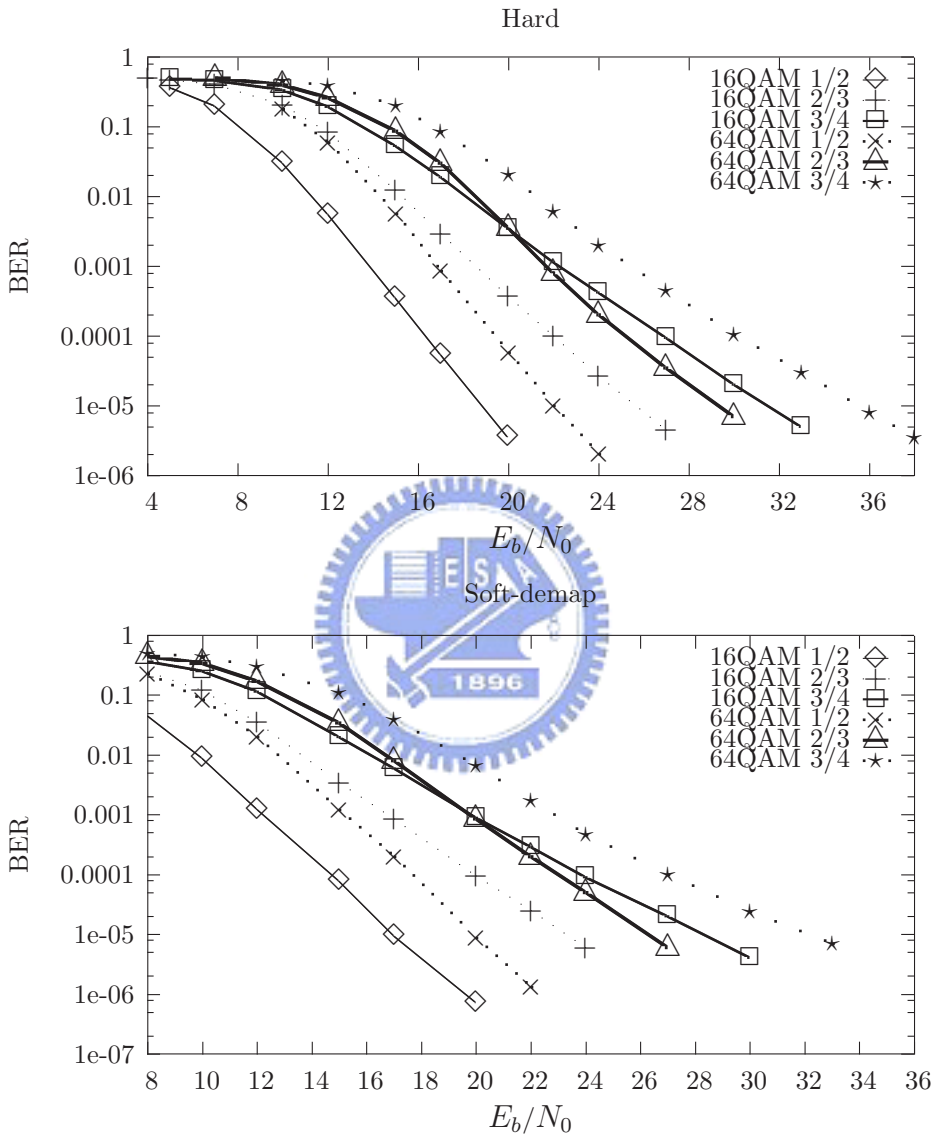

Figure 5.8: System performance of punctured codes with different coding rates under the Rayleigh flat fading channel for Hard and Soft-demap.

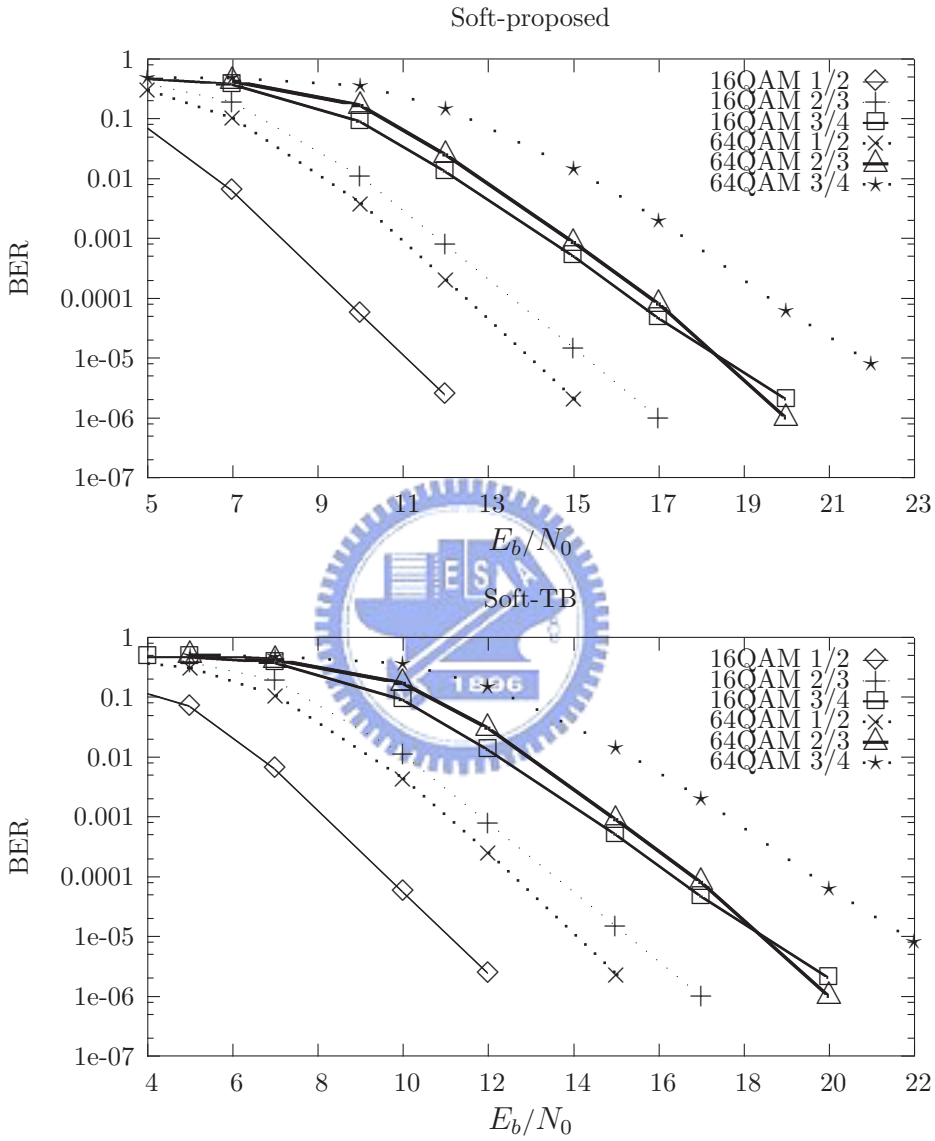

Figure 5.9: System performance of punctured codes with different coding rates under the Rayleigh flat fading channel for Soft-proposed and Soft-TB.

Chapter 6

Realization of the Systematic Bit-wise Decomposition Metric

6.1 Preliminary

Traditionally, realization of the Viterbi decoder can be divided into three units [13, 14], as shown in Fig. 6.1. The input data is used in the branch metric unit (BMU) to calculate the branch metrics for each new time step. These metrics are then fed to the add-compare-select unit (ACSU), which accumulates the branch metrics as the path metric (PM) stored in the path metric memory (PMM) according to the ACS-recursion. The survivor memory unit (SMU) processes the decisions which are being made in ACSU, and outputs the estimated path with a latency of at least D, called the survivor depth. Other than the combination design of interleaver and decoder, we will provide a dual-mode (Soft-proposed/Soft-TB) system architecture for BMU.

6.2 Architecture of Branch Metric Unit

In this section, we will provide a systematic architecture for BMU, which avails the recursiveness nature of the proposed bit metric decomposition formulas. Our architecture only

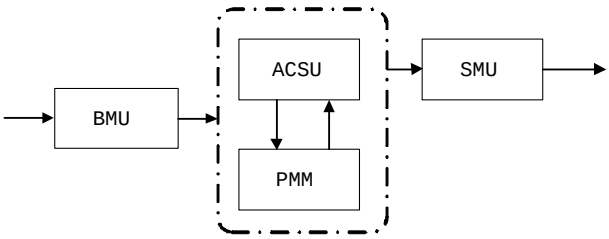

Figure 6.1: A simplified block diagram of the Viterbi decoder

requires the first-bit function table, and can be applied for 2^{2m}-QAM modulations for every $2 \leq m \leq m_{\max}$, if $(m_{\max} - 2)$ metric transition units (MTUs) is serially connected.

Under the setting of IEEE 802.11a/g, an OFDM signal consists of 96 2^{2m}-QAM symbols, and each 2^{2m}-QAM symbol was mapped from m coded-and-interlaved bits. The decoding sequences from left to right can be divided into 6 rows, where each row consists of 16 QAM quadrature symbols. For example, the first row in Fig. 1.3 contains $\{r_0, r_6, r_{12}, \ldots, r_{90}\}$, and the symbols in $\{r_1, r_7, r_{13}, \ldots, r_{91}\}$ form the second row. An internal control variable, named Index_c, is used to keep the record of which column of QAM quadrature symbol in Fig. 1.3-block the BMU is currently used. Consequently, Index_c is initially zero for each new 96 QAM symbol block, and is updated according to the rule of Index_c = (Index_c+1) mod 16. Another internal control variable, Sym_bit, is used to adjust the demapped bit number in each QAM symbol according to the interleaver rule. It is equal to $(6 \times m - 1)$ initially for each new 96 QAM symbol block, and is reduced by one when Index_c equals 0. We also record the position of the QAM quadrature component (in the 96 QAM symbol block) that is currently used. As a result, position $= 6 \times \text{Index\_c} + 5 - \lfloor \text{Sym\_bit}/m \rfloor$, where $\lfloor \cdot \rfloor$ denotes the floor function. All the internal control variables are periodically updated at the time a new QAM quadrature symbol enters the BMU. Notably, for 2^{2m}-QAM demodulation, each QAM quadrature symbol has to be re-accessed m times; for example, the BMU needs to generate $192 = 2 \times 96$ soft bit metrics for 16QAM demodulation in Fig. 1.4.

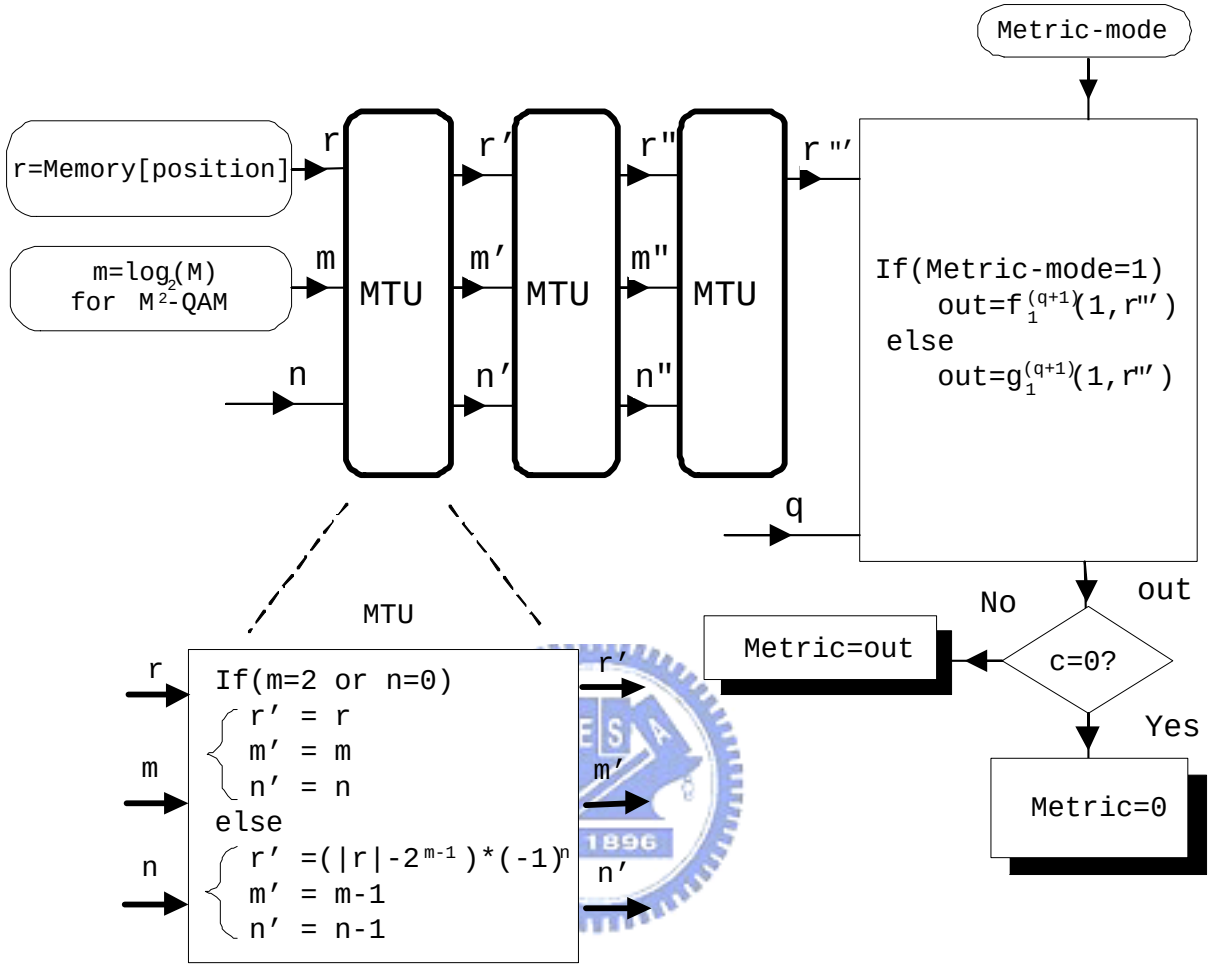


```
First,we receive 96 2^2m -QAM symbols in memory, and
    set Index_c=position=0,Sym_bit=6*m-1 and q=m-1.
Starting from the 2nd r, perform in sequence:
    Index_c = (Index_c+1) mod 16;
    if(Index_c=0) Sym_bit = Sym_bit-1;
    position = 6*Index_c+5-⌊Sym_bit/m⌋;
    q = (Index_c+Sym_bit)  mod m;
    n = m-1-q;
```

Figure 6.2: A dual-mode BMU architecture with $(m_{\max}-2)$ serially connected MTU's can perform the bit metric evaluations for 2^{2m}-QAM, where $2 \le m \le m_{\max}$. Here, $m_{\max} = 5$. All the constants in the formulas of Index_c, Sym_bit and position, such as 5 $(= \mathbf{6}-1)$, **6** and **16**, are chosen according to the 6×16 interleaver block used in IEEE 802.11a/g standard.

One can easily combine the implementation of both the proposed and Tosato/Bisaglia metrics by providing two first-bit metric function tables. As shown in Fig. 6.2, two metric calculation modes are set as:

"Metric-mode = 1" is for Soft-proposed, and
"Metric-mode = 0" is for Soft-TB.

A forth internal control variable, q = (Index_c+Sym_bit) mod m, is used to determine the bit metric function number. When q is decided, either function $f_1^{(q+1)}(\cdot,\cdot)$ or function $g_1^{(q+1)}(\cdot,\cdot)$ is used, depending on the Metric-mode. The last internal control variable, n, is simply $m-1-q$. This dual-mode BMU architecture is depicted in Fig. 6.2.

Our BMU requires two external input signals, which are *(i)* the received QAM quadrature symbol r that are derived from the proper position of the 96 symbol block, and *(ii)* $m = \log_2(M)$ if what has been received is M^2-QAM symbol.

Finally, since the soft bit metric equals zero when the branch bit c is zero, the BMU only evaluates bit metric values for $c = 1$. The case for "$c = 0$" is then handled by a check box appended at the output end of the BMU.

Chapter 7

Concluding Remarks

In this thesis, we obtained a recursive bit-decomposed metric formula through the approximation of symbol-based Euclidean metric. We subsequently compare the performances of the proposed soft bit-decomposed metric, the simplified bit metrics proposed in [5] and the straightforward hard-decision decoding system. As anticipated, the proposed soft bit-decomposed metric and the simplified bit metrics in [5] perform better than Hard in all respects. A realization of the proposed soft bit-decomposed metric is also presented that can perform all bit metric evaluation for 2^{2m}-QAM, where $2 \leq m \leq 5$.

The superiority of our proposed bit-decomposed metric over the simplified bit metrics proposed in [5] is a little more apparent under a fading environment and a higher QAM modulation. By assuming a Rayleigh flat fading channel with perfect channel knowledge , the performance difference between these two methods is a little larger (than that under the AWGN channel). Also, we observed that in a fading environment, the performance superiority of Soft-proposed and Soft-TB over the Hard extends to 8.5 dB under 256QAM modulation at BER = 10^{-5}.

Appendix A

Detailed Derivation of Bit-wise Metric for Soft-decision Decoding of 64QAM, 256QAM, 1024QAM Modulations

Define a bit-wise soft-demapping metric for an M-ary rectangular QAM symbol by

$$f_j(r,c) = (1/2)r^2 + a_{j,c,\rho}r + b_{j,c,\rho} \text{ for } 1 \le j \le (1/2)\log_2(M), \tag{A.1}$$

where r is the real-valued received QAM symbol, j indexes the soft bit-functions, c is the binary label on the decoding trellis, and $\rho = \rho(r)$ designates the dependence of the coefficients $a_{j,c,\rho}$ and $b_{j,c,\rho}$ on r.

The dependence of $a_{j,c,\rho}$ and $b_{j,c,\rho}$ on r is defined as follows. The range of r (i.e., the real line $\Re$) is partitioned into q contiguous sub-ranges $\mathcal{I}_1, \mathcal{I}_2, \ldots, \mathcal{I}_q$, where $\mathcal{I}_\rho = (\lambda_{\rho-1}, \lambda_\rho]$, and $\lambda_0 = -\infty$ and $\lambda_q = \infty$. Also both $a_{j,c,\rho}$ and $b_{j,c,\rho}$ remain constants in sub-range $\mathcal{I}_\rho$. Hence, the true soft ML metric is approximated by

$$\sum_{j=1}^{(1/2)\log_2(M)} f_j(r,c).$$

A.1 Derivation of Bit-wise Metric of 64QAM Modulation

Suppose that Gray code mapping is employed for 64QAM mapping, i.e., -7, -5, -3, -1, $+1$, $+3$, $+5$ and $+7$ respectively map to 000, 001, 011, 010, 110, 111, 101, and 100. Also, assume that each codeword is transmitted over the AWGN channel. Then the squared error criterion (or cost function) is given by

$$\begin{aligned}
W(f_1, f_2, f_3) \;=\; & \frac{1}{8\sqrt{\pi N_0}} \left(\int_{-\infty}^{\infty} \left[f_1(r,0) + f_2(r,0) + f_3(r,0) - (r+7)^2 \right]^2 e^{-(r+7)^2/N_0} dr \right. \\
& + \int_{-\infty}^{\infty} \left[f_1(r,0) + f_2(r,0) + f_3(r,1) - (r+5)^2 \right]^2 e^{-(r+5)^2/N_0} dr \\
& + \int_{-\infty}^{\infty} \left[f_1(r,0) + f_2(r,1) + f_3(r,1) - (r+3)^2 \right]^2 e^{-(r+3)^2/N_0} dr \\
& + \int_{-\infty}^{\infty} \left[f_1(r,0) + f_2(r,1) + f_3(r,0) - (r+1)^2 \right]^2 e^{-(r+1)^2/N_0} dr \\
& + \int_{-\infty}^{\infty} \left[f_1(r,1) + f_2(r,1) + f_3(r,0) - (r-1)^2 \right]^2 e^{-(r-1)^2/N_0} dr \\
& + \int_{-\infty}^{\infty} \left[f_1(r,1) + f_2(r,1) + f_3(r,1) - (r-3)^2 \right]^2 e^{-(r-3)^2/N_0} dr \\
& + \int_{-\infty}^{\infty} \left[f_1(r,1) + f_2(r,0) + f_3(r,1) - (r-5)^2 \right]^2 e^{-(r-5)^2/N_0} dr \\
& \left. + \int_{-\infty}^{\infty} \left[f_1(r,1) + f_2(r,0) + f_3(r,0) - (r-7)^2 \right]^2 e^{-(r-7)^2/N_0} dr \right),
\end{aligned}$$

where N_0 is the single-sided noise power per hertz. Substituting (A.1) into the above cost function, we obtain

$$
\begin{aligned}
& W(f_1, f_2, f_3) \\
= \; & \frac{1}{8\sqrt{\pi N_0}} \left(\sum_{\rho=1}^{q} \int_{\lambda_{\rho-1}}^{\lambda_\rho} \left[(a_{1,0,\rho} + a_{2,0,\rho} + a_{3,0,\rho} - 14)r + (b_{1,0,\rho} + b_{2,0,\rho} + b_{3,0,\rho} - 49) \right]^2 e^{-(r+7)^2/N_0} dr \right. \\
& + \sum_{\rho=1}^{q} \int_{\lambda_{\rho-1}}^{\lambda_\rho} \left[(a_{1,0,\rho} + a_{2,0,\rho} + a_{3,1,\rho} - 10)r + (b_{1,0,\rho} + b_{2,0,\rho} + b_{3,1,\rho} - 25) \right]^2 e^{-(r+5)^2/N_0} dr \\
& + \sum_{\rho=1}^{q} \int_{\lambda_{\rho-1}}^{\lambda_\rho} \left[(a_{1,0,\rho} + a_{2,1,\rho} + a_{3,1,\rho} - 6)r + (b_{1,0,\rho} + b_{2,1,\rho} + b_{3,1,\rho} - 9) \right]^2 e^{-(r+3)^2/N_0} dr \\
& + \sum_{\rho=1}^{q} \int_{\lambda_{\rho-1}}^{\lambda_\rho} \left[(a_{1,0,\rho} + a_{2,1,\rho} + a_{3,0,\rho} - 2)r + (b_{1,0,\rho} + b_{2,1,\rho} + b_{3,0,\rho} - 1) \right]^2 e^{-(r+1)^2/N_0} dr \\
& + \sum_{\rho=1}^{q} \int_{\lambda_{\rho-1}}^{\lambda_\rho} \left[(a_{1,1,\rho} + a_{2,1,\rho} + a_{3,0,\rho} + 2)r + (b_{1,1,\rho} + b_{2,1,\rho} + b_{3,0,\rho} - 1) \right]^2 e^{-(r-1)^2/N_0} dr \\
& + \sum_{\rho=1}^{q} \int_{\lambda_{\rho-1}}^{\lambda_\rho} \left[(a_{1,1,\rho} + a_{2,1,\rho} + a_{3,1,\rho} + 6)r + (b_{1,1,\rho} + b_{2,1,\rho} + b_{3,1,\rho} - 9) \right]^2 e^{-(r-3)^2/N_0} dr \\
& + \sum_{\rho=1}^{q} \int_{\lambda_{\rho-1}}^{\lambda_\rho} \left[(a_{1,1,\rho} + a_{2,0,\rho} + a_{3,1,\rho} + 10)r + (b_{1,1,\rho} + b_{2,0,\rho} + b_{3,1,\rho} - 25) \right]^2 e^{-(r-5)^2/N_0} dr \\
& \left. + \sum_{\rho=1}^{q} \int_{\lambda_{\rho-1}}^{\lambda_\rho} \left[(a_{1,1,\rho} + a_{2,0,\rho} + a_{3,0,\rho} + 14)r + (b_{1,1,\rho} + b_{2,0,\rho} + b_{3,0,\rho} - 49) \right]^2 e^{-(r-7)^2/N_0} dr \right).
\end{aligned}
$$

For each ρ, we can list the equations involving in the above cost function as follows:

$$a_{1,0,\rho} + a_{2,0,\rho} + a_{3,0,\rho} - 14 = 0 \qquad b_{1,0,\rho} + b_{2,0,\rho} + b_{3,0,\rho} - 49 = 0 \tag{A.2a}$$

$$a_{1,0,\rho} + a_{2,0,\rho} + a_{3,1,\rho} - 10 = 0 \qquad b_{1,0,\rho} + b_{2,0,\rho} + b_{3,1,\rho} - 25 = 0 \tag{A.2b}$$

$$a_{1,0,\rho} + a_{2,1,\rho} + a_{3,1,\rho} - 6 = 0 \qquad b_{1,0,\rho} + b_{2,1,\rho} + b_{3,1,\rho} - 9 = 0 \tag{A.2c}$$

$$a_{1,0,\rho} + a_{2,1,\rho} + a_{3,0,\rho} - 2 = 0 \qquad b_{1,0,\rho} + b_{2,1,\rho} + b_{3,0,\rho} - 1 = 0 \tag{A.2d}$$

$$a_{1,1,\rho} + a_{2,1,\rho} + a_{3,0,\rho} + 2 = 0 \qquad b_{1,1,\rho} + b_{2,1,\rho} + b_{3,0,\rho} - 1 = 0 \tag{A.2e}$$

$$a_{1,1,\rho} + a_{2,1,\rho} + a_{3,1,\rho} + 6 = 0 \qquad b_{1,1,\rho} + b_{2,1,\rho} + b_{3,1,\rho} - 9 = 0 \tag{A.2f}$$

$$a_{1,1,\rho} + a_{2,0,\rho} + a_{3,1,\rho} + 10 = 0 \qquad b_{1,1,\rho} + b_{2,0,\rho} + b_{3,1,\rho} - 25 = 0 \tag{A.2g}$$

$$a_{1,1,\rho} + a_{2,0,\rho} + a_{3,0,\rho} + 14 = 0 \qquad b_{1,1,\rho} + b_{2,0,\rho} + b_{3,0,\rho} - 49 = 0 \tag{A.2h}$$

Then applying the Algorithm Q to Eqs. (A.2a)–(A.2h) yields:

iteration	:	seed			:	set
1	:	(A.2a),	(A.2b), (A.2c), (A.2e)		:	A_1
2	:	(A.2a),	(A.2b),	(A.2c), (A.2e)	:	—
3	:	(A.2b),	(A.2c),	(A.2d), (A.2e)	:	A_2
4	:	(A.2b), (A.2c),	(A.2d),	(A.2e)	:	—
5	:	(A.2d),	(A.2e),	(A.2f), (A.2g)	:	A_3
6	:	(A.2d), (A.2e),	(A.2f),	(A.2g)	:	—
7	:	(A.2d), (A.2f),	(A.2g),	(A.2h)	:	A_4
8	:	(A.2d), (A.2f), (A.2g),	(A.2h)		:	—

Therefore, q is equal to 4.

Then, the solutions for each set are:

$$
\begin{aligned}
A_1(\rho=1) \quad : \quad & \begin{cases}
a_{1,0,1} = 6 - a_{2,1,1} - a_{3,1,1} \\
a_{1,1,1} = -6 - a_{2,1,1} - a_{3,1,1} \\
a_{2,0,1} = 4 + a_{2,1,1} \\
a_{3,0,1} = 4 + a_{3,1,1} \\
b_{1,0,1} = 9 - b_{2,1,1} - b_{3,1,1} \\
b_{1,1,1} = -23 - b_{2,1,1} - b_{3,1,1} \\
b_{2,0,1} = 16 + b_{2,1,1} \\
b_{3,0,1} = 24 + b_{3,1,1}
\end{cases} \\
A_2(\rho=2) \quad : \quad & \begin{cases}
a_{1,0,2} = 6 - a_{2,1,2} - a_{3,1,2} \\
a_{1,1,2} = 2 - a_{2,1,2} - a_{3,1,2} \\
a_{2,0,2} = 4 + a_{2,1,2} \\
a_{3,0,2} = -4 + a_{3,1,2} \\
b_{1,0,2} = b_{1,1,2} = 9 - b_{2,1,2} - b_{3,1,2} \\
b_{2,0,2} = 16 + b_{2,1,2} \\
b_{3,0,2} = -8 + b_{3,1,2}
\end{cases} \\
A_3(\rho=3) \quad : \quad & \begin{cases}
a_{1,0,3} = -2 - a_{2,1,3} - a_{3,1,3} \\
a_{1,1,3} = -6 - a_{2,1,3} - a_{3,1,3} \\
a_{2,0,3} = -4 + a_{2,1,3} \\
a_{3,0,3} = 4 + a_{3,1,3} \\
b_{1,0,3} = b_{1,1,3} = 9 - b_{2,1,3} - b_{3,1,3} \\
b_{2,0,3} = 16 + b_{2,1,3} \\
b_{3,0,3} = -8 + b_{3,1,3}
\end{cases} \\
A_4(\rho=4) \quad : \quad & \begin{cases}
a_{1,0,4} = 6 - a_{2,1,4} - a_{3,1,4} \\
a_{1,1,4} = -6 - a_{2,1,4} - a_{3,1,4} \\
a_{2,0,4} = -4 + a_{2,1,4} \\
a_{3,0,4} = -4 + a_{3,1,4} \\
b_{1,0,4} = -23 - b_{2,1,4} - b_{3,1,4} \\
b_{1,1,4} = 9 - b_{2,1,4} - b_{3,1,4} \\
b_{2,0,4} = 16 + b_{2,1,4} \\
b_{3,0,4} = 24 + b_{3,1,4}
\end{cases}
\end{aligned}
$$

For $q = 4$, the cost function can be further written as:

$$
\begin{aligned}
& W(\boldsymbol{\lambda}) \\
= \; & \frac{1}{8\sqrt{\pi N_0}} \left(\int_{\lambda_0}^{\lambda_1} \left[(a_{1,0,1} + a_{2,0,1} + a_{3,0,1} - 14)r + (b_{1,0,1} + b_{2,0,1} + b_{3,0,1} - 49) \right]^2 e^{-(r+7)^2/N_0} dr \right. \\
& + \int_{\lambda_0}^{\lambda_1} \left[(a_{1,0,1} + a_{2,0,1} + a_{3,1,1} - 10)r + (b_{1,0,1} + b_{2,0,1} + b_{3,1,1} - 25) \right]^2 e^{-(r+5)^2/N_0} dr \\
& + \int_{\lambda_0}^{\lambda_1} \left[(a_{1,0,1} + a_{2,1,1} + a_{3,1,1} - 6)r + (b_{1,0,1} + b_{2,1,1} + b_{3,1,1} - 9) \right]^2 e^{-(r+3)^2/N_0} dr \\
& + \int_{\lambda_0}^{\lambda_1} \left[(a_{1,0,1} + a_{2,1,1} + a_{3,0,1} - 2)r + (b_{1,0,1} + b_{2,1,1} + b_{3,0,1} - 1) \right]^2 e^{-(r+1)^2/N_0} dr \\
& + \int_{\lambda_0}^{\lambda_1} \left[(a_{1,1,1} + a_{2,1,1} + a_{3,0,1} + 2)r + (b_{1,1,1} + b_{2,1,1} + b_{3,0,1} - 1) \right]^2 e^{-(r-1)^2/N_0} dr \\
& + \int_{\lambda_0}^{\lambda_1} \left[(a_{1,1,1} + a_{2,1,1} + a_{3,1,1} + 6)r + (b_{1,1,1} + b_{2,1,1} + b_{3,1,1} - 9) \right]^2 e^{-(r-3)^2/N_0} dr \\
& + \int_{\lambda_0}^{\lambda_1} \left[(a_{1,1,1} + a_{2,0,1} + a_{3,1,1} + 10)r + (b_{1,1,1} + b_{2,0,1} + b_{3,1,1} - 25) \right]^2 e^{-(r-5)^2/N_0} dr \\
& + \int_{\lambda_0}^{\lambda_1} \left[(a_{1,1,1} + a_{2,0,1} + a_{3,0,1} + 14)r + (b_{1,1,1} + b_{2,0,1} + b_{3,0,1} - 49) \right]^2 e^{-(r-7)^2/N_0} dr \\
& + \int_{\lambda_1}^{\lambda_2} \left[(a_{1,0,2} + a_{2,0,2} + a_{3,0,2} - 14)r + (b_{1,0,2} + b_{2,0,2} + b_{3,0,2} - 49) \right]^2 e^{-(r+7)^2/N_0} dr \\
& + \int_{\lambda_1}^{\lambda_2} \left[(a_{1,0,2} + a_{2,0,2} + a_{3,1,2} - 10)r + (b_{1,0,2} + b_{2,0,2} + b_{3,1,2} - 25) \right]^2 e^{-(r+5)^2/N_0} dr \\
& + \int_{\lambda_1}^{\lambda_2} \left[(a_{1,0,2} + a_{2,1,2} + a_{3,1,2} - 6)r + (b_{1,0,2} + b_{2,1,2} + b_{3,1,2} - 9) \right]^2 e^{-(r+3)^2/N_0} dr \\
& + \int_{\lambda_1}^{\lambda_2} \left[(a_{1,0,2} + a_{2,1,2} + a_{3,0,2} - 2)r + (b_{1,0,2} + b_{2,1,2} + b_{3,0,2} - 1) \right]^2 e^{-(r+1)^2/N_0} dr \\
& + \int_{\lambda_1}^{\lambda_2} \left[(a_{1,1,2} + a_{2,1,2} + a_{3,0,2} + 2)r + (b_{1,1,2} + b_{2,1,2} + b_{3,0,2} - 1) \right]^2 e^{-(r-1)^2/N_0} dr \\
& + \int_{\lambda_1}^{\lambda_2} \left[(a_{1,1,2} + a_{2,1,2} + a_{3,1,2} + 6)r + (b_{1,1,2} + b_{2,1,2} + b_{3,1,2} - 9) \right]^2 e^{-(r-3)^2/N_0} dr \\
& + \int_{\lambda_1}^{\lambda_2} \left[(a_{1,1,2} + a_{2,0,2} + a_{3,1,2} + 10)r + (b_{1,1,2} + b_{2,0,2} + b_{3,1,2} - 25) \right]^2 e^{-(r-5)^2/N_0} dr \\
& + \int_{\lambda_1}^{\lambda_2} \left[(a_{1,1,2} + a_{2,0,2} + a_{3,0,2} + 14)r + (b_{1,1,2} + b_{2,0,2} + b_{3,0,2} - 49) \right]^2 e^{-(r-7)^2/N_0} dr
\end{aligned}
$$

$$
\begin{aligned}
&+\int_{\lambda_2}^{\lambda_3}\left[(a_{1,0,3}+a_{2,0,3}+a_{3,0,3}-14)r+(b_{1,0,3}+b_{2,0,3}+b_{3,0,3}-49)\right]^2 e^{-(r+7)^2/N_0}dr\\
&+\int_{\lambda_2}^{\lambda_3}\left[(a_{1,0,3}+a_{2,0,3}+a_{3,1,3}-10)r+(b_{1,0,3}+b_{2,0,3}+b_{3,1,3}-25)\right]^2 e^{-(r+5)^2/N_0}dr\\
&+\int_{\lambda_2}^{\lambda_3}\left[(a_{1,0,3}+a_{2,1,3}+a_{3,1,3}-6)r+(b_{1,0,3}+b_{2,1,3}+b_{3,1,3}-9)\right]^2 e^{-(r+3)^2/N_0}dr\\
&+\int_{\lambda_2}^{\lambda_3}\left[(a_{1,0,3}+a_{2,1,3}+a_{3,0,3}-2)r+(b_{1,0,3}+b_{2,1,3}+b_{3,0,3}-1)\right]^2 e^{-(r+1)^2/N_0}dr\\
&+\int_{\lambda_2}^{\lambda_3}\left[(a_{1,1,3}+a_{2,1,3}+a_{3,0,3}+2)r+(b_{1,1,3}+b_{2,1,3}+b_{3,0,3}-1)\right]^2 e^{-(r-1)^2/N_0}dr\\
&+\int_{\lambda_2}^{\lambda_3}\left[(a_{1,1,3}+a_{2,1,3}+a_{3,1,3}+6)r+(b_{1,1,3}+b_{2,1,3}+b_{3,1,3}-9)\right]^2 e^{-(r-3)^2/N_0}dr\\
&+\int_{\lambda_2}^{\lambda_3}\left[(a_{1,1,3}+a_{2,0,3}+a_{3,1,3}+10)r+(b_{1,1,3}+b_{2,0,3}+b_{3,1,3}-25)\right]^2 e^{-(r-5)^2/N_0}dr\\
&+\int_{\lambda_2}^{\lambda_3}\left[(a_{1,1,3}+a_{2,0,3}+a_{3,0,3}+14)r+(b_{1,1,3}+b_{2,0,3}+b_{3,0,3}-49)\right]^2 e^{-(r-7)^2/N_0}dr\\
&+\int_{\lambda_3}^{\lambda_4}\left[(a_{1,0,4}+a_{2,0,4}+a_{3,0,4}-14)r+(b_{1,0,4}+b_{2,0,4}+b_{3,0,4}-49)\right]^2 e^{-(r+7)^2/N_0}dr\\
&+\int_{\lambda_3}^{\lambda_4}\left[(a_{1,0,4}+a_{2,0,4}+a_{3,1,4}-10)r+(b_{1,0,4}+b_{2,0,4}+b_{3,1,4}-25)\right]^2 e^{-(r+5)^2/N_0}dr\\
&+\int_{\lambda_3}^{\lambda_4}\left[(a_{1,0,4}+a_{2,1,4}+a_{3,1,4}-6)r+(b_{1,0,4}+b_{2,1,4}+b_{3,1,4}-9)\right]^2 e^{-(r+3)^2/N_0}dr\\
&+\int_{\lambda_3}^{\lambda_4}\left[(a_{1,0,4}+a_{2,1,4}+a_{3,0,4}-2)r+(b_{1,0,4}+b_{2,1,4}+b_{3,0,4}-1)\right]^2 e^{-(r+1)^2/N_0}dr\\
&+\int_{\lambda_3}^{\lambda_4}\left[(a_{1,1,4}+a_{2,1,4}+a_{3,0,4}+2)r+(b_{1,1,4}+b_{2,1,4}+b_{3,0,4}-1)\right]^2 e^{-(r-1)^2/N_0}dr\\
&+\int_{\lambda_3}^{\lambda_4}\left[(a_{1,1,4}+a_{2,1,4}+a_{3,1,4}+6)r+(b_{1,1,4}+b_{2,1,4}+b_{3,1,4}-9)\right]^2 e^{-(r-3)^2/N_0}dr\\
&+\int_{\lambda_3}^{\lambda_4}\left[(a_{1,1,4}+a_{2,0,4}+a_{3,1,4}+10)r+(b_{1,1,4}+b_{2,0,4}+b_{3,1,4}-25)\right]^2 e^{-(r-5)^2/N_0}dr\\
&+\int_{\lambda_3}^{\lambda_4}\left[(a_{1,1,4}+a_{2,0,4}+a_{3,0,4}+14)r+(b_{1,1,4}+b_{2,0,4}+b_{3,0,4}-49)\right]^2 e^{-(r-7)^2/N_0}dr\Bigg)
\end{aligned}
$$

$$
\begin{aligned}
= \; & \frac{8}{\sqrt{\pi N_0}} \left(\int_{-\infty}^{\lambda_1} (r+4)^2 \, e^{-(r+1)^2/N_0} dr + \int_{-\infty}^{\lambda_1} 16 e^{-(r-3)^2/N_0} dr \right. \\
& + \int_{-\infty}^{\lambda_1} (r-4)^2 \, e^{-(r-5)^2/N_0} dr + \int_{-\infty}^{\lambda_1} 4\,(r-2)^2 \, e^{-(r-7)^2/N_0} dr \\
& + \int_{\lambda_1}^{\lambda_2} (r+4)^2 \, e^{-(r+7)^2/N_0} dr + \int_{\lambda_1}^{\lambda_2} r^2 e^{-(r-3)^2/N_0} dr \\
& + \int_{\lambda_1}^{\lambda_2} 4r^2 e^{-(r-5)^2/N_0} dr + \int_{\lambda_1}^{\lambda_2} 4\,(r-2)^2 \, e^{-(r-7)^2/N_0} dr \\
& + \int_{\lambda_2}^{\lambda_3} 4\,(r+2)^2 \, e^{-(r+7)^2/N_0} dr + \int_{\lambda_2}^{\lambda_3} 4r^2 e^{-(r+5)^2/N_0} dr \\
& + \int_{\lambda_2}^{\lambda_3} r^2 e^{-(r+3)^2/N_0} dr + \int_{\lambda_2}^{\lambda_3} (r-4)^2 \, e^{-(r-7)^2/N_0} dr \\
& + \int_{\lambda_3}^{\infty} 4\,(r+2)^2 \, e^{-(r+7)^2/N_0} dr + \int_{\lambda_3}^{\infty} (r+4)^2 \, e^{-(r+5)^2/N_0} dr \\
& \left. + \int_{\lambda_3}^{\infty} 16 e^{-(r+3)^2/N_0} dr + \int_{\lambda_3}^{\infty} (r-4)^2 \, e^{-(r-1)^2/N_0} dr \right)
\end{aligned}
$$

The partial differentiations of the above cost function with respect to λ_1, λ_2 and λ_3 are:

$$
\begin{aligned}
\frac{\partial W(\boldsymbol{\lambda})}{\lambda_1} = \; & \frac{8}{\sqrt{\pi N_0}} \Big((\lambda_1+4)^2 \, e^{-(\lambda_1+1)^2/N_0} + 16 e^{-(\lambda_1-3)^2/N_0} \\
& + (\lambda_1-4)^2 \, e^{-(\lambda_1-5)^2/N_0} + 4\,(\lambda_1-2)^2 \, e^{-(\lambda_1-7)^2/N_0} \\
& - (\lambda_1+4)^2 \, e^{-(\lambda_1+7)^2/N_0} - \lambda_1^2 e^{-(\lambda_1-3)^2/N_0} \\
& - 4\lambda_1^2 e^{-(\lambda_1-5)^2/N_0} - 4\,(\lambda_1-2)^2 \, e^{-(\lambda_1-7)^2/N_0} \Big)
\end{aligned}
$$

$$
\begin{aligned}
\frac{\partial W(\boldsymbol{\lambda})}{\lambda_2} = \; & \frac{8}{\sqrt{\pi N_0}} \Big((\lambda_2+4)^2 \, e^{-(\lambda_2+7)^2/N_0} + \lambda_2^2 e^{-(\lambda_2-3)^2/N_0} \\
& + 4\lambda_2^2 e^{-(\lambda_2-5)^2/N_0} + 4\,(\lambda_2-2)^2 \, e^{-(\lambda_2-7)^2/N_0} \\
& - 4\,(\lambda_2+2)^2 \, e^{-(\lambda_2+7)^2/N_0} - 4\lambda_2^2 e^{-(\lambda_2+5)^2/N_0} \\
& - \lambda_2^2 e^{-(\lambda_2+3)^2/N_0} - (\lambda_2-4)^2 \, e^{-(\lambda_2-7)^2/N_0} \Big)
\end{aligned}
$$

$$\begin{aligned}\frac{\partial W(\boldsymbol{\lambda})}{\lambda_3} &= \frac{8}{\sqrt{\pi N_0}}\Big(4\left(\lambda_3+2\right)^2 e^{-(\lambda_3+7)^2/N_0}+4\lambda_3^2 e^{-(\lambda_3+5)^2/N_0}\\ &\quad +\lambda_3^2 e^{-(\lambda_3+3)^2/N_0}+\left(\lambda_3-4\right)^2 e^{-(\lambda_3-7)^2/N_0}\\ &\quad -4\left(\lambda_3+2\right)^2 e^{-(\lambda_3+7)^2/N_0}-\left(\lambda_3+4\right)^2 e^{-(\lambda_3+5)^2/N_0}\\ &\quad -16e^{-(\lambda_3+3)^2/N_0}-\left(\lambda_3-4\right)^2 e^{-(\lambda_3-1)^2/N_0}\Big).\end{aligned}$$

By setting the above equations to be zero we have $\lambda_1 = -4$, $\lambda_2 = 0$, and $\lambda_3 = 4$ which minimize the cost function. Consequently, the cost function is reduced to

$$\begin{aligned}W(f_1,f_2,f_3) &= \frac{8}{\sqrt{\pi N_0}}\Big(\int_{-\infty}^{-4}(r+4)^2 e^{-(r+1)^2/N_0}dr+\int_{-\infty}^{-4}16e^{-(r-3)^2/N_0}dr\\ &\quad +\int_{-\infty}^{-4}(r-4)^2 e^{-(r-5)^2/N_0}dr+\int_{-\infty}^{-4}4\left(r-2\right)^2 e^{-(r-7)^2/N_0}dr\\ &\quad +\int_{-4}^{0}(r+4)^2 e^{-(r+7)^2/N_0}dr+\int_{-4}^{0}r^2 e^{-(r-3)^2/N_0}dr\\ &\quad +\int_{-4}^{0}4r^2 e^{-(r-5)^2/N_0}dr+\int_{-4}^{0}4\left(r-2\right)^2 e^{-(r-7)^2/N_0}dr\\ &\quad +\int_{0}^{4}4\left(r+2\right)^2 e^{-(r+7)^2/N_0}dr+\int_{0}^{4}4r^2 e^{-(r+5)^2/N_0}dr\\ &\quad +\int_{0}^{4}r^2 e^{-(r+3)^2/N_0}dr+\int_{0}^{4}(r-4)^2 e^{-(r-7)^2/N_0}dr\\ &\quad +\int_{4}^{\infty}4\left(r+2\right)^2 e^{-(r+7)^2/N_0}dr+\int_{4}^{\infty}(r+4)^2 e^{-(r+5)^2/N_0}dr\\ &\quad +\int_{4}^{\infty}16e^{-(r+3)^2/N_0}dr+\int_{4}^{\infty}(r-4)^2 e^{-(r-1)^2/N_0}dr\Big)\\ &= \frac{88\sqrt{N_0}}{\sqrt{\pi}}e^{-81/N_0}-\frac{112\sqrt{N_0}}{\sqrt{\pi}}e^{-49/N_0}-\frac{160\sqrt{N_0}}{\sqrt{\pi}}e^{-25/N_0}-\frac{72\sqrt{N_0}}{\sqrt{\pi}}e^{-9/N_0}\\ &\quad +12(18+N_0)\operatorname{erfc}\left(\frac{3}{\sqrt{N_0}}\right)+16(50+N_0)\operatorname{erfc}\left(\frac{5}{\sqrt{N_0}}\right)\\ &\quad +8(98+N_0)\operatorname{erfc}\left(\frac{7}{\sqrt{N_0}}\right)-12(66+N_0)\operatorname{erfc}\left(\frac{9}{\sqrt{N_0}}\right).\end{aligned}$$

We summarize the bit-wise metrics as follows.

$$\rho=\begin{cases}1, & \text{if } r\le -4;\\ 2, & \text{if } -4<r\le 0;\\ 3, & \text{if } 0<r\le 4;\\ 4, & \text{if } r>4\end{cases}$$

$$
\begin{aligned}
f_1(r,c) &= \frac{1}{3}r^2 + a_{1,c,\rho}r + b_{1,c,\rho} \\
&= \frac{1}{3}r^2 + [-a_{2,1,\rho} - a_{3,1,\rho} - 2(1-2c) + 8(1-2c)\cdot \mathbf{1}\{(1-2c)r \le 0 \vee (1-2c)r \ge 4\}]\, r \\
&\quad +[(9 - b_{2,1,\rho} - b_{3,1,\rho}) - 32\cdot \mathbf{1}\{(1-2c)r \ge 4\}] \\
f_2(r,c) &= \frac{1}{3}r^2 + a_{2,c,\rho}r + b_{2,c,\rho} \\
&= \frac{1}{3}r^2 + [a_{2,1,\rho} - 4(1-c)\cdot \mathrm{sgn}(r)]r + [b_{2,1,\rho} + 16(1-c)] \\
f_3(r,c) &= \frac{1}{3}r^2 + a_{3,c,\rho}r + b_{3,c,\rho} \\
&= \frac{1}{3}r^2 + [a_{3,1,\rho} - (4 - 8\cdot \mathrm{u}(-|r|\cdot(|r|-4)))(1-c)\cdot \mathrm{sgn}(r)]r \\
&\quad +[b_{3,1,\rho} + (-8 + 32\cdot \mathrm{u}(|r|-4))(1-c)]
\end{aligned}
$$

By the nature of Viterbi algorithm, only those terms that depend on c affect the decoding behavior. Hence, the equivalent bit-wise metrics are:

$$
\begin{aligned}
f_1^{\mathrm{eq}}(r,c) &= -2(1-2c)r + 8(1-2c)r\cdot \mathbf{1}\{(1-2c)r \le 0 \vee (1-2c)r \ge 4\} - 32\cdot \mathbf{1}\{(1-2c)r \ge 4\} \\
f_2^{\mathrm{eq}}(r,c) &= -4(1-c)|r| + 16(1-c) \\
f_3^{\mathrm{eq}}(r,c) &= -(4 - 8\cdot \mathrm{u}(-|r|\cdot(|r|-4)))(1-c)|r| + (-8 + 32\cdot \mathrm{u}(|r|-4))(1-c).
\end{aligned}
$$

Since the branch metric of Viterbi algorithm can be the relative metric between information bits 0 and 1, the above metrics can be further reduced to

$$
\begin{cases}
f_1^{\mathrm{64QAM}}(c,r) &= c(|r-4| + |r| + |r+4| - 8)\cdot \mathrm{sgn}(-r) \\
f_2^{\mathrm{64QAM}}(c,r) &= c(|4 - |r||)\cdot \mathrm{sgn}(|r|-4) \\
f_3^{\mathrm{64QAM}}(c,r) &= c(||r|-4| - 2)
\end{cases}
$$

Finally, we can use the nature of recursive from 16QAM's metrics to represent 64QAM's metrics.

$$
\begin{cases}
f_1^{\mathrm{64QAM}}(c,r) &= c(|r-4| + |r| + |r+4| - 8)\cdot \mathrm{sgn}(-r) \\
f_2^{\mathrm{64QAM}}(c,r) &= f_1^{\mathrm{16QAM}}(c, 4 - |r|) \\
f_3^{\mathrm{64QAM}}(c,r) &= f_2^{\mathrm{16QAM}}(c, |r|-4)
\end{cases}
$$

A.2 Derivation of Bit-wise Metric of 256QAM Modulation

Suppose that Gray code mapping is employed for 256QAM mapping, i.e., -15, -13, -11, -9, -7, -5, -3, -1, $+1$, $+3$, $+5$, $+7$, $+9$, $+11$, $+13$ and $+15$ respectively map to 0000, 0001, 0011, 0010, 0110, 0111, 0101, 0100,1100, 1101, 1111, 1110, 1010, 1011, 1001, and 1000. Then the squared error criterion (or cost function) is given by

$$
\begin{aligned}
& W(f_1, f_2, f_3, f_4) \\
= \; & \frac{1}{16\sqrt{\pi N_0}} \left(\int_{-\infty}^{\infty} \left[f_1(r,0) + f_2(r,0) + f_3(r,0) + f_4(r,0) - (r+15)^2 \right]^2 e^{-(r_1+15)^2/N_0} dr \right. \\
& + \int_{-\infty}^{\infty} \left[f_1(r,0) + f_2(r,0) + f_3(r,0) + f_4(r,1) - (r+13)^2 \right]^2 e^{-(r_1+13)^2/N_0} dr \\
& + \int_{-\infty}^{\infty} \left[f_1(r,0) + f_2(r,0) + f_3(r,1) + f_4(r,1) - (r+11)^2 \right]^2 e^{-(r_1+11)^2/N_0} dr \\
& + \int_{-\infty}^{\infty} \left[f_1(r,0) + f_2(r,0) + f_3(r,1) + f_4(r,0) - (r+9)^2 \right]^2 e^{-(r_1+9)^2/N_0} dr \\
& + \int_{-\infty}^{\infty} \left[f_1(r,0) + f_2(r,1) + f_3(r,1) + f_4(r,0) - (r+7)^2 \right]^2 e^{-(r_1+7)^2/N_0} dr \\
& + \int_{-\infty}^{\infty} \left[f_1(r,0) + f_2(r,1) + f_3(r,1) + f_4(r,1) - (r+5)^2 \right]^2 e^{-(r_1+5)^2/N_0} dr \\
& + \int_{-\infty}^{\infty} \left[f_1(r,0) + f_2(r,1) + f_3(r,0) + f_4(r,1) - (r+3)^2 \right]^2 e^{-(r_1+3)^2/N_0} dr \\
& + \int_{-\infty}^{\infty} \left[f_1(r,0) + f_2(r,1) + f_3(r,0) + f_4(r,0) - (r+1)^2 \right]^2 e^{-(r_1+1)^2/N_0} dr \\
& + \int_{-\infty}^{\infty} \left[f_1(r,1) + f_2(r,1) + f_3(r,0) + f_4(r,0) - (r-1)^2 \right]^2 e^{-(r_1-1)^2/N_0} dr \\
& + \int_{-\infty}^{\infty} \left[f_1(r,1) + f_2(r,1) + f_3(r,0) + f_4(r,1) - (r-3)^2 \right]^2 e^{-(r_1-3)^2/N_0} dr \\
& + \int_{-\infty}^{\infty} \left[f_1(r,1) + f_2(r,1) + f_3(r,1) + f_4(r,1) - (r-5)^2 \right]^2 e^{-(r_1-5)^2/N_0} dr \\
& + \int_{-\infty}^{\infty} \left[f_1(r,1) + f_2(r,1) + f_3(r,1) + f_4(r,0) - (r-7)^2 \right]^2 e^{-(r_1-7)^2/N_0} dr \\
& + \int_{-\infty}^{\infty} \left[f_1(r,1) + f_2(r,0) + f_3(r,1) + f_4(r,0) - (r-9)^2 \right]^2 e^{-(r_1-9)^2/N_0} dr \\
& + \int_{-\infty}^{\infty} \left[f_1(r,1) + f_2(r,0) + f_3(r,1) + f_4(r,1) - (r-11)^2 \right]^2 e^{-(r_1-11)^2/N_0} dr \\
& + \int_{-\infty}^{\infty} \left[f_1(r,1) + f_2(r,0) + f_3(r,0) + f_4(r,1) - (r-13)^2 \right]^2 e^{-(r_1-13)^2/N_0} dr \\
& \left. + \int_{-\infty}^{\infty} \left[f_1(r,1) + f_2(r,0) + f_3(r,0) + f_4(r,0) - (r-15)^2 \right]^2 e^{-(r_1-15)^2/N_0} dr \right),
\end{aligned}
$$

where N_0 is the single-sided noise power per hertz. substituting (A.1) into the above cost function, we obtain

$$
\begin{aligned}
W(f_1,f_2,f_3,f_4) &= \frac{1}{16\sqrt{\pi N_0}}\left(\sum_{\rho=1}^{q}\int_{\lambda_{\rho-1}}^{\lambda_\rho}[(a_{1,0,\rho}+a_{2,0,\rho}+a_{3,0,\rho}+a_{4,0,\rho}-30)r\right.\\
&+(b_{1,0,\rho}+b_{2,0,\rho}+b_{3,0,\rho}+b_{4,0,\rho}-225)]^2e^{-(r+15)^2/N_0}dr\\
&+\sum_{\rho=1}^{q}\int_{\lambda_{\rho-1}}^{\lambda_\rho}[(a_{1,0,\rho}+a_{2,0,\rho}+a_{3,0,\rho}+a_{4,1,\rho}-26)r\\
&+(b_{1,0,\rho}+b_{2,0,\rho}+b_{3,0,\rho}+b_{4,1,\rho}-169)]^2e^{-(r+13)^2/N_0}dr\\
&+\sum_{\rho=1}^{q}\int_{\lambda_{\rho-1}}^{\lambda_\rho}[(a_{1,0,\rho}+a_{2,0,\rho}+a_{3,1,\rho}+a_{4,1,\rho}-22)r\\
&+(b_{1,0,\rho}+b_{2,0,\rho}+b_{3,1,\rho}+b_{4,1,\rho}-121)]^2e^{-(r+11)^2/N_0}dr\\
&+\sum_{\rho=1}^{q}\int_{\lambda_{\rho-1}}^{\lambda_\rho}[(a_{1,0,\rho}+a_{2,0,\rho}+a_{3,1,\rho}+a_{4,0,\rho}-18)r\\
&+(b_{1,0,\rho}+b_{2,0,\rho}+b_{3,1,\rho}+b_{4,0,\rho}-81)]^2e^{-(r+9)^2/N_0}dr\\
&+\sum_{\rho=1}^{q}\int_{\lambda_{\rho-1}}^{\lambda_\rho}[(a_{1,0,\rho}+a_{2,1,\rho}+a_{3,1,\rho}+a_{4,0,\rho}-14)r\\
&+(b_{1,0,\rho}+b_{2,1,\rho}+b_{3,1,\rho}+b_{4,0,\rho}-49)]^2e^{-(r+7)^2/N_0}dr\\
&+\sum_{\rho=1}^{q}\int_{\lambda_{\rho-1}}^{\lambda_\rho}[(a_{1,0,\rho}+a_{2,1,\rho}+a_{3,1,\rho}+a_{4,1,\rho}-10)r\\
&+(b_{1,0,\rho}+b_{2,1,\rho}+b_{3,1,\rho}+b_{4,1,\rho}-25)]^2e^{-(r+5)^2/N_0}dr\\
&+\sum_{\rho=1}^{q}\int_{\lambda_{\rho-1}}^{\lambda_\rho}[(a_{1,0,\rho}+a_{2,1,\rho}+a_{3,0,\rho}+a_{4,1,\rho}-6)r\\
&+(b_{1,0,\rho}+b_{2,1,\rho}+b_{3,0,\rho}+b_{4,1,\rho}-9)]^2e^{-(r+3)^2/N_0}dr\\
&+\sum_{\rho=1}^{q}\int_{\lambda_{\rho-1}}^{\lambda_\rho}[(a_{1,0,\rho}+a_{2,1,\rho}+a_{3,0,\rho}+a_{4,0,\rho}-2)r\\
&+(b_{1,0,\rho}+b_{2,1,\rho}+b_{3,0,\rho}+b_{4,0,\rho}-1)]^2e^{-(r+1)^2/N_0}dr\\
&+\sum_{\rho=1}^{q}\int_{\lambda_{\rho-1}}^{\lambda_\rho}[(a_{1,1,\rho}+a_{2,1,\rho}+a_{3,0,\rho}+a_{4,0,\rho}+2)r\\
&+(b_{1,1,\rho}+b_{2,1,\rho}+b_{3,0,\rho}+b_{4,0,\rho}-1)]^2e^{-(r-1)^2/N_0}dr\\
&+\sum_{\rho=1}^{q}\int_{\lambda_{\rho-1}}^{\lambda_\rho}[(a_{1,1,\rho}+a_{2,1,\rho}+a_{3,0,\rho}+a_{4,1,\rho}+6)r\\
&+(b_{1,1,\rho}+b_{2,1,\rho}+b_{3,0,\rho}+b_{4,1,\rho}-9)]^2e^{-(r-3)^2/N_0}dr\\
&+\sum_{\rho=1}^{q}\int_{\lambda_{\rho-1}}^{\lambda_\rho}[(a_{1,1,\rho}+a_{2,1,\rho}+a_{3,1,\rho}+a_{4,1,\rho}+10)r\\
&+(b_{1,1,\rho}+b_{2,1,\rho}+b_{3,1,\rho}+b_{4,1,\rho}-25)]^2e^{-(r-5)^2/N_0}dr
\end{aligned}
$$

$$+\sum_{\rho=1}^{q}\int_{\lambda_{\rho-1}}^{\lambda_\rho}[(a_{1,1,\rho}+a_{2,1,\rho}+a_{3,1,\rho}+a_{4,0,\rho}+14)r$$
$$+(b_{1,1,\rho}+b_{2,1,\rho}+b_{3,1,\rho}+b_{4,0,\rho}-49)]^2e^{-(r-7)^2/N_0}dr$$
$$+\sum_{\rho=1}^{q}\int_{\lambda_{\rho-1}}^{\lambda_\rho}[(a_{1,1,\rho}+a_{2,0,\rho}+a_{3,1,\rho}+a_{4,0,\rho}+18)r$$
$$+(b_{1,1,\rho}+b_{2,0,\rho}+b_{3,1,\rho}+b_{4,0,\rho}-81)]^2e^{-(r-9)^2/N_0}dr$$
$$+\sum_{\rho=1}^{q}\int_{\lambda_{\rho-1}}^{\lambda_\rho}[(a_{1,1,\rho}+a_{2,0,\rho}+a_{3,1,\rho}+a_{4,1,\rho}+22)r$$
$$+(b_{1,1,\rho}+b_{2,0,\rho}+b_{3,1,\rho}+b_{4,1,\rho}-121)]^2e^{-(r-11)^2/N_0}dr$$
$$+\sum_{\rho=1}^{q}\int_{\lambda_{\rho-1}}^{\lambda_\rho}[(a_{1,1,\rho}+a_{2,0,\rho}+a_{3,0,\rho}+a_{4,1,\rho}+26)r$$
$$+(b_{1,1,\rho}+b_{2,0,\rho}+b_{3,0,\rho}+b_{4,1,\rho}-169)]^2e^{-(r-13)^2/N_0}dr$$
$$+\sum_{\rho=1}^{q}\int_{\lambda_{\rho-1}}^{\lambda_\rho}[(a_{1,1,\rho}+a_{2,0,\rho}+a_{3,0,\rho}+a_{4,0,\rho}+30)r$$
$$+(b_{1,1,\rho}+b_{2,0,\rho}+b_{3,0,\rho}+b_{4,0,\rho}-225)]^2e^{-(r-15)^2/N_0}dr\Big).$$

For each ρ, we can list the equations involving in the above cost function as follows:

$$a_{1,0,\rho} + a_{2,0,\rho} + a_{3,0,\rho} + a_{4,0,\rho} - 30 = 0 \qquad b_{1,0,\rho} + b_{2,0,\rho} + b_{3,0,\rho} + b_{4,0,\rho} - 225 = 0 \quad \text{(A.3a)}$$

$$a_{1,0,\rho} + a_{2,0,\rho} + a_{3,0,\rho} + a_{4,1,\rho} - 26 = 0 \qquad b_{1,0,\rho} + b_{2,0,\rho} + b_{3,0,\rho} + b_{4,1,\rho} - 169 = 0 \quad \text{(A.3b)}$$

$$a_{1,0,\rho} + a_{2,0,\rho} + a_{3,1,\rho} + a_{4,1,\rho} - 22 = 0 \qquad b_{1,0,\rho} + b_{2,0,\rho} + b_{3,1,\rho} + b_{4,1,\rho} - 121 = 0 \quad \text{(A.3c)}$$

$$a_{1,0,\rho} + a_{2,0,\rho} + a_{3,1,\rho} + a_{4,0,\rho} - 18 = 0 \qquad b_{1,0,\rho} + b_{2,0,\rho} + b_{3,1,\rho} + b_{4,0,\rho} - 81 = 0 \quad \text{(A.3d)}$$

$$a_{1,0,\rho} + a_{2,1,\rho} + a_{3,1,\rho} + a_{4,0,\rho} - 14 = 0 \qquad b_{1,0,\rho} + b_{2,1,\rho} + b_{3,1,\rho} + b_{4,0,\rho} - 49 = 0 \quad \text{(A.3e)}$$

$$a_{1,0,\rho} + a_{2,1,\rho} + a_{3,1,\rho} + a_{4,1,\rho} - 10 = 0 \qquad b_{1,0,\rho} + b_{2,1,\rho} + b_{3,1,\rho} + b_{4,1,\rho} - 25 = 0 \quad \text{(A.3f)}$$

$$a_{1,0,\rho} + a_{2,1,\rho} + a_{3,0,\rho} + a_{4,1,\rho} - 6 = 0 \qquad b_{1,0,\rho} + b_{2,1,\rho} + b_{3,0,\rho} + b_{4,1,\rho} - 9 = 0 \quad \text{(A.3g)}$$

$$a_{1,0,\rho} + a_{2,1,\rho} + a_{3,0,\rho} + a_{4,0,\rho} - 2 = 0 \qquad b_{1,0,\rho} + b_{2,1,\rho} + b_{3,0,\rho} + b_{4,0,\rho} - 1 = 0 \quad \text{(A.3h)}$$

$$a_{1,1,\rho} + a_{2,1,\rho} + a_{3,0,\rho} + a_{4,0,\rho} + 2 = 0 \qquad b_{1,1,\rho} + b_{2,1,\rho} + b_{3,0,\rho} + b_{4,0,\rho} - 1 = 0 \quad \text{(A.3i)}$$

$$a_{1,1,\rho} + a_{2,1,\rho} + a_{3,0,\rho} + a_{4,1,\rho} + 6 = 0 \qquad b_{1,1,\rho} + b_{2,1,\rho} + b_{3,0,\rho} + b_{4,1,\rho} - 9 = 0 \quad \text{(A.3j)}$$

$$a_{1,1,\rho} + a_{2,1,\rho} + a_{3,1,\rho} + a_{4,1,\rho} + 10 = 0 \qquad b_{1,1,\rho} + b_{2,1,\rho} + b_{3,1,\rho} + b_{4,1,\rho} - 25 = 0 \quad \text{(A.3k)}$$

$$a_{1,1,\rho} + a_{2,1,\rho} + a_{3,1,\rho} + a_{4,0,\rho} + 14 = 0 \qquad b_{1,1,\rho} + b_{2,1,\rho} + b_{3,1,\rho} + b_{4,0,\rho} - 49 = 0 \quad \text{(A.3l)}$$

$$a_{1,1,\rho} + a_{2,0,\rho} + a_{3,1,\rho} + a_{4,0,\rho} + 18 = 0 \qquad b_{1,1,\rho} + b_{2,0,\rho} + b_{3,1,\rho} + b_{4,0,\rho} - 81 = 0 \quad \text{(A.3m)}$$

$$a_{1,1,\rho} + a_{2,0,\rho} + a_{3,1,\rho} + a_{4,1,\rho} + 22 = 0 \qquad b_{1,1,\rho} + b_{2,0,\rho} + b_{3,1,\rho} + b_{4,1,\rho} - 121 = 0 \quad \text{(A.3n)}$$

$$a_{1,1,\rho} + a_{2,0,\rho} + a_{3,0,\rho} + a_{4,1,\rho} + 26 = 0 \qquad b_{1,1,\rho} + b_{2,0,\rho} + b_{3,0,\rho} + b_{4,1,\rho} - 169 = 0 \quad \text{(A.3o)}$$

$$a_{1,1,\rho} + a_{2,0,\rho} + a_{3,0,\rho} + a_{4,0,\rho} + 30 = 0 \qquad b_{1,1,\rho} + b_{2,0,\rho} + b_{3,0,\rho} + b_{4,0,\rho} - 225 = 0 \quad \text{(A.3p)}$$

Then applying the Algorithm Q to Eqs. (A.3a)–(A.3p) yields:

iteration	:			seed			: set
1	:			(A.3a),	(A.3b), (A.3c), (A.3e), (A.3i)		: A_1
2	:		(A.3a),	(A.3b),	(A.3c), (A.3e), (A.3i)		: —
3	:		(A.3b),	(A.3c),	(A.3d), (A.3e), (A.3i)		: A_2
4	:	(A.3b),	(A.3c),	(A.3d),	(A.3e), (A.3i)		: —
5	:		(A.3d),	(A.3e),	(A.3f), (A.3g), (A.3i)		: A_3
6	:		(A.3d), (A.3e),	(A.3f),	(A.3g), (A.3i)		: —
7	:		(A.3d), (A.3f),	(A.3g),	(A.3h), (A.3i)		: A_4
8	:	(A.3d),	(A.3f),	(A.3g),	(A.3h),	(A.3i)	: —
9	:			(A.3h)	(A.3i),	(A.3j), (A.3k), (A.3m)	: A_5
10	:			(A.3h), (A.3i),	(A.3j),	(A.3k), (A.3m)	: —
11	:			(A.3h), (A.3j),	(A.3k),	(A.3l), (A.3m)	: A_6
12	:		(A.3h),	(A.3j),	(A.3k),	(A.3l), (A.3m)	: —
13	:			(A.3h), (A.3l),	(A.3m),	(A.3n), (A.3o)	: A_7
14	:		(A.3h),	(A.3l),	(A.3m),	(A.3n), (A.3o)	: —
15	:		(A.3h),	(A.3l),	(A.3n),	(A.3o), (A.3p)	: A_8
16	:	(A.3h),	(A.3l),	(A.3n),	(A.3o),	(A.3p)	: —

Therefore, q is equal to 8.

Then the solutions for each set are:

$$
A_1(\rho=1) \quad : \quad \begin{cases}
a_{1,0,1} = 10 - a_{2,1,1} - a_{3,1,1} - a_{4,1,1} \\
a_{1,1,1} = -10 - a_{2,1,1} - a_{3,1,1} - a_{4,1,1} \\
a_{2,0,1} = 12 + a_{2,1,1} \\
a_{3,0,1} = 4 + a_{3,1,1} \\
a_{4,0,1} = 4 + a_{4,1,1} \\
b_{1,0,1} = -7 - b_{2,1,1} - b_{3,1,1} - b_{4,1,1} \\
b_{1,1,1} = -103 - b_{2,1,1} - b_{3,1,1} - b_{4,1,1} \\
b_{2,0,1} = 128 + b_{2,1,1} \\
b_{3,0,1} = 48 + b_{3,1,1} \\
b_{4,0,1} = 56 + b_{4,1,1}
\end{cases}
$$

$$
A_2(\rho=2) \quad : \quad \begin{cases}
a_{1,0,2} = 18 - a_{2,1,2} - a_{3,1,2} - a_{4,1,2} \\
a_{1,1,2} = -2 - a_{2,1,2} - a_{3,1,2} - a_{4,1,2} \\
a_{2,0,2} = 4 + a_{2,1,2} \\
a_{3,0,2} = 4 + a_{3,1,2} \\
a_{4,0,2} = -4 + a_{4,1,2} \\
b_{1,0,2} = 89 - b_{2,1,2} - b_{3,1,2} - b_{4,1,2} \\
b_{1,1,2} = -7 - b_{2,1,2} - b_{3,1,2} - b_{4,1,2} \\
b_{2,0,2} = 32 + b_{2,1,2} \\
b_{3,0,2} = 48 + b_{3,1,2} \\
b_{4,0,2} = -40 + b_{4,1,2}
\end{cases}
$$

$$
A_3(\rho=3) \quad : \quad \begin{cases}
a_{1,0,3} = 10 - a_{2,1,3} - a_{3,1,3} - a_{4,1,3} \\
a_{1,1,3} = -2 - a_{2,1,3} - a_{3,1,3} - a_{4,1,3} \\
a_{2,0,3} = 4 + a_{2,1,3} \\
a_{3,0,3} = -4 + a_{3,1,3} \\
a_{4,0,3} = 4 + a_{4,1,3} \\
b_{1,0,3} = 25 - b_{2,1,3} - b_{3,1,3} - b_{4,1,3} \\
b_{1,1,3} = -7 - b_{2,1,3} - b_{3,1,3} - b_{4,1,3} \\
b_{2,0,3} = 32 + b_{2,1,3} \\
b_{3,0,3} = -16 + b_{3,1,3} \\
b_{4,0,3} = 24 + b_{4,1,3}
\end{cases}
$$

$$
\begin{aligned}
A_4(\rho=4) \quad : \quad & \begin{cases}
a_{1,0,4} = 10 - a_{2,1,4} - a_{3,1,4} - a_{4,1,4} \\
a_{1,1,4} = 6 - a_{2,1,4} - a_{3,1,4} - a_{4,1,4} \\
a_{2,0,4} = 12 + a_{2,1,4} \\
a_{3,0,4} = -4 + a_{3,1,4} \\
a_{4,0,4} = -4 + a_{4,1,4} \\
b_{1,0,4} = 25 - b_{2,1,4} - b_{3,1,4} - b_{4,1,4} \\
b_{1,1,4} = 25 - b_{2,1,4} - b_{3,1,4} - b_{4,1,4} \\
b_{2,0,4} = 64 + b_{2,1,4} \\
b_{3,0,4} = -16 + b_{3,1,4} \\
b_{4,0,4} = -8 + b_{4,1,4}
\end{cases} \\
A_5(\rho=5) \quad : \quad & \begin{cases}
a_{1,0,5} = -6 - a_{2,1,5} - a_{3,1,5} - a_{4,1,5} \\
a_{1,1,5} = -10 - a_{2,1,5} - a_{3,1,5} - a_{4,1,5} \\
a_{2,0,5} = -12 + a_{2,1,5} \\
a_{3,0,5} = 4 + a_{3,1,5} \\
a_{4,0,5} = 4 + a_{4,1,5} \\
b_{1,0,5} = 25 - b_{2,1,5} - b_{3,1,5} - b_{4,1,5} \\
b_{1,1,5} = 25 - b_{2,1,5} - b_{3,1,5} - b_{4,1,5} \\
b_{2,0,5} = 64 + b_{2,1,5} \\
b_{3,0,5} = -16 + b_{3,1,5} \\
b_{4,0,5} = -8 + b_{4,1,5}
\end{cases} \\
A_6(\rho=6) \quad : \quad & \begin{cases}
a_{1,0,6} = 2 - a_{2,1,6} - a_{3,1,6} - a_{4,1,6} \\
a_{1,1,6} = -10 - a_{2,1,6} - a_{3,1,6} - a_{4,1,6} \\
a_{2,0,6} = -4 + a_{2,1,6} \\
a_{3,0,6} = 4 + a_{3,1,6} \\
a_{4,0,6} = -4 + a_{4,1,6} \\
b_{1,0,6} = -7 - b_{2,1,6} - b_{3,1,6} - b_{4,1,6} \\
b_{1,1,6} = 25 - b_{2,1,6} - b_{3,1,6} - b_{4,1,6} \\
b_{2,0,6} = 32 + b_{2,1,6} \\
b_{3,0,6} = -16 + b_{3,1,6} \\
b_{4,0,6} = 24 + b_{4,1,6}
\end{cases}
\end{aligned}
$$

$$A_7(\rho=7) \quad : \quad \begin{cases} a_{1,0,7} = 2 - a_{2,1,7} - a_{3,1,7} - a_{4,1,7} \\ a_{1,1,7} = -18 - a_{2,1,7} - a_{3,1,7} - a_{4,1,7} \\ a_{2,0,7} = -4 + a_{2,1,7} \\ a_{3,0,7} = -4 + a_{3,1,7} \\ a_{4,0,7} = 4 + a_{4,1,7} \\ b_{1,0,7} = -7 - b_{2,1,7} - b_{3,1,7} - b_{4,1,7} \\ b_{1,1,7} = 89 - b_{2,1,7} - b_{3,1,7} - b_{4,1,7} \\ b_{2,0,7} = 32 + b_{2,1,7} \\ b_{3,0,7} = 48 + b_{3,1,7} \\ b_{4,0,7} = -40 + b_{4,1,7} \end{cases}$$

$$A_8(\rho=8) \quad : \quad \begin{cases} a_{1,0,8} = 10 - a_{2,1,8} - a_{3,1,8} - a_{4,1,8} \\ a_{1,1,8} = -10 - a_{2,1,8} - a_{3,1,8} - a_{4,1,8} \\ a_{2,0,8} = -12 + a_{2,1,8} \\ a_{3,0,8} = -4 + a_{3,1,8} \\ a_{4,0,8} = -4 + a_{4,1,8} \\ b_{1,0,8} = -103 - b_{2,1,8} - b_{3,1,8} - b_{4,1,8} \\ b_{1,1,8} = -7 - b_{2,1,8} - b_{3,1,8} - b_{4,1,8} \\ b_{2,0,8} = 128 + b_{2,1,8} \\ b_{3,0,8} = 48 + b_{3,1,8} \\ b_{4,0,8} = 56 + b_{4,1,8} \end{cases}$$

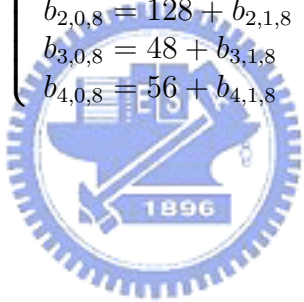

For $q = 8$, the cost function can be further written as:

$$W(\boldsymbol{\lambda}) = \frac{1}{16\sqrt{\pi N_0}}$$
$$\left(\int_{\lambda_0}^{\lambda_1}[(a_{1,0,1}+a_{2,0,1}+a_{3,0,1}+a_{4,0,1}-30)r+(b_{1,0,1}+b_{2,0,1}+b_{3,0,1}+b_{4,0,1}-225)]^2 e^{-(r+15)^2/N_0}dr\right.$$
$$+\int_{\lambda_0}^{\lambda_1}[(a_{1,0,1}+a_{2,0,1}+a_{3,0,1}+a_{4,1,1}-26)r+(b_{1,0,1}+b_{2,0,1}+b_{3,0,1}+b_{4,1,1}-169)]^2 e^{-(r+13)^2/N_0}dr$$
$$+\int_{\lambda_0}^{\lambda_1}[(a_{1,0,1}+a_{2,0,1}+a_{3,1,1}+a_{4,1,1}-22)r+(b_{1,0,1}+b_{2,0,1}+b_{3,1,1}+b_{4,1,1}-121)]^2 e^{-(r+11)^2/N_0}dr$$
$$+\int_{\lambda_0}^{\lambda_1}[(a_{1,0,1}+a_{2,0,1}+a_{3,1,1}+a_{4,0,1}-18)r+(b_{1,0,1}+b_{2,0,1}+b_{3,1,1}+b_{4,0,1}-81)]^2 e^{-(r+9)^2/N_0}dr$$
$$+\int_{\lambda_0}^{\lambda_1}[(a_{1,0,1}+a_{2,1,1}+a_{3,1,1}+a_{4,0,1}-14)r+(b_{1,0,1}+b_{2,1,1}+b_{3,1,1}+b_{4,0,1}-49)]^2 e^{-(r+7)^2/N_0}dr$$
$$+\int_{\lambda_0}^{\lambda_1}[(a_{1,0,1}+a_{2,1,1}+a_{3,1,1}+a_{4,1,1}-10)r+(b_{1,0,1}+b_{2,1,1}+b_{3,1,1}+b_{4,1,1}-25)]^2 e^{-(r+5)^2/N_0}dr$$
$$+\int_{\lambda_0}^{\lambda_1}[(a_{1,0,1}+a_{2,1,1}+a_{3,0,1}+a_{4,1,1}-6)r+(b_{1,0,1}+b_{2,1,1}+b_{3,0,1}+b_{4,1,1}-9)]^2 e^{-(r+3)^2/N_0}dr$$
$$+\int_{\lambda_0}^{\lambda_1}[(a_{1,0,1}+a_{2,1,1}+a_{3,0,1}+a_{4,0,1}-2)r+(b_{1,0,1}+b_{2,1,1}+b_{3,0,1}+b_{4,0,1}-1)]^2 e^{-(r+1)^2/N_0}dr$$
$$+\int_{\lambda_0}^{\lambda_1}[(a_{1,1,1}+a_{2,1,1}+a_{3,0,1}+a_{4,0,1}+2)r+(b_{1,1,1}+b_{2,1,1}+b_{3,0,1}+b_{4,0,1}-1)]^2 e^{-(r-1)^2/N_0}dr$$
$$+\int_{\lambda_0}^{\lambda_1}[(a_{1,1,1}+a_{2,1,1}+a_{3,0,1}+a_{4,1,1}+6)r+(b_{1,1,1}+b_{2,1,1}+b_{3,0,1}+b_{4,1,1}-9)]^2 e^{-(r-3)^2/N_0}dr$$
$$+\int_{\lambda_0}^{\lambda_1}[(a_{1,1,1}+a_{2,1,1}+a_{3,1,1}+a_{4,1,1}+10)r+(b_{1,1,1}+b_{2,1,1}+b_{3,1,1}+b_{4,1,1}-25)]^2 e^{-(r-5)^2/N_0}dr$$
$$+\int_{\lambda_0}^{\lambda_1}[(a_{1,1,1}+a_{2,1,1}+a_{3,1,1}+a_{4,0,1}+14)r+(b_{1,1,1}+b_{2,1,1}+b_{3,1,1}+b_{4,0,1}-49)]^2 e^{-(r-7)^2/N_0}dr$$
$$+\int_{\lambda_0}^{\lambda_1}[(a_{1,1,1}+a_{2,0,1}+a_{3,1,1}+a_{4,0,1}+18)r+(b_{1,1,1}+b_{2,0,1}+b_{3,1,1}+b_{4,0,1}-81)]^2 e^{-(r-9)^2/N_0}dr$$
$$+\int_{\lambda_0}^{\lambda_1}[(a_{1,1,1}+a_{2,0,1}+a_{3,1,1}+a_{4,1,1}+22)r+(b_{1,1,1}+b_{2,0,1}+b_{3,1,1}+b_{4,1,1}-121)]^2 e^{-(r-11)^2/N_0}dr$$
$$+\int_{\lambda_0}^{\lambda_1}[(a_{1,1,1}+a_{2,0,1}+a_{3,0,1}+a_{4,1,1}+26)r+(b_{1,1,1}+b_{2,0,1}+b_{3,0,1}+b_{4,1,1}-169)]^2 e^{-(r-13)^2/N_0}dr$$
$$+\int_{\lambda_0}^{\lambda_1}\left.[(a_{1,1,1}+a_{2,0,1}+a_{3,0,1}+a_{4,0,1}+30)r+(b_{1,1,1}+b_{2,0,1}+b_{3,0,1}+b_{4,0,1}-225)]^2 e^{-(r-15)^2/N_0}dr\right)$$

$$+\int_{\lambda_1}^{\lambda_2}\left[(a_{1,0,2}+a_{2,0,2}+a_{3,0,2}+a_{4,0,2}-30)r+(b_{1,0,2}+b_{2,0,2}+b_{3,0,2}+b_{4,0,2}-225)\right]^2 e^{-(r+15)^2/N_0}dr$$
$$+\int_{\lambda_1}^{\lambda_2}\left[(a_{1,0,2}+a_{2,0,2}+a_{3,0,2}+a_{4,1,2}-26)r+(b_{1,0,2}+b_{2,0,2}+b_{3,0,2}+b_{4,1,2}-169)\right]^2 e^{-(r+13)^2/N_0}dr$$
$$+\int_{\lambda_1}^{\lambda_2}\left[(a_{1,0,2}+a_{2,0,2}+a_{3,1,2}+a_{4,1,2}-22)r+(b_{1,0,2}+b_{2,0,2}+b_{3,1,2}+b_{4,1,2}-121)\right]^2 e^{-(r+11)^2/N_0}dr$$
$$+\int_{\lambda_1}^{\lambda_2}\left[(a_{1,0,2}+a_{2,0,2}+a_{3,1,2}+a_{4,0,2}-18)r+(b_{1,0,2}+b_{2,0,2}+b_{3,1,2}+b_{4,0,2}-81)\right]^2 e^{-(r+9)^2/N_0}dr$$
$$+\int_{\lambda_1}^{\lambda_2}\left[(a_{1,0,2}+a_{2,1,2}+a_{3,1,2}+a_{4,0,2}-14)r+(b_{1,0,2}+b_{2,1,2}+b_{3,1,2}+b_{4,0,2}-49)\right]^2 e^{-(r+7)^2/N_0}dr$$
$$+\int_{\lambda_1}^{\lambda_2}\left[(a_{1,0,2}+a_{2,1,2}+a_{3,1,2}+a_{4,1,2}-10)r+(b_{1,0,2}+b_{2,1,2}+b_{3,1,2}+b_{4,1,2}-25)\right]^2 e^{-(r+5)^2/N_0}dr$$
$$+\int_{\lambda_1}^{\lambda_2}\left[(a_{1,0,2}+a_{2,1,2}+a_{3,0,2}+a_{4,1,2}-6)r+(b_{1,0,2}+b_{2,1,2}+b_{3,0,2}+b_{4,1,2}-9)\right]^2 e^{-(r+3)^2/N_0}dr$$
$$+\int_{\lambda_1}^{\lambda_2}\left[(a_{1,0,2}+a_{2,1,2}+a_{3,0,2}+a_{4,0,2}-2)r+(b_{1,0,2}+b_{2,1,2}+b_{3,0,2}+b_{4,0,2}-1)\right]^2 e^{-(r+1)^2/N_0}dr$$
$$+\int_{\lambda_1}^{\lambda_2}\left[(a_{1,1,2}+a_{2,1,2}+a_{3,0,2}+a_{4,0,2}+2)r+(b_{1,1,2}+b_{2,1,2}+b_{3,0,2}+b_{4,0,2}-1)\right]^2 e^{-(r-1)^2/N_0}dr$$
$$+\int_{\lambda_1}^{\lambda_2}\left[(a_{1,1,2}+a_{2,1,2}+a_{3,0,2}+a_{4,1,2}+6)r+(b_{1,1,2}+b_{2,1,2}+b_{3,0,2}+b_{4,1,2}-9)\right]^2 e^{-(r-3)^2/N_0}dr$$
$$+\int_{\lambda_1}^{\lambda_2}\left[(a_{1,1,2}+a_{2,1,2}+a_{3,1,2}+a_{4,1,2}+10)r+(b_{1,1,2}+b_{2,1,2}+b_{3,1,2}+b_{4,1,2}-25)\right]^2 e^{-(r-5)^2/N_0}dr$$
$$+\int_{\lambda_1}^{\lambda_2}\left[(a_{1,1,2}+a_{2,1,2}+a_{3,1,2}+a_{4,0,2}+14)r+(b_{1,1,2}+b_{2,1,2}+b_{3,1,2}+b_{4,0,2}-49)\right]^2 e^{-(r-7)^2/N_0}dr$$
$$+\int_{\lambda_1}^{\lambda_2}\left[(a_{1,1,2}+a_{2,0,2}+a_{3,1,2}+a_{4,0,2}+18)r+(b_{1,1,2}+b_{2,0,2}+b_{3,1,2}+b_{4,0,2}-81)\right]^2 e^{-(r-9)^2/N_0}dr$$
$$+\int_{\lambda_1}^{\lambda_2}\left[(a_{1,1,2}+a_{2,0,2}+a_{3,1,2}+a_{4,1,2}+22)r+(b_{1,1,2}+b_{2,0,2}+b_{3,1,2}+b_{4,1,2}-121)\right]^2 e^{-(r-11)^2/N_0}dr$$
$$+\int_{\lambda_1}^{\lambda_2}\left[(a_{1,1,2}+a_{2,0,2}+a_{3,0,2}+a_{4,1,2}+26)r+(b_{1,1,2}+b_{2,0,2}+b_{3,0,2}+b_{4,1,2}-169)\right]^2 e^{-(r-13)^2/N_0}dr$$
$$+\int_{\lambda_1}^{\lambda_2}\left[(a_{1,1,2}+a_{2,0,2}+a_{3,0,2}+a_{4,0,2}+30)r+(b_{1,1,2}+b_{2,0,2}+b_{3,0,2}+b_{4,0,2}-225)\right]^2 e^{-(r-15)^2/N_0}dr$$

$$+\int_{\lambda_2}^{\lambda_3}\left[(a_{1,0,3}+a_{2,0,3}+a_{3,0,3}+a_{4,0,3}-30)r+(b_{1,0,3}+b_{2,0,3}+b_{3,0,3}+b_{4,0,3}-225)\right]^2 e^{-(r+15)^2/N_0}dr$$
$$+\int_{\lambda_2}^{\lambda_3}\left[(a_{1,0,3}+a_{2,0,3}+a_{3,0,3}+a_{4,1,3}-26)r+(b_{1,0,3}+b_{2,0,3}+b_{3,0,3}+b_{4,1,3}-169)\right]^2 e^{-(r+13)^2/N_0}dr$$
$$+\int_{\lambda_2}^{\lambda_3}\left[(a_{1,0,3}+a_{2,0,3}+a_{3,1,3}+a_{4,1,3}-22)r+(b_{1,0,3}+b_{2,0,3}+b_{3,1,3}+b_{4,1,3}-121)\right]^2 e^{-(r+11)^2/N_0}dr$$
$$+\int_{\lambda_2}^{\lambda_3}\left[(a_{1,0,3}+a_{2,0,3}+a_{3,1,3}+a_{4,0,3}-18)r+(b_{1,0,3}+b_{2,0,3}+b_{3,1,3}+b_{4,0,3}-81)\right]^2 e^{-(r+9)^2/N_0}dr$$
$$+\int_{\lambda_2}^{\lambda_3}\left[(a_{1,0,3}+a_{2,1,3}+a_{3,1,3}+a_{4,0,3}-14)r+(b_{1,0,3}+b_{2,1,3}+b_{3,1,3}+b_{4,0,3}-49)\right]^2 e^{-(r+7)^2/N_0}dr$$
$$+\int_{\lambda_2}^{\lambda_3}\left[(a_{1,0,3}+a_{2,1,3}+a_{3,1,3}+a_{4,1,3}-10)r+(b_{1,0,3}+b_{2,1,3}+b_{3,1,3}+b_{4,1,3}-25)\right]^2 e^{-(r+5)^2/N_0}dr$$
$$+\int_{\lambda_2}^{\lambda_3}\left[(a_{1,0,3}+a_{2,1,3}+a_{3,0,3}+a_{4,1,3}-6)r+(b_{1,0,3}+b_{2,1,3}+b_{3,0,3}+b_{4,1,3}-9)\right]^2 e^{-(r+3)^2/N_0}dr$$
$$+\int_{\lambda_2}^{\lambda_3}\left[(a_{1,0,3}+a_{2,1,3}+a_{3,0,3}+a_{4,0,3}-2)r+(b_{1,0,3}+b_{2,1,3}+b_{3,0,3}+b_{4,0,3}-1)\right]^2 e^{-(r+1)^2/N_0}dr$$
$$+\int_{\lambda_2}^{\lambda_3}\left[(a_{1,1,3}+a_{2,1,3}+a_{3,0,3}+a_{4,0,3}+2)r+(b_{1,1,3}+b_{2,1,3}+b_{3,0,3}+b_{4,0,3}-1)\right]^2 e^{-(r-1)^2/N_0}dr$$
$$+\int_{\lambda_2}^{\lambda_3}\left[(a_{1,1,3}+a_{2,1,3}+a_{3,0,3}+a_{4,1,3}+6)r+(b_{1,1,3}+b_{2,1,3}+b_{3,0,3}+b_{4,1,3}-9)\right]^2 e^{-(r-3)^2/N_0}dr$$
$$+\int_{\lambda_2}^{\lambda_3}\left[(a_{1,1,3}+a_{2,1,3}+a_{3,1,3}+a_{4,1,3}+10)r+(b_{1,1,3}+b_{2,1,3}+b_{3,1,3}+b_{4,1,3}-25)\right]^2 e^{-(r-5)^2/N_0}dr$$
$$+\int_{\lambda_2}^{\lambda_3}\left[(a_{1,1,3}+a_{2,1,3}+a_{3,1,3}+a_{4,0,3}+14)r+(b_{1,1,3}+b_{2,1,3}+b_{3,1,3}+b_{4,0,3}-49)\right]^2 e^{-(r-7)^2/N_0}dr$$
$$+\int_{\lambda_2}^{\lambda_3}\left[(a_{1,1,3}+a_{2,0,3}+a_{3,1,3}+a_{4,0,3}+18)r+(b_{1,1,3}+b_{2,0,3}+b_{3,1,3}+b_{4,0,3}-81)\right]^2 e^{-(r-9)^2/N_0}dr$$
$$+\int_{\lambda_2}^{\lambda_3}\left[(a_{1,1,3}+a_{2,0,3}+a_{3,1,3}+a_{4,1,3}+22)r+(b_{1,1,3}+b_{2,0,3}+b_{3,1,3}+b_{4,1,3}-121)\right]^2 e^{-(r-11)^2/N_0}dr$$
$$+\int_{\lambda_2}^{\lambda_3}\left[(a_{1,1,3}+a_{2,0,3}+a_{3,0,3}+a_{4,1,3}+26)r+(b_{1,1,3}+b_{2,0,3}+b_{3,0,3}+b_{4,1,3}-169)\right]^2 e^{-(r-13)^2/N_0}dr$$
$$+\int_{\lambda_2}^{\lambda_3}\left[(a_{1,1,3}+a_{2,0,3}+a_{3,0,3}+a_{4,0,3}+30)r+(b_{1,1,3}+b_{2,0,3}+b_{3,0,3}+b_{4,0,3}-225)\right]^2 e^{-(r-15)^2/N_0}dr$$

$$+\int_{\lambda_3}^{\lambda_4}\left[(a_{1,0,4}+a_{2,0,4}+a_{3,0,4}+a_{4,0,4}-30)r+(b_{1,0,4}+b_{2,0,4}+b_{3,0,4}+b_{4,0,4}-225)\right]^2 e^{-(r+15)^2/N_0}dr$$
$$+\int_{\lambda_3}^{\lambda_4}\left[(a_{1,0,4}+a_{2,0,4}+a_{3,0,4}+a_{4,1,4}-26)r+(b_{1,0,4}+b_{2,0,4}+b_{3,0,4}+b_{4,1,4}-169)\right]^2 e^{-(r+13)^2/N_0}dr$$
$$+\int_{\lambda_3}^{\lambda_4}\left[(a_{1,0,4}+a_{2,0,4}+a_{3,1,4}+a_{4,1,4}-22)r+(b_{1,0,4}+b_{2,0,4}+b_{3,1,4}+b_{4,1,4}-121)\right]^2 e^{-(r+11)^2/N_0}dr$$
$$+\int_{\lambda_3}^{\lambda_4}\left[(a_{1,0,4}+a_{2,0,4}+a_{3,1,4}+a_{4,0,4}-18)r+(b_{1,0,4}+b_{2,0,4}+b_{3,1,4}+b_{4,0,4}-81)\right]^2 e^{-(r+9)^2/N_0}dr$$
$$+\int_{\lambda_3}^{\lambda_4}\left[(a_{1,0,4}+a_{2,1,4}+a_{3,1,4}+a_{4,0,4}-14)r+(b_{1,0,4}+b_{2,1,4}+b_{3,1,4}+b_{4,0,4}-49)\right]^2 e^{-(r+7)^2/N_0}dr$$
$$+\int_{\lambda_3}^{\lambda_4}\left[(a_{1,0,4}+a_{2,1,4}+a_{3,1,4}+a_{4,1,4}-10)r+(b_{1,0,4}+b_{2,1,4}+b_{3,1,4}+b_{4,1,4}-25)\right]^2 e^{-(r+5)^2/N_0}dr$$
$$+\int_{\lambda_3}^{\lambda_4}\left[(a_{1,0,4}+a_{2,1,4}+a_{3,0,4}+a_{4,1,4}-6)r+(b_{1,0,4}+b_{2,1,4}+b_{3,0,4}+b_{4,1,4}-9)\right]^2 e^{-(r+3)^2/N_0}dr$$
$$+\int_{\lambda_3}^{\lambda_4}\left[(a_{1,0,4}+a_{2,1,4}+a_{3,0,4}+a_{4,0,4}-2)r+(b_{1,0,4}+b_{2,1,4}+b_{3,0,4}+b_{4,0,4}-1)\right]^2 e^{-(r+1)^2/N_0}dr$$
$$+\int_{\lambda_3}^{\lambda_4}\left[(a_{1,1,4}+a_{2,1,4}+a_{3,0,4}+a_{4,0,4}+2)r+(b_{1,1,4}+b_{2,1,4}+b_{3,0,4}+b_{4,0,4}-1)\right]^2 e^{-(r-1)^2/N_0}dr$$
$$+\int_{\lambda_3}^{\lambda_4}\left[(a_{1,1,4}+a_{2,1,4}+a_{3,0,4}+a_{4,1,4}+6)r+(b_{1,1,4}+b_{2,1,4}+b_{3,0,4}+b_{4,1,4}-9)\right]^2 e^{-(r-3)^2/N_0}dr$$
$$+\int_{\lambda_3}^{\lambda_4}\left[(a_{1,1,4}+a_{2,1,4}+a_{3,1,4}+a_{4,1,4}+10)r+(b_{1,1,4}+b_{2,1,4}+b_{3,1,4}+b_{4,1,4}-25)\right]^2 e^{-(r-5)^2/N_0}dr$$
$$+\int_{\lambda_3}^{\lambda_4}\left[(a_{1,1,4}+a_{2,1,4}+a_{3,1,4}+a_{4,0,4}+14)r+(b_{1,1,4}+b_{2,1,4}+b_{3,1,4}+b_{4,0,4}-49)\right]^2 e^{-(r-7)^2/N_0}dr$$
$$+\int_{\lambda_3}^{\lambda_4}\left[(a_{1,1,4}+a_{2,0,4}+a_{3,1,4}+a_{4,0,4}+18)r+(b_{1,1,4}+b_{2,0,4}+b_{3,1,4}+b_{4,0,4}-81)\right]^2 e^{-(r-9)^2/N_0}dr$$
$$+\int_{\lambda_3}^{\lambda_4}\left[(a_{1,1,4}+a_{2,0,4}+a_{3,1,4}+a_{4,1,4}+22)r+(b_{1,1,4}+b_{2,0,4}+b_{3,1,4}+b_{4,1,4}-121)\right]^2 e^{-(r-11)^2/N_0}dr$$
$$+\int_{\lambda_3}^{\lambda_4}\left[(a_{1,1,4}+a_{2,0,4}+a_{3,0,4}+a_{4,1,4}+26)r+(b_{1,1,4}+b_{2,0,4}+b_{3,0,4}+b_{4,1,4}-169)\right]^2 e^{-(r-13)^2/N_0}dr$$
$$+\int_{\lambda_3}^{\lambda_4}\left[(a_{1,1,4}+a_{2,0,4}+a_{3,0,4}+a_{4,0,4}+30)r+(b_{1,1,4}+b_{2,0,4}+b_{3,0,4}+b_{4,0,4}-225)\right]^2 e^{-(r-15)^2/N_0}dr$$

$$+\int_{\lambda_4}^{\lambda_5}\left[(a_{1,0,5}+a_{2,0,5}+a_{3,0,5}+a_{4,0,5}-30)r+(b_{1,0,5}+b_{2,0,5}+b_{3,0,5}+b_{4,0,5}-225)\right]^2 e^{-(r+15)^2/N_0}dr$$
$$+\int_{\lambda_4}^{\lambda_5}\left[(a_{1,0,5}+a_{2,0,5}+a_{3,0,5}+a_{4,1,5}-26)r+(b_{1,0,5}+b_{2,0,5}+b_{3,0,5}+b_{4,1,5}-169)\right]^2 e^{-(r+13)^2/N_0}dr$$
$$+\int_{\lambda_4}^{\lambda_5}\left[(a_{1,0,5}+a_{2,0,5}+a_{3,1,5}+a_{4,1,5}-22)r+(b_{1,0,5}+b_{2,0,5}+b_{3,1,5}+b_{4,1,5}-121)\right]^2 e^{-(r+11)^2/N_0}dr$$
$$+\int_{\lambda_4}^{\lambda_5}\left[(a_{1,0,5}+a_{2,0,5}+a_{3,1,5}+a_{4,0,5}-18)r+(b_{1,0,5}+b_{2,0,5}+b_{3,1,5}+b_{4,0,5}-81)\right]^2 e^{-(r+9)^2/N_0}dr$$
$$+\int_{\lambda_4}^{\lambda_5}\left[(a_{1,0,5}+a_{2,1,5}+a_{3,1,5}+a_{4,0,5}-14)r+(b_{1,0,5}+b_{2,1,5}+b_{3,1,5}+b_{4,0,5}-49)\right]^2 e^{-(r+7)^2/N_0}dr$$
$$+\int_{\lambda_4}^{\lambda_5}\left[(a_{1,0,5}+a_{2,1,5}+a_{3,1,5}+a_{4,1,5}-10)r+(b_{1,0,5}+b_{2,1,5}+b_{3,1,5}+b_{4,1,5}-25)\right]^2 e^{-(r+5)^2/N_0}dr$$
$$+\int_{\lambda_4}^{\lambda_5}\left[(a_{1,0,5}+a_{2,1,5}+a_{3,0,5}+a_{4,1,5}-6)r+(b_{1,0,5}+b_{2,1,5}+b_{3,0,5}+b_{4,1,5}-9)\right]^2 e^{-(r+3)^2/N_0}dr$$
$$+\int_{\lambda_4}^{\lambda_5}\left[(a_{1,0,5}+a_{2,1,5}+a_{3,0,5}+a_{4,0,5}-2)r+(b_{1,0,5}+b_{2,1,5}+b_{3,0,5}+b_{4,0,5}-1)\right]^2 e^{-(r+1)^2/N_0}dr$$
$$+\int_{\lambda_4}^{\lambda_5}\left[(a_{1,1,5}+a_{2,1,5}+a_{3,0,5}+a_{4,0,5}+2)r+(b_{1,1,5}+b_{2,1,5}+b_{3,0,5}+b_{4,0,5}-1)\right]^2 e^{-(r-1)^2/N_0}dr$$
$$+\int_{\lambda_4}^{\lambda_5}\left[(a_{1,1,5}+a_{2,1,5}+a_{3,0,5}+a_{4,1,5}+6)r+(b_{1,1,5}+b_{2,1,5}+b_{3,0,5}+b_{4,1,5}-9)\right]^2 e^{-(r-3)^2/N_0}dr$$
$$+\int_{\lambda_4}^{\lambda_5}\left[(a_{1,1,5}+a_{2,1,5}+a_{3,1,5}+a_{4,1,5}+10)r+(b_{1,1,5}+b_{2,1,5}+b_{3,1,5}+b_{4,1,5}-25)\right]^2 e^{-(r-5)^2/N_0}dr$$
$$+\int_{\lambda_4}^{\lambda_5}\left[(a_{1,1,5}+a_{2,1,5}+a_{3,1,5}+a_{4,0,5}+14)r+(b_{1,1,5}+b_{2,1,5}+b_{3,1,5}+b_{4,0,5}-49)\right]^2 e^{-(r-7)^2/N_0}dr$$
$$+\int_{\lambda_4}^{\lambda_5}\left[(a_{1,1,5}+a_{2,0,5}+a_{3,1,5}+a_{4,0,5}+18)r+(b_{1,1,5}+b_{2,0,5}+b_{3,1,5}+b_{4,0,5}-81)\right]^2 e^{-(r-9)^2/N_0}dr$$
$$+\int_{\lambda_4}^{\lambda_5}\left[(a_{1,1,5}+a_{2,0,5}+a_{3,1,5}+a_{4,1,5}+22)r+(b_{1,1,5}+b_{2,0,5}+b_{3,1,5}+b_{4,1,5}-121)\right]^2 e^{-(r-11)^2/N_0}dr$$
$$+\int_{\lambda_4}^{\lambda_5}\left[(a_{1,1,5}+a_{2,0,5}+a_{3,0,5}+a_{4,1,5}+26)r+(b_{1,1,5}+b_{2,0,5}+b_{3,0,5}+b_{4,1,5}-169)\right]^2 e^{-(r-13)^2/N_0}dr$$
$$+\int_{\lambda_4}^{\lambda_5}\left[(a_{1,1,5}+a_{2,0,5}+a_{3,0,5}+a_{4,0,5}+30)r+(b_{1,1,5}+b_{2,0,5}+b_{3,0,5}+b_{4,0,5}-225)\right]^2 e^{-(r-15)^2/N_0}dr$$

$$+\int_{\lambda_5}^{\lambda_6}\left[(a_{1,0,6}+a_{2,0,6}+a_{3,0,6}+a_{4,0,6}-30)r+(b_{1,0,6}+b_{2,0,6}+b_{3,0,6}+b_{4,0,6}-225)\right]^2 e^{-(r+15)^2/N_0}dr$$
$$+\int_{\lambda_5}^{\lambda_6}\left[(a_{1,0,6}+a_{2,0,6}+a_{3,0,6}+a_{4,1,6}-26)r+(b_{1,0,6}+b_{2,0,6}+b_{3,0,6}+b_{4,1,6}-169)\right]^2 e^{-(r+13)^2/N_0}dr$$
$$+\int_{\lambda_5}^{\lambda_6}\left[(a_{1,0,6}+a_{2,0,6}+a_{3,1,6}+a_{4,1,6}-22)r+(b_{1,0,6}+b_{2,0,6}+b_{3,1,6}+b_{4,1,6}-121)\right]^2 e^{-(r+11)^2/N_0}dr$$
$$+\int_{\lambda_5}^{\lambda_6}\left[(a_{1,0,6}+a_{2,0,6}+a_{3,1,6}+a_{4,0,6}-18)r+(b_{1,0,6}+b_{2,0,6}+b_{3,1,6}+b_{4,0,6}-81)\right]^2 e^{-(r+9)^2/N_0}dr$$
$$+\int_{\lambda_5}^{\lambda_6}\left[(a_{1,0,6}+a_{2,1,6}+a_{3,1,6}+a_{4,0,6}-14)r+(b_{1,0,6}+b_{2,1,6}+b_{3,1,6}+b_{4,0,6}-49)\right]^2 e^{-(r+7)^2/N_0}dr$$
$$+\int_{\lambda_5}^{\lambda_6}\left[(a_{1,0,6}+a_{2,1,6}+a_{3,1,6}+a_{4,1,6}-10)r+(b_{1,0,6}+b_{2,1,6}+b_{3,1,6}+b_{4,1,6}-25)\right]^2 e^{-(r+5)^2/N_0}dr$$
$$+\int_{\lambda_5}^{\lambda_6}\left[(a_{1,0,6}+a_{2,1,6}+a_{3,0,6}+a_{4,1,6}-6)r+(b_{1,0,6}+b_{2,1,6}+b_{3,0,6}+b_{4,1,6}-9)\right]^2 e^{-(r+3)^2/N_0}dr$$
$$+\int_{\lambda_5}^{\lambda_6}\left[(a_{1,0,6}+a_{2,1,6}+a_{3,0,6}+a_{4,0,6}-2)r+(b_{1,0,6}+b_{2,1,6}+b_{3,0,6}+b_{4,0,6}-1)\right]^2 e^{-(r+1)^2/N_0}dr$$
$$+\int_{\lambda_5}^{\lambda_6}\left[(a_{1,1,6}+a_{2,1,6}+a_{3,0,6}+a_{4,0,6}+2)r+(b_{1,1,6}+b_{2,1,6}+b_{3,0,6}+b_{4,0,6}-1)\right]^2 e^{-(r-1)^2/N_0}dr$$
$$+\int_{\lambda_5}^{\lambda_6}\left[(a_{1,1,6}+a_{2,1,6}+a_{3,0,6}+a_{4,1,6}+6)r+(b_{1,1,6}+b_{2,1,6}+b_{3,0,6}+b_{4,1,6}-9)\right]^2 e^{-(r-3)^2/N_0}dr$$
$$+\int_{\lambda_5}^{\lambda_6}\left[(a_{1,1,6}+a_{2,1,6}+a_{3,1,6}+a_{4,1,6}+10)r+(b_{1,1,6}+b_{2,1,6}+b_{3,1,6}+b_{4,1,6}-25)\right]^2 e^{-(r-5)^2/N_0}dr$$
$$+\int_{\lambda_5}^{\lambda_6}\left[(a_{1,1,6}+a_{2,1,6}+a_{3,1,6}+a_{4,0,6}+14)r+(b_{1,1,6}+b_{2,1,6}+b_{3,1,6}+b_{4,0,6}-49)\right]^2 e^{-(r-7)^2/N_0}dr$$
$$+\int_{\lambda_5}^{\lambda_6}\left[(a_{1,1,6}+a_{2,0,6}+a_{3,1,6}+a_{4,0,6}+18)r+(b_{1,1,6}+b_{2,0,6}+b_{3,1,6}+b_{4,0,6}-81)\right]^2 e^{-(r-9)^2/N_0}dr$$
$$+\int_{\lambda_5}^{\lambda_6}\left[(a_{1,1,6}+a_{2,0,6}+a_{3,1,6}+a_{4,1,6}+22)r+(b_{1,1,6}+b_{2,0,6}+b_{3,1,6}+b_{4,1,6}-121)\right]^2 e^{-(r-11)^2/N_0}dr$$
$$+\int_{\lambda_5}^{\lambda_6}\left[(a_{1,1,6}+a_{2,0,6}+a_{3,0,6}+a_{4,1,6}+26)r+(b_{1,1,6}+b_{2,0,6}+b_{3,0,6}+b_{4,1,6}-169)\right]^2 e^{-(r-13)^2/N_0}dr$$
$$+\int_{\lambda_5}^{\lambda_6}\left[(a_{1,1,6}+a_{2,0,6}+a_{3,0,6}+a_{4,0,6}+30)r+(b_{1,1,6}+b_{2,0,6}+b_{3,0,6}+b_{4,0,6}-225)\right]^2 e^{-(r-15)^2/N_0}dr$$

$$+\int_{\lambda_6}^{\lambda_7}\left[(a_{1,0,7}+a_{2,0,7}+a_{3,0,7}+a_{4,0,7}-30)r+(b_{1,0,7}+b_{2,0,7}+b_{3,0,7}+b_{4,0,7}-225)\right]^2 e^{-(r+15)^2/N_0}dr$$
$$+\int_{\lambda_6}^{\lambda_7}\left[(a_{1,0,7}+a_{2,0,7}+a_{3,0,7}+a_{4,1,7}-26)r+(b_{1,0,7}+b_{2,0,7}+b_{3,0,7}+b_{4,1,7}-169)\right]^2 e^{-(r+13)^2/N_0}dr$$
$$+\int_{\lambda_6}^{\lambda_7}\left[(a_{1,0,7}+a_{2,0,7}+a_{3,1,7}+a_{4,1,7}-22)r+(b_{1,0,7}+b_{2,0,7}+b_{3,1,7}+b_{4,1,7}-121)\right]^2 e^{-(r+11)^2/N_0}dr$$
$$+\int_{\lambda_6}^{\lambda_7}\left[(a_{1,0,7}+a_{2,0,7}+a_{3,1,7}+a_{4,0,7}-18)r+(b_{1,0,7}+b_{2,0,7}+b_{3,1,7}+b_{4,0,7}-81)\right]^2 e^{-(r+9)^2/N_0}dr$$
$$+\int_{\lambda_6}^{\lambda_7}\left[(a_{1,0,7}+a_{2,1,7}+a_{3,1,7}+a_{4,0,7}-14)r+(b_{1,0,7}+b_{2,1,7}+b_{3,1,7}+b_{4,0,7}-49)\right]^2 e^{-(r+7)^2/N_0}dr$$
$$+\int_{\lambda_6}^{\lambda_7}\left[(a_{1,0,7}+a_{2,1,7}+a_{3,1,7}+a_{4,1,7}-10)r+(b_{1,0,7}+b_{2,1,7}+b_{3,1,7}+b_{4,1,7}-25)\right]^2 e^{-(r+5)^2/N_0}dr$$
$$+\int_{\lambda_6}^{\lambda_7}\left[(a_{1,0,7}+a_{2,1,7}+a_{3,0,7}+a_{4,1,7}-6)r+(b_{1,0,7}+b_{2,1,7}+b_{3,0,7}+b_{4,1,7}-9)\right]^2 e^{-(r+3)^2/N_0}dr$$
$$+\int_{\lambda_6}^{\lambda_7}\left[(a_{1,0,7}+a_{2,1,7}+a_{3,0,7}+a_{4,0,7}-2)r+(b_{1,0,7}+b_{2,1,7}+b_{3,0,7}+b_{4,0,7}-1)\right]^2 e^{-(r+1)^2/N_0}dr$$
$$+\int_{\lambda_6}^{\lambda_7}\left[(a_{1,1,7}+a_{2,1,7}+a_{3,0,7}+a_{4,0,7}+2)r+(b_{1,1,7}+b_{2,1,7}+b_{3,0,7}+b_{4,0,7}-1)\right]^2 e^{-(r-1)^2/N_0}dr$$
$$+\int_{\lambda_6}^{\lambda_7}\left[(a_{1,1,7}+a_{2,1,7}+a_{3,0,7}+a_{4,1,7}+6)r+(b_{1,1,7}+b_{2,1,7}+b_{3,0,7}+b_{4,1,7}-9)\right]^2 e^{-(r-3)^2/N_0}dr$$
$$+\int_{\lambda_6}^{\lambda_7}\left[(a_{1,1,7}+a_{2,1,7}+a_{3,1,7}+a_{4,1,7}+10)r+(b_{1,1,7}+b_{2,1,7}+b_{3,1,7}+b_{4,1,7}-25)\right]^2 e^{-(r-5)^2/N_0}dr$$
$$+\int_{\lambda_6}^{\lambda_7}\left[(a_{1,1,7}+a_{2,1,7}+a_{3,1,7}+a_{4,0,7}+14)r+(b_{1,1,7}+b_{2,1,7}+b_{3,1,7}+b_{4,0,7}-49)\right]^2 e^{-(r-7)^2/N_0}dr$$
$$+\int_{\lambda_6}^{\lambda_7}\left[(a_{1,1,7}+a_{2,0,7}+a_{3,1,7}+a_{4,0,7}+18)r+(b_{1,1,7}+b_{2,0,7}+b_{3,1,7}+b_{4,0,7}-81)\right]^2 e^{-(r-9)^2/N_0}dr$$
$$+\int_{\lambda_6}^{\lambda_7}\left[(a_{1,1,7}+a_{2,0,7}+a_{3,1,7}+a_{4,1,7}+22)r+(b_{1,1,7}+b_{2,0,7}+b_{3,1,7}+b_{4,1,7}-121)\right]^2 e^{-(r-11)^2/N_0}dr$$
$$+\int_{\lambda_6}^{\lambda_7}\left[(a_{1,1,7}+a_{2,0,7}+a_{3,0,7}+a_{4,1,7}+26)r+(b_{1,1,7}+b_{2,0,7}+b_{3,0,7}+b_{4,1,7}-169)\right]^2 e-(r-13)^2/N_0dr$$
$$+\int_{\lambda_6}^{\lambda_7}\left[(a_{1,1,7}+a_{2,0,7}+a_{3,0,7}+a_{4,0,7}+30)r+(b_{1,1,7}+b_{2,0,7}+b_{3,0,7}+b_{4,0,7}-225)\right]^2 e^{-(r-15)^2/N_0}dr$$

$$
\begin{aligned}
&+\int_{\lambda_7}^{\lambda_8}\left[(a_{1,0,8}+a_{2,0,8}+a_{3,0,8}+a_{4,0,8}-30)r+(b_{1,0,8}+b_{2,0,8}+b_{3,0,8}+b_{4,0,8}-225)\right]^2 e^{-(r+15)^2/N_0}dr\\
&+\int_{\lambda_7}^{\lambda_8}\left[(a_{1,0,8}+a_{2,0,8}+a_{3,0,8}+a_{4,1,8}-26)r+(b_{1,0,8}+b_{2,0,8}+b_{3,0,8}+b_{4,1,8}-169)\right]^2 e^{-(r+13)^2/N_0}dr\\
&+\int_{\lambda_7}^{\lambda_8}\left[(a_{1,0,8}+a_{2,0,8}+a_{3,1,8}+a_{4,1,8}-22)r+(b_{1,0,8}+b_{2,0,8}+b_{3,1,8}+b_{4,1,8}-121)\right]^2 e^{-(r+11)^2/N_0}dr\\
&+\int_{\lambda_7}^{\lambda_8}\left[(a_{1,0,8}+a_{2,0,8}+a_{3,1,8}+a_{4,0,8}-18)r+(b_{1,0,8}+b_{2,0,8}+b_{3,1,8}+b_{4,0,8}-81)\right]^2 e^{-(r+9)^2/N_0}dr\\
&+\int_{\lambda_7}^{\lambda_8}\left[(a_{1,0,8}+a_{2,1,8}+a_{3,1,8}+a_{4,0,8}-14)r+(b_{1,0,8}+b_{2,1,8}+b_{3,1,8}+b_{4,0,8}-49)\right]^2 e^{-(r+7)^2/N_0}dr\\
&+\int_{\lambda_7}^{\lambda_8}\left[(a_{1,0,8}+a_{2,1,8}+a_{3,1,8}+a_{4,1,8}-10)r+(b_{1,0,8}+b_{2,1,8}+b_{3,1,8}+b_{4,1,8}-25)\right]^2 e^{-(r+5)^2/N_0}dr\\
&+\int_{\lambda_7}^{\lambda_8}\left[(a_{1,0,8}+a_{2,1,8}+a_{3,0,8}+a_{4,1,8}-6)r+(b_{1,0,8}+b_{2,1,8}+b_{3,0,8}+b_{4,1,8}-9)\right]^2 e^{-(r+3)^2/N_0}dr\\
&+\int_{\lambda_7}^{\lambda_8}\left[(a_{1,0,8}+a_{2,1,8}+a_{3,0,8}+a_{4,0,8}-2)r+(b_{1,0,8}+b_{2,1,8}+b_{3,0,8}+b_{4,0,8}-1)\right]^2 e^{-(r+1)^2/N_0}dr\\
&+\int_{\lambda_7}^{\lambda_8}\left[(a_{1,1,8}+a_{2,1,8}+a_{3,0,8}+a_{4,0,8}+2)r+(b_{1,1,8}+b_{2,1,8}+b_{3,0,8}+b_{4,0,8}-1)\right]^2 e^{-(r-1)^2/N_0}dr\\
&+\int_{\lambda_7}^{\lambda_8}\left[(a_{1,1,8}+a_{2,1,8}+a_{3,0,8}+a_{4,1,8}+6)r+(b_{1,1,8}+b_{2,1,8}+b_{3,0,8}+b_{4,1,8}-9)\right]^2 e^{-(r-3)^2/N_0}dr\\
&+\int_{\lambda_7}^{\lambda_8}\left[(a_{1,1,8}+a_{2,1,8}+a_{3,1,8}+a_{4,1,8}+10)r+(b_{1,1,8}+b_{2,1,8}+b_{3,1,8}+b_{4,1,8}-25)\right]^2 e^{-(r-5)^2/N_0}dr\\
&+\int_{\lambda_7}^{\lambda_8}\left[(a_{1,1,8}+a_{2,1,8}+a_{3,1,8}+a_{4,0,8}+14)r+(b_{1,1,8}+b_{2,1,8}+b_{3,1,8}+b_{4,0,8}-49)\right]^2 e^{-(r-7)^2/N_0}dr\\
&+\int_{\lambda_7}^{\lambda_8}\left[(a_{1,1,8}+a_{2,0,8}+a_{3,1,8}+a_{4,0,8}+18)r+(b_{1,1,8}+b_{2,0,8}+b_{3,1,8}+b_{4,0,8}-81)\right]^2 e^{-(r-9)^2/N_0}dr\\
&+\int_{\lambda_7}^{\lambda_8}\left[(a_{1,1,8}+a_{2,0,8}+a_{3,1,8}+a_{4,1,8}+22)r+(b_{1,1,8}+b_{2,0,8}+b_{3,1,8}+b_{4,1,8}-121)\right]^2 e^{-(r-11)^2/N_0}dr\\
&+\int_{\lambda_7}^{\lambda_8}\left[(a_{1,1,8}+a_{2,0,8}+a_{3,0,8}+a_{4,1,8}+26)r+(b_{1,1,8}+b_{2,0,8}+b_{3,0,8}+b_{4,1,8}-169)\right]^2 e^{-(r-13)^2/N_0}dr\\
&+\int_{\lambda_7}^{\lambda_8}\left[(a_{1,1,8}+a_{2,0,8}+a_{3,0,8}+a_{4,0,8}+30)r+(b_{1,1,8}+b_{2,0,8}+b_{3,0,8}+b_{4,0,8}-225)\right]^2 e^{-(r-15)^2/N_0}dr\Bigg).
\end{aligned}
$$

By substituting all equations obtained in $A_i(\rho=i)$, $1\le i\le 8$, into the above equation

we have

$$
\begin{aligned}
W(\boldsymbol{\lambda}) \;=\; & \frac{1}{16\sqrt{\pi N_0}}\left(\int_{-\infty}^{\lambda_1}(8r+96)^2e^{-(r+9)^2/N_0}dr+\int_{-\infty}^{\lambda_1}(-32)^2e^{-(r+5)^2/N_0}dr\right.\\
&+\int_{-\infty}^{\lambda_1}(8r+32)^2e^{-(r+3)^2/N_0}dr+\int_{-\infty}^{\lambda_1}(16r+96)^2e^{-(r+1)^2/N_0}dr\\
&+\int_{-\infty}^{\lambda_1}(-64)^2e^{-(r-3)^2/N_0}dr+\int_{-\infty}^{\lambda_1}(-128)^2e^{-(r-5)^2/N_0}dr\\
&+\int_{-\infty}^{\lambda_1}(8r-96)^2e^{-(r-7)^2/N_0}dr+\int_{-\infty}^{\lambda_1}(24r)^2e^{-(r-9)^2/N_0}dr\\
&+\int_{-\infty}^{\lambda_1}(24r-96)^2e^{-(r-11)^2/N_0}dr+\int_{-\infty}^{\lambda_1}(32r-96)^2e^{-(r-13)^2/N_0}dr\\
&+\int_{-\infty}^{\lambda_1}(40r-96)^2e^{-(r-15)^2/N_0}dr\\
&+\int_{\lambda_1}^{\lambda_2}(-8r-96)^2e^{-(r+15)^2/N_0}dr+\int_{\lambda_1}^{\lambda_2}(8r+64)^2e^{-(r+5)^2/N_0}dr\\
&+\int_{\lambda_1}^{\lambda_2}(16r+128)^2e^{-(r+3)^2/N_0}dr+\int_{\lambda_1}^{\lambda_2}(16r+96)^2e^{-(r+1)^2/N_0}dr\\
&+\int_{\lambda_1}^{\lambda_2}(8r+32)^2e^{-(r-3)^2/N_0}dr+\int_{\lambda_1}^{\lambda_2}(8r-32)^2e^{-(r-5)^2/N_0}dr\\
&+\int_{\lambda_1}^{\lambda_2}(8r-96)^2e^{-(r-7)^2/N_0}dr+\int_{\lambda_1}^{\lambda_2}(16r-96)^2e^{-(r-9)^2/N_0}dr\\
&+\int_{\lambda_1}^{\lambda_2}(24r-96)^2e^{-(r-11)^2/N_0}dr+\int_{\lambda_1}^{\lambda_2}(32r-96)^2e^{-(r-13)^2/N_0}dr\\
&+\int_{\lambda_1}^{\lambda_2}(32r-192)^2e^{-(r-15)^2/N_0}dr\\
&+\int_{\lambda_2}^{\lambda_3}(-16r-160)^2e^{-(r+15)^2/N_0}dr+\int_{\lambda_2}^{\lambda_3}(-16r-128)^2e^{-(r+13)^2/N_0}dr\\
&+\int_{\lambda_2}^{\lambda_3}(-8r-64)^2e^{-(r+11)^2/N_0}dr+\int_{\lambda_2}^{\lambda_3}(8r+32)^2e^{-(r+1)^2/N_0}dr\\
&+\int_{\lambda_2}^{\lambda_3}(-32)^2e^{-(r-3)^2/N_0}dr+\int_{\lambda_2}^{\lambda_3}(8r-32)^2e^{-(r-5)^2/N_0}dr\\
&+\int_{\lambda_2}^{\lambda_3}(16r-32)^2e^{-(r-7)^2/N_0}dr+\int_{\lambda_2}^{\lambda_3}(24r-32)^2e^{-(r-9)^2/N_0}dr\\
&+\int_{\lambda_2}^{\lambda_3}(24r-96)^2e^{-(r-11)^2/N_0}dr+\int_{\lambda_2}^{\lambda_3}(24r-160)^2e^{-(r-13)^2/N_0}dr\\
&+\int_{\lambda_2}^{\lambda_3}(32r-192)^2e^{-(r-15)^2/N_0}dr
\end{aligned}
$$

$$+\int_{\lambda_3}^{\lambda_4}(-16r-160)^2e^{-(r+15)^2/N_0}dr+\int_{\lambda_3}^{\lambda_4}(-8r-96)^2e^{-(r+13)^2/N_0}dr$$
$$+\int_{\lambda_3}^{\lambda_4}(-32)^2e^{-(r+11)^2/N_0}dr+\int_{\lambda_3}^{\lambda_4}(-8r-32)^2e^{-(r+7)^2/N_0}dr$$
$$+\int_{\lambda_3}^{\lambda_4}(8r)^2e^{-(r-3)^2/N_0}dr+\int_{\lambda_3}^{\lambda_4}(16r)^2e^{-(r-5)^2/N_0}dr$$
$$+\int_{\lambda_3}^{\lambda_4}(16r-32)^2e^{-(r-7)^2/N_0}dr+\int_{\lambda_3}^{\lambda_4}(32r)^2e^{-(r-9)^2/N_0}dr$$
$$+\int_{\lambda_3}^{\lambda_4}(40r-32)^2e^{-(r-11)^2/N_0}dr+\int_{\lambda_3}^{\lambda_4}(40r-96)^2e^{-(r-13)^2/N_0}dr$$
$$+\int_{\lambda_3}^{\lambda_4}(40r-160)^2e^{-(r-15)^2/N_0}dr$$
$$+\int_{\lambda_4}^{\lambda_5}(-40r-160)^2e^{-(r+15)^2/N_0}dr+\int_{\lambda_4}^{\lambda_5}(-40r-96)^2e^{-(r+13)^2/N_0}dr$$
$$+\int_{\lambda_4}^{\lambda_5}(-40r-32)^2e^{-(r+11)^2/N_0}dr+\int_{\lambda_4}^{\lambda_5}(-32r)^2e^{-(r+9)^2/N_0}dr$$
$$+\int_{\lambda_4}^{\lambda_5}(-16r-32)^2e^{-(r+7)^2/N_0}dr+\int_{\lambda_4}^{\lambda_5}(-16r)^2e^{-(r+5)^2/N_0}dr$$
$$+\int_{\lambda_4}^{\lambda_5}(-8r)^2e^{-(r+3)^2/N_0}dr+\int_{\lambda_4}^{\lambda_5}(8r-32)^2e^{-(r-7)^2/N_0}dr$$
$$+\int_{\lambda_4}^{\lambda_5}(-32)^2e^{-(r-11)^2/N_0}dr+\int_{\lambda_4}^{\lambda_5}(8r-96)^2e^{-(r-13)^2/N_0}dr$$
$$+\int_{\lambda_4}^{\lambda_5}(16r-160)^2e^{-(r-15)^2/N_0}dr$$
$$+\int_{\lambda_5}^{\lambda_6}(-32r-192)^2e^{-(r+15)^2/N_0}dr+\int_{\lambda_5}^{\lambda_6}(-24r-160)^2e^{-(r+13)^2/N_0}dr$$
$$+\int_{\lambda_5}^{\lambda_6}(-24r-96)^2e^{-(r+11)^2/N_0}dr+\int_{\lambda_5}^{\lambda_6}(-24r-32)^2e^{-(r+9)^2/N_0}dr$$
$$+\int_{\lambda_5}^{\lambda_6}(-16r-32)^2e^{-(r+7)^2/N_0}dr+\int_{\lambda_5}^{\lambda_6}(-8r-32)^2e^{-(r+5)^2/N_0}dr$$
$$+\int_{\lambda_5}^{\lambda_6}(-32)^2e^{-(r+3)^2/N_0}dr+\int_{\lambda_5}^{\lambda_6}(-8r+32)^2e^{-(r-1)^2/N_0}dr$$
$$+\int_{\lambda_5}^{\lambda_6}(8r-64)^2e^{-(r-11)^2/N_0}dr+\int_{\lambda_5}^{\lambda_6}(16r-128)^2e^{-(r-13)^2/N_0}dr$$
$$+\int_{\lambda_5}^{\lambda_6}(16r-160)^2e^{-(r-15)^2/N_0}dr$$

$$
\begin{aligned}
&+\int_{\lambda_6}^{\lambda_7}(-32r-192)^2e^{-(r+15)^2/N_0}dr+\int_{\lambda_6}^{\lambda_7}(-32r-96)^2e^{-(r+13)^2/N_0}dr\\
&+\int_{\lambda_6}^{\lambda_7}(-24r-96)^2e^{-(r+11)^2/N_0}dr+\int_{\lambda_6}^{\lambda_7}(-16r-96)^2e^{-(r+9)^2/N_0}dr\\
&+\int_{\lambda_6}^{\lambda_7}(-8r-96)^2e^{-(r+7)^2/N_0}dr+\int_{\lambda_6}^{\lambda_7}(-8r-32)^2e^{-(r+5)^2/N_0}dr\\
&+\int_{\lambda_6}^{\lambda_7}(-8r+32)^2e^{-(r+3)^2/N_0}dr+\int_{\lambda_6}^{\lambda_7}(-16r+96)^2e^{-(r-1)^2/N_0}dr\\
&+\int_{\lambda_6}^{\lambda_7}(-16r+128)^2e^{-(r-3)^2/N_0}dr+\int_{\lambda_6}^{\lambda_7}(-8r+64)^2e^{-(r-5)^2/N_0}dr\\
&+\int_{\lambda_6}^{\lambda_7}(8r-96)^2e^{-(r-15)^2/N_0}dr\\
&+\int_{\lambda_7}^{\infty}(-40r-96)^2e^{-(r+15)^2/N_0}dr+\int_{\lambda_7}^{\infty}(-32r-96)^2e^{-(r+13)^2/N_0}dr\\
&+\int_{\lambda_7}^{\infty}(-24r-96)^2e^{-(r+11)^2/N_0}dr+\int_{\lambda_7}^{\infty}(-24r)^2e^{-(r+9)^2/N_0}dr\\
&+\int_{\lambda_7}^{\infty}(-8r-96)^2e^{-(r+7)^2/N_0}dr+\int_{\lambda_7}^{\infty}(-128)^2e^{-(r+5)^2/N_0}dr\\
&+\int_{\lambda_7}^{\infty}(-64)^2e^{-(r+3)^2/N_0}dr+\int_{\lambda_7}^{\infty}(-16r+96)^2e^{-(r-1)^2/N_0}dr\\
&+\int_{\lambda_7}^{\infty}(-8r+32)^2e^{-(r-3)^2/N_0}dr+\int_{\lambda_7}^{\infty}(-32)^2e^{-(r-5)^2/N_0}dr\\
&+\int_{\lambda_7}^{\infty}(-8r+96)^2e^{-(r-9)^2/N_0}dr\Bigg).
\end{aligned}
$$

The partial differentiations of the above cost function with respect to λ_1,λ_2,λ_3,λ_4,λ_5,λ_6,

and λ_7 are:

$$\begin{aligned}
\frac{\partial W(\boldsymbol{\lambda})}{\partial \lambda_1} = \frac{1}{16\sqrt{\pi N_0}} \Big(& (8\lambda_1+96)^2 e^{-(\lambda_1+9)^2/N_0} + (-32)^2 e^{-(\lambda_1+5)^2/N_0} \\
& + (8\lambda_1+32)^2 e^{-(\lambda_1+3)^2/N_0} + (16\lambda_1+96)^2 e^{-(\lambda_1+1)^2/N_0} \\
& + (-64)^2 e^{-(\lambda_1-3)^2/N_0} + (-128)^2 e^{-(\lambda_1-5)^2/N_0} \\
& + (8\lambda_1-96)^2 e^{-(\lambda_1-7)^2/N_0} + (24\lambda_1)^2 e^{-(\lambda_1-9)^2/N_0} \\
& + (24\lambda_1-96)^2 e^{-(\lambda_1-11)^2/N_0} + (32\lambda_1-96)^2 e^{-(\lambda_1-13)^2/N_0} \\
& + (40\lambda_1-96)^2 e^{-(\lambda_1-15)^2/N_0} - (-8\lambda_1-96)^2 e^{-(\lambda_1+15)^2/N_0} \\
& - (8\lambda_1+64)^2 e^{-(\lambda_1+5)^2/N_0} - (16\lambda_1+128)^2 e^{-(\lambda_1+3)^2/N_0} \\
& - (16\lambda_1+96)^2 e^{-(\lambda_1+1)^2/N_0} - (8\lambda_1+32)^2 e^{-(\lambda_1-3)^2/N_0} \\
& - (8\lambda_1-32)^2 e^{-(\lambda_1-5)^2/N_0} - (8\lambda_1-96)^2 e^{-(\lambda_1-7)^2/N_0} \\
& - (16\lambda_1-96)^2 e^{-(\lambda_1-9)^2/N_0} - (24\lambda_1-96)^2 e^{-(\lambda_1-11)^2/N_0} \\
& - (32\lambda_1-96)^2 e^{-(\lambda_1-13)^2/N_0} - (32\lambda_1-192)^2 e^{-(\lambda_1-15)^2/N_0} \Big),
\end{aligned}$$

$$
\begin{aligned}
\frac{\partial W(\boldsymbol{\lambda})}{\partial \lambda_2} \;=\; & \frac{1}{16\sqrt{\pi N_0}} \Big((-8\lambda_2 - 96)^2 e^{-(\lambda_2+15)^2/N_0} + (8\lambda_2 + 64)^2 e^{-(\lambda_2+5)^2/N_0} \\
& + (16\lambda_2 + 128)^2 e^{-(\lambda_2+3)^2/N_0} + (16\lambda_2 + 96)^2 e^{-(\lambda_2+1)^2/N_0} \\
& + (8\lambda_2 + 32)^2 e^{-(\lambda_2-3)^2/N_0} + (8\lambda_2 - 32)^2 e^{-(\lambda_2-5)^2/N_0} \\
& + (8\lambda_2 - 96)^2 e^{-(\lambda_2-7)^2/N_0} + (16\lambda_2 - 96)^2 e^{-(\lambda_2-9)^2/N_0} \\
& + (24\lambda_2 - 96)^2 e^{-(\lambda_2-11)^2/N_0} + (32\lambda_2 - 96)^2 e^{-(\lambda_2-13)^2/N_0} \\
& + (32\lambda_2 - 192)^2 e^{-(\lambda_2-15)^2/N_0} - (-16\lambda_2 - 160)^2 e^{-(\lambda_2+15)^2/N_0} \\
& - (-16\lambda_2 - 128)^2 e^{-(\lambda_2+13)^2/N_0} - (-8\lambda_2 - 64)^2 e^{-(\lambda_2+11)^2/N_0} \\
& - (8\lambda_2 + 32)^2 e^{-(\lambda_2+1)^2/N_0} - (-32)^2 e^{-(\lambda_2-3)^2/N_0} \\
& - (8\lambda_2 - 32)^2 e^{-(\lambda_2-5)^2/N_0} - (16\lambda_2 - 32)^2 e^{-(\lambda_2-7)^2/N_0} \\
& - (24\lambda_2 - 32)^2 e^{-(\lambda_2-9)^2/N_0} - (24\lambda_2 - 96)^2 e^{-(\lambda_2-11)^2/N_0} \\
& - (24\lambda_2 - 160)^2 e^{-(\lambda_2-13)^2/N_0} - (32\lambda_2 - 192)^2 e^{-(\lambda_2-15)^2/N_0} \Big) ,
\end{aligned}
$$

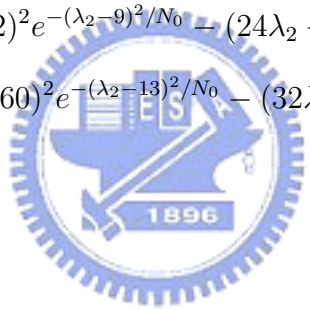

$$
\begin{aligned}
\frac{\partial W(\boldsymbol{\lambda})}{\partial \lambda_3} \;=\; & \frac{1}{16\sqrt{\pi N_0}} \Big((-16\lambda_3 - 160)^2 e^{-(\lambda_3+15)^2/N_0} + (-16\lambda_3 - 128)^2 e^{-(\lambda_3+13)^2/N_0} \\
& + (-8\lambda_3)^2 e^{-(\lambda_3+11)^2/N_0} + (8\lambda_3 + 32)^2 e^{-(\lambda_3+1)^2/N_0} \\
& + (-32)^2 e^{-(\lambda_3-3)^2/N_0} + (8\lambda_3 - 32)^2 e^{-(\lambda_3-5)^2/N_0} \\
& + (16\lambda_3 - 32)^2 e^{-(\lambda_3-7)^2/N_0} + (24\lambda_3 - 32)^2 e^{-(\lambda_3-9)^2/N_0} \\
& + (24\lambda_3 - 96)^2 e^{-(\lambda_3-11)^2/N_0} + (24\lambda_3 - 160)^2 e^{-(\lambda_3-13)^2/N_0} \\
& + (32\lambda_3 - 192)^2 e^{-(\lambda_3-15)^2/N_0} \\
& - (-16\lambda_3 - 160)^2 e^{-(\lambda_3+15)^2/N_0} - (-8\lambda_3 - 96)^2 e^{-(\lambda_3+13)^2/N_0} \\
& - (-32)^2 e^{-(\lambda_3+11)^2/N_0} - (-8\lambda_3 - 32)^2 e^{-(\lambda_3+7)^2/N_0} \\
& - (8\lambda_3)^2 e^{-(\lambda_3-3)^2/N_0} - (16\lambda_3)^2 e^{-(\lambda_3-5)^2/N_0} \\
& - (16\lambda_3 - 32)^2 e^{-(\lambda_3-7)^2/N_0} - (32\lambda_3)^2 e^{-(\lambda_3-9)^2/N_0} \\
& - (40\lambda_3 - 32)^2 e^{-(\lambda_3-11)^2/N_0} - (40\lambda_3 - 96)^2 e^{-(\lambda_3-13)^2/N_0} \\
& - (40\lambda_3 - 160)^2 e^{-(\lambda_3-15)^2/N_0} \Big),
\end{aligned}
$$

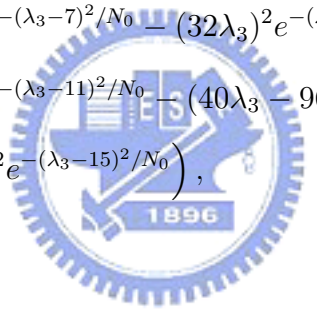

$$
\begin{aligned}
\frac{\partial W(\boldsymbol{\lambda})}{\partial \lambda_4} = \frac{1}{16\sqrt{\pi N_0}} \Big(& (-16\lambda_4 - 160)^2 e^{-(\lambda_4+15)^2/N_0} + (-8\lambda_4 - 96)^2 e^{-(\lambda_4+13)^2/N_0} \\
& + (-32)^2 e^{-(\lambda_4+11)^2/N_0} + (-8\lambda_4 - 32)^2 e^{-(\lambda_4+7)^2/N_0} \\
& + (8\lambda_4)^2 e^{-(\lambda_4-3)^2/N_0} + (16\lambda_4)^2 e^{-(\lambda_4-5)^2/N_0} \\
& + (16\lambda_4 - 32)^2 e^{-(\lambda_4-7)^2/N_0} + (32\lambda_4)^2 e^{-(\lambda_4-9)^2/N_0} \\
& + (40\lambda_4 - 32)^2 e^{-(\lambda_4-11)^2/N_0} + (40\lambda_4 - 96)^2 e^{-(\lambda_4-13)^2/N_0} \\
& + (40\lambda_4 - 160)^2 e^{-(\lambda_4-15)^2/N_0} \\
& - (-40\lambda_4 - 160)^2 e^{-(\lambda_4+15)^2/N_0} - (-40\lambda_4 - 96)^2 e^{-(\lambda_4+13)^2/N_0} \\
& - (-40\lambda_4 - 32)^2 e^{-(\lambda_4+11)^2/N_0} - (-32\lambda_4)^2 e^{-(\lambda_4+9)^2/N_0} \\
& - (-16\lambda_4 - 32)^2 e^{-(\lambda_4+7)^2/N_0} - (-16\lambda_4)^2 e^{-(\lambda_4+5)^2/N_0} \\
& - (-8\lambda_4)^2 e^{-(\lambda_4+3)^2/N_0} - (8\lambda_4 - 32)^2 e^{-(\lambda_4-7)^2/N_0} \\
& - (-32)^2 e^{-(\lambda_4-11)^2/N_0} - (8\lambda_4 - 96)^2 e^{-(\lambda_4-13)^2/N_0} \\
& - (16\lambda_4 - 160)^2 e^{-(\lambda_4-15)^2/N_0} \Big),
\end{aligned}
$$

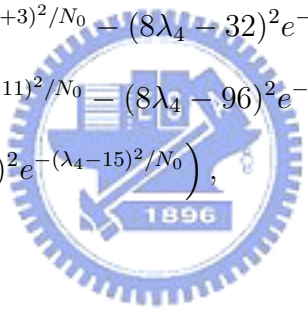

$$
\begin{aligned}
\frac{\partial W(\boldsymbol{\lambda})}{\partial \lambda_5} \;=\; & \frac{1}{16\sqrt{\pi N_0}}\Big((-40\lambda_5-160)^2 e^{-(\lambda_5+15)^2/N_0}+(-40\lambda_5-96)^2 e^{-(\lambda_5+13)^2/N_0} \\
& +(-40\lambda_5-32)^2 e^{-(\lambda_5+11)^2/N_0}+(-32\lambda_5)^2 e^{-(\lambda_5+9)^2/N_0} \\
& +(-16\lambda_5-32)^2 e^{-(\lambda_5+7)^2/N_0}+(-16\lambda_5)^2 e^{-(\lambda_5+5)^2/N_0} \\
& +(-8\lambda_5)^2 e^{-(\lambda_5+3)^2/N_0}+(8\lambda_5-32)^2 e^{-(\lambda_5-7)^2/N_0} \\
& +(-32)^2 e^{-(\lambda_5-11)^2/N_0}+(8\lambda_5-96)^2 e^{-(\lambda_5-13)^2/N_0} \\
& +(16\lambda_5-160)^2 e^{-(\lambda_5-15)^2/N_0} \\
& -(-32\lambda_5-192)^2 e^{-(\lambda_5+15)^2/N_0}-(-24\lambda_5-160)^2 e^{-(\lambda_5+13)^2/N_0} \\
& -(-24\lambda_5-96)^2 e^{-(\lambda_5+11)^2/N_0}-(-24\lambda_5-32)^2 e^{-(\lambda_5+9)^2/N_0} \\
& -(-16\lambda_5-32)^2 e^{-(\lambda_5+7)^2/N_0}-(-8\lambda_5-32)^2 e^{-(\lambda_5+5)^2/N_0} \\
& -(-32)^2 e^{-(\lambda_5+3)^2/N_0}-(-8\lambda_5+32)^2 e^{-(\lambda_5-1)^2/N_0} \\
& -(8\lambda_5)^2 e^{-(\lambda_5-11)^2/N_0}-(16\lambda_5-128)^2 e^{-(\lambda_5-13)^2/N_0} \\
& -(16\lambda_5-160)^2 e^{-(\lambda_5-15)^2/N_0}\Big),
\end{aligned}
$$

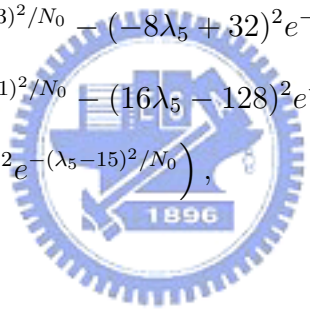

$$
\begin{aligned}
\frac{\partial W(\boldsymbol{\lambda})}{\partial \lambda_6} \;=\; & \frac{1}{16\sqrt{\pi N_0}} \Big((-32\lambda_6 - 192)^2 e^{-(\lambda_6+15)^2/N_0} + (-24\lambda_6 - 160)^2 e^{-(\lambda_6+13)^2/N_0} \\
& + (-24\lambda_6 - 96)^2 e^{-(\lambda_6+11)^2/N_0} + (-24\lambda_6 - 32)^2 e^{-(\lambda_6+9)^2/N_0} \\
& + (-16\lambda_6 - 32)^2 e^{-(\lambda_6+7)^2/N_0} + (-8\lambda_6 - 32)^2 e^{-(\lambda_6+5)^2/N_0} \\
& + (-32)^2 e^{-(\lambda_6+3)^2/N_0} + (-8\lambda_6 + 32)^2 e^{-(\lambda_6-1)^2/N_0} \\
& + (8\lambda_6 - 64)^2 e^{-(\lambda_6-11)^2/N_0} + (16\lambda_6 - 128)^2 e^{-(\lambda_6-13)^2/N_0} \\
& + (16\lambda_6 - 160)^2 e^{-(\lambda_6-15)^2/N_0} \\
& - (-32\lambda_6 - 192)^2 e^{-(\lambda_6+15)^2/N_0} - (-32\lambda_6 - 96)^2 e^{-(\lambda_6+13)^2/N_0} \\
& - (-24\lambda_6 - 96)^2 e^{-(\lambda_6+11)^2/N_0} - (-16\lambda_6 - 96)^2 e^{-(\lambda_6+9)^2/N_0} \\
& - (-8\lambda_6 - 96)^2 e^{-(\lambda_6+7)^2/N_0} - (-8\lambda_6 - 32)^2 e^{-(\lambda_6+5)^2/N_0} \\
& - (-8\lambda_6 + 32)^2 e^{-(\lambda_6+3)^2/N_0} - (-16\lambda_6 + 96)^2 e^{-(\lambda_6-1)^2/N_0} \\
& - (-16\lambda_6 + 128)^2 e^{-(\lambda_6-3)^2/N_0} - (-8\lambda_6 + 64)^2 e^{-(\lambda_6-5)^2/N_0} \\
& - (8\lambda_6 - 96)^2 e^{-(\lambda_6-15)^2/N_0} \Big),
\end{aligned}
$$

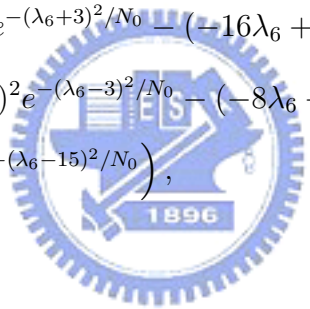

$$
\begin{aligned}
\frac{\partial W(\boldsymbol{\lambda})}{\partial \lambda_7} &= \frac{1}{16\sqrt{\pi N_0}}\Big((-32\lambda_7-192)^2 e^{-(\lambda_7+15)^2/N_0} + (-32\lambda_7-96)^2 e^{-(\lambda_7+13)^2/N_0} \\
&\quad +(-24\lambda_7-96)^2 e^{-(\lambda_7+11)^2/N_0} + (-16\lambda_7-96)^2 e^{-(\lambda_7+9)^2/N_0} \\
&\quad +(-8\lambda_7-96)^2 e^{-(\lambda_7+7)^2/N_0} + (-8\lambda_7-32)^2 e^{-(\lambda_7+5)^2/N_0} \\
&\quad +(-8\lambda_7+32)^2 e^{-(\lambda_7+3)^2/N_0} + (-16\lambda_7+96)^2 e^{-(\lambda_7-1)^2/N_0} \\
&\quad +(-16\lambda_7+128)^2 e^{-(\lambda_7-3)^2/N_0} + (-8\lambda_7+64)^2 e^{-(\lambda_7-5)^2/N_0} \\
&\quad +(8\lambda_7-96)^2 e^{-(\lambda_7-15)^2/N_0} \\
&\quad -(-40\lambda_7-96)^2 e^{-(\lambda_7+15)^2/N_0} - (-32\lambda_7-96)^2 e^{-(\lambda_7+13)^2/N_0} \\
&\quad -(-24\lambda_7-96)^2 e^{-(\lambda_7+11)^2/N_0} - (-24\lambda_7)^2 e^{-(\lambda_7+9)^2/N_0} \\
&\quad -(-8\lambda_7-96)^2 e^{-(\lambda_7+7)^2/N_0} - (-128)^2 e^{-(\lambda_7+5)^2/N_0} \\
&\quad -(-64)^2 e^{-(\lambda_7+3)^2/N_0} - (-16\lambda_7+96)^2 e^{-(\lambda_7-1)^2/N_0} \\
&\quad -(-8\lambda_7+32)^2 e^{-(\lambda_7-3)^2/N_0} - (-32)^2 e^{-(\lambda_7-5)^2/N_0} \\
&\quad -(-8\lambda_7+96)^2 e^{-(\lambda_7-9)^2/N_0}\Big).
\end{aligned}
$$

By setting the above equations to be zero we have $\lambda_1 = -12$, $\lambda_2 = -8$, $\lambda_3 = -4$, $\lambda_4 = 0$, $\lambda_5 = 4$, $\lambda_6 = 8$, and $\lambda_7 = 12$ which minimize the cost function. Consequently, the cost function is reduced to:

$$
\begin{aligned}
W(f_1,f_2,f_3,f_4) \;=\; & \frac{4}{\sqrt{\pi N_0}}\left(\int_{-\infty}^{-12}(r+12)^2e^{-(r+9)^2/N_0}dr+\int_{-\infty}^{-12}(-4)^2e^{-(r+5)^2/N_0}dr\right.\\
&+\int_{-\infty}^{-12}(r+4)^2e^{-(r+3)^2/N_0}dr+\int_{-\infty}^{-12}(2r+12)^2e^{-(r+1)^2/N_0}dr\\
&+\int_{-\infty}^{-12}(-8)^2e^{-(r-3)^2/N_0}dr+\int_{-\infty}^{-12}(-16)^2e^{-(r-5)^2/N_0}dr\\
&+\int_{-\infty}^{-12}(r-12)^2e^{-(r-7)^2/N_0}dr+\int_{-\infty}^{-12}(3r)^2e^{-(r-9)^2/N_0}dr\\
&+\int_{-\infty}^{-12}(3r-12)^2e^{-(r-11)^2/N_0}dr+\int_{-\infty}^{-12}(4r-12)^2e^{-(r-13)^2/N_0}dr\\
&+\int_{-\infty}^{-12}(5r-12)^2e^{-(r-15)^2/N_0}dr\\
&+\int_{-12}^{-8}(-r-12)^2e^{-(r+15)^2/N_0}dr+\int_{-12}^{-8}(r+8)^2e^{-(r+5)^2/N_0}dr\\
&+\int_{-12}^{-8}(2r+16)^2e^{-(r+3)^2/N_0}dr+\int_{-12}^{-8}(2r+12)^2e^{-(r+1)^2/N_0}dr\\
&+\int_{-12}^{-8}(r+4)^2e^{-(r-3)^2/N_0}dr+\int_{-12}^{-8}(r-4)^2e^{-(r-5)^2/N_0}dr\\
&+\int_{-12}^{-8}(r-12)^2e^{-(r-7)^2/N_0}dr+\int_{-12}^{-8}(2r-12)^2e^{-(r-9)^2/N_0}dr\\
&+\int_{-12}^{-8}(3r-12)^2e^{-(r-11)^2/N_0}dr+\int_{-12}^{-8}(4r-12)^2e^{-(r-13)^2/N_0}dr\\
&+\int_{-12}^{-8}(4r-24)^2e^{-(r-15)^2/N_0}dr\\
&+\int_{-8}^{-4}(-2r-20)^2e^{-(r+15)^2/N_0}dr+\int_{-8}^{-4}(-2r-16)^2e^{-(r+13)^2/N_0}dr\\
&+\int_{-8}^{-4}(-r-8)^2e^{-(r+11)^2/N_0}dr+\int_{-8}^{-4}(r+4)^2e^{-(r+1)^2/N_0}dr\\
&+\int_{-8}^{-4}(-4)^2e^{-(r-3)^2/N_0}dr+\int_{-8}^{-4}(r-4)^2e^{-(r-5)^2/N_0}dr\\
&+\int_{-8}^{-4}(2r-4)^2e^{-(r-7)^2/N_0}dr+\int_{-8}^{-4}(3r-4)^2e^{-(r-9)^2/N_0}dr\\
&+\int_{-8}^{-4}(3r-12)^2e^{-(r-11)^2/N_0}dr+\int_{-8}^{-4}(3r-20)^2e^{-(r-13)^2/N_0}dr\\
&+\int_{-8}^{-4}(4r-24)^2e^{-(r-15)^2/N_0}dr
\end{aligned}
$$

$$
\begin{aligned}
&+\int_{-4}^{0}(-2r-20)^2e^{-(r+15)^2/N_0}dr+\int_{-4}^{0}(-r-12)^2e^{-(r+13)^2/N_0}dr\\
&+\int_{-4}^{0}(-4)^2e^{-(r+11)^2/N_0}dr+\int_{-4}^{0}(-r-4)^2e^{-(r+7)^2/N_0}dr\\
&+\int_{-4}^{0}(r)^2e^{-(r-3)^2/N_0}dr+\int_{-4}^{0}(2r)^2e^{-(r-5)^2/N_0}dr\\
&+\int_{-4}^{0}(2r-4)^2e^{-(r-7)^2/N_0}dr+\int_{-4}^{0}(4r)^2e^{-(r-9)^2/N_0}dr\\
&+\int_{-4}^{0}(5r-4)^2e^{-(r-11)^2/N_0}dr+\int_{-4}^{0}(5r-12)^2e^{-(r-13)^2/N_0}dr\\
&+\int_{-4}^{0}(5r-20)^2e^{-(r-15)^2/N_0}dr\\
&+\int_{0}^{4}(-5r-20)^2e^{-(r+15)^2/N_0}dr+\int_{0}^{4}(-5r-12)^2e^{-(r+13)^2/N_0}dr\\
&+\int_{0}^{4}(-5r-4)^2e^{-(r+11)^2/N_0}dr+\int_{0}^{4}(-4r)^2e^{-(r+9)^2/N_0}dr\\
&+\int_{0}^{4}(-2r-4)^2e^{-(r+7)^2/N_0}dr+\int_{0}^{4}(-2r)^2e^{-(r+5)^2/N_0}dr\\
&+\int_{0}^{4}(-r)^2e^{-(r+3)^2/N_0}dr+\int_{0}^{4}(r-4)^2e^{-(r-7)^2/N_0}dr\\
&+\int_{0}^{4}(-4)^2e^{-(r-11)^2/N_0}dr+\int_{0}^{4}(r-12)^2e^{-(r-13)^2/N_0}dr\\
&+\int_{0}^{4}(2r-20)^2e^{-(r-15)^2/N_0}dr\\
&+\int_{4}^{8}(-4r-24)^2e^{-(r+15)^2/N_0}dr+\int_{4}^{8}(-3r-20)^2e^{-(r+13)^2/N_0}dr\\
&+\int_{4}^{8}(-3r-12)^2e^{-(r+11)^2/N_0}dr+\int_{4}^{8}(-3r-4)^2e^{-(r+9)^2/N_0}dr\\
&+\int_{4}^{8}(-2r-4)^2e^{-(r+7)^2/N_0}dr+\int_{4}^{8}(-r-4)^2e^{-(r+5)^2/N_0}dr\\
&+\int_{4}^{8}(-4)^2e^{-(r+3)^2/N_0}dr+\int_{4}^{8}(-r+4)^2e^{-(r-1)^2/N_0}dr\\
&+\int_{4}^{8}(r-8)^2e^{-(r-11)^2/N_0}dr+\int_{4}^{8}(2r-16)^2e^{-(r-13)^2/N_0}dr\\
&+\int_{4}^{8}(2r-20)^2e^{-(r-15)^2/N_0}dr
\end{aligned}
$$

$$
\begin{aligned}
&+\int_8^{12}(-4r-24)^2e^{-(r+15)^2/N_0}dr+\int_8^{12}(-4r-12)^2e^{-(r+13)^2/N_0}dr\\
&+\int_8^{12}(-3r-12)^2e^{-(r+11)^2/N_0}dr+\int_8^{12}(-2r-12)^2e^{-(r+9)^2/N_0}dr\\
&+\int_8^{12}(-r-12)^2e^{-(r+7)^2/N_0}dr+\int_8^{12}(-r-4)^2e^{-(r+5)^2/N_0}dr\\
&+\int_8^{12}(-r+4)^2e^{-(r+3)^2/N_0}dr+\int_8^{12}(-2r+12)^2e^{-(r-1)^2/N_0}dr\\
&+\int_8^{12}(-2r+16)^2e^{-(r-3)^2/N_0}dr+\int_8^{12}(-r+8)^2e^{-(r-5)^2/N_0}dr\\
&+\int_8^{12}(r-12)^2e^{-(r-15)^2/N_0}dr\\
&+\int_{12}^{\infty}(-5r-12)^2e^{-(r+15)^2/N_0}dr+\int_{12}^{\infty}(-4r-12)^2e^{-(r+13)^2/N_0}dr\\
&+\int_{12}^{\infty}(-3r-12)^2e^{-(r+11)^2/N_0}dr+\int_{12}^{\infty}(-3r)^2e^{-(r+9)^2/N_0}dr\\
&+\int_{12}^{\infty}(-r-12)^2e^{-(r+7)^2/N_0}dr+\int_{12}^{\infty}(-16)^2e^{-(r+5)^2/N_0}dr\\
&+\int_{12}^{\infty}(8)^2e^{-(r+3)^2/N_0}dr+\int_{12}^{\infty}(-2r+12)^2e^{-(r-1)^2/N_0}dr\\
&+\int_{12}^{\infty}(-r+4)^2e^{-(r-3)^2/N_0}dr+\int_{12}^{\infty}(-4)^2e^{-(r-5)^2/N_0}dr\\
&+\int_{12}^{\infty}(-r+12)^2e^{-(r-9)^2/N_0}dr\Big)\\
=\;&-\frac{396\sqrt{N_0}}{\sqrt{\pi}}e^{-729/N_0}-\frac{368\sqrt{N_0}}{\sqrt{\pi}}e^{-441/N_0}+\frac{364\sqrt{N_0}}{\sqrt{\pi}}e^{-361/N_0}+\frac{632\sqrt{N_0}}{\sqrt{\pi}}e^{-289/N_0}\\
&-\frac{188\sqrt{N_0}}{\sqrt{\pi}}e^{-225/N_0}-\frac{628\sqrt{N_0}}{\sqrt{\pi}}e^{-169/N_0}-\frac{952\sqrt{N_0}}{\sqrt{\pi}}e^{-121/N_0}-\frac{444\sqrt{N_0}}{\sqrt{\pi}}e^{-81/N_0}\\
&-\frac{168\sqrt{N_0}}{\sqrt{\pi}}e^{-49/N_0}-\frac{240\sqrt{N_0}}{\sqrt{\pi}}e^{-25/N_0}-\frac{84\sqrt{N_0}}{\sqrt{\pi}}e^{-9/N_0}\\
&+(252+4N_0)\operatorname{erfc}\left(\frac{3}{\sqrt{N_0}}\right)+(1200+24N_0)\operatorname{erfc}\left(\frac{5}{\sqrt{N_0}}\right)+(1176+12N_0)\operatorname{erfc}\left(\frac{7}{\sqrt{N_0}}\right)\\
&+(3996+14N_0)\operatorname{erfc}\left(\frac{9}{\sqrt{N_0}}\right)+(10472+52N_0)\operatorname{erfc}\left(\frac{1}{1}\sqrt{N_0}\right)+(8146+34N_0)\operatorname{erfc}\left(\frac{1}{3}\sqrt{N_0}\right)\\
&+(2820+2N_0)\operatorname{erfc}\left(\frac{1}{5}\sqrt{N_0}\right)-(10744+44N_0)\operatorname{erfc}\left(\frac{1}{7}\sqrt{N_0}\right)-(6916+18N_0)\operatorname{erfc}\left(\frac{1}{9}\sqrt{N_0}\right)\\
&+(7728+24N_0)\operatorname{erfc}\left(\frac{2}{1}\sqrt{N_0}\right)+(10692+18N_0)\operatorname{erfc}\left(\frac{2}{7}\sqrt{N_0}\right)
\end{aligned}
$$

.

We summarize the bit-wise metrics as follows.

$$\rho = \begin{cases} 1, & \text{if } r \le -12; \\ 2, & \text{if } -12 < r \le -8; \\ 3, & \text{if } -8 < r \le -4; \\ 4, & \text{if } -4 < r \le 0; \\ 5, & \text{if } 0 < r \le 4; \\ 6, & \text{if } 4 < r \le 8; \\ 7, & \text{if } 8 < r \le 12; \\ 8, & \text{if } r > 12 \end{cases}$$

$$\begin{aligned}
f_1(r,c) &= \frac{1}{3}r^2 + a_{1,c,\rho}r + b_{1,c,\rho} \\
&= \frac{1}{3}r^2 + [-a_{2,1,\rho} - a_{3,1,\rho} - 2(1-2c) + 8(1-2c)\cdot \mathbf{1}\{(1-2c)r \le 0 \vee (1-2c)r \ge 4\}]\, r \\
&\quad +[(9 - b_{2,1,\rho} - b_{3,1,\rho}) - 32 \cdot \mathbf{1}\{(1-2c)r \ge 4\}] \\
f_2(r,c) &= \frac{1}{4}r^2 + a_{2,c,\rho}r + b_{2,c,\rho} \\
&= \frac{1}{4}r^2 + [a_{2,1,\rho} - (4 + 8\cdot \mathrm{u}((|r|-4)\cdot(|r|-12)))(1-c)\cdot \mathrm{sgn}(r)]r \\
&\quad +[b_{2,1,\rho} + (32 + (8*(12-4) - 32)\mathrm{u}((|r|-4)(|r|+4)) \\
&\quad +(8*(12+4) - 32)\mathrm{u}((|r|-12)(|r|+12)))(1-c)] \\
f_3(r,c) &= \frac{1}{4}r^2 + a_{3,c,\rho}r + b_{3,c,\rho} \\
&= \frac{1}{4}r^2 + [a_{3,1,\rho} - (4 - 8\cdot \mathrm{u}(-|r|\cdot(|r|-8)))(1-c)\cdot \mathrm{sgn}(r)]r \\
&\quad +[b_{3,1,\rho} + (-16 + 64\cdot \mathrm{u}(|r|-4))(1-c)] \\
f_4(r,c) &= \frac{1}{4}r^2 + a_{3,c,\rho}r + b_{3,c,\rho} \\
&= \frac{1}{4}r^2 + [a_{4,1,\rho} - (4 - 8\cdot \mathrm{u}(-|r|\cdot(|r|-8)) + 8\cdot \mathrm{u}(-(|r|-8)(|r|-12)))(1-c)\cdot \mathrm{sgn}(r)]r \\
&\quad +[b_{4,1,\rho} + (-8 + 32\cdot \mathrm{u}(|r|-4) - 64\cdot \mathrm{u}(|r|-8) + 96\cdot \mathrm{u}(|r|-12))(1-c)]
\end{aligned}$$

By the nature of Viterbi algorithm, only those terms that depend on c affect the decoding

behavior. Hence, the equivalent metrics are

$$
\begin{aligned}
f_1^{\text{eq}}(r,c) &= -2(1-2c)r + 8(1-2c)r \cdot \mathbf{1}\{(1-2c)r \le 0 \vee (1-2c)r \ge 4\} - 32 \cdot \mathbf{1}\{(1-2c)r \ge 4\} \\
f_2^{\text{eq}}(r,c) &= -(4 + 8 \cdot \mathrm{u}((|r|-4)\cdot(|r|-12)))(1-c)|r| \\
&\quad +[32 + (8*(12-4)-32)\mathrm{u}((|r|-4)(|r|+4)) \\
&\quad +(8*(12+4)-32)\mathrm{u}((|r|-12)(|r|+12))](1-c) \\
f_3^{\text{eq}}(r,c) &= -(4 - 8 \cdot \mathrm{u}(-|r|\cdot(|r|-8)))(1-c)|r| + (-16 + 64 \cdot \mathrm{u}(|r|-4))(1-c) \\
f_4^{\text{eq}}(r,c) &= -(4 - 8 \cdot \mathrm{u}(-|r|\cdot(|r|-8)) + 8 \cdot \mathrm{u}(-(|r|-8)(|r|-12)))(1-c)|r| \\
&\quad +[-8 + 32 \cdot \mathrm{u}(|r|-4) - 64 \cdot \mathrm{u}(|r|-8) + 96 \cdot \mathrm{u}(|r|-12)](1-c),
\end{aligned}
$$

Since the branch metric of Viterbi algorithm can be the relative metric between information bits 0 and 1, the above metrics can be further reduced to

$$
\begin{cases}
f_1^{256\text{QAM}}(c,r) &= c(|r-8| + |r-4| + |r| + |r+4| + |r+8| - 24)\cdot \mathrm{sgn}(-r) \\
f_2^{256\text{QAM}}(c,r) &= c(|4-|r|| + |8-|r|| + |12-|r|| - 8)\cdot \mathrm{sgn}(-r) \\
f_3^{256\text{QAM}}(c,r) &= c(|4-||r|-8||)\cdot \mathrm{sgn}(||r|-8|-4) \\
f_4^{256\text{QAM}}(c,r) &= c(||8-|r||-4|-2)
\end{cases}
$$

Finally, we can use the nature of recursive from 64QAM's metrics to represent 256QAM's metrics.

$$
\begin{cases}
f_1^{256\text{QAM}}(c,r) &= c(|r-8| + |r-4| + |r| + |r+4| + |r+8| - 24)\cdot \mathrm{sgn}(-r) \\
f_2^{256\text{QAM}}(c,r) &= f_1^{64\text{QAM}}(c, 8-|r|) \\
f_3^{256\text{QAM}}(c,r) &= f_2^{64\text{QAM}}(c, |r|-8) \\
f_4^{256\text{QAM}}(c,r) &= f_3^{64\text{QAM}}(c, 8-|r|)
\end{cases}
$$

A.3 Derivation of Bit-wise Metric of 1024QAM Modulation

Suppose that Gray code mapping is employed for 256QAM mapping, i.e. -31, -29, -27, -25, -23, -21, -19, -17, -15, -13, -11, -9, -7, -5, -3, -1, $+1$, $+3$, $+5$, $+7$, $+9$, $+11$, $+13$, $+15$, $+17$, $+19$, $+21$, $+23$, $+25$, $+27$, $+29$ and $+31$ respectively map to 00000, 00001, 00011, 00010, 00110, 00111, 00101, 00100, 01100, 01101, 01111, 01110, 01010, 01011, 01001, 01000, 11000, 11001, 11011, 11010, 11110, 11111, 11101, 11100, 10100, 10101, 10111, 10110, 10010, 10011, 10001, and 10000. Then the squared error criterion (or cost function)is given by

$$W(f_1,f_2,f_3,f_4,f_5)=\frac{1}{32\sqrt{\pi N_0}}$$
$$\Bigg(\int_{-\infty}^{\infty}\left[f_1(r_1,0)+f_2(r_1,0)+f_3(r_1,0)+f_4(r_1,0)+f_5(r_1,0)-(r_1+31)^2\right]^2 e^{-(r_1+31)^2/N_0}dr_1$$
$$+\int_{-\infty}^{\infty}\left[f_1(r_1,0)+f_2(r_1,0)+f_3(r_1,0)+f_4(r_1,0)+f_5(r_1,1)-(r_1+29)^2\right]^2 e^{-(r_1+29)^2/N_0}dr_1$$
$$+\int_{-\infty}^{\infty}\left[f_1(r_1,0)+f_2(r_1,0)+f_3(r_1,0)+f_4(r_1,1)+f_5(r_1,1)-(r_1+27)^2\right]^2 e^{-(r_1+27)^2/N_0}dr_1$$
$$+\int_{-\infty}^{\infty}\left[f_1(r_1,0)+f_2(r_1,0)+f_3(r_1,0)+f_4(r_1,1)+f_5(r_1,0)-(r_1+25)^2\right]^2 e^{-(r_1+25)^2/N_0}dr_1$$
$$+\int_{-\infty}^{\infty}\left[f_1(r_1,0)+f_2(r_1,0)+f_3(r_1,1)+f_4(r_1,1)+f_5(r_1,0)-(r_1+23)^2\right]^2 e^{-(r_1+23)^2/N_0}dr_1$$
$$+\int_{-\infty}^{\infty}\left[f_1(r_1,0)+f_2(r_1,0)+f_3(r_1,1)+f_4(r_1,1)+f_5(r_1,1)-(r_1+21)^2\right]^2 e^{-(r_1+21)^2/N_0}dr_1$$
$$+\int_{-\infty}^{\infty}\left[f_1(r_1,0)+f_2(r_1,0)+f_3(r_1,1)+f_4(r_1,0)+f_5(r_1,1)-(r_1+19)^2\right]^2 e^{-(r_1+19)^2/N_0}dr_1$$
$$+\int_{-\infty}^{\infty}\left[f_1(r_1,0)+f_2(r_1,0)+f_3(r_1,1)+f_4(r_1,0)+f_5(r_1,0)-(r_1+17)^2\right]^2 e^{-(r_1+17)^2/N_0}dr_1$$
$$+\int_{-\infty}^{\infty}\left[f_1(r_1,0)+f_2(r_1,1)+f_3(r_1,1)+f_4(r_1,0)+f_5(r_1,0)-(r_1+15)^2\right]^2 e^{-(r_1+15)^2/N_0}dr_1$$
$$+\int_{-\infty}^{\infty}\left[f_1(r_1,0)+f_2(r_1,1)+f_3(r_1,1)+f_4(r_1,0)+f_5(r_1,1)-(r_1+13)^2\right]^2 e^{-(r_1+13)^2/N_0}dr_1$$
$$+\int_{-\infty}^{\infty}\left[f_1(r_1,0)+f_2(r_1,1)+f_3(r_1,1)+f_4(r_1,1)+f_5(r_1,1)-(r_1+11)^2\right]^2 e^{-(r_1+11)^2/N_0}dr_1$$
$$+\int_{-\infty}^{\infty}\left[f_1(r_1,0)+f_2(r_1,1)+f_3(r_1,1)+f_4(r_1,1)+f_5(r_1,0)-(r_1+9)^2\right]^2 e^{-(r_1+9)^2/N_0}dr_1$$
$$+\int_{-\infty}^{\infty}\left[f_1(r_1,0)+f_2(r_1,1)+f_3(r_1,0)+f_4(r_1,1)+f_5(r_1,0)-(r_1+7)^2\right]^2 e^{-(r_1+7)^2/N_0}dr_1$$
$$+\int_{-\infty}^{\infty}\left[f_1(r_1,0)+f_2(r_1,1)+f_3(r_1,0)+f_4(r_1,1)+f_5(r_1,1)-(r_1+5)^2\right]^2 e^{-(r_1+5)^2/N_0}dr_1$$
$$+\int_{-\infty}^{\infty}\left[f_1(r_1,0)+f_2(r_1,1)+f_3(r_1,0)+f_4(r_1,0)+f_5(r_1,1)-(r_1+3)^2\right]^2 e^{-(r_1+3)^2/N_0}dr_1$$
$$+\int_{-\infty}^{\infty}\left[f_1(r_1,0)+f_2(r_1,1)+f_3(r_1,0)+f_4(r_1,0)+f_5(r_1,0)-(r_1+1)^2\right]^2 e^{-(r_1+1)^2/N_0}dr_1$$
$$+\int_{-\infty}^{\infty}\left[f_1(r_1,1)+f_2(r_1,1)+f_3(r_1,0)+f_4(r_1,0)+f_5(r_1,0)-(r_1-1)^2\right]^2 e^{-(r_1-1)^2/N_0}dr_1$$
$$+\int_{-\infty}^{\infty}\left[f_1(r_1,1)+f_2(r_1,1)+f_3(r_1,0)+f_4(r_1,0)+f_5(r_1,1)-(r_1-3)^2\right]^2 e^{-(r_1-3)^2/N_0}dr_1$$

$$
\begin{aligned}
&+\int_{-\infty}^{\infty}\left[f_1(r_1,1)+f_2(r_1,1)+f_3(r_1,0)+f_4(r_1,1)+f_5(r_1,1)-(r_1-5)^2\right]^2 e^{-(r_1-5)^2/N_0}dr_1\\
&+\int_{-\infty}^{\infty}\left[f_1(r_1,1)+f_2(r_1,1)+f_3(r_1,0)+f_4(r_1,1)+f_5(r_1,0)-(r_1-7)^2\right]^2 e^{-(r_1-7)^2/N_0}dr_1\\
&+\int_{-\infty}^{\infty}\left[f_1(r_1,1)+f_2(r_1,1)+f_3(r_1,1)+f_4(r_1,1)+f_5(r_1,0)-(r_1-9)^2\right]^2 e^{-(r_1-9)^2/N_0}dr_1\\
&+\int_{-\infty}^{\infty}\left[f_1(r_1,1)+f_2(r_1,1)+f_3(r_1,1)+f_4(r_1,1)+f_5(r_1,1)-(r_1-11)^2\right]^2 e^{-(r_1-11)^2/N_0}dr_1\\
&+\int_{-\infty}^{\infty}\left[f_1(r_1,1)+f_2(r_1,1)+f_3(r_1,1)+f_4(r_1,0)+f_5(r_1,1)-(r_1-13)^2\right]^2 e^{-(r_1-13)^2/N_0}dr_1\\
&+\int_{-\infty}^{\infty}\left[f_1(r_1,1)+f_2(r_1,1)+f_3(r_1,1)+f_4(r_1,0)+f_5(r_1,0)-(r_1-15)^2\right]^2 e^{-(r_1-15)^2/N_0}dr_1\\
&+\int_{-\infty}^{\infty}\left[f_1(r_1,1)+f_2(r_1,0)+f_3(r_1,1)+f_4(r_1,0)+f_5(r_1,0)-(r_1-17)^2\right]^2 e^{-(r_1-17)^2/N_0}dr_1\\
&+\int_{-\infty}^{\infty}\left[f_1(r_1,1)+f_2(r_1,0)+f_3(r_1,1)+f_4(r_1,0)+f_5(r_1,1)-(r_1-19)^2\right]^2 e^{-(r_1-19)^2/N_0}dr_1\\
&+\int_{-\infty}^{\infty}\left[f_1(r_1,1)+f_2(r_1,0)+f_3(r_1,1)+f_4(r_1,1)+f_5(r_1,1)-(r_1-21)^2\right]^2 e^{-(r_1-21)^2/N_0}dr_1\\
&+\int_{-\infty}^{\infty}\left[f_1(r_1,1)+f_2(r_1,0)+f_3(r_1,1)+f_4(r_1,1)+f_5(r_1,0)-(r_1-23)^2\right]^2 e^{-(r_1-23)^2/N_0}dr_1\\
&+\int_{-\infty}^{\infty}\left[f_1(r_1,1)+f_2(r_1,0)+f_3(r_1,0)+f_4(r_1,1)+f_5(r_1,0)-(r_1-25)^2\right]^2 e^{-(r_1-25)^2/N_0}dr_1\\
&+\int_{-\infty}^{\infty}\left[f_1(r_1,1)+f_2(r_1,0)+f_3(r_1,0)+f_4(r_1,1)+f_5(r_1,1)-(r_1-27)^2\right]^2 e^{-(r_1-27)^2/N_0}dr_1\\
&+\int_{-\infty}^{\infty}\left[f_1(r_1,1)+f_2(r_1,0)+f_3(r_1,0)+f_4(r_1,0)+f_5(r_1,1)-(r_1-29)^2\right]^2 e^{-(r_1-29)^2/N_0}dr_1\\
&+\int_{-\infty}^{\infty}\left[f_1(r_1,1)+f_2(r_1,0)+f_3(r_1,0)+f_4(r_1,0)+f_5(r_1,0)-(r_1-31)^2\right]^2 e^{-(r_1-31)^2/N_0}dr_1\Bigg),
\end{aligned}
$$

For each ρ, we can list the equations involving in the above cost function as follows:

$$a_{1,0,\rho} + a_{2,0,\rho} + a_{3,0,\rho} + a_{4,0,\rho} + a_{5,0,\rho} - 62 = 0 \quad (A.4a)$$

$$a_{1,0,\rho} + a_{2,0,\rho} + a_{3,0,\rho} + a_{4,0,\rho} + a_{5,1,\rho} - 58 = 0 \quad (A.4b)$$

$$a_{1,0,\rho} + a_{2,0,\rho} + a_{3,0,\rho} + a_{4,1,\rho} + a_{5,1,\rho} - 54 = 0 \quad (A.4c)$$

$$a_{1,0,\rho} + a_{2,0,\rho} + a_{3,0,\rho} + a_{4,1,\rho} + a_{5,0,\rho} - 50 = 0 \quad (A.4d)$$

$$a_{1,0,\rho} + a_{2,0,\rho} + a_{3,1,\rho} + a_{4,1,\rho} + a_{5,0,\rho} - 46 = 0 \quad (A.4e)$$

$$a_{1,0,\rho} + a_{2,0,\rho} + a_{3,1,\rho} + a_{4,1,\rho} + a_{5,1,\rho} - 42 = 0 \quad (A.4f)$$

$$a_{1,0,\rho} + a_{2,0,\rho} + a_{3,1,\rho} + a_{4,0,\rho} + a_{5,1,\rho} - 38 = 0 \quad (A.4g)$$

$$a_{1,0,\rho} + a_{2,0,\rho} + a_{3,1,\rho} + a_{4,0,\rho} + a_{5,0,\rho} - 34 = 0 \quad (A.4h)$$

$$a_{1,0,\rho} + a_{2,1,\rho} + a_{3,1,\rho} + a_{4,0,\rho} + a_{5,0,\rho} - 30 = 0 \quad (A.4i)$$

$$a_{1,0,\rho} + a_{2,1,\rho} + a_{3,1,\rho} + a_{4,0,\rho} + a_{5,1,\rho} - 26 = 0 \quad (A.4j)$$

$$a_{1,0,\rho} + a_{2,1,\rho} + a_{3,1,\rho} + a_{4,1,\rho} + a_{5,1,\rho} - 22 = 0 \quad (A.4k)$$

$$a_{1,0,\rho} + a_{2,1,\rho} + a_{3,1,\rho} + a_{4,1,\rho} + a_{5,0,\rho} - 18 = 0 \quad (A.4l)$$

$$a_{1,0,\rho} + a_{2,1,\rho} + a_{3,0,\rho} + a_{4,1,\rho} + a_{5,0,\rho} - 14 = 0 \quad (A.4m)$$

$$a_{1,0,\rho} + a_{2,1,\rho} + a_{3,0,\rho} + a_{4,1,\rho} + a_{5,1,\rho} - 10 = 0 \quad (A.4n)$$

$$a_{1,0,\rho} + a_{2,1,\rho} + a_{3,0,\rho} + a_{4,0,\rho} + a_{5,1,\rho} - 6 = 0 \quad (A.4o)$$

$$a_{1,0,\rho} + a_{2,1,\rho} + a_{3,0,\rho} + a_{4,0,\rho} + a_{5,0,\rho} - 2 = 0 \quad (A.4p)$$

$$a_{1,1,\rho} + a_{2,1,\rho} + a_{3,0,\rho} + a_{4,0,\rho} + a_{5,0,\rho} + 2 = 0 \quad (A.5a)$$

$$a_{1,1,\rho} + a_{2,1,\rho} + a_{3,0,\rho} + a_{4,0,\rho} + a_{5,1,\rho} + 6 = 0 \quad (A.5b)$$

$$a_{1,1,\rho} + a_{2,1,\rho} + a_{3,0,\rho} + a_{4,1,\rho} + a_{5,1,\rho} + 10 = 0 \quad (A.5c)$$

$$a_{1,1,\rho} + a_{2,1,\rho} + a_{3,0,\rho} + a_{4,1,\rho} + a_{5,0,\rho} + 14 = 0 \quad (A.5d)$$

$$a_{1,1,\rho} + a_{2,1,\rho} + a_{3,1,\rho} + a_{4,1,\rho} + a_{5,0,\rho} + 18 = 0 \quad (A.5e)$$

$$a_{1,1,\rho} + a_{2,1,\rho} + a_{3,1,\rho} + a_{4,1,\rho} + a_{5,1,\rho} + 22 = 0 \quad (A.5f)$$

$$a_{1,1,\rho} + a_{2,1,\rho} + a_{3,1,\rho} + a_{4,0,\rho} + a_{5,1,\rho} + 26 = 0 \quad (A.5g)$$

$$a_{1,1,\rho} + a_{2,1,\rho} + a_{3,1,\rho} + a_{4,0,\rho} + a_{5,0,\rho} + 30 = 0 \quad (A.5h)$$

$$a_{1,1,\rho} + a_{2,0,\rho} + a_{3,1,\rho} + a_{4,0,\rho} + a_{5,0,\rho} + 34 = 0 \quad (A.5i)$$

$$a_{1,1,\rho} + a_{2,0,\rho} + a_{3,1,\rho} + a_{4,0,\rho} + a_{5,1,\rho} + 38 = 0 \quad (A.5j)$$

$$a_{1,1,\rho} + a_{2,0,\rho} + a_{3,1,\rho} + a_{4,1,\rho} + a_{5,1,\rho} + 42 = 0 \quad (A.5k)$$

$$a_{1,1,\rho} + a_{2,0,\rho} + a_{3,1,\rho} + a_{4,1,\rho} + a_{5,0,\rho} + 46 = 0 \quad (A.5l)$$

$$a_{1,1,\rho} + a_{2,0,\rho} + a_{3,0,\rho} + a_{4,1,\rho} + a_{5,0,\rho} + 50 = 0 \quad (A.5m)$$

$$a_{1,1,\rho} + a_{2,0,\rho} + a_{3,0,\rho} + a_{4,1,\rho} + a_{5,1,\rho} + 54 = 0 \quad (A.5n)$$

$$a_{1,1,\rho} + a_{2,0,\rho} + a_{3,0,\rho} + a_{4,0,\rho} + a_{5,1,\rho} + 58 = 0 \quad (A.5o)$$

$$a_{1,1,\rho} + a_{2,0,\rho} + a_{3,0,\rho} + a_{4,0,\rho} + a_{5,0,\rho} + 62 = 0 \quad (A.5p)$$

$$b_{1,0,\rho} + b_{2,0,\rho} + b_{3,0,\rho} + b_{4,0,\rho} + b_{5,0,\rho} - 961 = 0 \quad \text{(A.4a)}$$

$$b_{1,0,\rho} + b_{2,0,\rho} + b_{3,0,\rho} + b_{4,0,\rho} + b_{5,1,\rho} - 841 = 0 \quad \text{(A.4b)}$$

$$b_{1,0,\rho} + b_{2,0,\rho} + b_{3,0,\rho} + b_{4,1,\rho} + b_{5,1,\rho} - 729 = 0 \quad \text{(A.4c)}$$

$$b_{1,0,\rho} + b_{2,0,\rho} + b_{3,0,\rho} + b_{4,1,\rho} + b_{5,0,\rho} - 625 = 0 \quad \text{(A.4d)}$$

$$b_{1,0,\rho} + b_{2,0,\rho} + b_{3,1,\rho} + b_{4,1,\rho} + b_{5,0,\rho} - 529 = 0 \quad \text{(A.4e)}$$

$$b_{1,0,\rho} + b_{2,0,\rho} + b_{3,1,\rho} + b_{4,1,\rho} + b_{5,1,\rho} - 441 = 0 \quad \text{(A.4f)}$$

$$b_{1,0,\rho} + b_{2,0,\rho} + b_{3,1,\rho} + b_{4,0,\rho} + b_{5,1,\rho} - 361 = 0 \quad \text{(A.4g)}$$

$$b_{1,0,\rho} + b_{2,0,\rho} + b_{3,1,\rho} + b_{4,0,\rho} + b_{5,0,\rho} - 289 = 0 \quad \text{(A.4h)}$$

$$b_{1,0,\rho} + b_{2,1,\rho} + b_{3,1,\rho} + b_{4,0,\rho} + b_{5,0,\rho} - 225 = 0 \quad \text{(A.4i)}$$

$$b_{1,0,\rho} + b_{2,1,\rho} + b_{3,1,\rho} + b_{4,0,\rho} + b_{5,1,\rho} - 169 = 0 \quad \text{(A.4j)}$$

$$b_{1,0,\rho} + b_{2,1,\rho} + b_{3,1,\rho} + b_{4,1,\rho} + b_{5,1,\rho} - 121 = 0 \quad \text{(A.4k)}$$

$$b_{1,0,\rho} + b_{2,1,\rho} + b_{3,1,\rho} + b_{4,1,\rho} + b_{5,0,\rho} - 81 = 0 \quad \text{(A.4l)}$$

$$b_{1,0,\rho} + b_{2,1,\rho} + b_{3,0,\rho} + b_{4,1,\rho} + b_{5,0,\rho} - 49 = 0 \quad \text{(A.4m)}$$

$$b_{1,0,\rho} + b_{2,1,\rho} + b_{3,0,\rho} + b_{4,1,\rho} + b_{5,1,\rho} - 25 = 0 \quad \text{(A.4n)}$$

$$b_{1,0,\rho} + b_{2,1,\rho} + b_{3,0,\rho} + b_{4,0,\rho} + b_{5,1,\rho} - 9 = 0 \quad \text{(A.4o)}$$

$$b_{1,0,\rho} + b_{2,1,\rho} + b_{3,0,\rho} + b_{4,0,\rho} + b_{5,0,\rho} - 1 = 0 \quad \text{(A.4p)}$$

$$b_{1,1,\rho} + b_{2,1,\rho} + b_{3,0,\rho} + b_{4,0,\rho} + b_{5,0,\rho} - 1 = 0 \quad \text{(A.5a)}$$

$$b_{1,1,\rho} + b_{2,1,\rho} + b_{3,0,\rho} + b_{4,0,\rho} + b_{5,1,\rho} - 9 = 0 \quad \text{(A.5b)}$$

$$b_{1,1,\rho} + b_{2,1,\rho} + b_{3,0,\rho} + b_{4,1,\rho} + b_{5,1,\rho} - 25 = 0 \quad \text{(A.5c)}$$

$$b_{1,1,\rho} + b_{2,1,\rho} + b_{3,0,\rho} + b_{4,1,\rho} + b_{5,0,\rho} - 49 = 0 \quad \text{(A.5d)}$$

$$b_{1,1,\rho} + b_{2,1,\rho} + b_{3,1,\rho} + b_{4,1,\rho} + b_{5,0,\rho} - 81 = 0 \quad \text{(A.5e)}$$

$$b_{1,1,\rho} + b_{2,1,\rho} + b_{3,1,\rho} + b_{4,1,\rho} + b_{5,1,\rho} - 121 = 0 \quad \text{(A.5f)}$$

$$b_{1,1,\rho} + b_{2,1,\rho} + b_{3,1,\rho} + b_{4,0,\rho} + b_{5,1,\rho} - 169 = 0 \quad \text{(A.5g)}$$

$$b_{1,1,\rho} + b_{2,1,\rho} + b_{3,1,\rho} + b_{4,0,\rho} + b_{5,0,\rho} - 225 = 0 \quad \text{(A.5h)}$$

$$b_{1,1,\rho} + b_{2,0,\rho} + b_{3,1,\rho} + b_{4,0,\rho} + b_{5,0,\rho} - 289 = 0 \quad \text{(A.5i)}$$

$$b_{1,1,\rho} + b_{2,0,\rho} + b_{3,1,\rho} + b_{4,0,\rho} + b_{5,1,\rho} - 361 = 0 \quad \text{(A.5j)}$$

$$b_{1,1,\rho} + b_{2,0,\rho} + b_{3,1,\rho} + b_{4,1,\rho} + b_{5,1,\rho} - 441 = 0 \quad \text{(A.5k)}$$

$$b_{1,1,\rho} + b_{2,0,\rho} + b_{3,1,\rho} + b_{4,1,\rho} + b_{5,0,\rho} - 529 = 0 \quad \text{(A.5l)}$$

$$b_{1,1,\rho} + b_{2,0,\rho} + b_{3,0,\rho} + b_{4,1,\rho} + b_{5,0,\rho} - 625 = 0 \quad \text{(A.5m)}$$

$$b_{1,1,\rho} + b_{2,0,\rho} + b_{3,0,\rho} + b_{4,1,\rho} + b_{5,1,\rho} - 729 = 0 \quad \text{(A.5n)}$$

$$b_{1,1,\rho} + b_{2,0,\rho} + b_{3,0,\rho} + b_{4,0,\rho} + b_{5,1,\rho} - 841 = 0 \quad \text{(A.5o)}$$

$$b_{1,1,\rho} + b_{2,0,\rho} + b_{3,0,\rho} + b_{4,0,\rho} + b_{5,0,\rho} - 961 = 0 \quad \text{(A.5p)}$$

Then applying the Algorithm Q to Eqs. (A.4a)–(A.5p) yields:

1 :	(A.4a), (A.4b), (A.4c), (A.4e), (A.4i), (A.5a)	: A_1
2 :	(A.4b), (A.4c), (A.4d), (A.4e), (A.4i), (A.5a)	: A_2
3 :	(A.4d), (A.4e), (A.4f), (A.4g), (A.4i), (A.5a)	: A_3
4 :	(A.4d), (A.4f), (A.4g), (A.4h), (A.4i), (A.5a)	: A_4
5 :	(A.4h), (A.4i), (A.4j), (A.4k), (A.4m), (A.5a)	: A_5
6 :	(A.4h), (A.4j), (A.4k), (A.4l), (A.4m), (A.5a)	: A_6
7 :	(A.4h), (A.4l), (A.4m), (A.4n), (A.4o), (A.5a)	: A_7
8 :	(A.4h), (A.4l), (A.4n), (A.4o), (A.4p), (A.5a)	: A_8
9 :	(A.4p), (A.5a), (A.5b), (A.5c), (A.5e), (A.5i)	: A_9
10 :	(A.4p), (A.5b), (A.5c), (A.5d), (A.5e), (A.5i)	: A_{10}
11 :	(A.4p), (A.5d), (A.5e), (A.5f), (A.5g), (A.5i)	: A_{11}
12 :	(A.4p), (A.5d), (A.5f), (A.5g), (A.5h), (A.5i)	: A_{12}
13 :	(A.4p), (A.5h), (A.5i), (A.5j), (A.5k), (A.5m)	: A_{13}
14 :	(A.4p), (A.5h), (A.5j), (A.5k), (A.5l), (A.5m)	: A_{14}
15 :	(A.4p), (A.5h), (A.5l), (A.5m), (A.5n), (A.5o)	: A_{15}
16 :	(A.4p), (A.5h), (A.5l), (A.5n), (A.5o), (A.5p)	: A_{16}

Therefore, q is equal to 16.

Then, the solutions for each set are:

$$
A_1(\rho=1) \quad : \quad \begin{cases}
a_{1,0,1} = 22 - a_{2,1,1} - a_{3,1,1} - a_{4,1,1} - a_{5,1,1} \\
a_{1,1,1} = -22 - a_{2,1,1} - a_{3,1,1} - a_{4,1,1} - a_{5,1,1} \\
a_{2,0,1} = 20 + a_{2,1,1} \\
a_{3,0,1} = 12 + a_{3,1,1} \\
a_{4,0,1} = 4 + a_{4,1,1} \\
a_{5,0,1} = 4 + a_{5,1,1} \\
b_{1,0,1} = -7 - b_{2,1,1} - b_{3,1,1} - b_{4,1,1} - b_{5,1,1} \\
b_{1,1,1} = -551 - b_{2,1,1} - b_{3,1,1} - b_{4,1,1} - b_{5,1,1} \\
b_{2,0,1} = 416 + b_{2,1,1} \\
b_{3,0,1} = 320 + b_{3,1,1} \\
b_{4,0,1} = 112 + b_{4,1,1} \\
b_{5,0,1} = 120 + b_{5,1,1}
\end{cases}
$$

$$
A_2(\rho=2) \quad : \quad \begin{cases}
a_{1,0,2} = 30 - a_{2,1,2} - a_{3,1,2} - a_{4,1,2} - a_{5,1,2} \\
a_{1,1,2} = -6 - a_{2,1,2} - a_{3,1,2} - a_{4,1,2} - a_{5,1,2} \\
a_{2,0,2} = 20 + a_{2,1,2} \\
a_{3,0,2} = 4 + a_{3,1,2} \\
a_{4,0,2} = 4 + a_{4,1,2} \\
a_{5,0,2} = -4 + a_{5,1,2} \\
b_{1,0,2} = 217 - b_{2,1,2} - b_{3,1,2} - b_{4,1,2} - b_{5,1,2} \\
b_{1,1,2} = -103 - b_{2,1,2} - b_{3,1,2} - b_{4,1,2} - b_{5,1,2} \\
b_{2,0,2} = 416 + b_{2,1,2} \\
b_{3,0,2} = 96 + b_{3,1,2} \\
b_{4,0,2} = 112 + b_{4,1,2} \\
b_{5,0,2} = -104 + b_{5,1,2}
\end{cases}
$$

$$
A_3(\rho=3) \quad : \quad \begin{cases}
a_{1,0,3} = 30 - a_{2,1,3} - a_{3,1,3} - a_{4,1,3} - a_{5,1,3} \\
a_{1,1,3} = -6 - a_{2,1,3} - a_{3,1,3} - a_{4,1,3} - a_{5,1,3} \\
a_{2,0,3} = 12 + a_{2,1,3} \\
a_{3,0,3} = 4 + a_{3,1,3} \\
a_{4,0,3} = -4 + a_{4,1,3} \\
a_{5,0,3} = 4 + a_{5,1,3} \\
b_{1,0,3} = 217 - b_{2,1,3} - b_{3,1,3} - b_{4,1,3} - b_{5,1,3} \\
b_{1,1,3} = -103 - b_{2,1,3} - b_{3,1,3} - b_{4,1,3} - b_{5,1,3} \\
b_{2,0,3} = 224 + b_{2,1,3} \\
b_{3,0,3} = 96 + b_{3,1,3} \\
b_{4,0,3} = -80 + b_{4,1,3} \\
b_{5,0,3} = 88 + b_{5,1,3}
\end{cases}
$$

$$
A_4(\rho=4) \quad : \quad \begin{cases}
a_{1,0,4} = 38 - a_{2,1,4} - a_{3,1,4} - a_{4,1,4} - a_{5,1,4} \\
a_{1,1,4} = -6 - a_{2,1,4} - a_{3,1,4} - a_{4,1,4} - a_{5,1,4} \\
a_{2,0,4} = 4 + a_{2,1,4} \\
a_{3,0,4} = 12 + a_{3,1,4} \\
a_{4,0,4} = -4 + a_{4,1,4} \\
a_{5,0,4} = -4 + a_{5,1,4} \\
b_{1,0,4} = 377 - b_{2,1,4} - b_{3,1,3} - b_{4,1,3} - b_{5,1,3} \\
b_{1,1,4} = -103 - b_{2,1,4} - b_{3,1,3} - b_{4,1,3} - b_{5,1,3} \\
b_{2,0,4} = 64 + b_{2,1,4} \\
b_{3,0,4} = 256 + b_{3,1,4} \\
b_{4,0,4} = -80 + b_{4,1,4} \\
b_{5,0,4} = -72 + b_{5,1,4}
\end{cases}
$$

$$
A_5(\rho=5) \quad : \quad \begin{cases}
a_{1,0,5} = 22 - a_{2,1,5} - a_{3,1,5} - a_{4,1,5} - a_{5,1,5} \\
a_{1,1,5} = 2 - a_{2,1,5} - a_{3,1,5} - a_{4,1,5} - a_{5,1,5} \\
a_{2,0,5} = 4 + a_{2,1,5} \\
a_{3,0,5} = -12 + a_{3,1,5} \\
a_{4,0,5} = 4 + a_{4,1,5} \\
a_{5,0,5} = 4 + a_{5,1,5} \\
b_{1,0,5} = 121 - b_{2,1,5} - b_{3,1,5} - b_{4,1,5} - b_{5,1,5} \\
b_{1,1,5} = 25 - b_{2,1,5} - b_{3,1,5} - b_{4,1,5} - b_{5,1,5} \\
b_{2,0,5} = 64 + b_{2,1,5} \\
b_{3,0,5} = -128 + b_{3,1,5} \\
b_{4,0,5} = 48 + b_{4,1,5} \\
b_{5,0,5} = 56 + b_{5,1,5}
\end{cases}
$$

$$
A_6(\rho=6) \quad : \quad \begin{cases}
a_{1,0,6} = 22 - a_{2,1,6} - a_{3,1,6} - a_{4,1,6} - a_{5,1,6} \\
a_{1,1,6} = 2 - a_{2,1,6} - a_{3,1,6} - a_{4,1,6} - a_{5,1,6} \\
a_{2,0,6} = 12 + a_{2,1,6} \\
a_{3,0,6} = -4 + a_{3,1,6} \\
a_{4,0,6} = 4 + a_{4,1,6} \\
a_{5,0,6} = -4 + a_{5,1,6} \\
b_{1,0,6} = 121 - b_{2,1,6} - b_{3,1,6} - b_{4,1,6} - b_{5,1,6} \\
b_{1,1,6} = 25 - b_{2,1,6} - b_{3,1,6} - b_{4,1,6} - b_{5,1,6} \\
b_{2,0,6} = 160 + b_{2,1,6} \\
b_{3,0,6} = -32 + b_{3,1,6} \\
b_{4,0,6} = 48 + b_{4,1,6} \\
b_{5,0,6} = -40 + b_{5,1,6}
\end{cases}
$$

$$
A_7(\rho=7) \quad : \quad \begin{cases}
a_{1,0,7} = 14 - a_{2,1,7} - a_{3,1,7} - a_{4,1,7} - a_{5,1,7} \\
a_{1,1,7} = 2 - a_{2,1,7} - a_{3,1,7} - a_{4,1,7} - a_{5,1,7} \\
a_{2,0,7} = 20 + a_{2,1,7} \\
a_{3,0,7} = -4 + a_{3,1,7} \\
a_{4,0,7} = -4 + a_{4,1,7} \\
a_{5,0,7} = 4 + a_{5,1,7} \\
b_{1,0,7} = 57 - b_{2,1,7} - b_{3,1,7} - b_{4,1,7} - b_{5,1,7} \\
b_{1,1,7} = 25 - b_{2,1,7} - b_{3,1,7} - b_{4,1,7} - b_{5,1,7} \\
b_{2,0,7} = 224 + b_{2,1,7} \\
b_{3,0,7} = -32 + b_{3,1,7} \\
b_{4,0,7} = -16 + b_{4,1,7} \\
b_{5,0,7} = 24 + b_{5,1,7}
\end{cases}
$$

$$
A_8(\rho=8) \quad : \quad \begin{cases}
a_{1,0,8} = 22 - a_{2,1,8} - a_{3,1,8} - a_{4,1,8} - a_{5,1,8} \\
a_{1,1,8} = 18 - a_{2,1,8} - a_{3,1,8} - a_{4,1,8} - a_{5,1,8} \\
a_{2,0,8} = 20 + a_{2,1,8} \\
a_{3,0,8} = -12 + a_{3,1,8} \\
a_{4,0,8} = -4 + a_{4,1,8} \\
a_{5,0,8} = -4 + a_{5,1,8} \\
b_{1,0,8} = 89 - b_{2,1,8} - b_{3,1,8} - b_{4,1,8} - b_{5,1,8} \\
b_{1,1,8} = 89 - b_{2,1,8} - b_{3,1,8} - b_{4,1,8} - b_{5,1,8} \\
b_{2,0,8} = 224 + b_{2,1,8} \\
b_{3,0,8} = -64 + b_{3,1,8} \\
b_{4,0,8} = -16 + b_{4,1,8} \\
b_{5,0,8} = -8 + b_{5,1,8}
\end{cases}
$$

$$
A_9(\rho=9) \quad : \quad \begin{cases}
a_{1,0,9} = -18 - a_{2,1,9} - a_{3,1,9} - a_{4,1,9} - a_{5,1,9} \\
a_{1,1,9} = -22 - a_{2,1,9} - a_{3,1,9} - a_{4,1,9} - a_{5,1,9} \\
a_{2,0,9} = -20 + a_{2,1,9} \\
a_{3,0,9} = 12 + a_{3,1,9} \\
a_{4,0,9} = 4 + a_{4,1,9} \\
a_{5,0,9} = 4 + a_{5,1,9} \\
b_{1,0,9} = 89 - b_{2,1,9} - b_{3,1,9} - b_{4,1,9} - b_{5,1,9} \\
b_{1,1,9} = 89 - b_{2,1,9} - b_{3,1,9} - b_{4,1,9} - b_{5,1,9} \\
b_{2,0,9} = 224 + b_{2,1,9} \\
b_{3,0,9} = -64 + b_{3,1,9} \\
b_{4,0,9} = -16 + b_{4,1,9} \\
b_{5,0,9} = -8 + b_{5,1,9}
\end{cases}
$$

$$
A_{10}(\rho=10) \quad : \quad \begin{cases}
a_{1,0,10} = -2 - a_{2,1,10} - a_{3,1,10} - a_{4,1,10} - a_{5,1,10} \\
a_{1,1,10} = -14 - a_{2,1,10} - a_{3,1,10} - a_{4,1,10} - a_{5,1,10} \\
a_{2,0,10} = -20 + a_{2,1,10} \\
a_{3,0,10} = 4 + a_{3,1,10} \\
a_{4,0,10} = 4 + a_{4,1,10} \\
a_{5,0,10} = -4 + a_{5,1,10} \\
b_{1,0,10} = 25 - b_{2,1,10} - b_{3,1,10} - b_{4,1,10} - b_{5,1,10} \\
b_{1,1,10} = 57 - b_{2,1,10} - b_{3,1,10} - b_{4,1,10} - b_{5,1,10} \\
b_{2,0,10} = 224 + b_{2,1,10} \\
b_{3,0,10} = -32 + b_{3,1,10} \\
b_{4,0,10} = -16 + b_{4,1,10} \\
b_{5,0,10} = 24 + b_{5,1,10}
\end{cases}
$$

$$A_{11}(\rho = 11) \quad : \quad \begin{cases} a_{1,0,11} = -2 - a_{2,1,11} - a_{3,1,11} - a_{4,1,11} - a_{5,1,11} \\ a_{1,1,11} = -22 - a_{2,1,11} - a_{3,1,11} - a_{4,1,11} - a_{5,1,11} \\ a_{2,0,11} = -12 + a_{2,1,11} \\ a_{3,0,11} = 4 + a_{3,1,11} \\ a_{4,0,11} = -4 + a_{4,1,11} \\ a_{5,0,11} = 4 + a_{5,1,11} \\ b_{1,0,11} = 25 - b_{2,1,11} - b_{3,1,11} - b_{4,1,11} - b_{5,1,11} \\ b_{1,1,11} = 121 - b_{2,1,11} - b_{3,1,11} - b_{4,1,11} - b_{5,1,11} \\ b_{2,0,11} = 160 + b_{2,1,11} \\ b_{3,0,11} = -32 + b_{3,1,11} \\ b_{4,0,11} = 48 + b_{4,1,11} \\ b_{5,0,11} = -40 + b_{5,1,11} \end{cases}$$

$$A_{12}(\rho = 12) \quad : \quad \begin{cases} a_{1,0,12} = -2 - a_{2,1,12} - a_{3,1,12} - a_{4,1,12} - a_{5,1,12} \\ a_{1,1,12} = -22 - a_{2,1,12} - a_{3,1,12} - a_{4,1,12} - a_{5,1,12} \\ a_{2,0,12} = -4 + a_{2,1,12} \\ a_{3,0,12} = 12 + a_{3,1,12} \\ a_{4,0,12} = -4 + a_{4,1,12} \\ a_{5,0,12} = -4 + a_{5,1,12} \\ b_{1,0,12} = 25 - b_{2,1,12} - b_{3,1,12} - b_{4,1,12} - b_{5,1,12} \\ b_{1,1,12} = 121 - b_{2,1,12} - b_{3,1,12} - b_{4,1,12} - b_{5,1,12} \\ b_{2,0,12} = 64 + b_{2,1,12} \\ b_{3,0,12} = -128 + b_{3,1,12} \\ b_{4,0,12} = 48 + b_{4,1,12} \\ b_{5,0,12} = 56 + b_{5,1,12} \end{cases}$$

$$A_{13}(\rho=13) \quad : \quad \begin{cases} a_{1,0,13} = 6 - a_{2,1,13} - a_{3,1,13} - a_{4,1,13} - a_{5,1,13} \\ a_{1,1,13} = -38 - a_{2,1,13} - a_{3,1,13} - a_{4,1,13} - a_{5,1,13} \\ a_{2,0,13} = -4 + a_{2,1,13} \\ a_{3,0,13} = -12 + a_{3,1,13} \\ a_{4,0,13} = 4 + a_{4,1,13} \\ a_{5,0,13} = 4 + a_{5,1,13} \\ b_{1,0,13} = -103 - b_{2,1,13} - b_{3,1,13} - b_{4,1,13} - b_{5,1,13} \\ b_{1,1,13} = 377 - b_{2,1,13} - b_{3,1,13} - b_{4,1,13} - b_{5,1,13} \\ b_{2,0,13} = 64 + b_{2,1,13} \\ b_{3,0,13} = 256 + b_{3,1,13} \\ b_{4,0,13} = -80 + b_{4,1,13} \\ b_{5,0,13} = -72 + b_{5,1,13} \end{cases}$$

$$A_{14}(\rho=14) \quad : \quad \begin{cases} a_{1,0,14} = 6 - a_{2,1,14} - a_{3,1,14} - a_{4,1,14} - a_{5,1,14} \\ a_{1,1,14} = -30 - a_{2,1,14} - a_{3,1,14} - a_{4,1,14} - a_{5,1,14} \\ a_{2,0,14} = -12 + a_{2,1,14} \\ a_{3,0,14} = -4 + a_{3,1,14} \\ a_{4,0,14} = 4 + a_{4,1,14} \\ a_{5,0,14} = -4 + a_{5,1,14} \\ b_{1,0,14} = -103 - b_{2,1,14} - b_{3,1,14} - b_{4,1,14} - b_{5,1,14} \\ b_{1,1,14} = 217 - b_{2,1,14} - b_{3,1,14} - b_{4,1,14} - b_{5,1,14} \\ b_{2,0,14} = 224 + b_{2,1,14} \\ b_{3,0,14} = 96 + b_{3,1,14} \\ b_{4,0,14} = -80 + b_{4,1,14} \\ b_{5,0,14} = 88 + b_{5,1,14} \end{cases}$$

$$A_{15}(\rho=15) \quad : \quad \begin{cases} a_{1,0,15} = 6 - a_{2,1,15} - a_{3,1,15} - a_{4,1,15} - a_{5,1,15} \\ a_{1,1,15} = -30 - a_{2,1,15} - a_{3,1,15} - a_{4,1,15} - a_{5,1,15} \\ a_{2,0,15} = -20 + a_{2,1,15} \\ a_{3,0,15} = -4 + a_{3,1,15} \\ a_{4,0,15} = -4 + a_{4,1,15} \\ a_{5,0,15} = 4 + a_{5,1,15} \\ b_{1,0,15} = -103 - b_{2,1,15} - b_{3,1,15} - b_{4,1,15} - b_{5,1,15} \\ b_{1,1,15} = 217 - b_{2,1,15} - b_{3,1,15} - b_{4,1,15} - b_{5,1,15} \\ b_{2,0,15} = 416 + b_{2,1,15} \\ b_{3,0,15} = 96 + b_{3,1,15} \\ b_{4,0,15} = 112 + b_{4,1,15} \\ b_{5,0,15} = -104 + b_{5,1,15} \end{cases}$$

$$A_{16}(\rho=16) \quad : \quad \begin{cases} a_{1,0,16} = 22 - a_{2,1,16} - a_{3,1,16} - a_{4,1,16} - a_{5,1,16} \\ a_{1,1,16} = -22 - a_{2,1,16} - a_{3,1,16} - a_{4,1,16} - a_{5,1,16} \\ a_{2,0,16} = -20 + a_{2,1,16} \\ a_{3,0,16} = -12 + a_{3,1,16} \\ a_{4,0,16} = -4 + a_{4,1,16} \\ a_{5,0,16} = -4 + a_{5,1,16} \\ b_{1,0,16} = -551 - b_{2,1,16} - b_{3,1,16} - b_{4,1,16} - b_{5,1,16} \\ b_{1,1,16} = -7 - b_{2,1,16} - b_{3,1,16} - b_{4,1,16} - b_{5,1,16} \\ b_{2,0,16} = 416 + b_{2,1,16} \\ b_{3,0,16} = 320 + b_{3,1,16} \\ b_{4,0,16} = 112 + b_{4,1,16} \\ b_{5,0,16} = 120 + b_{5,1,16} \end{cases}$$

By taking a similar procedure demonstrated in previous subsections we obtain the optimal thresholds are -28, -24, -20, -16, -12, -8, -4, 0, 4, 8, 12, 16, 20, 24, and 28. By substituting these thresholds into the above equations we have

$$
\begin{aligned}
A_1(r \le -28) \quad &: \quad \begin{cases} f_1^{eq}(r,c) = -11c \cdot r - 136c \\ f_2^{eq}(r,c) = -5c \cdot r - 104c \\ f_3^{eq}(r,c) = -3c \cdot r - 80c \\ f_4^{eq}(r,c) = -c \cdot r - 28c \\ f_5^{eq}(r,c) = -c \cdot r - 30c \end{cases} \\
A_2(-28 < r \le -24) \quad &: \quad \begin{cases} f_1^{eq}(r,c) = -9c \cdot r - 80c \\ f_1^{eq}(r,c) = -5c \cdot r - 104c \\ f_2^{eq}(r,c) = -c \cdot r - 24c \\ f_3^{eq}(r,c) = -c \cdot r - 28c \\ f_4^{eq}(r,c) = c \cdot r + 26c \end{cases} \\
A_3(-24 < r \le -20) \quad &: \quad \begin{cases} f_1^{eq}(r,c) = -9c \cdot r - 80c \\ f_1^{eq}(r,c) = -3c \cdot r - 56c \\ f_2^{eq}(r,c) = -c \cdot r - 24c \\ f_3^{eq}(r,c) = c \cdot r + 20c \\ f_4^{eq}(r,c) = -c \cdot r - 22c \end{cases} \\
A_4(-20 < r \le -16) \quad &: \quad \begin{cases} f_1^{eq}(r,c) = -11c \cdot r - 120c \\ f_1^{eq}(r,c) = -c \cdot r - 16c \\ f_2^{eq}(r,c) = -3c \cdot r - 64c \\ f_3^{eq}(r,c) = c \cdot r + 20c \\ f_4^{eq}(r,c) = c \cdot r + 18c \end{cases} \\
A_5(-16 < r \le -12) \quad &: \quad \begin{cases} f_1^{eq}(r,c) = -5c \cdot r - 24c \\ f_1^{eq}(r,c) = -c \cdot r - 16c \\ f_2^{eq}(r,c) = 3c \cdot r + 32c \\ f_3^{eq}(r,c) = -c \cdot r - 12c \\ f_4^{eq}(r,c) = -c \cdot r - 14c \end{cases} \\
A_6(-12 < r \le -8) \quad &: \quad \begin{cases} f_1^{eq}(r,c) = -5c \cdot r - 24c \\ f_1^{eq}(r,c) = -3c \cdot r - 40c \\ f_2^{eq}(r,c) = c \cdot r + 8c \\ f_3^{eq}(r,c) = -c \cdot r - 12c \\ f_4^{eq}(r,c) = c \cdot r + 10c \end{cases}
\end{aligned}
$$

$$
\begin{aligned}
A_7(-8 < r \le -4) \quad : \quad & \begin{cases} f_1^{eq}(r,c) = -3c \cdot r - 8c \\ f_1^{eq}(r,c) = -5c \cdot r - 56c \\ f_2^{eq}(r,c) = c \cdot r + 8c \\ f_3^{eq}(r,c) = c \cdot r + 4c \\ f_4^{eq}(r,c) = -c \cdot r - 6c \end{cases} \\
A_8(-4 < r \le 0) \quad : \quad & \begin{cases} f_1^{eq}(r,c) = -c \cdot r \\ f_1^{eq}(r,c) = -5c \cdot r - 56c \\ f_2^{eq}(r,c) = 3c \cdot r + 16c \\ f_3^{eq}(r,c) = c \cdot r + 4c \\ f_4^{eq}(r,c) = c \cdot r + 2c \end{cases} \\
A_9(0 < r \le 4) \quad : \quad & \begin{cases} f_1^{eq}(r,c) = -c \cdot r \\ f_1^{eq}(r,c) = 5c \cdot r - 56c \\ f_2^{eq}(r,c) = -3c \cdot r + 16c \\ f_3^{eq}(r,c) = -c \cdot r + 4c \\ f_4^{eq}(r,c) = -c \cdot r + 2c \end{cases} \\
A_{10}(4 < r \le 8) \quad : \quad & \begin{cases} f_1^{eq}(r,c) = -3c \cdot r + 8c \\ f_1^{eq}(r,c) = 5c \cdot r - 56c \\ f_2^{eq}(r,c) = -c \cdot r + 8c \\ f_3^{eq}(r,c) = -c \cdot r + 4c \\ f_4^{eq}(r,c) = c \cdot r - 6c \end{cases} \\
A_{11}(8 < r \le 12) \quad : \quad & \begin{cases} f_1^{eq}(r,c) = -5c \cdot r + 24c \\ f_1^{eq}(r,c) = 3c \cdot r - 40c \\ f_2^{eq}(r,c) = -c \cdot r + 8c \\ f_3^{eq}(r,c) = c \cdot r - 12c \\ f_4^{eq}(r,c) = -c \cdot r + 10c \end{cases} \\
A_{12}(12 < r \le 16) \quad : \quad & \begin{cases} f_1^{eq}(r,c) = -5c \cdot r + 24c \\ f_1^{eq}(r,c) = c \cdot r - 16c \\ f_2^{eq}(r,c) = -3c \cdot r + 32c \\ f_3^{eq}(r,c) = c \cdot r - 12c \\ f_4^{eq}(r,c) = c \cdot r - 14c \end{cases}
\end{aligned}
$$

$$
\begin{array}{lll}
A_{13}(16 < r \le 20) & : & \begin{cases} f_1^{\text{eq}}(r,c) = -11c \cdot r + 120c \\ f_1^{\text{eq}}(r,c) = c \cdot r - 16 \\ f_2^{\text{eq}}(r,c) = 3c \cdot r - 64c \\ f_3^{\text{eq}}(r,c) = -c \cdot r + 20c \\ f_4^{\text{eq}}(r,c) = -c \cdot r + 18c \end{cases} \\
A_{14}(20 < r \le 24) & : & \begin{cases} f_1^{\text{eq}}(r,c) = -9c \cdot r + 80c \\ f_1^{\text{eq}}(r,c) = 3c \cdot r - 56c \\ f_2^{\text{eq}}(r,c) = c \cdot r - 24c \\ f_3^{\text{eq}}(r,c) = -c \cdot r + 20c \\ f_4^{\text{eq}}(r,c) = c \cdot r - 22c \end{cases} \\
A_{15}(24 < r \le 28) & : & \begin{cases} f_1^{\text{eq}}(r,c) = -9c \cdot r + 80c \\ f_1^{\text{eq}}(r,c) = 5c \cdot r - 104c \\ f_2^{\text{eq}}(r,c) = c \cdot r - 24c \\ f_3^{\text{eq}}(r,c) = c \cdot r - 28c \\ f_4^{\text{eq}}(r,c) = -c \cdot r + 26c \end{cases} \\
A_{16}(28 < r) & : & \begin{cases} f_1^{\text{eq}}(r,c) = -11c \cdot r + 136c \\ f_2^{\text{eq}}(r,c) = 5c \cdot r - 104c \\ f_3^{\text{eq}}(r,c) = 3c \cdot r - 80c \\ f_4^{\text{eq}}(r,c) = c \cdot r - 28c \\ f_5^{\text{eq}}(r,c) = c \cdot r - 30c \end{cases}
\end{array}
$$

Since the branch metric of Viterbi algorithm can be the relative metric between information bits 0 and 1, the above metrics can be further reduced to

$$
\begin{cases}
f_1^{1024\text{QAM}}(c,r) &= c(|r-28|+|r-20|+|r-16|+|r-8|+|r-4|+|r|+|r+4| \\
&\quad +|r+8|+|r+16|+|r+20|+|r+28|-136)\cdot \text{sgn}(-r) \\
f_2^{1024\text{QAM}}(c,r) &= c(|8-|r||+|12-|r||+|16-|r||+|20-|r||+|24-|r||-24)\cdot \text{sgn}(|r|-16) \\
f_3^{1024\text{QAM}}(c,r) &= c(|4-||r|-16||+|8-||r|-16||+|12-||r|-16||-8)\cdot \text{sgn}(||r|-16|-8) \\
f_4^{1024\text{QAM}}(c,r) &= c(|4-||16-|r||-8|)\cdot \text{sgn}(||16-|r||-8||-4) \\
f_5^{1024\text{QAM}}(c,r) &= c(||8-||r|-16||-4|-2)
\end{cases}
$$

Finally, we can use the nature of recursive from 256QAM's metrics to represent 1024QAM's metrics.

$$
\begin{cases}
f_1^{1024\text{QAM}}(c,r) &= c(|r-28|+|r-20|+|r-16|+|r-8|+|r-4|+|r|+|r+4| \\
&\quad +|r+8|+|r+16|+|r+20|+|r+28|-136)\cdot \text{sgn}(-r) \\
f_2^{1024\text{QAM}}(c,r) &= f_1^{256\text{QAM}}(c,16-|r|) \\
f_3^{1024\text{QAM}}(c,r) &= f_2^{256\text{QAM}}(c,|r|-16) \\
f_4^{1024\text{QAM}}(c,r) &= f_3^{256\text{QAM}}(c,16-|r|) \\
f_5^{1024\text{QAM}}(c,r) &= f_4^{256\text{QAM}}(c,|r|-16)
\end{cases}
$$

Appendix B

An Intuitive Soft-demapping Decoding for 16QAM and 64QAM Modulations

B.1 Soft-demapping Metric of 16QAM Modulation

An intuitive approach to soft-demap bit-interleaved coded modulation signals is to directly quantize the received vector according to the *inverse* of modulation mapping function [3]. According to the constellation of 16QAM (cf. Fig. B.1), when Gray code mapping is applied to 16QAM modulation, where $s(0,0) = -3$, $s(0,1) = -1$, $s(1,1) = 1$ and $s(1,0) = 3$, the inverse mapping for the first bit position is $b_0^{-1}(-3) = 0$, $b_0^{-1}(-1) = 0$, $b_0^{-1}(1) = 1$ and $b_0^{-1}(3) = 1$; Similarly, the inverse mapping for the second bit position can be obtained as $b_1^{-1}(-3) = 0$, $b_1^{-1}(-1) = 1$, $b_1^{-1}(1) = 1$ and $b_1^{-1}(3) = 0$. According to these specified inverse mapping values, we can then form two continuous demapping functions as:

$$b_0^{-1}(r) = \begin{cases} 0, & \text{for } r < -1; \\ (1+r)/2, & \text{for } -1 \le r < 1; \\ 1, & \text{for } r \ge 1 \end{cases} \quad \text{and} \quad b_1^{-1}(r) = \begin{cases} 0, & \text{for } r < -3; \\ (3+r)/2, & \text{for } -3 \le r < -1; \\ 1, & \text{for } -1 \le r < 1; \\ (3-r)/2, & \text{for } 1 \le r < 3; \\ 0, & \text{for } r \ge 3, \end{cases}$$

which is shown in Fig. 2.1.

A finite-level soft-demapping is simply a stair-cased approximation of $b_0^{-1}(\cdot)$ and $b_1^{-1}(\cdot)$

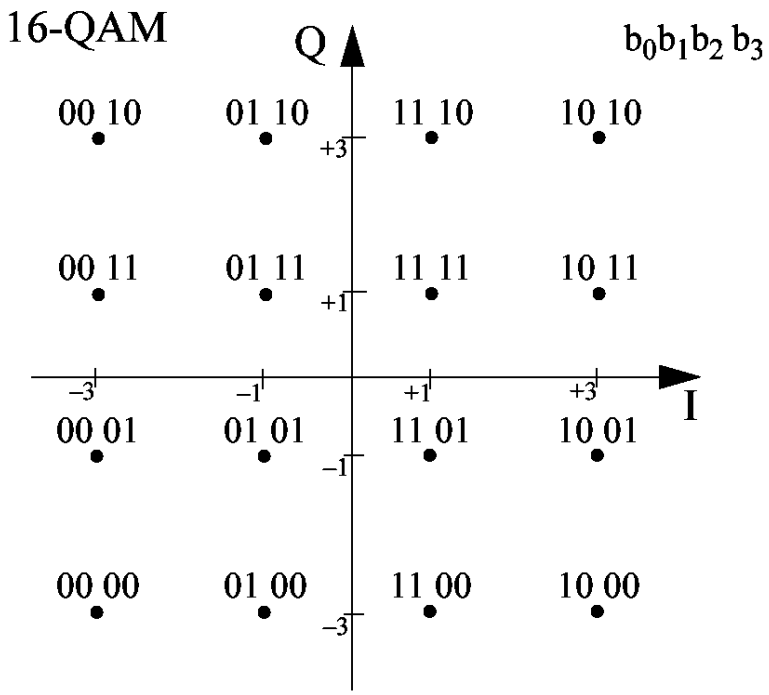

Figure B.1: 16QAM constellation with Gray code applied in 802.11a/g.

that combines the metric with quantization. An example of stair-cased approximation for eight-level quantization is illustrated in Fig. B.2, where values of demapping function have been multiplied by seven for implementation convenience (3-bit quantization). In this case, 0 and 7 represent the code bits 0 and 1, respectively, in the calculation of Euclidean metrics.

B.2 Soft-demapping Metric of 64QAM Modulation

According to the constellation of 64QAM (cf. Fig. B.3), when Gray code mapping is applied to 16QAM modulation, where $s(0,0,0) = -7$, $s(0,0,1) = -5$, $s(0,1,1) = -3$, $s(0,1,0) = -1$, $s(1,1,0) = 1$, $s(1,1,1) = 3$, $s(1,0,1) = 5$ and $s(1,0,0) = 7$, the inverse mapping for the first bit position is $b_0^{-1}(-7) = 0$, $b_0^{-1}(-5) = 0$, $b_0^{-1}(-3) = 0$, $b_0^{-1}(-1) = 0$, $b_0^{-1}(1) = 1$, $b_0^{-1}(3) = 1$, $b_0^{-1}(5) = 1$ and $b_0^{-1}(7) = 1$; Similarly, the inverse mapping for the second bit position can be obtained as $b_1^{-1}(-7) = 0$, $b_1^{-1}(-5) = 0$, $b_1^{-1}(-3) = 1$, $b_1^{-1}(-1) = 1$,

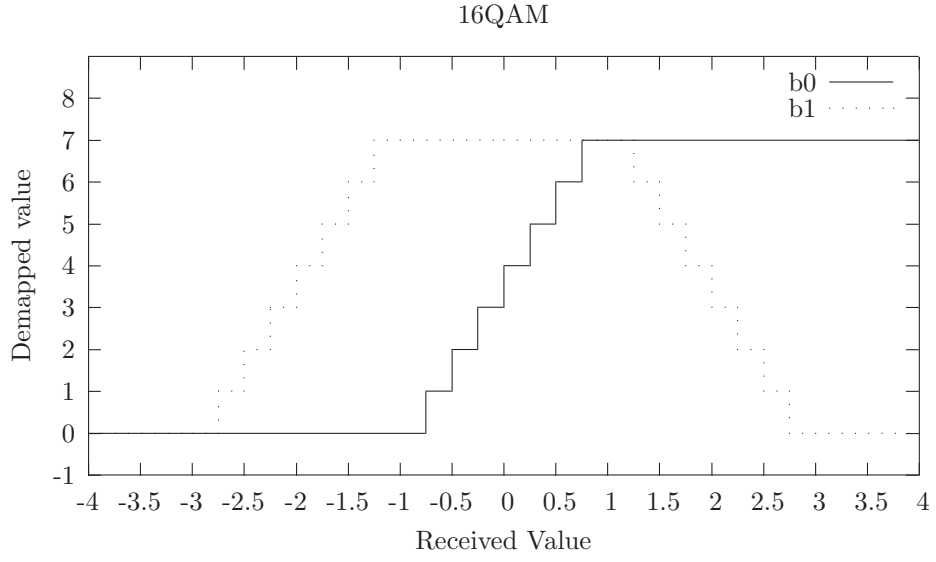

Figure B.2: 8-level stair-case approximation to $b_0^{-1}(\cdot)$ and $b_1^{-1}(\cdot)$.

$b_1^{-1}(1) = 1$, $b_1^{-1}(3) = 1$, $b_1^{-1}(5) = 0$ and $b_1^{-1}(7) = 0$, and for the third bit position as $b_2^{-1}(-7) = 0$, $b_2^{-1}(-5) = 1$, $b_2^{-1}(-3) = 1$, $b_2^{-1}(-1) = 0$, $b_2^{-1}(1) = 0$, $b_2^{-1}(3) = 1$, $b_2^{-1}(5) = 1$ and $b_2^{-1}(7) = 0$. According to these specified inverse mapping values, we can then form three continuous demapping functions as:

$$b_0^{-1}(r) = \begin{cases} 0, & \text{for } r < -1; \\ (1+r)/2, & \text{for } -1 \le r < 1; \\ 1, & \text{for } r \ge 1 \end{cases} \quad \text{and} \quad b_1^{-1}(r) = \begin{cases} 0, & \text{for } r < -5; \\ (5+r)/2, & \text{for } -5 \le r < -3; \\ 1, & \text{for } -3 \le r < 3; \\ (5-r)/2, & \text{for } 3 \le r < 5; \\ 0, & \text{for } r \ge 5. \end{cases}$$

$$b_2^{-1}(r) = \begin{cases} 0, & \text{for } r < -7; \\ (7+r)/2, & \text{for } -7 \le r < -5; \\ 1, & \text{for } -5 \le r < -3; \\ (-1-r)/2, & \text{for } -3 \le r < -1; \\ 0, & \text{for } -1 \le r < 1; \\ (-1+r)/2, & \text{for } 1 \le r < 3; \\ 1, & \text{for } 3 \le r < 5; \\ (7-r)/2, & \text{for } 5 \le r < 7; \\ 0, & \text{for } r \ge 7, \end{cases}$$

which is illustrated in Fig. B.4.

A finite-level soft-demapping is simply a stair-cased approximation of $b_0^{-1}(\cdot)$, $b_1^{-1}(\cdot)$ and $b_2^{-1}(\cdot)$ that combines the metric with quantization. An example of stair-cased approximation for eight-level quantization is illustrated in Fig. B.5, where values of demapping function have been multiplied by seven for implementation convenience (3-bit quantization). In this case, 0 and 7 represent the code bits 0 and 1, respectively, in the calculation of Euclidean metrics. Similar design rule can be easily extended to the higher QAM modulations and other modulation signal mapping such as 256QAM and 1024QAM modulations.

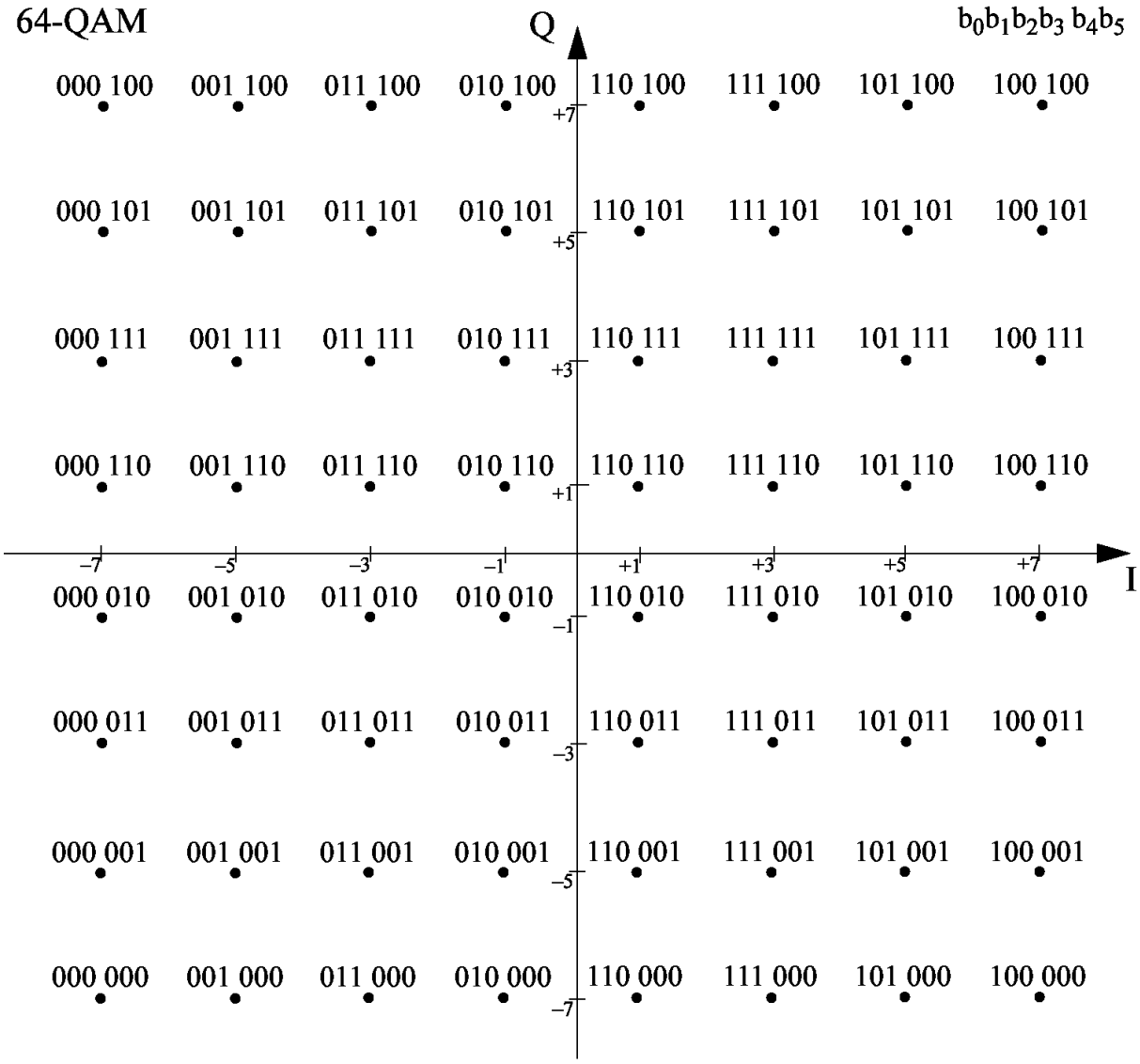

Figure B.3: 16QAM constellation with Gray code applied in 802.11a/g.

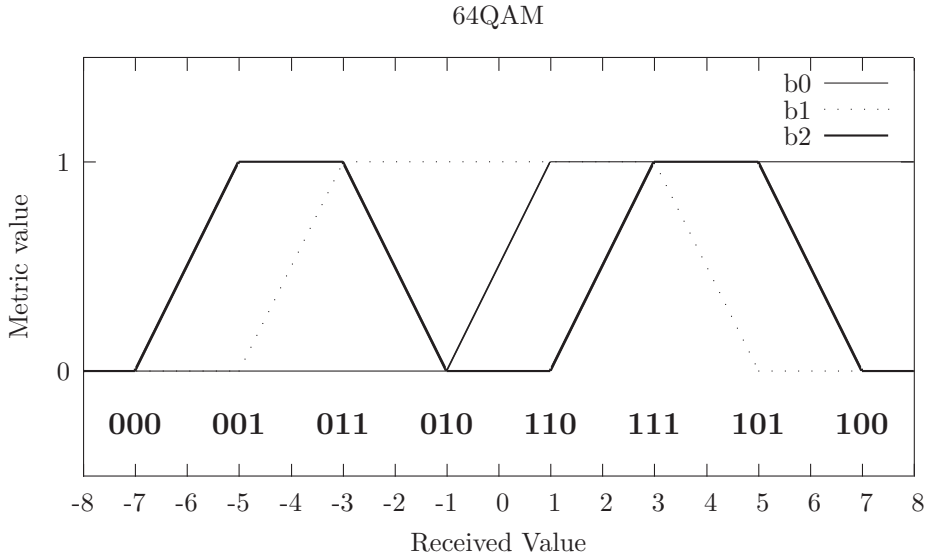

Figure B.4: The metric values of Soft-demap for 64QAM.

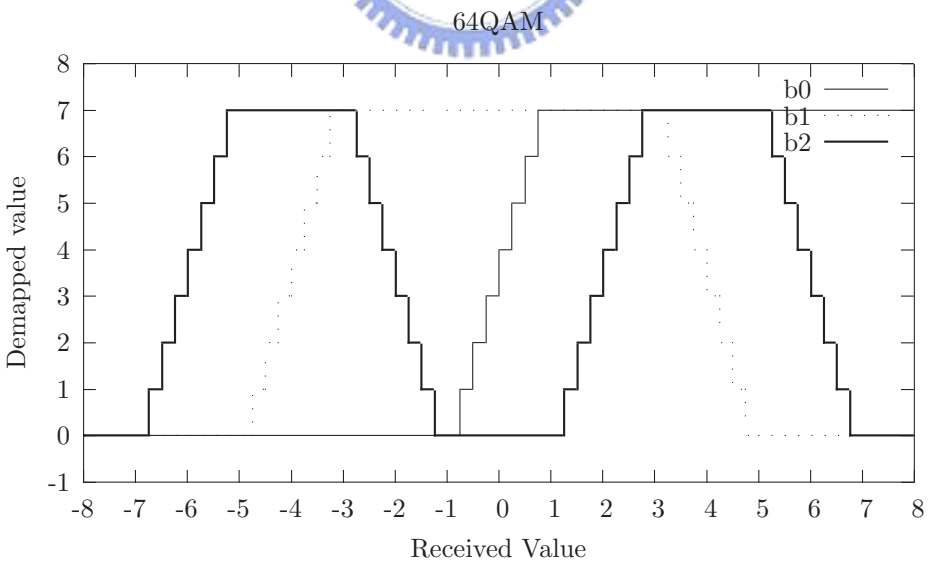

Figure B.5: 8-level stair-case approximation to $b_0^{-1}(\cdot)$, $b_1^{-1}(\cdot)$ and $b_2^{-1}(\cdot)$.

Appendix C

Theoretical Performances and Simulations of QAM Modulation over AWGN and Rayleigh Flat Fading Channels

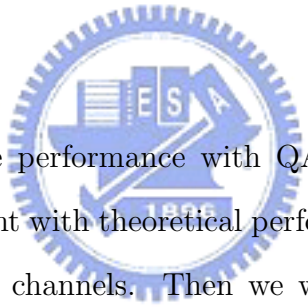

In this appendix, we discuss the performance with QAM modulation without coding to assure that our system is consistent with theoretical performance of QAM modulation under AWGN and Rayleigh flat fading channels. Then we want to figure out the relationship between bit error rate and symbol error rate under the AWGN and Rayleigh flat fading channels.

C.1 Theoretical Performances of QAM Modulation over AWGN Channel

For rectangular signal constellations in which $M = 2^k$ where k is even, the QAM signal constellation is equivalent to two PAM signals on quadrature carriers, each having $\sqrt{M} = 2^{k/2}$ signals points. Since the signals in the phase-quadrature components can be perfectly separated at the demodulator, the probability of error for QAM is easily determined from the probability of error for PAM [8]. Specifically, the probability of a correct decision for the

M-ary QAM system is

$$P_{correct} = (1 - P_{\sqrt{M}})^2$$

where $P_{\sqrt{M}}$ is the probability of error of an $\sqrt{M}$-ary PAM with one-half the average power in each quadrature signal of the equivalent QAM system. By appropriately modifying the probability of error for M-ary PAM, we obtain

$$P_{\sqrt{M}} = 2(1 - \frac{1}{\sqrt{M}}) \cdot Q(\sqrt{\frac{3}{M-1}\frac{E_s}{N_0}})$$

where $\frac{E_s}{N_0}$ is the average SNR per symbol. Therefore, the probability of a symbol error for the M-ary QAM is

$$P_{symbol} = 1 - (1 - P_{\sqrt{M}})^2$$

Note that this result is exact for $M = 2^k$ when k is odd, there is no equivalent $\sqrt{M}$-ary PAM system. If we employ the optimum detector that bases its decisions on the optimum distance metrics, it is relatively straightforward to show that the symbol error probability is tightly upper-bounded as:

$$\begin{aligned} P_{symbol} &= 1 - [1 - 2(1 - \frac{1}{\sqrt{M}}) \cdot Q(\sqrt{\frac{3}{M-1}\frac{E_s}{N_0}})]^2 \\ &\leqslant 1 - [1 - 2Q(\sqrt{\frac{3}{M-1}\frac{E_s}{N_0}})]^2 \\ &\leqslant 4Q(\sqrt{\frac{3}{M-1}\frac{E_s}{N_0}}) \\ &= 4Q(\sqrt{\frac{3k}{M-1}\frac{E_b}{N_0}}) \end{aligned}$$

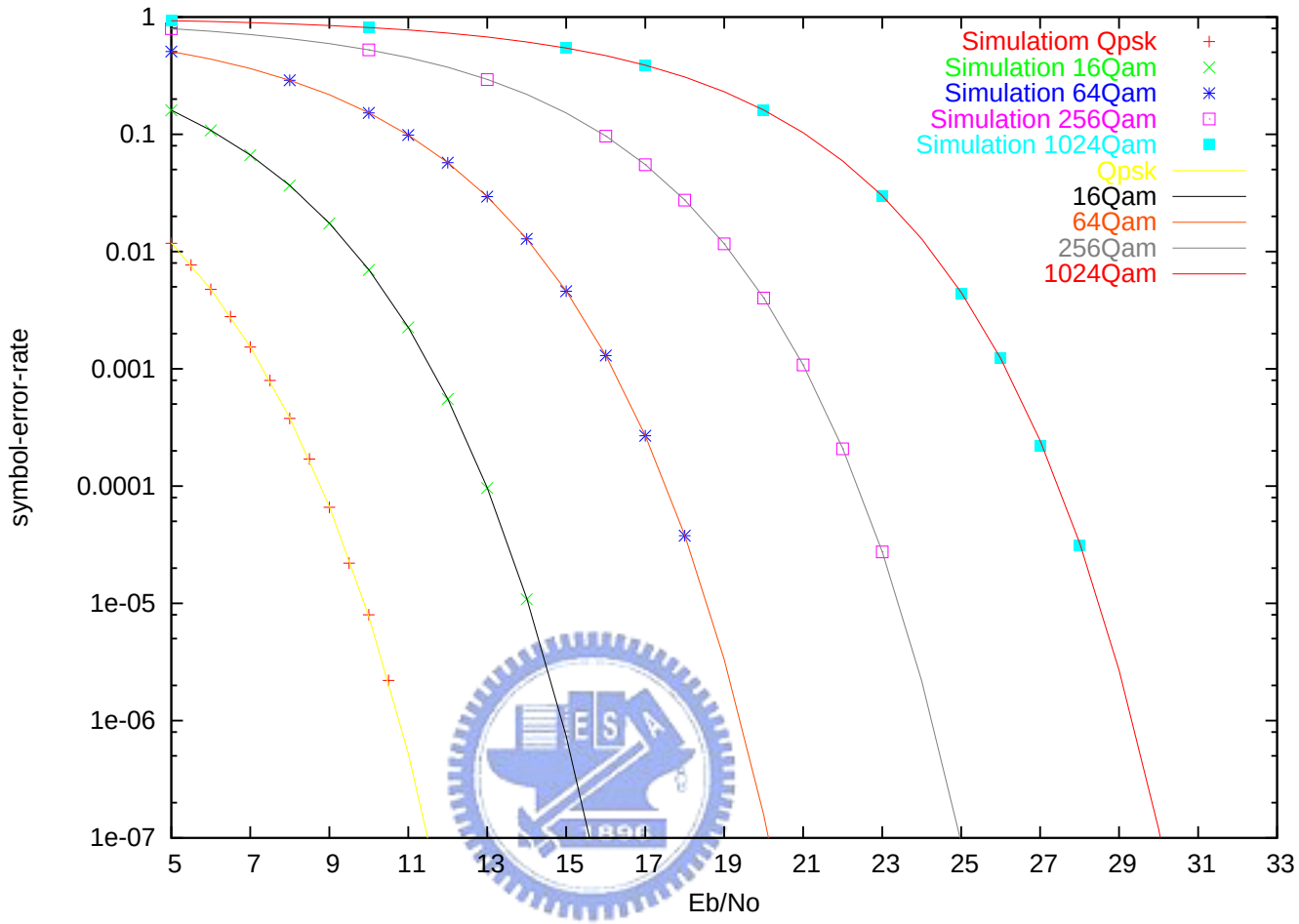

Figure C.1: Symbol error probability versus E_b/N_0 for QAM modulations under the AWGN channel.

For any $k \geqslant 1$, where $\frac{E_b}{N_0}$ is the average SNR per bit. The probability of a symbol error is plotted in as a function of the average SNR per bit. Fig. C.1 shows the symbol error rate probability of theory and our simulations.

C.1.1 Bit Error Probabilities from Symbol Error Probabilities under AWGN Channel

In this subsection, we want to discuss the relationship between symbol error rate and bit error rate [9]. To compute an equivalent bit error probability, or bit error rate (BER), from

a symbol error probability, two approaches may be taken depending on the structure of the signal space and the mapping of the signal space points into equivalent bit sequences.

In the first case, we assume that in going from one signal point to an adjacent signal point, only one bit in the binary word representing the signal point changes. Such is the case, for example, with M-ary PSK if a Gray code is used to identify the signal points, or in the case of QAM as shown with the mapping in Fig. B.1 and Fig. B.3. Since the probability of mistaking an adjacent signal point for the actual signal point is a more probable error than is that of mistaking it for a nonadjacent signal point, assuming P_s is small, it follows that the most probable number of bit errors for each symbol error is one. Since there are $k = \log_2 M$ bits represented by each symbol in an M-ary system, it follows that the bit error probability is related to the symbol error probability for systems where the above assumptions hold by

$$P_b = \frac{P_s}{\log_2 M}$$

Another intuitive approach is to record the distribution of the numbers of error bits in each error symbols. If we know the distribution of these numbers of error bits, we can use formula to derive the bit error probability from the symbol error probability.

$$P_b = \frac{P_s}{k} \sum_{i=1}^{k} i * P_{error}^{k} \tag{C.1}$$

$$\tag{C.2}$$

Table C.1 to Table C.5 record the simulation results and the theoretical values, we can find that the bit error rates derived from symbol error rates really can simplify (C.2) to $P_b = P_s/log_2 M$ in AWGN channel.

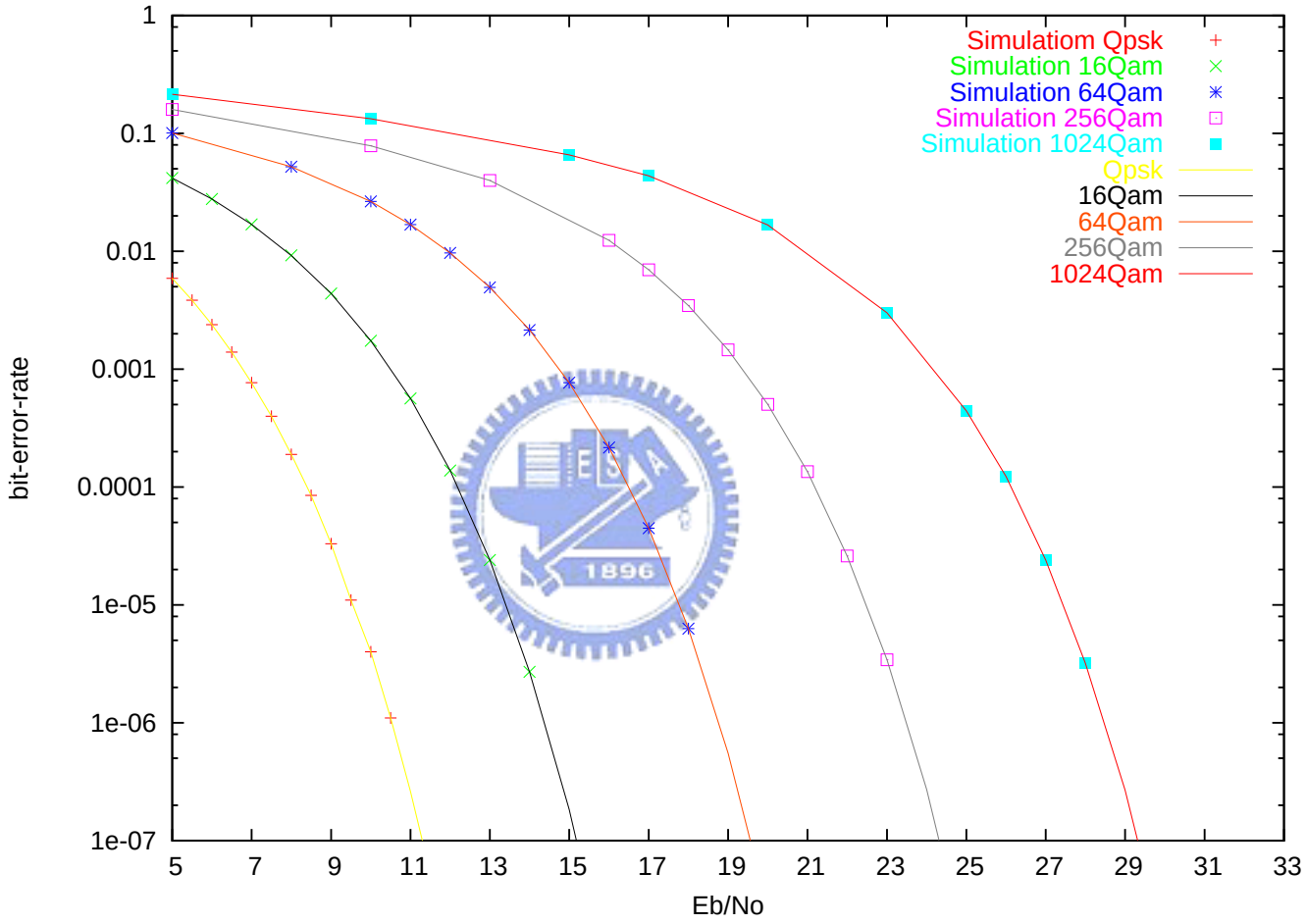

Figure C.2: Bit error probability versus E_b/N_0 for QAM modulations under the AWGN channel.

Table C.1: Symbol error rates of theory and simulation are consistent, and the bit error rate of simulation result also conforms to the distributions of the bit error numbers in the error symbols. Formula P_b=$(1*P_{error}^{1bit}+2*P_{error}^{2bit})*P_s/2$

Qpsk under AWGN channel						
E_b/N_0	*Theory* P_s	*Simul.* P_s	*Simul.* P_b	$1bit$ P_{error}	$2bit$ P_{error}	*Formula.* P_b
5	0.0118723	0.01177	0.005904	0.99670	0.00329	0.005904
5.5	0.00770955	0.00768	0.003847	0.998031556	0.001968444	0.003847559
6	0.00477088	0.004768	0.002386	0.998871242	0.001128758	0.002386691
6.5	0.00279765	0.00279	0.001395	0.999586312	0.000413688	0.001395577
7	0.00154475	0.001532	0.000767	0.999720093	0.000279907	0.000766214
7.5	0.000797434	0.000796	0.000399	0.999830592	0.000169408	0.000398067
8	0.000381779	0.000378	0.000189	0.999959639	4.03608E-05	0.000189008
8.5	0.000167992	0.00017	0.000085	0.999927078	7.29217E-05	8.50062E-05
9	6.72533E-05	0.000066	0.000033	1	0	0.000033
9.5	2.42176E-05	0.000022	0.000011	1	0	0.000011
10	0.00000774	0.000008	0.000004	1	0	0.000004
10.5	0.00000216	0.0000022	0.0000011	1	0	0.0000011

C.2 Theoretical Performances of QAM Modulation over Rayleigh Flat Fading Channel

The symbol error probability for QAM modulations was found in last subsection to be of the form :

$$P_{symbol,QAM} = 1-(1-P_{\sqrt{M}})^2 \quad \text{(C.3)}$$

$$= 2*P_{\sqrt{M}}-P_{\sqrt{M}}^2 \quad \text{(C.4)}$$

where $P_{\sqrt{M}}$ is the symbol error probability of $\sqrt{M}$-ary amplitude-shift keying given by

Table C.2: Symbol error rates of theory and simulation are consistent, and the bit error rate of simulation result also conforms to the distributions of the bit error numbers in the error symbols. Formula P_b=(1*P_{error}^{1bit}+2*P_{error}^{2bit}+3*P_{error}^{3bit}+4*P_{error}^{4bit}) *P_s/4

16QAM under AWGN channel							
E_b/N_0	*Theory* P_s	*Simul.* P_s	*Simul.* P_b	1*bit* P_{error}	2*bit* P_{error}	3*bit* P_{error}	*Formula.* P_b
5	0.160549	0.16004	0.041755	0.95637	0.0436	1.3E-06	0.041755
6	0.108378	0.107968	0.027767	0.97129	0.0287	0	0.0277668
7	0.0667155	0.066512	0.016914	0.98278	0.0172	0	0.016914
8	0.0366468	0.036504	0.00922	0.99083	0.0091	0	0.009209
9	0.0174842	0.017428	0.004376	0.99567	0.0043	0	0.004376
10	0.00700429	0.006956	0.001742	0.99835	0.0016	0	0.001742
11	0.00225755	0.002256	0.000564	0.99942	0.0005	0	0.0005643
12	0.000554558	0.000552	0.000138	0.99976	0.0002	0	0.000138
13	9.69328E-05	0.000096	0.000024	1	0	0	0.000024
14	1.10528E-05	0.00001084	0.00000271	1	0	0	0.00000271

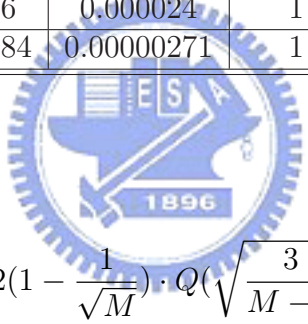

$$P_{\sqrt{M}} = 2(1 - \frac{1}{\sqrt{M}}) \cdot Q(\sqrt{\frac{3}{M-1}\frac{E_s}{N_0}}) \tag{C.5}$$

For large E_b/N_0, the second term in (C.4) is much smaller than the first term, bur we will include both terms in proper integral expressions are given for both $Q(x)$ and$Q^2(x)$ as

$$Q(x) = \frac{1}{\pi}\int_0^{\pi/2} exp(-\frac{x^2}{2\sin^2\phi})d\phi \quad and \quad Q^2(x) = \frac{1}{\pi}\int_0^{\pi/4} exp(-\frac{x^2}{2\sin^2\phi})d\phi$$

then we can obtain the symbol error rate under the Rayleigh flat fading channel:

Table C.3: Symbol error rates of theory and simulation are consistent, and the bit error rate of simulation result also conforms to the distributions of the bit error numbers in the error symbols. Formula P_b=(1*P_{error}^{1bit}+2*P_{error}^{2bit}+3*P_{error}^{3bit} +4*P_{error}^{4bit}+5*P_{error}^{5bit}+6*P_{error}^{6bit})*P_s/6

64QAM under AWGN channel								
E_b/N_0	*Theory* P_s	*Simul.* P_s	*Simul.* P_b	1*bit* P_{error}	2*bit* P_{error}	3*bit* P_{error}	4*bit* P_{error}	*Formula.* P_b
5	0.50875	0.5082	0.1007	0.816	0.181	0.0038	2.29E-05	0.1006
8	0.28928	0.2886	0.052	0.915	0.0851	4.8E-05	0	0.0522
10	0.15286	0.1524	0.0264	0.959	0.0412	6.7E-07	0	0.02641
11	0.09873	0.0985	0.0168	0.974	0.0258	0	0	0.01683
12	0.05749	0.0573	0.0097	0.985	0.0149	0	0	0.00969
13	0.02945	0.0294	0.0049	0.993	0.0076	0	0	0.00493
14	0.01288	0.01286	0.00215	0.996	0.00358	0	0	0.00215
15	0.00463	0.004596	0.000767	0.998	0.00130	0	0	0.000767
16	0.00130	0.001296	0.000216	0.999	0.00052	0	0	0.0002161
17	0.000267	0.000268	0.0000448	1	0	0	0	0.0000448
18	3.8E-05	0.000038	0.0000063	1	0	0	0	0.0000063

$$\overline{P}_{s,Rayleigh} = \frac{4}{\pi}(1-\frac{1}{\sqrt{M}})\int_0^{\pi/2}\frac{1}{1+2\sigma^2 B(\phi)}d\phi$$
$$-\frac{4}{\pi}(1-\frac{1}{\sqrt{M}})^2\int_0^{\pi/4}\frac{1}{1+2\sigma^2 B(\phi)}d\phi$$

where

$$2\sigma^2 = \frac{E_s}{N_0} \quad and \quad B(\phi) = \frac{3}{2(M-1)}\frac{1}{\sin^2\phi}$$

Another way to analyze the symbol error rate under the Rayleigh flat fading channel can be easier understood as follows. The frequency-nonselective channel results in multiplicative distortion of the transmitted signal $s_l(t)$, the received equivalent low-pass signal in one signaling interval is

$$r_l(t) = \alpha e^{-j\phi} s_l(t) + z(t), \quad 0 \leqslant t \leqslant T$$

where $Z(t)$ represents the complex-valued white Gaussian noise process corrupting the signal. Let us assume that the channel fading is sufficiently slow that the phase shift ϕ can be estimated from the received signal without error. In that case, we can achieve ideal coherent detection of the received signal. Thus, the received signal can be processed by passing it through a matched filter in the case of M QAM systems. One method that we can use to determine the performance of the binary communication systems is to evaluate the decision variables and from these determine the probability of error. However, we have already done this for a fixed (time-invariant) channel. That is, for a fixed attenuation α we know the probability of error for M QAM modulation as

$$\begin{aligned} P_{symbol,QAM}(\gamma_b) &= 1 - (1 - P_{\sqrt{M}}(\gamma_b))^2 \\ &= 2 * P_{\sqrt{M}}(\gamma_b) - P^2_{\sqrt{M}}(\gamma_b) \\ P_{\sqrt{M}}(\gamma_b) &= 2(1 - \frac{1}{\sqrt{M}}) \cdot Q(\sqrt{\frac{3}{M-1}\frac{\gamma_b}{N_0}}), \end{aligned}$$

where $\gamma_b = \alpha^2 E_s/N_0$. We view this formula as conditional error probabilities, where the condition is that α is fixed. To obtain the error probabilities when α is random, we must average the probability density function of γ_b. That is, we must evaluate the integral

$$P_{s,Rayleigh} = \int_0^\infty P_{symbol,QAM}(\gamma_b) \cdot p(\gamma_b) d\gamma_b$$

where $p(\gamma_b)$ is the probability density function of γ_b when α is random. When α is Rayleigh-distributed, α^2 has a chi-square probability distribution with two degrees of freedom. Consequently, γ_b also is chi-square-distributed. It is easily shown that

$$p_{\gamma_b} = \frac{1}{\overline{\gamma}_b} e^{-\gamma_b/\overline{\gamma}_b}, \quad \gamma_b \geqslant 0$$

where $\overline{\gamma}_b$ is the average signal-to-noise ratio, defined as

$$\overline{\gamma}_b = \frac{E_s}{N_0} E(\alpha^2)$$

The term $E(\alpha^2)$ is simply the average value of α^2. Fig. C.3 shows the symbol error rate probability of theory and our simulations under the Rayleigh flat fading channel. Fig. C.4 shows the symbol error rate probability of theory and our simulations under the Rayleigh flat fading channel and AWGN channel.

C.2.1 Bit Error Probabilities from Symbol Error Probabilities under Rayleigh Flat Fading Channel

Traditionally, we can use $P_b = \frac{P_s}{\log_2 M}$ to derive the bit error rate from already known symbol error rate. But after we scrutinize the records about the number of error bits in the error symbols, we find it is a slight distortion in this method. Table C.6 to Table C.10 record the simulation results and the theoretical values under the Rayleigh flat fading channel. Fig. C.5 shows the bit error rate probability of traditionally method and our simulations under the Rayleigh flat fading channel. Finally, we can get such a conclusion about the relationship between symbol error rate and bit error rate. With the higher of the E_b/N_0, the inferential lines of bit error rate will get closer to the real simulations.

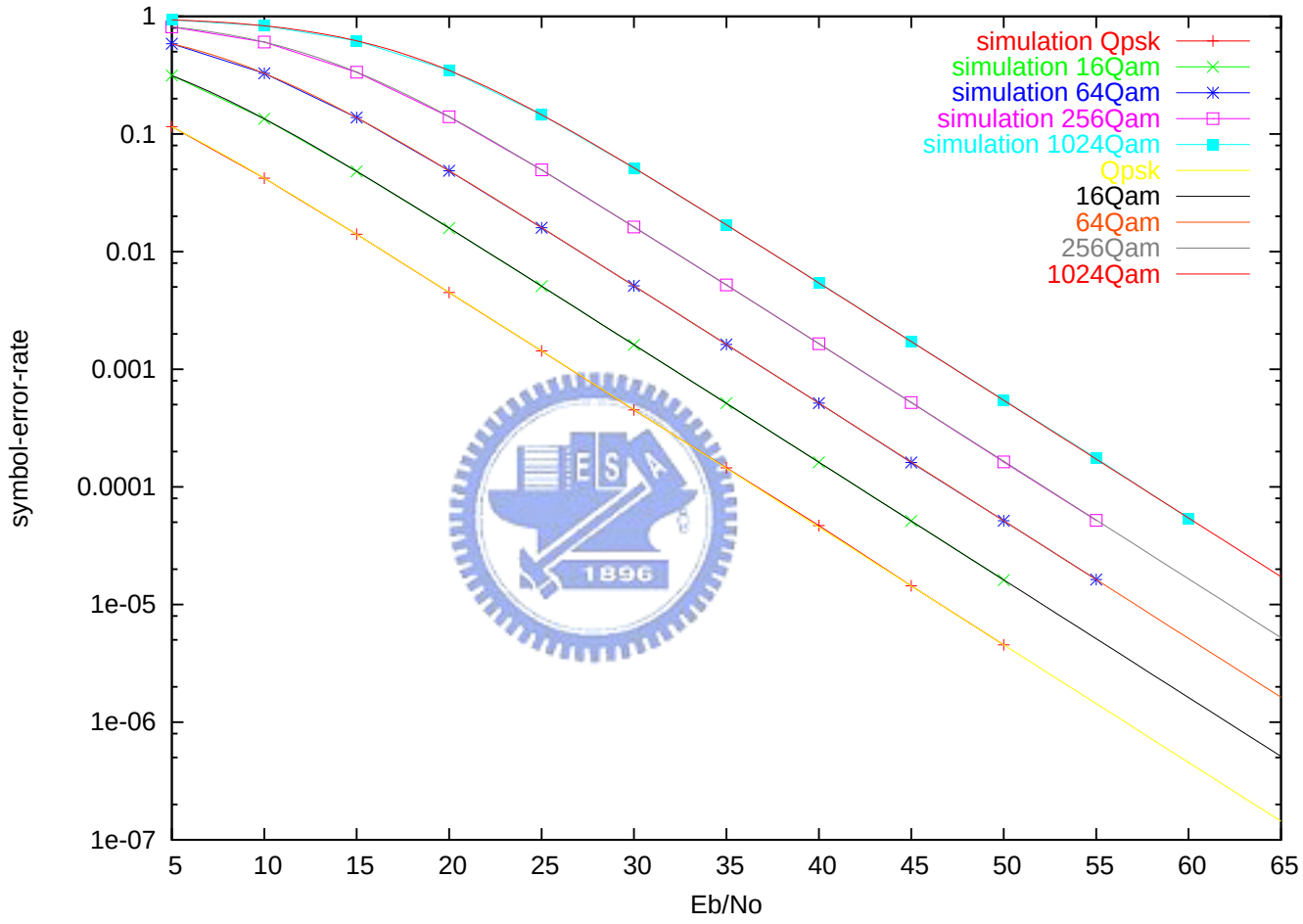

Figure C.3: Symbol error probability versus E_b/N_0 for QAM modulations under the Rayleigh flat fading channel.

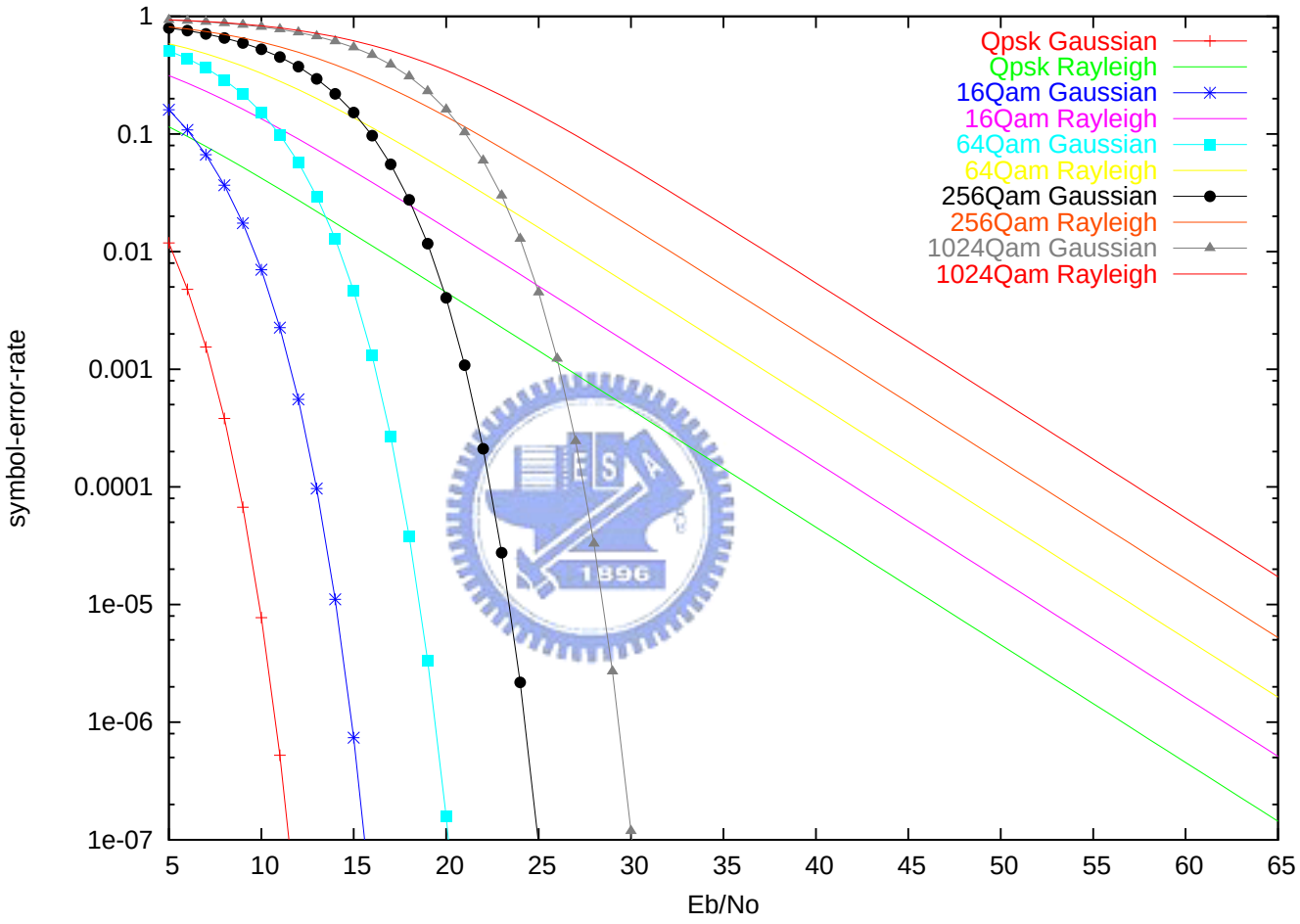

Figure C.4: Symbol error probability versus E_b/N_0 for QAM modulations under the AWGN and Rayleigh flat fading channels.

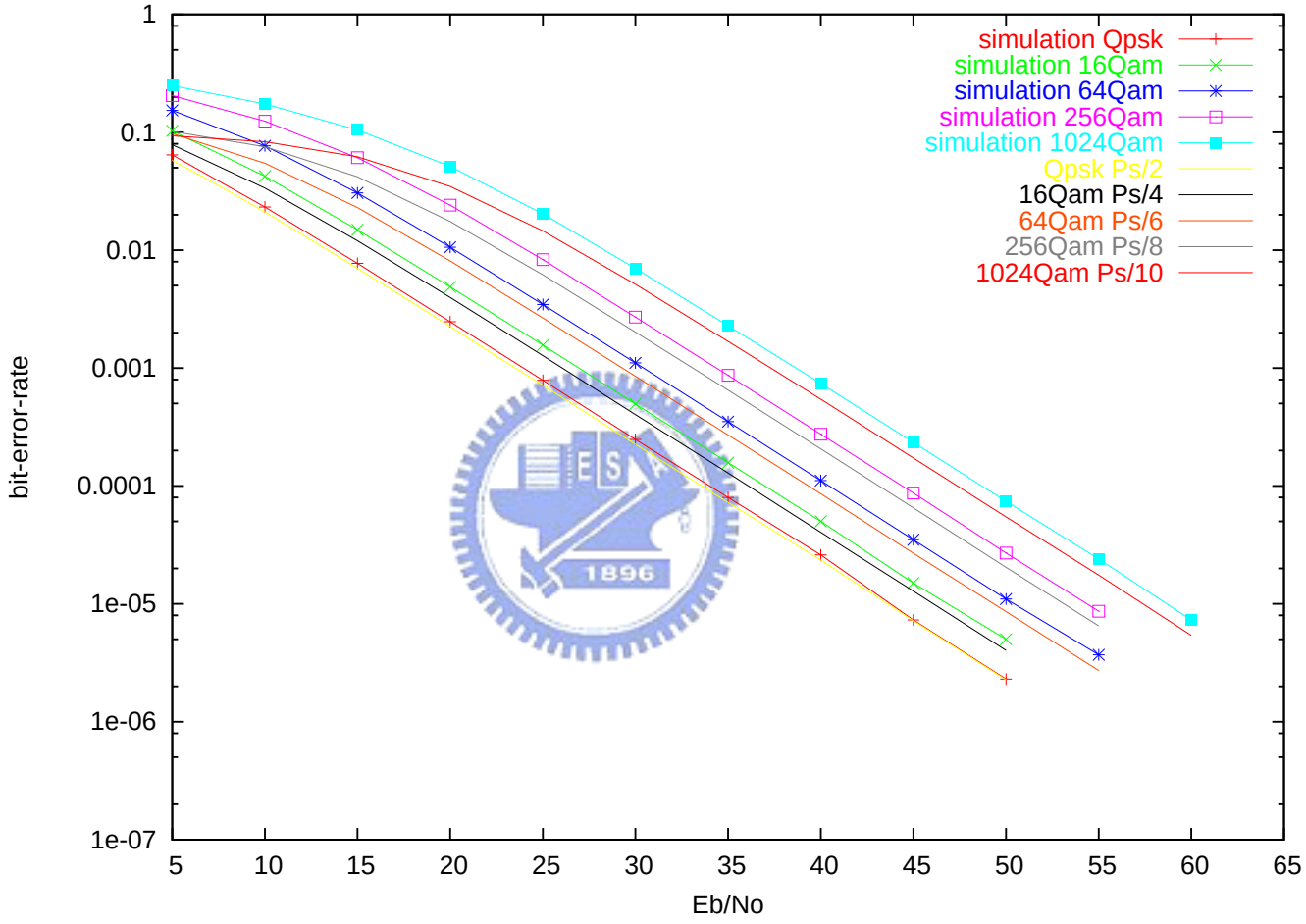

Figure C.5: Bit error probability versus E_b/N_0 for QAM modulations under the Rayleigh flat fading channel.

Table C.4: Symbol error rates of theory and simulation are consistent, and the bit error rate of simulation result also conforms to the distributions of the bit error numbers in the error symbols. Formula P_b=(1*P_{error}^{1bit}+2*P_{error}^{2bit}+3*P_{error}^{3bit}+4*P_{error}^{4bit} +5*P_{error}^{5bit}+6*P_{error}^{6bit}+7*P_{error}^{7bit}+8*P_{error}^{8bit})*P_s/8

256QAM under AWGN channel					
E_b/N_0	*Theory* P_s	*Simul.* P_s	*Simul.* P_b	1*bit* P_{error}	2*bit* P_{error}
5	0.796408	0.796288	0.159249	0.524451866	0.363660629
10	0.525592	0.525096	0.078498	0.807792762	0.188496301
13	0.294254	0.293576	0.039895	0.912897653	0.087065499
16	0.0967384	0.096488	0.012367	0.974652612	0.025347388
17	0.0552126	0.054976	0.006969	0.985916955	0.014083045
18	0.0275839	0.027488	0.00346	0.992863877	0.007136123
19	0.0116892	0.011624	0.001457	0.996845038	0.003154962
20	0.00403837	0.004016	0.000502	0.999085616	0.000914384
21	0.00108161	0.00108	0.000135	1	0
22	0.000210678	0.000208	0.000026	1	0
23	2.75209E-05	0.00002744	0.00000343	1	0

3*bit* P_{error}	4*bit* P_{error}	5*bit* P_{error}	6*bit* P_{error}	*Formula.* P_b
0.09990847	0.011483004	0.000489566	6.46566E-06	0.159249356
0.00369191	1.90269E-05	0	0	0.07849773
3.68475E-05	0	0	0	0.039894747
0	0	0	0	0.012366715
0	0	0	0	0.006968779
0	0	0	0	0.00346052
0	0	0	0	0.001457584
0	0	0	0	0.000502459
0	0	0	0	0.000135
0	0	0	0	0.000026
0	0	0	0	0.00000343

Table C.5: Symbol error rates of theory and simulation are consistent, and the bit error rate of simulation result also conforms to the distributions of the bit error numbers in the error symbols. Formula P_b=(1*P_{error}^{1bit}+2*P_{error}^{2bit}+3*P_{error}^{3bit}+4*P_{error}^{4bit} +5*P_{error}^{5bit}+6*P_{error}^{6bit}+7*P_{error}^{7bit}+8*P_{error}^{8bit} +9*P_{error}^{9bit}+10*P_{error}^{10bit})*P_s/10

1024QAM under AWGN channel					
E_b/N_0	*Theory* P_s	*Simul.* P_s	*Simul.* P_b	1*bit* P_{error}	2*bit* P_{error}
5	0.930807	0.93078	0.21471	0.2518	0.3526
10	0.814896	0.81463	0.1333	0.5022	0.3738
15	0.544463	0.54379	0.065679	0.7965	0.1991
17	0.389009	0.38832	0.043626	0.8768	0.1229
20	0.161122	0.16062	0.016765	0.9579	0.0421
23	0.0299324	0.02982	0.003004	0.9924	0.0076
25	0.00449938	0.00442	0.000443	0.9986	0.0014
26	0.00122714	0.00123	0.000123	0.9997	0.0003
27	0.000244515	0.00024	0.000024	1	0
28	3.28644E-05	0.000032	0.0000032	1	0

3*bit* P_{error}	4*bit* P_{error}	5*bit* P_{error}	6*bit* P_{error}	7*bit* P_{error}	8*bit* P_{error}	*Formula.* P_b
0.2612	0.108	0.0239	0.0023	2.94E-05	9.0E-08	0.214710
0.1097	0.0136	0.00065	1.1E-05	0	0	0.1333
0.0043	2.43E-05	0	0	0	0	0.065679
0.00027	0	0	0	0	0	0.04363
5.29E-07	0	0	0	0	0	0.01674
0	0	0	0	0	0	0.003004
0	0	0	0	0	0	0.0004426
0	0	0	0	0	0	0.000123
0	0	0	0	0	0	0.000024
0	0	0	0	0	0	0.0000032

Table C.6: Symbol error rates of theory and simulation are consistent, and the bit error rate of simulation result also conforms to the distributions of the bit error numbers in the error symbols. Formula P_b=$(1*P_{error}^{1bit}+2*P_{error}^{2bit})*P_s/2$

Qpsk under Rayleigh flat fading channel						
E_b/N_0	*Theory* P_s	*Simul.* P_s	*Simul.* P_b	1*bit* P_{error}	2*bit* P_{error}	*Formula.* P_b
5	0.115273	0.115478	0.064282	0.88663	0.11336	0.064284675
6	0.0954077	0.095371	0.052986	0.88878	0.11121	0.052988928
7	0.0784119	0.078294	0.043447	0.89024	0.10975	0.043443673
8	0.0640557	0.063994	0.03543	0.88993	0.11006	0.035518684
10	0.0421319	0.042121	0.02326	0.89514	0.10485	0.023268879
13	0.0219135	0.021927	0.01207	0.89884	0.10115	0.012072564
15	0.0140236	0.014034	0.00772	0.89988	0.10011	0.007719519
18	0.00711514	0.007116	0.003917	0.89914	0.10085	0.003916836
20	0.00451	0.004498	0.002476	0.89830	0.10169	0.002477711
23	0.00226926	0.002243	0.001234	0.89935	0.10064	0.001234376
25	0.0014339	0.001433	0.000788	0.90022	0.09977	0.000787991
30	0.000454217	0.000451	0.000248	0.90251	0.09748	0.000247482
35	0.000143714	0.000145	0.00008	0.90138	0.09861	7.96496E-05
40	4.54541E-05	0.000047	0.000026	0.90298	0.09701	2.57797E-05
45	1.43746E-05	0.0000144	0.0000073	1	0	0.0000072
50	0.000004545	0.00000454	0.0000023	1	0	0.00000227

Table C.7: Symbol error rates of theory and simulation are consistent, and the bit error rate of simulation result also conforms to the distributions of the bit error numbers in the error symbols. Formula P_b=(1*P_{error}^{1bit}+2*P_{error}^{2bit}+3*P_{error}^{3bit}+4*P_{error}^{4bit}) *P_s/4

16QAM under Rayleigh flat fading channel								
E_b/N_0	*Theory* P_s	*Simul.* P_s	*Simul.* P_b	1*bit* P_{error}	2*bit* P_{error}	3*bit* P_{error}	4*bit* P_{error}	*Formula.* P_b
5	0.3138	0.3138	0.103	0.743	0.207	0.044	0.0067	0.103
10	0.1346	0.13456	0.042	0.785	0.176	0.034	0.0051	0.042
15	0.04810	0.0481	0.0149	0.801	0.164	0.030	0.0045	0.0149
20	0.015870	0.01587	0.00488	0.807	0.159	0.029	0.0043	0.00488
25	0.005088	0.00509	0.00156	0.808	0.159	0.029	0.0042	0.001563
30	0.001616	0.001615	0.000496	0.808	0.158	0.029	0.0045	0.0004963
35	0.000512	0.000514	0.000158	0.809	0.159	0.028	0.0041	0.000158
40	0.000162	0.000162	0.00005	0.809	0.156	0.029	0.0054	4.99E-05
45	5.12E-05	0.0000513	0.000015	0.808	0.157	0.031	0.0047	1.52E-05
50	1.62E-05	0.0000161	0.000005	0.810	0.157	0.028	0.0054	4.97E-06

Table C.8: Symbol error rates of theory and simulation are consistent, and the bit error rate of simulation result also conforms to the distributions of the bit error numbers in the error symbols. Formula P_b=(1*P_{error}^{1bit}+2*P_{error}^{2bit}+3*P_{error}^{3bit} +4*P_{error}^{4bit}+5*P_{error}^{5bit}+6*P_{error}^{6bit})*P_s/6

64QAM under Rayleigh flat fading channel					
E_b/N_0	*Theory* P_s	*Simul.* P_s	*Simul.* P_b	1*bit* P_{error}	2*bit* P_{error}
5	0.586	0.585	0.1534	0.5988	0.2729
10	0.327	0.3276	0.0767	0.7013	0.2183
15	0.1376	0.1378	0.0307	0.7485	0.1885
20	0.0487	0.04868	0.0106	0.7655	0.1777
25	0.01599	0.015968	0.0035	0.7713	0.1744
30	0.00512	0.005117	0.0011	0.7728	0.1727
35	0.00163	0.001626	0.00035	0.7729	0.1730
40	0.000515	0.000515	0.00011	0.7733	0.1729
45	0.000163	0.000161	0.000035	0.7761	0.1689
50	5.15E-05	0.0000515	0.000011	0.7738	0.1731
55	1.63E-05	0.0000163	0.0000037	0.7738	0.1739

3*bit* P_{error}	4*bit* P_{error}	5*bit* P_{error}	6*bit* P_{error}	*Formula.* P_b
0.09227	0.0290	0.00617	0.000647	0.15337
0.05885	0.0173	0.00366	0.000385	0.0767
0.04621	0.0135	0.00279	0.000291	0.03066
0.04198	0.0120	0.00251	0.000211	0.01062
0.03996	0.0116	0.00230	0.000253	0.003479
0.04008	0.0116	0.00235	0.000264	0.001107
0.03978	0.0115	0.00242	0.000251	0.000351
0.03990	0.0112	0.00235	0.000214	0.0001112
0.04037	0.0119	0.00225	0.000341	3.478E-05
0.03892	0.0109	0.00295	0.000210	1.11E-05
0.03582	0.0142	0.00208	0	3.68E-06

Table C.9: Symbol error rates of theory and simulation are consistent, and the bit error rate of simulation result also conforms to the distributions of the bit error numbers in the error symbols. Formula P_b=(1*P_{error}^{1bit}+2*P_{error}^{2bit}+3*P_{error}^{3bit}+4*P_{error}^{4bit} +5*P_{error}^{5bit}+6*P_{error}^{6bit}+7*P_{error}^{7bit}+8*P_{error}^{8bit})*P_s/8

256QAM under Rayleigh flat fading channel					
E_b/N_0	*Theory* P_s	*Simul.* P_s	*Simul.* P_b	1*bit* P_{error}	2*bit* P_{error}
5	0.8147	0.8142	0.20457	0.40587	0.3224
10	0.6039	0.6038	0.124213	0.57388	0.2760
15	0.3357	0.335514	0.060935	0.68268	0.2230
20	0.1403	0.140212	0.02409	0.73135	0.1947
25	0.04948	0.049482	0.008322	0.74988	0.1833
30	0.0162	0.01617	0.00271	0.75316	0.1813
35	0.005197	0.005208	0.000868	0.75689	0.1798
40	0.0016499	0.00165	0.000275	0.75557	0.1802
45	0.000522	0.000521	0.000087	0.76042	0.1757
50	0.00016525	0.000163	0.000027	0.75598	0.1772
55	0.0000522	0.000052	0.00000864	0.76371	0.1697

3*bit* P_{error}	4*bit* P_{error}	5*bit* P_{error}	6*bit* P_{error}	7*bit* P_{error}	8*bit* P_{error}	*Formula.* P_b
0.1678	0.07210	0.024518	0.006103	0.001036	9.577E-05	0.20456
0.0987	0.03668	0.011366	0.002756	0.000454	4.718E-05	0.12421
0.0635	0.02206	0.006755	0.001563	0.000265	2.197E-05	0.06093
0.0502	0.01709	0.005086	0.001254	0.000197	2.207E-05	0.02408
0.0454	0.01547	0.004635	0.001050	0.000159	1.298E-05	0.00832
0.0450	0.01474	0.004607	0.000998	0.000151	2.269E-05	0.00270
0.0430	0.01472	0.004203	0.001094	0.000150	1.765E-05	0.00086
0.0440	0.01433	0.004239	0.001132	0.000388	3.236E-05	0.000276
0.0440	0.01437	0.004132	0.001086	0.000191	0	8.661E-05
0.0456	0.01570	0.004591	0.000865	0	0	2.726E-05
0.0482	0.01324	0.004006	0.000890	0.000222	0	8.6397E-06

Table C.10: Symbol error rates of theory and simulation are consistent, and the bit error rate of simulation result also conforms to the distributions of the bit error numbers in the error symbols. Formula P_b=(1*P_{error}^{1bit}+2*P_{error}^{2bit}+3*P_{error}^{3bit}+4*P_{error}^{4bit} +5*P_{error}^{5bit}+6*P_{error}^{6bit}+7*P_{error}^{7bit}+8*P_{error}^{8bit} +9*P_{error}^{9bit}+10*P_{error}^{10bit})*P_s/10

1024QAM under Rayleigh flat fading channel							
E_b/N_0	*Theory* P_s	*Simul.* P_s	*Simul.* P_b	1*bit* P_{error}	2*bit* P_{error}	3*bit* P_{error}	4*bit* P_{error}
5	0.93409	0.93452	0.249104	0.21634	0.29135	0.24568	0.14653
10	0.830626	0.830518	0.174076	0.38368	0.31989	0.17357	0.07949
15	0.63	0.62	0.104901	0.55868	0.27850	0.10275	0.04025
20	0.347162	0.347162	0.051435	0.75743	0.19155	0.04178	0.00785
25	0.1457	0.14557	0.02031	0.72314	0.19776	0.05169	0.01874
30	0.05148	0.051408	0.00701	0.74331	0.18509	0.04710	0.01665
35	0.0169	0.01685	0.002285	0.74860	0.18076	0.04694	0.01645
40	0.00541	0.00544	0.00074	0.74693	0.18337	0.04618	0.01622
45	0.001718	0.001725	0.000234	0.74911	0.17974	0.04710	0.01488
50	0.000544	0.000546	0.000074	0.75246	0.17900	0.04723	0.01525
55	0.000173	0.000175	0.000024	0.75143	0.18122	0.04318	0.01567
60	0.0000544	0.000054	0.0000073	0.75136	0.18865	0.03816	0.01672

5*bit* P_{error}	6*bit* P_{error}	7*bit* P_{error}	8*bit* P_{error}	9*bit* P_{error}	10*bit* P_{error}	*Formula.* P_b
0.06771	0.02408	0.00675	0.001305	0.000217	1.189E-05	0.24905
0.03040	0.00973	0.00258	0.000550	8.0586E-05	4.78E-06	0.17406
0.01413	0.00432	0.00108	0.000223	3.119E-05	2.5E-06	0.10485
0.00120	0.00015	1.59E-05	1.827E-06	1.073E-07	0	0.0518
0.00618	0.00184	0.000512	0.000104861	1.39E-05	0	0.02031
0.00567	0.00162	0.000445	8.416E-05	9.35E-06	0	0.00700
0.00522	0.00147	0.000457	4.428E-05	2.95E-05	0	0.00228
0.00566	0.00135	0.000218	4.361E-05	0	0	0.00073
0.00707	0.00171	0.000244	0.000122	0	0	0.00023
0.00438	0.00131	0.000302	5.035E-05	0	0	7.346E-05
0.00591	0.00175	0.000799	0	0	0	2.365E-05
0.00327	0.00109	0.000727	0	0	0	7.225E-06

Bibliography

[1] M.R.G. Butler, S. Armour, P. N. Fletcher, A. R. Nix and D. R. Bull, newblock "Viterbi decoding strategies for 5GHz wireless LAN systems," *Vehicular Technology Conference (VTC 2001)*, vol. 1, pp. 77–81, September 2001.

[2] J. A. Heller and I. M. Jacobs, "Viterbi decoding for satellite and space communication," *IEEE Trans. Commun.*, vol. 19, no. 5, pp. 835–848, Oct. 1971.

[3] Chen-Yi Lee, *Key Technologies in Wideband Wireless Networks — Baseband Transceiver for Multi-Mode Wireless Communications*, An MOEA (Ministry of Economic Affair) Project of Project Code: 91-EC-17-A-03-S1-0005, Taiwan, R.O.C., August 1, 2002 ∼ July 31, 2005.

[4] R. Pyndiah, A. Picard and A. Glavieux, "Performance of block turbo coded 16-QAM and 64-QAM modulations," in *Proc. of IEEE GLOBECOM '95*, vol. 2, no. 13-17, pp. 1039-1043, Singapore, Nov. 1995.

[5] F. Tosato and P. Bisaglia, "Simplified soft-output demapper for binary interleaved COFDM with application to HIPERLAN/2," *HP Labs 2001 Technical Report*, HP-2001-246, 2001.

[6] E. Zehavi, "8-PSK trellis codes for a Rayleigh channel," in *IEEE Trans. Commun.*, vol. 40, no. 5, pp. 873-884, May. 1992.

[7] Richard van N. R. Prasad, *OFDM for Wireless Multimedia Communications,* Artech House, May. 1997.

[8] J. G. Proakis, *Digital communications*, 4th edition, McGraw Hill, pp. 108-111, Sept. 2001.

[9] R. E. Zimer and R. Peterson, *Introduction to Digital Communications*, 2th edition, Prentice Hall, pp. 332–341, Nov. 2001.

[10] ETSI TS 101 475, *Broadbadn Radio Access Networks (BRAN); HIPERLAN Type 2; Physical (PHY) layer*, v1.2.2, 2001.

[11] IEEE Std 802.11a-1999, *Part 11: Wireless LAN Medium Access Control (MAC) and Physical Layer (PHY) specifications: High-speed Physical Layer in the 5 GHz band*, Sept. 1999.

[12] IEEE Draft 802.11g, *Part 11: Wireless LAN Medium Access Control (MAC) and Physical Layer (PHY) specifications: Further Higher Data Rate Extension in the 2.4 GHz band*, Draft 8.2, Apr. 2003.

[13] Fettweis, G., "Algebraic survivor memory management design for Viterbi detectors," *Communications, IEEE Transactions.*, vol. 43, Iss. 9, pp. 2458–2463, Sept. 1995.

[14] Chi-Ying Tsui; Cheng, R.S.-K.; Ling, C., "Low power ACS unit design for the Viterbi decoder," *Circuits and Systems, 1999. ISCAS '99. Proceedings of the 1999 IEEE International Symposium.*, vol. 1,30, pp. 137–140, June. 1999.

[15] Chia-Wei,Chang;Po-Ning,chen "On Bit-wise Decomposition of M-ary Symbol Metric," *ICICS2003.*, Oct. 2003 .

[16] Caire, G.; Taricco, G.; Biglieri, E., " Bit-interleaved coded modulation," *Information Theory, IEEE Transactions.*, vol. 44, Iss. 3, pp. 927–946, May. 1998.